MODELING THE EARTHQUAKE RESPONSE OF OLDER REINFORCED CONCRETE BEAM-COLUMN BUILDING JOINTS

Adam G. Theiss

A thesis submitted in partial fulfillment of the
requirements for the degree of

Master of Science in Civil Engineering

University of Washington

2005

Program Authorized to Offer Degree: Department of
Civil and Environmental Engineering

University of Washington
Graduate School

This is to certify that I have examined this copy of a master's thesis by

Adam G. Theiss

and have found that it is complete and satisfactory in all respects,
and that any and all revisions required by the final
examining committee have been made.

Committee Members:

____
Laura N. Lowes

____
Greg R. Miller

____
Dawn E. Lehman

Date:______________________

TABLE OF CONTENTS

LIST OF FIGURES

Figure Number Page

LIST OF TABLES

Table Number Page

ACKNOWLEDGEMENTS

The author wishes to thank all those people at the Pacific Earthquake Engineering Research Center, the Valle Program, and the UW Structural Engineering and Mechanics department who where instrumental in the completion of this work through their assistance and knowledge. Special thanks go to Professor Laura Lowes for the opportunity and her guidance. Final thanks go to my friends at LTH, my family, and most importantly, my fiancée Elizabeth. Their support made this thesis possible.

Chapter 1

Introduction

1.1. Introduction to Research

The research presented in this paper investigates the use of inelastic beam-column joint models to improve accuracy and increase resolution of demand predictions for the analysis of older, reinforced concrete frames towards improved performance-based earthquake engineering methodologies. Performance-based earthquake engineering (PBEE) of structures requires accurate prediction of local and global load and deformation demands for variable levels of earthquake loading. Past experimental investigation (Alire 2002, Walker 2001, Mazzoni and Moehle 2001, Clyde et al. 2000, Lowes and Moehle 1999, Leon 1990, Meinheit and Jirsa 1977, Park and Ruitong 1988, Durrani and Wight 1985) as well as damage observed following recent earthquakes (EERI 1994) indicate that under even moderate levels of earthquake loading, sufficient stiffness and strength loss due to beam-column joint damage may have a significant impact on the response of an older concrete building. Given the indications that beam-column joint response determines system behavior, this research works toward explicitly simulating inelastic joint action to accurately predict overall building and component demands, thus assisting in the development of PBEE methodologies.

The earthquake response of a single case study building, the Holiday Inn in Van Nuys, California, has been considered in this study's attempt to improve accuracy and increase resolution of demand predictions by modeling inelastic beam-column joint behavior. This building has been studied extensively (Blume and Assoc. 1973, Islam 1996, Li and Jirsa 1998, Trifunac et al. 1999, Browning et al. 2000, De la Llera et al. 2002, Barin and Pincheira 2002, Paspuleti 2002) and acceleration and damage data are available characterizing the response of the building to the 1994 Northridge earthquake. Simulation of structural response has been accomplished using the OpenSees analysis platform (http://opensees.berkeley.edu) developed as part of the Pacific Earthquake Engineering Research (PEER) Center research effort (http://peer.berkeley.edu).

Eight joint models, created from three beam-column joint element formulations and three calibration approaches developed previously, have been implemented to simulate seismic joint response in older reinforced concrete buildings. These models are evaluated through a quantitative and qualitative comparison of simulated and observed response for a series of joint sub-assemblages tested at the University of Washington (Walker 2001 and Alire 2002). Further evaluation of the most promising models is then completed through comparison of the simulated and observed response for the case study building under the Northridge earthquake. Based on the modeling of inelastic beam-column joint behavior undertaken here, the results of this study include recommendations for the simulation of joint response in order improve accuracy and increase resolution of demand predictions when modeling older, reinforced concrete frames.

1.2. Research Objectives

The objectives of the research presented here are:

1. To develop a series of inelastic joint models using the results of previous research. These results include previously proposed joint element formulations, calibration approaches and experimental data.
2. To evaluate the proposed joint models through qualitative and quantitative comparisons of simulated and observed response for a series of joint sub-assemblages tested by others in the laboratory at University of Washington and thereby identify a preferred model.
3. To investigate the impact of explicit simulation of inelastic joint action on the prediction of structural response, and component and system demands, under earthquake loading.
4. To develop recommendations for simulation of inelastic joint action in order to improve the accuracy and increase resolution of demand predictions for older reinforced concrete structures.

1.3. Motivation for Research

The objective of traditional, prescriptive building codes is the design of a structure to meet the minimum life-safety standards under moderate to severe earthquake loading. While this approach ensures minimum loss of life, it does not address the potential for structural damage, the loss of building contents or disruption of building use. Thus, in recent years, the earthquake engineering community has begun to embrace PBEE.

The drive to apply PBEE to the overall building design in the United States arose in the aftermath of the 1989 Loma Prieta and 1994 Northridge earthquakes. Buildings that were designed using the standard code procedures to meet life safety performance levels were observed also to suffer extensive and economically debilitating damage as a result of moderate earthquake ground motion. Research coordinated by the Pacific Earthquake Engineering Research (PEER) Center is working toward enabling designers to predict the economic impact, characterized in terms of repair cost and building downtime, of a particular level of earthquake loading as well as to quantify the uncertainty associated with this prediction.

The PBEE design methodology will allow engineers to provide building owners with structures that meet specific risk and performance objectives. For example, buildings will be designed with the objective of immediate occupancy or repairable-damage, for specific levels of earthquake loading, such as peak ground acceleration with a 10% probability of exceedance in 50 years. Thus PBEE, consisting of performance-based structural design and assessment, provides a framework for earthquake engineers to meet the socio-economic demands of facility owners in developed countries such as Japan and the United States. The research presented here is part of the PEER Center's efforts to develop and advance analysis and design tools for PBEE so that they are readily available to practicing engineers.

Research and Simulation Tools to Enable PBEE

The PBEE process comprises a series of steps to enable the determination of the potential economic impact due to earthquake damage. For a preliminary structural design, this process initiates with a probabilistic site hazard assessment and the development of earthquake ground motion records representing variable levels of earthquake hazard. Next, structural analysis is preformed to predict the component load and deformation demands as well as system-wide demands such as floor accelerations. Then, empirical models are employed to link demands with damage; higher resolution simulation data enable more accurate prediction of component damage (Pagni 2003). Finally, damage measures are used to predict decision variables, such as repair cost and downtime, which can be used by building owners to assess the adequacy of the design. If the design does not meet the owner's requirements, then the design is refined and the process repeated.

To accomplish the above process, earthquake engineers require a series of simulation tools and models. Of particular interest to the current study is the prediction of structural and component demands under earthquake loading. As suggested by the discussion above, uncertainty in assessing the earthquake risk can be reduced by increasing the accuracy and resolution with which demands are computed. For beam-column joints, explicit simulation of joint response enables prediction of joint load and deformation demands. This can reduce the uncertainty and inaccuracy in prediction of joint as well as beam and column damage.

1.4. Previous Research

The results of multiple previous experimental and analytical studies provide a basis for accomplishing the objectives of this research project. In particular, beam-column joint element formulations, one-dimensional constitutive models, and model calibration approaches developed by other researchers facilitated the development of beam-column joint models to be used for the accurate simulation of older reinforced-concrete buildings. Additionally, experimental data of beam-column joint sub-assemblages provided by UW researchers were used to evaluate the eight proposed joint models. The sub-assemblage and full-frame simulations were carried out using OpenSees, the analysis platform developed as part of the PEER Center research initiative.

OpenSees

OpenSees is integral to achieving the PEER Center's goal of advancing performance-based earthquake engineering. OpenSees is "a software framework for the nonlinear finite element modeling and analysis of the seismic response of structural and geotechnical systems" (http://opensees.berkeley.edu). It serves as the primary computational platform for PEER sponsored research geared toward advancing performance–based earthquake engineering. Previous studies by other researchers resulted in the development of several beam-column joint element formulations and constitutive models that have been implemented in the OpenSees platform and made available for use by the earthquake engineering research community.

This research takes advantage of the newly available modeling tools in OpenSees to simulate seismic beam-column joint behavior using sub-assemblage and full-frame building response data. The sub-assemblage response data is the result of experimental work completed at the University of Washington (Walker 2001 and Alire 2002), while the full-frame building response data is taken from the case study building, which has been monitored during past earthquakes. These data sources are elaborated below.

PEER/UW Beam-Column Joint Tests

The University of Washington has engaged in a multi-phase research project to characterize the performance of older reinforced-concrete joints. The PEER sponsored project commenced with Greg Mosier's (2000) review of pervious research to determine the parameters that determine the response of this type of joint known for its non-ductile detailing. This review concluded that behavior was determined primarily by joint shear stress demand, cyclic displacement history and concrete compressive strength. A review of building plans for structures designed between 1920 and 1970 identified the ranges of these parameters used typically in older construction. On the basis of this information, a two-part experimental investigation comprised of pseudo-static loading of eleven, full-scale building joint sub-assemblages was developed and performed. Test parameters included in the tests were joint shear stress demand, concrete compressive strength, and load history. The results of the investigation are documented in Walker (2001) and Alire (2002).

From the eleven specimens tested by Walker and Alire, five specific specimens were identified as being the most valuable for the use in evaluating models to be used to simulate the response of joints in the case study building. These specimens address the test parameters of joint shear stress demand, concrete compressive strength, and load history. Three of the tests span the range of nominal joint shear stress demand predicted for the case study building. Also, three of the five tests consist of subjecting specimens of identical design to three different cyclic load histories, while two concrete compressive strengths are used between the five specimens, normal and high.

A Case Study: The Holiday Inn of Van Nuys, CA

In the 1960s, building codes did not require many of the design details that are required today to ensure ductile response under earthquake loading. The Van Nuys Holiday Inn building is typical of buildings constructed during this period and included a number of design details that could be expected to result in brittle failure under earthquake loading: 1) short, inadequate confined splices of column longitudinal bars that are located above the floor slab in a region that could be expected to experience substantial inelastic flexural deformation demand, 2) the potential for column rather than beam yielding, 3) inadequate column shear strength, 4) insufficient transverse joint reinforcement, and 5) high joint shear stress demand.

In 2001, the Van Nuys Holiday Inn building was chosen by the PEER Center researchers to be one of three testbeds to support the development of PBEE methodologies. The Van Nuys building was chosen for a number of reasons. The primary reasons were 1) the building has a relatively simple layout and framing system and has design details typical of pre-1970s construction on the West Coast of the United States, 2) the building was instrumented with accelerometers that provide acceleration data from multiple earthquakes including the 1994 Northridge earthquake, and 3) the presence of this instrumentation has ensured that engineers inspect the building carefully following nearby earthquakes. This resulted in available data characterizing the damage sustained by the building during several earthquakes including the Northridge earthquake.

A two-dimensional, full frame model of the case study building was developed by Paspuleti (2002) as part of the PEER research program. The model evaluated the effectiveness of the inelastic modeling capabilities available in OpenSees by comparing the displacement response and mode failures of the building. The research presented here extends that research by introducing joint models to explore the impact on overall predicted response for older reinforced concrete buildings.

1.5. Report Layout

This research project investigates the use of inelastic beam-column joint models to improve accuracy and increase resolution of demand predictions for the analysis of older, reinforced concrete frames. The layout of this report reflects the natural progression taken from a survey of previous research, to joint model development and sub-assemblage simulation, to the full-frame simulation of the case study building with models of the under-reinforced beam-column joints. A breakdown of the following four chapters and their content is as follows:

- Chapter 2 presents a review of previous research containing nonlinear analyses of the Van Nuys Holiday Inn building.
- Chapter 3 presents results of previous research focused on improving understanding of nonlinear response on older beam-column joints and to develop models for use in simulating this response.
- Chapter 4 presents the results of a comparison of simulated and observed response histories for the selected five specimens of the UW under-reinforced beam-column joint test series.
- Chapter 5 presents the results of implementing joint elements into sub-assemblage and full frame simulations of the Van Nuys Holiday Inn building.
- Chapter 6 summarizes and concludes the research.

Chapter 2

The Case Study Building

2.1. Introduction

The ultimate objective of this research is the simulation of the inelastic response of beam-column joints in older reinforced concrete frames. A reinforced concrete case study building designed in 1965 was chosen to assist in achieving this objective. The Van Nuys Holiday Inn building in Van Nuys, California is a seven story building with a highly regular framing plan with eight bays in the east-west (longitudinal) direction and three in the north-south (transverse) direction. The building has detailing typical of 1960's construction, which is considered inadequate for seismic zones by today's standards. These details include no transverse steel in the beam-column joints. The building was retrofitted following the Northridge earthquake, but this study considers the building in its pre-Northridge earthquake condition.

An important aspect of the Van Nuys Holiday Inn as is the extensive instrumentation of the building and the resulting collection of seismic response data. The building was instrumented with accelerometers producing nine channels of data prior to the 1971 San Fernando earthquake. This instrumentation was upgraded and expanded to sixteen channels of data in 1980 as part of the California Strong Motion Instrumentation Program (CSMIP). Since then, acceleration response data from the 1987 Whittier Narrows and the 1994 Northridge earthquakes has also been collected as well as post-earthquake damage evaluations (Trifunac et al. 1999).

Due to the building's instrumentation, regular structure, non-ductile detailing, and the availability of data characterizing post-earthquake response, it has been the focus of many past research projects (e.g. Islam 1996, Li and Jirsa 1998, Browning et al. 2000, de la Llera et al. 2002, Barin and Pincheira 2002, Paspuleti 2002). While these projects have sought to evaluate simulation models for reinforced concrete elements with non-ductile detailing subjected to earthquake loading, none have included explicit simulation of inelastic joint action. Given that following both the San Fernando (Islam 1996) and Northridge earthquakes (Trifunac et al. 1999), the building exhibited joint damage, it is appropriate to use the building as a test case for inelastic joint modeling in older reinforced concrete buildings.

This chapter describes the case study building as well as the model of the building developed by Paspuleti (2002). This model is representative of the non-linear structural models developed by previous researchers, and it is of particular interest to the current study as it is the basis of the modeling effort documented here. The current study extends the Paspuleti model using the proposed joint models in order to simulate the inelastic response of beam-column joints in older reinforced concrete frames.

2.2. Case Study Building Details

General Details

The Holiday Inn of Van Nuys, CA is an older reinforced-concrete moment frame building located in the heart of the San Fernando Valley. The building was design in 1965 using the 1963 ACI-318 code and construction was completed a short time later. It has seven stories, four rows of columns in the east-west direction, and nine rows of columns in the north-south direction. The interior of the building consists of slab-column frames while the exterior frames are beam-slab-column moment frames. Drawings of the building layout, elevations, and connection details are provided in Appendix D. Pertinent design details include the following:

- The total building height is 65’ - 8 ½” with a ground story height of 13’ – 6”, a second story height of 8’ – 8 ½”, and a typical story height of 8’ – 8”.
- The footprint of the building is 62 feet (north-south direction) by 150 feet (east-west direction).
- The typical exterior columns are 14” x 20” oriented with the weak axis perpendicular to the longitudinal axis of the building.
- The typical depth of the spandrel beams is 22.5” except for those on the second floor which have a depth of 30”.

- The interior columns are 20” x 20” on the ground floor and 18” x 18” on the remaining floors.
- The typical slab thickness is 8 ½”, while the slab for the second floor is 10” and the roof is 8”.

Design Inadequacies and Failure Mechanisms

As mentioned previously in Section 1.4, building codes prior to 1970 were such that reinforced concrete buildings were designed with details that may allows for non-ductile response under earthquake loading. In part, the inadequacy of older designs stems from the use of small lateral load in the design process; small lateral loads resulted in gravity loads controlling the design and consequently detailing insufficient to ensure ductile response under earthquake loads. For the case study building, the non-ductile detailing of particular concern include the following which are discussed in detail below:

- Beam-column joint reinforcement
- Transverse column reinforcement
- Column lap compression splices
- Beam-slab splices
- Hooked reinforcement
- M_c/M_b: ration of the moment capacities of the column and beams

Beam-Column Joint Reinforcement

Prior to the 1971 edition of the ACI Building Code Requirements (ACI 318-71) design recommendations, there was no requirement for the inclusion of transverse reinforcement in beam-column joints in the seismic regions. Since the case study building was built prior to 1971 it has virtually no transverse reinforcement steel. One would expect the lack of this critical reinforcement in the joints would leave the joints susceptible to the loss of bond capacity for the beam and column longitudinal reinforcement, as well as joint shear failure. Experimental testing has been found to support this assertion. Walker (2001) indicates that a lack of transverse reinforcement in concrete beam-column joints results in brittle failure and limited ductility under earthquake loading.

Transverse Column Reinforcement

Calculations by Paspuleti (2002) indicate that the transverse reinforcement in the columns was spaced at distances that greatly exceed today's standards. The stirrup design was originally completed using shear forces calculated using linear analyses under design lateral loads. The resulting transverse reinforcement in the columns is No. 3, Grade 40 ties at 12" spacing. In comparison, the current code provisions (ACI 318-02) use the maximum moment capacity of the frame elements so that the stirrup spacing is a maximum of 4" with No. 3 ties (Paspuleti 2002). This large stirrup spacing leads to columns prone to brittle shear-failures prior to developing their full flexural strength. Such failures were noted in the damage evaluation of the case study building after the Northridge earthquake.

Column Lap Compression Splices

With the relatively low lateral loads of the 1960's codes, gravity governed the building design, the columns were designed as compression members, and compression splices of the column longitudinal steel were placed just above each floor slab. Since the splices were compression controlled, their lengths were 24 bar diameters for the interior frame and 36 bar diameters for the external frame members. Present day standards require 30 bar diameters with a minimum length of 12". Additionally, transverse steel was inadequately designed to confine the region around the splice, and the location of the splices is undesirable if the moment in the column near the joint was to approach the nominal moment. Given these details, it is not surprising that limited tensile capacity and ductility at the splice locations was observed during the Northridge earthquake.

Beam-Slab Splices

Design inadequacies in the splices for the interior beam-slab steel may also arise in older reinforced concrete structures. For the case study building, the longitudinal bottom reinforcement steel of the slabs has 18" lap splices at the transverse column lines.

Assuming flexural cracks would occur along the column line, the bars had only nine inches to develop anchorage. Based on the resulting inadequate development length one would expect premature pullout during flexural loading.

Hooked Reinforcement

Typically in reinforced concrete buildings built prior to the UBC (1967) and the ACI (ACI 318-71), the transverse steel hoops in the beams and columns were not terminated using the present day standard of 135° seismic hooks as specified by ACI 318-02, Section 21.4.4. The expected result of these inadequate bar termination practices are poor concrete confinement and reduced ductility.

M_c/M_b: Ratio of the Moment Capacities of the Column and Beam

A final area of potential design inadequacy with respect to today's requirements is the ratio of beam to column moment capacity. Current design standards require a column to have a strength ratio of 1.2 to ensure the columns do not yield in flexure (ACI 318-02 21.4.2.2). Column yielding can potentially result in a soft story mechanism.

2.3. Observed Earthquake Response

As discussed in Section 2.1, prior to the 1971 San Fernando earthquake the case study building was instrumented with nine accelerometers. Following the1971 earthquake the instrumentation was upgraded and expanded to 16 sensors. Figure 2.3.1 illustrates the location and orientation of the sensors. A vertical acceleration of 1% *g* (where *g* represents the acceleration of gravity) triggers the sensors resulting in digitized acceleration response records (CSMIP 1994). Acceleration data are available for 11 ground motion events, with the most notable being the 1994 Northridge, the 1987 Whittier Narrows, and the 1971 San Fernando earthquakes. Acceleration data for these events are given in Table 2.3.1 (Trifunac et al. 1999).

Based on the acceleration data the approximate period of the case study building can be determined before and after the strong ground motions. The approximate period for the building early in the ground motions and at peak response are given in

Table 2.3.2. The determination of the shift in period that the case study building exhibits as the ground motion progresses is an indication of the building's damage and inelastic response.

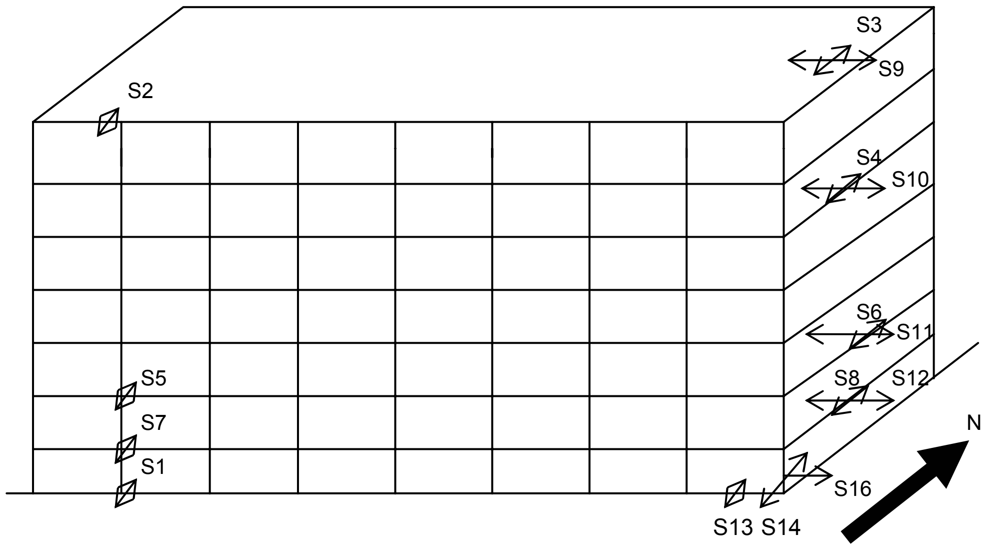

Figure 2.3.1: Sensor location and orientation in the Holiday Inn of Van Nuys.

Table 2.3.1: Select strong ground motion events (Trifunac et al., 1999)

Earthquake	Date	M	R (km)	PGA (cm/sec^2)		PGA (cm/sec^2)		PGA (cm/sec^2)	
				Trans	Long	Trans	Long	Trans	Long
San Fernando	02/09/71	6.6	22	240	130	27	23	5.3	9.7
Whittier	10/01/87	5.9	41	160	--	8.7	--	1.8	--
Northridge	01/17/94	6.7	7.2	390	440	40	51	12	7.9

Table 2.3.2: Approximate case study building periods (Islam, 1996)

	Longitudinal	Transverse
Pre-1971 San Fernando, ambient vibration	0.52 sec	0.40 sec
San Fernando earthquake:		
Early part	0.70	0.70
During peak response	1.5	1.6
Northridge earthquake:		
Early part (0-10 s)	1.5	2.2
Middle part (10-20)	2.1	2.2
Towards end (>25)	2.4	2.0

The documentation of the post-earthquake damage evaluation and repair of the building provide understanding of the building response to the earthquake loading. As a result of the San Fernando earthquake, with a peak ground acceleration of 130 cm/sec^2 in the longitudinal direction and 240 cm/sec^2 in the transverse direction, the structural damage consisted of repairing a single beam-column joint located in the north-east corner of the building. The nonstructural damage, however, was severe and contributed 80% of the total repair costs, which was the equivalent of 10% of the initial construction costs (Trifunac et al. 1999).

For the Northridge event, with a peak ground acceleration of 440 cm/sec^2 in the longitudinal direction and 390 cm/sec^2 in the transverse direction, shaking, structural response, and damage were more severe in comparison to the San Fernando event. Extensive damage to the structural system was observed in the external, longitudinal moment frames (Trifunac et al., 1999). Shear failures of the columns and beam-column joints were noted as well as spalling of the concrete cover over reinforcement bars, buckling of reinforcement bars and severe cracking of the joints and columns. Damage to the south frame occurred at six location, with five of those locations being at the 5th floor joints as shown in Figure 2.3.2a. On the north frame, cracking to the columns and joints occurred at 12 locations between the 2nd and 5th floors as shown in Figure 2.3.2b. The extent of the damage was such that the building was red flagged and evacuated by the city of Los Angeles. Trifunac and Hao (2001) indicate that the nonstructural damage was also significant. Every guest room experienced some damage. The large relative motions and deformations of the interior walls resulted in ripped wallpaper, damaged ceramic bathroom tiles and crack bathtubs.

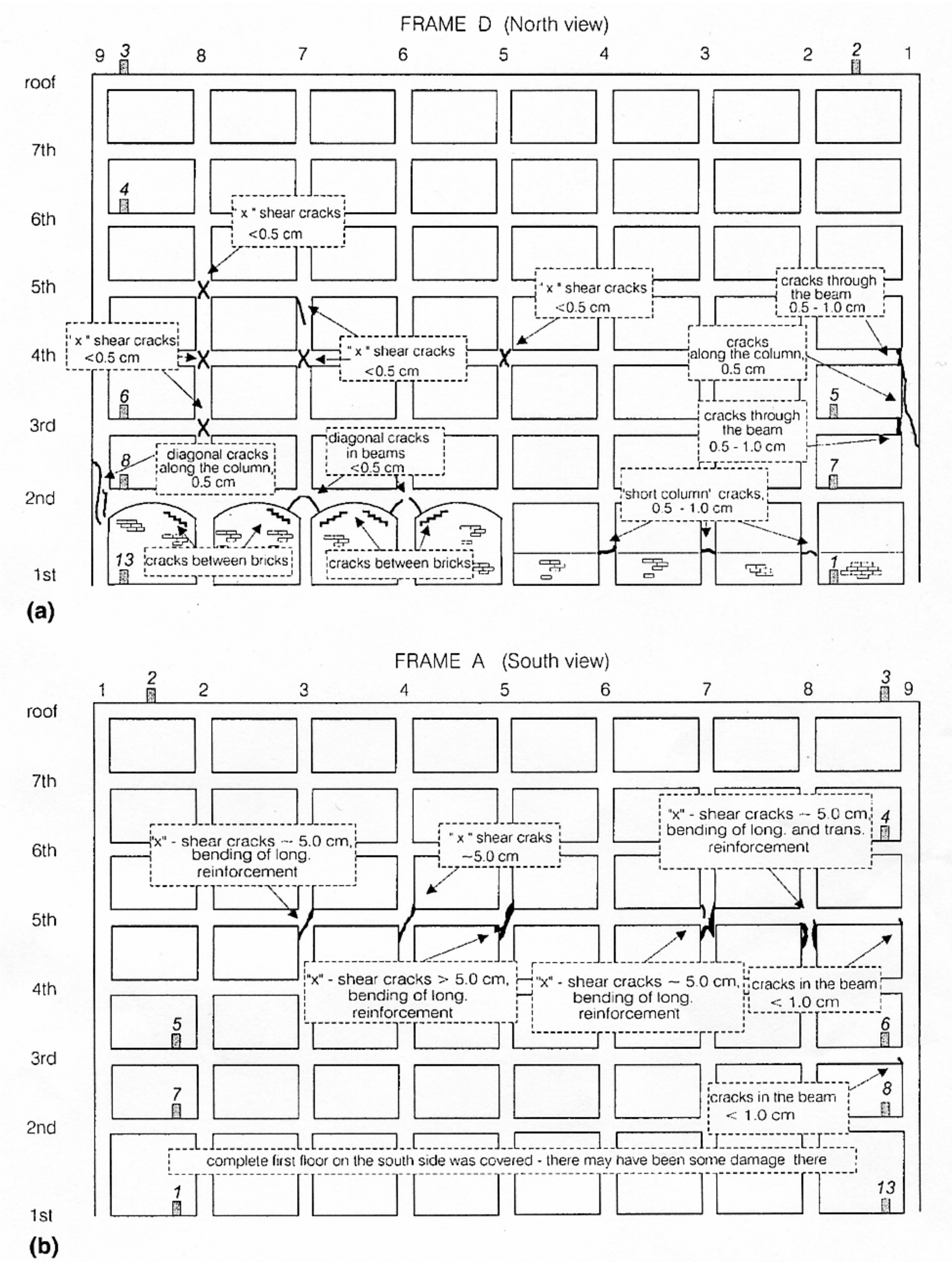

Figure 2.3.2: The primary damage to a) the south and b) the north external moment frames (Trifunac et al., 1999).

2.4. Nonlinear Modeling Procedures

This section briefly summarizes the modeling approaches used by Paspuleti within OpenSees to model the case study building. Specifically addressed are the element material properties, element formulations, and section discretization used to simulate the structure. Also discussed are the approaches taken to model the failure mechanisms of the building components.

Notable assumptions applied to the modeling of the case study building include:

- beam-column joints were assumed to be rigid or flexible. Rigid joints were modeled using rigid offsets equal to the joint dimensions. Flexible joints set the rigid offsets to zero so that the beam lengths were defined by the center lines of the columns.
- the soil-structure interaction was assumed to be negligible. The column bases were rigidly fixed to the ground.
- the mass of the building is lumped at the nodes at the beam column intersections.

Concrete Material Properties

Various one-dimensional concrete material models from OpenSees were tested by Paspuleti. The concrete material model ultimately chosen for use was *Concrete01,* which models concrete with zero tensile strength (http://opensees.berkeley.edu). In compression the material model simulates a parabolic stress-strain response to the point of maximum strength. Strength deteriorates linearly with strain beyond this point to a residual strength and then maintains this residual strength. Concrete is assumed to respond plastically in compression, with an elastic modulus (used for unloading) equal to the compression stress-strain curve for zero strain.

Initially, the Kent-Park-Scott model (1971) was used to define the confined compressive concrete response curve. This model indicated only marginal increases in compressive strength and ductility due to the wide confinement spacing and the 90° bends in the hoops. Thus all the concrete was assumed to behave as “unconfined” concrete with no increase in strength or ductility due to the limited confinement. Further, the reduction in compressive strength predicted by the model (0.05 • f'_c at $\varepsilon = 0.004$) resulted in substantial model strength deterioration in the post yield regime. Consequently, the reduction in strength was modified to a more modest 80% of f'_c. The strains are consistent with the results of Mander et al. (1971).

Steel Material Properties

Paspuleti implemented the *Steel02* model in defining the one-dimensional stress-strain response of the reinforcement steel. *Steel02* uses a simple bilinear envelope for the steel loading and a uniaxial Menegotto-Pinto model to capture the more complex unloading behavior (http://opensees.berkeley.edu). Two strengths of steel were modeled using *Steel02*. The beam and slab longitudinal steel was modeled with a yield strength, fy, of 50 ksi, and the column longitudinal reinforcement was modeled with an fy of 75 ksi (Paspuleti 2002).

Beam-Column Element Formulation

Several beam-column element formulations are available in the OpenSees environment. These were evaluated for accuracy and robustness by Paspuleti, and a lumped-plasticity model was implemented. The specific formulation used is denoted *beamWithHinges2* in OpenSees. This formulation places fiber sections at the end of the hinge instead of the middle which is expected to provide more accurate results. Scott (2001) provides a complete discussion of the model. The length of the element between the plastic "hinge" regions of the formulation are modeled as linear elastic where the modulus of elasticity is taken from the concrete and the effective element moment of inertia is taken as a percentage of the gross section moment of inertia. The percentage of gross section moment of inertia was manipulated to achieve the fundamental period of 1.5 seconds for the building measured at the beginning of the Northridge earthquake (Islam, 1996).

The length of the plastic "hinge" regions of the beam-column elements, L_h, significantly impacts predicted element response. The hinge lengths used were previously varied. They were defined as either the depth of the beam-column element, h

or as $0.5h$. While more involved models were available this was taken as an acceptable approximation (Park et al. 1982).

Section Definition and Discretization

A fiber discretization of the beam-column elements was considered beneficial for this model given that the formulation is defined using only the well known geometry of the gross concrete section, the documented reinforcement size and pattern, and the experimentally well-defined, one-dimensional steel and concrete material models. The *beamWithHinges2* element requires that fiber cross-sections be defined for the quadrature points in each hinge. The cross-sections for the desired beam, slab or column are built from the concrete and steel materials discussed above. The sections are discretized using a maximum mesh size of 0.5 inches in the direction perpendicular to the axis of bending which gives accurate section response with reasonable computational demand.

Modeling of Failure Mechanisms

A review of the design detailing for the case study building leads to the inadequacies indicated in Section 2.2. Given the noted inadequacies in the column transverse and longitudinal detailing and the lack of beam-column joint transverse detailing, shear failure in the columns and joint regions and splice failure in the columns would be expected to occur. From the damage evaluations of the case study building completed by Trifunac and Hao (2001) after the 1994 Northridge earthquake, it is apparent that these failure mechanisms did occur.

The Paspuleti model specifically models the failure mechanisms of the columns. It particularly models the shear and splice failures that may occur as discussed below. However, no joint failure mechanisms were implemented by Paspuleti or any past researchers (e.g. Islam,1996, Li and Jirsa 1998, Browning et al. 2000, De la Llera et al. 2002, Barin and Pincheira 2002). In all cases, the beam-column joints were assumed to be rigid in both flexure and shear.

Shear Failure Model

Paspueleti investigated different models for the simulation of the column shear failure mechanism. The models, identified as ACI, UCSD, and FEMA, were characterized by maximum shear strengths based on the gross cross-sections defined for each column element. For a shear critical column, the shear failure model allows the column response to be controlled by flexure until the shear demand exceeds the shear capacity. The brittle shear failure results in essentially no lateral stiffness, but the column maintains its axial load carrying capacity. The three shear failure models, ACI, UCSD, and FEMA, were defined using the recommendations of ACI 318-02, Kowalsky and Priestley (2000) and FEMA 356 respectively. Paspuleti ultimately chose the UCSD approach to model the column shear based on the analyses they completed. However, according to the work of Cammarillo (2003), the ACI model is the most desirable for modeling column shear and is the preferred choice in this study.

There are a few points of the shear models implemented by Paspuleti that differ from the originally proposed models. Details of the model implementations and how they differ from the originals are discussed below.

1. The FEMA356 model implements the recommendations of FEMA 356 except that the full strength of the transverse steel is used. FEMA 356 recommends using half the strength if the ties are spaced greater than 50% of the section depth. Also, FEMA356 recommends limited ductility capacity after the shear capacity is reached. Paspuleti defines the shear failure as brittle with essentially no ductility. The FEMA356 model is the most conservative with shear strengths ranging from 28% to 115% of the maximum shear demand assuming that the column develops nominal flexural strength at both ends.
2. The UCSD model implements the recommendations of Kowalsky and Priestley (2000). The one exception to this is that the model uses a minimum concrete shear strength factor corresponding to a large ductility demand to define the concrete contribution to the shear capacity. Kowalsky and Priestley model the concrete contribution to the shear capacity s a function of ductility demand, but at the time the

model was developed, it was not possible to define shear strength be a function of ductility demand within OpenSees. Contributions to the shear capacity also come from the transverse steel, and the axial load on the member. The UCSD model is moderately conservative with shear strengths ranging from 55% to 194% of the maximum demand. The equations used by Paspuleti to calculate the shear strength for the UCSD model are as follows

$$V_n = V_c + V_s + V_p$$ **Equation 2.4.1**

where,

$$V_c = \alpha\beta\gamma\sqrt{f_c^{'}}(0.8A_g)$$ **Equation 2.4.2**

$$V_p = P(\frac{D-C}{2L})$$ **Equation 2.4.3**

$$V_s = A_v f_y \left(\frac{D'}{s}\right)\cot\theta$$ **Equation 2.4.4**

Here, V_p represents the strength attributed to the axial load, P is the axial load, D is the column width and D' is the confined core diameter. θ represents the assumed angle of inclination between the shear cracks and the vertical column axis and is assumed to be 30 degrees. The γ factor is a measure of the allowable shear stress and is a function of curvature ductility. The α accounts for the column aspect ratio and is given by the equation $1 \le \alpha = 3 - \frac{M}{VD} \le 1.5$. The factor β is a modifier that accounts for the longitudinal steel ratio, and is given by the equation

$$\beta = 0.5 + 20\rho_l \le 1$$ **Equation 2.4.5**

where, ρ_l is the longitudinal steel ratio.

3. The ACI model implements the recommendations of ACI 318-02 except that the concrete is assumed to contribute to shear strength in the plastic-hinge region (ACI 318-02 recommends that the concrete contribution to shear capacity be ignored for members that will experience flexural yielding). The ACI model is least conservative of all the models with shear strengths ranging from 96% to 254% of the maximum

demand. The equations used to calculate the shear strength capacity for the ACI model are as below.

$$V_n = V_c + V_s \qquad \textbf{Equation 2.4.6}$$

where,

$$V_s = \frac{A_v f_y d}{s} \qquad \textbf{Equation 2.4.7}$$

and,

$$V_c = 2\left[1 + \frac{N_u}{2000 A_g}\right]\sqrt{f_c^{'}}\, b_w d \qquad \textbf{Equation 2.4.8}$$

where, V_s is the strength provided in terms of the area A_v, yield strength f_y, spacing s of the shear reinforcement and d is the effective depth. N_u is the factored axial load and b_w is the width of the section.

Splice Failure Model

Splice failure of the columns was simulated through the modification of the one-dimensional stress-strain curve of the longitudinal reinforcing steel located in the fiber cross-section nearest the splice location. A reduction in yield strength and a negative post-yield stiffness per the recommendations of FEMA 356 and ACI 318-02 are the modifications that are included. The reduction in strength is found using

$$f_{y,splice} = f_{y,actual} * \left(\frac{l_b}{l_d}\right) \qquad \textbf{Equation 2.4.9}$$

where, l_b is the provided lap-splice length ($24d_b$ for interior columns and $36d_b$ for exterior columns) and l_d is the design lap-splice length calculated using

$$l_d = \left[\frac{3}{40}\frac{f_y}{\sqrt{f_c^{'}}}\frac{1}{\left(\dfrac{c + K_{tr}}{d_b}\right)}\right] d_b \qquad \textbf{Equation 2.4.10}$$

In Equation 2.4.10, c is the smaller of (1) the distance from the center of bar being developed to the nearest concrete surface, and of (2) one-half the center-to-center spacing of bars being developed. Also, the term $\left(\frac{c+K_{tr}}{d_b}\right)$ cannot exceed 2.5, and

$$K_{tr} = \frac{A_{tr} f_{yt}}{1500sn} \qquad \textbf{Equation 2.4.11}$$

where, A_{tr} is the area of the transverse reinforcement in plane of splitting. f_{yt} is the yield strength of longitudinal reinforcement, s is the spacing of transverse reinforcement (within l_d) and n is the number of bars being developed.

Lateral Load Pattern

Various lateral load patterns were implemented by Paspuleti, but the one of interest here is based on recommendations by the FEMA 356. In this pattern the normalized story load is a function of the floor height, h, and the fundamental period of the structure, 1.5 sec. The load pattern suggested by FEMA 356 applies increased lateral forces to the upper levels of the building. This distribution is intended to capture the higher mode effects in the seismic response and is defined by the following exponential equation.

$$F_x = C_{vx} V \qquad \text{and} \qquad C_{vx} = \frac{w_x h_x^{\ k}}{\sum_{i=1}^{n} w_i h_i^{\ k}} \qquad \textbf{Equation 2.4.12}$$

Here, C_{vx} is the vertical distribution factor, V is the total base shear, w_i and w_x are the weight at level i or x, h_i or h_x are the height in feet or meters from the base to level i or x, and k is an exponent related to the structure period ($k = 1.0$ for $T \leq 0.5$, $k = 2.0$ for $T \geq 2.5$, linear interpolation for intermediate values of T). If k is equal to 1.0, the resulting distribution is triangular, and if k is 2.0 the distribution is parabolic. For the case study building, the T is 1.5 and k is interpolated as 1.5.

2.5. Nonlinear Modeling Results

The results of the older, reinforced concrete case study building evaluate the accuracy with which the nonlinear modeling procedures predict the building response and failure mode for earthquake loading. The impact of modeling parameters and assumptions on the calculated response was also explored. The results are presented below in three sections: pushover analysis, dynamic analysis, and parameter study.

Pushover Analysis

From the pushover analyses results, the variation in model parameters were shown to have little impact (6%) on base shear demand and significant impact (19%) on the displacement at which failure occurs. Furthermore, the pushover analysis results indicated that this analysis method may be used to predict the mechanism that determines earthquake response of a non-ductile reinforced concrete frame. Observed shear damage of the 4^{th} and 5^{th} story columns was predicted by a pushover analysis. Finally, the pushover analyses with the baseline model indicate that the predicted failure mechanism is relatively insensitive to the load distribution. A similar failure mechanism was observed for different load distributions (uniform, triangular and FEMA 356).

Dynamic Analysis

The dynamic analyses that use the baseline model predicted a peak displacement with a high level of accuracy. However, dynamic analysis did not accurately predict the displacement history. The predicted time and direction of peak displacement did not correspond with the observed.

The dynamic analyses also predicted that the exterior frame was more severely damaged than the interior frame. Shear failures of the fourth and fifth story columns of the exterior frame which were observed during the Northridge earthquake were predicted. However, the analyses did not predict the observed splice failures in some of the ground story columns.

Parameter Study

The parameter study showed that none of the parameter models had a significant impact on the case study building seismic response during the 1994 Northridge earthquake. Furthermore, the seismic response impact due to parameter variation for the brittle model was found to be more significant than the response impact of the flexure model except in terms of the hinge length. Also, it was determined that for higher intensity earthquakes there was less variation compared to the lower and moderate intensity earthquakes because the building was failing regardless of the modeling assumptions. Finally, at any earthquake hazard level, variability in shear strength had less impact than the variability in earthquake ground motion on the variability of maximum inter-story.

Chapter 3

Previous Joint Behavior Research

3.1. Introduction

The results of experimental testing and observations of older reinforced concrete building damage resulting from recent earthquakes indicate that beam-column joint response may contribute to the response of structural systems. Thus, in order to simulate the seismic behavior of this type of building, the seismic response of the joints must first be understood and accurately modeled. This chapter surveys the previous research on reinforced concrete joint behavior and highlights those studies used to develop, calibrate and evaluate joint models necessary for simulating the seismic response of older reinforced concrete buildings.

Numerous analytical and experimental investigations have been completed by previous researchers regarding the inelastic response of reinforced concrete joints. The previous experimental research provides an understanding of the design parameters that determine the seismic joint response of older, pre-1967 beam-column joints, as well as data used in evaluating and calibrating proposed inelastic joint models. Specifically provided is a detailed discussion of a series of cruciform tests conducted at the University of Washington (UW) by Lehman, Stanton, Walker (2001), and Alire (2002). The analytical investigations have provided the current study numerical beam-column joint models for use in the analysis of reinforced concrete frames. Focus is brought onto three potential models, two developed at UW and Stanford (Altoontash and Deierlein 2003, Lowes et al. 2004) and the rotational spring model. These joint models are used to simulate the response of a selection of the cruciforms tested at UW. The results of these analyses are used as a basis for modeling the beam-column joints in the case study building.

3.2. The Earthquake Response of Beam-Column Joints

Numerous experimental studies have investigated the earthquake response of reinforced concrete beam-column joints. The results of these tests provide an understanding of the design and load parameters that determine earthquake response of joints. The following sections identify the important parameters of seismic response for all reinforced concrete joints primarily with detailing typical of modern construction, as well as only those joints representative of older construction.

Design Parameters that Determine Joint Response

Previous research has led to the determination of some primary parameters regarding the inelastic response of reinforced concrete joints. Variations of the design and load parameters within and between previous investigations have lead to some understanding of seismic damage patterns and progression. Four design parameters and one load parameter are discussed below along with their proposed response impact. Concrete strength and displacement history are also important parameters, but they are not discussed here.

- *Nominal Joint Shear Stress Demand:* The results of multiple studies indicate that joint performance, as defined by the extent of damage and/or the drift level at which strength loss initiates, deteriorates with joint shear stress demand (Walker 2001, Durrani and Wight 1982, Meinheit and Jirsa 1977) equal to

  $$v_j = V_j / A_j \qquad \textbf{Equation 3.2.1}$$

  Where V_j is the joint shear force and A_j is the joint area.
- *Transverse Steel Ratio:* The results of multiple studies suggest that increasing the volume of joint transverse reinforcement reduces joint damage and delays the onset of joint failure (Durrani and Wight 1982).
- *Bond Index:* For joints with continuous beam reinforcement, the bond index is the average bond stress demand along the beam reinforcing steel, assuming that the steel yields in compression and tension on opposite sides of the joint. The results of multiple studies indicate that increased bond stress demand results in increased

damage and reduced drift capacity (Alire 2002, Leon 1990, Park and Ruitong 1988).

- *Column Axial Load:* For much of the previous experimental data, axial load of the specimens was applied at the top of the column and maintained at a constant level throughout the test. Bonnaci and Pantazopoulou (1993) assembled data from 86 joint tests and conclude that column axial load has no discernable affect on joint strength. Mosier (2000) reaches a similar conclusion using a database of 29 test programs and considering data only from joints that sustained joint damge in shear. However, the impact of column axial load on joint performance is not well documented in the literature. Bonnaci and Pantazopoulou (1993) hypothesize that axial load affects joint deformation but note that insufficient data are available to test this hypothesis. Kitiyama et al. (1987) conclude, on the basis of data from numerous joint tests conducted in Japan, that higher axial load deteriorates the joint strut mechanism more rapidly. Given the limited impact of column axial load on joint strength and the limited data characterizing the impact of axial load on joint performance, it is unclear how significant large variations in column axial load are toward the observed damage patterns.
- *Column Splice:* Some of the past research consists of specimens which have column longitudinal steel that is spliced above the joint. For these joints, splice lengths and confining reinforcement are considered inadequate by today's standards. The results of these studies indicate that inadequately designed splices may affect sub-assemblage strength and drift capacity thus impacting whether joint damage will progress under simulated earthquake loading.

Design Parameters Characteristic of pre-1967 Joints

The vast majority of the tests identified above included specimens representative of "modern" construction; relatively few experimental investigations have considered the earthquake response of older beam-column joints, with design details typical of pre-1967 design and construction. Prior to 1967 the UBC did not specifically address the design of joints; similarly, the ACI code did not until 1971. Modern design methods were adopted in 1980s for the UBC and ACI codes, and both have been modified to reflect current design methods.

Mosier (2000) review drawings for 15 building designed for construction on the west coast prior to 1979 to determine representative design and load details for beam-column joints designed in this period. Table 3.2.1 shows the results of this review for critical design parameters as well as the range of values of these parameters for the test case building. From Table 3.2.1, one can conclude that the beam-column joints in the Van Nuys building are typical of pre 1967 construction do to the lack of transverse reinforcement and high joint shear stress demand.

Table 3.2.1: Critical design parameters from Mosier (2000) study and the case study building.

	Volumetric Transverse Steel Ratio (%)			**Shear Stress Demand / *f'c***			**Beam Bar Bond Index** $\beta = \frac{d_b}{h_c}\frac{f_y}{2\sqrt{f_c^{'}}}$ **Equation 3.2.2**		
Design Year	Ave.	Min.	Max.	Ave.	Min.	Max.	Ave.	Min.	Max.
Pre-1967	0.0	0.0	0.2	0.21	0.09	0.30	21	12	38
1967-1979	0.9	0.0	2.1	0.15	0.06	0.29	23	14	43
Van Nuys Building	0.0	0.0	0.0	0.33	0.23	0.45	23	19	29

On the basis of the conclusions identified above, one could expect that older beam-column joints would exhibit non-ductile damage due to earthquake loads that overload the unconfined joint core.

3.3. Experimental Data for Older Joints: the UW Test Series

Of the studies in Section 3.2 that consider older joints, the series of 11 beam-column joint sub-assemblages tested at the University of Washington by Stanton, Lehman, Walker (2001), and Alire (2002) represent a unique dataset that is of particular interest to the current study. This series of tests evaluates the earthquake response of 2/3 scale interior beam-column joint sub-assemblages from planar frames with shear stress demand levels, anchorage stress demand levels and material properties that span the ranges observed by Mosier (2000). Details of these 11 joints are given below.

Beam-Column Joint Design Details and Load Parameters

The joints in the UW test series were designed with reinforcement detailing and load levels representative of pre-1967 construction. Figure 3.3.1 shows a typical joint sub-assemblage. The same geometry was used for all the specimens, but the reinforcement was varied such that $\sum M_c / \sum M_b$ was about equal to 1.2 and the bond demand is relatively constant. Table 3.3.1 shows the range of critical parameters for the joints included in the UW study. These parameters fall within the ranges observed by Mosier (2000) in pre-1967 design and encompass the range of values observed in the Van Nuys building. Thus, the data from these tests are appropriate for evaluating the the proposed models for simulating the earthquake response of the Van Nuys building.

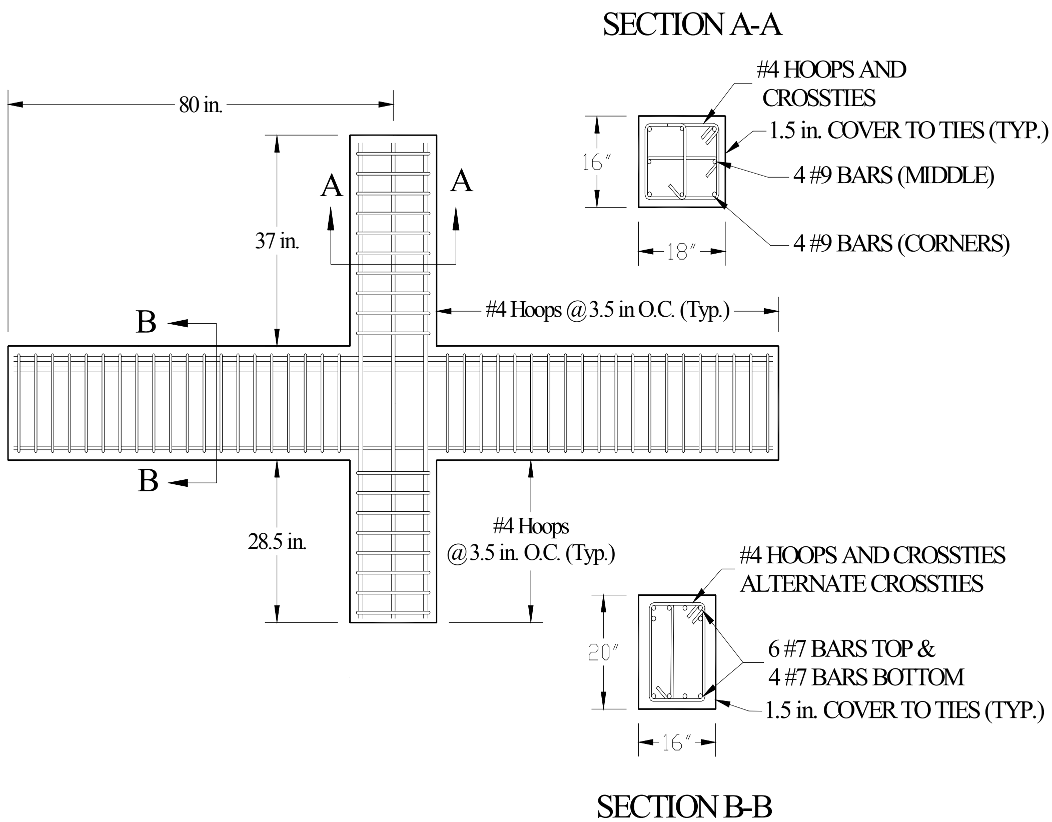

Figure 3.3.1: Geometry and reinforcement for PEER 2250 (Walker 2001).

Table 3.3.1: UW joint test matrix (Alire 2002)

Specimen Name	f'_{ct} (psi)	$v_{jt}/\sqrt{f'_{ct}}$	v_{jt}/f'_{ct}	Bond Index (top)	Bond Index (bot.)	$P/(A_g f'_{ct})$
PEER-1450	5,000	9.10	0.14	23.00	16.45	0.10
PEER-2250	5,000	14.80	0.22	23.00	23.00	0.10
CD15-1450	5,000	9.10	0.14	23.00	16.45	0.10
CD30-1450	5,000	9.10	0.14	23.00	16.45	0.10
CD30-2250	5,000	14.80	0.22	23.00	23.00	0.10
PADH-1450	5,000	9.10	0.14	23.00	16.45	0.10
PADH-2250	5,000	14.80	0.22	23.00	23.00	0.10
PEER-0850	5,000	5.70	0.08d	23.00	23.00	0.10
PEER-0995	9,500	8.50	0.09	16.68	16.68	0.10
PEER-1595	9,500	14.40	0.15	14.32	14.32	0.10
PEER-4150	5,000	29.30	0.41	29.61	29.61	0.10

In addition to design details representative of the joints in the case study building, the UW test data are especially appropriate for use in the current study because the UW test program includes:

- Four different displacement histories. This provides a comprehensive set of displacement histories for use in evaluating the proposed joint models.
- Electronic data sets: The availability of the forces and deformations experienced by the beams, column, joint, and beam longitudinal reinforcement facilitated the accurate calibration of the one dimensional joint material models as presented in Section 4.3.
- Different failure modes: The cruciforms tested by Walker (2001) and Alire (2002) have varying failure modes; the joint core can fail in shear, the beams can fail in flexure, or the longitudinal bars can lose bond strength through the joint. The ability of the joint formulations to model the different joint failure modes is significant in the model evaluation.

From the 11 possible cruciforms in the UW test program, a subset of five was chosen to span the range of joint shear stress demands as well as displacement history indicated by Mosier (2000) and found in the case study building. Thus, a subset of five test specimens (PEER-0995, PEER-2250, PEER-4150, CD30-2250, PADH-2250) was used to calibrate and evaluate the beam-column joint models.

The three PEER[1]-**** tests span a range of nominal joint shear stress demands and, as a result, exhibit three different joint failure modes. For the PEER-0995 inelastic action is isolated primarily in the beams, with the joint exhibiting relatively little damage. For the PEER-2250 specimen, significant joint damage is observed as well as a reduction in the drift level at which strength loss occurs; however, the joint is sufficiently strong that the beams reach nominal flexural strength. For the PEER-4150 joint specimen, the nominal joint shear stress demand is sufficiently high that the joint exhibits shear failure prior to beam hinging.

The three ****-2250 specimens span a range of displacement histories. The PEER-2250 specimen used the PEER (**P**acific **E**arthquake **E**ngineering **R**esearch) history which is representative of load histories used by past researchers and may be representative of a long-duration seismic event (Alire 2002). The CD30-2250 uses the CD30 (**C**onstant amplitude **D**isplacement to **3.0**% drift) load history which mimics the loading of fairly constant amplitude earthquakes, while in comparison, the PADH (**P**ulse **A**symmetric **D**isplacement **H**istory) is used to simulate near fault loading. The three different load histories allow the model calibrations of the one-dimensional material models to account for the variability and impact of load history on seismic joint response.

Walker (2001) and Alire (2002) present a significant amount of data for each of the specimens tested. For the current study, in which the response data are used to calibrate and evaluate a series of proposal joint model, three specific response characteristics are important: the observed failure mode of the specimen, the column shear-drift response, and the joint response. The observed failure mode may be compared with the simulated failure model to validate the model. The ideal model will

[1] The specimen name scheme developed by Alire (2002) starts with a four-letter tag that identifies the loading protocol used, here the tag **PEER** refers to a displacement history consisting of three cycles each to increasing maximum drift demands. This is followed by two numbers that identify the design joint shear stress demand as a fraction of f'c, for example the PEER-4150 specimen had a design joint shear stress demand of 0.**41**fc. The final two numbers of the specimen name identify the concrete compressive strength; for the specimens used in this study the concrete compressive strengths were **50**00 psi and **95**00 psi.

represent the observed column shear versus drift history, including initial stiffness, yield and maximum strength, unloading stiffness, and drift capacity.

3.4. Models for Prediction of Joint Response

The previous research discussed in Sections 3.2 and 3.3 indicate that the seismic response of reinforced concrete beam-column joints is complex. A number of design parameters affect the strength, stiffness and drift capacity of the joint, and ultimately determine the damage experienced by the joint, either overloading of the joint core concrete in shear and/or overloading of beam-bar anchorage. Simulation of this complex behavior requires a beam-column joint model that accurately predicts the strength, stiffness and drift capacity and consequently the damage of the joint. Thus, the ideal joint model must be complex enough to support the simulation of multiple response mechanisms, yet simple enough to ensure computationally efficient. Also, the calibration procedures for the constitutive models that define the joint response must be sufficiently objective and transparent.

Previously proposed approaches to joint modeling range in sophistication from a zero-length rotational spring element (e.g., El-Metwally and Chen 1988) to high-resolution continuum modeling of the joint region (e.g., Elmorsi et al. 1998). These previously proposed models also vary in their ease of implementation and calibration, computational efficiency, modeling robustness, and the ability to predict observed joint seismic response. In the following paragraphs, previously proposed beam-column joint models are reviewed with the objective of identifying one or two preferred models for use in simulating the response of the case study building.

Simple Joint Response Models

Many models proposed previously for simulating seismic joint response are relatively simple and robust, and therefore appropriate for use in the full-frame seismic simulation of the case study building. These simple joint models typically required that the user make a number of assumptions about the joint response or have access to experimental data for use in model calibration. Examples of these simple models include:

- Modification of the plastic hinge model in the beam-column elements to account for inelastic deformation associated with joint deformation as well as flexural hinging of the beam-column (e.g., Otani 1974, Anderson and Townsend 1977).
- A zero-area rotational spring placed between the beams and columns (e.g., El-Metwally & Chen 1988).
- A zero-area rotational spring with rigid zones defining the joint area (e.g., Alath & Kunnath 1995, Deng et al. 2000).
- Two zero-area rotational springs placed between a beam and column line with one spring calibrated to simulate inelastic response associated with failure of the joint core under shear loading and one spring calibrated to simulate inelastic action associated with anchorage failure of beam or column reinforcing steel bond-slip (Biddah and Ghobarah 1999).
- Finite-area super-elements with multiple zero-area rotational springs (Altoontash and Deierlein 2003, Lowes et al. 2004).

Otani (1974) and Anderson and Townsend (1977) represent some of the earliest work regarding the introduction of discrete inelastic beam-column joint action into the behavior of reinforced concrete frames. They calibrated plastic-hinges within the beam-column elements to represent the joint behavior as well as the inelastic flexural response of the frame members. Despite being computationally efficient, this lumped modeling approach does not directly model the joint, much less the joint response mechanisms, making calibration of the rotational springs difficult.

The next generation in joint modeling approaches (El-Metwally & Chen 1988, Alath & Kunnath 1995, and Deng et al. 2000) addressed the modeling and calibration limitations of the previous work by separating the joint behavior from that of the beams and columns. Alath and Kunnath (1995) and Deng et al. (2000) attempted to more accurately model the kinematics of the joint region by including rigid zones that define the joint area in the plane of the frame and take into account the flexural rigidity of the joint. The calibration of the joint element behavior is typically carried out empirically using joint moment-rotation data from cruciform sub-assemblage tests. This modeling approach proves to be accurate and computationally efficient, as well as somewhat less opaque than the earlier approach. However, it also fails to distinguish between the responses of the joint mechanisms, and it does not completely satisfy the joint kinematics.

Biddah & Ghobarah (1999) attempted to address the limitations of the lumped rotational spring model by implemented two rotational springs to separately model joint shear and bond-slip. The joint shear spring was calibrated using the softened truss theory (Hsu 1988) and a hysteretic model was implemented for the bond spring. While this approach has the ability to model separate joint response mechanisms, the benefits of this approach in comparison to the single rotational spring model are outweighed by the involved calibration procedures required.

Altoontash and Deierlein (2003) and Lowes et al. (2004) have used the previously proposed simple joint models as a basis for the development of beam-column joint models for the OpenSees platform. Lowes et al. (2004) developed a model for seismic joint response that attempts to balance the accuracy and objectivity of more complex joint models with the computational efficiency and robustness of the previously proposed, simple joint models. They developed a two-dimensional, finite area super-element that requires relatively few user assumptions and allows for relatively good computational efficiency while explicitly accounting for the joint response mechanisms. The element is composed of thirteen components, one shear-panel, eight bar-slip, and four interface-shear components, all of which require separate one-dimensional load-deformation response histories. One-dimensional constitutive models have been developed in conjunction with the joint formulation to assist in the calibration of the various rotational springs.

Altoontash and Deierlein (2003) developed their closely related versatile model for beam-column joints. This model is also relatively computational efficient and robust with adequate accuracy and modeling objectivity. The modeling approach varies by explicitly simulating five components of joint response, one shear panel component and four components for the rotations at the joint interfaces.

Complex Joint Response Models

Some past researchers have simulated the complex, reinforced-concrete joint response using continuum-type elements and fine discretization of the joint region. Planar continuum elements were implemented to model the internal joint structure, standard line elements were used to define the frame elements outside of the joint, and transition zones were used to ensure compatibility between the two element types. Examples of these complex joint response models include:

- Elmorsi et al. (1998)
- Ziyaeifar & Noguchi (2000)
- Fleury et al. (2000)

Elmorsi et al. (1998) simulated joint response using a variety of elements. They modeled the concrete core of the joint using inelastic plane stress elements, the reinforcement steel with truss elements, and bond regions with discrete bond-link elements. Quadrilateral transition elements were implemented to model the plastic hinge regions of the beams and columns.

Ziyaeifar & Noguchi (2000) simulated joint response using transition beam-column elements with higher order shape functions connected to a joint element. The transitional elements were capable of modeling shear distortion in the vicinity of the joint. This approach modeled both material and geometric nonlinearities.

Fleury et al. (2000) implemented various elements to simulate joint response. They modeled the concrete core of the joint and the smeared effect of the transverse reinforcement using plane stress elements, the beam steel using a mesh of quadrilateral elements, the column steel using truss elements, and the connections of the beams, columns and joints using transition elements.

These more complex joint response models, while more accurately representing the joint response than the simple models, have limited practical applications. The complex models require a significant increase in computational effort that is impractical for full frame analyses, and the robustness of these complex approaches is questionable for a wide range of joint designs and model parameters. Thus, while past studies have shown this high resolution approach to have significant potential, they are not appropriate for the current research.

3.5. Selection of Joint Response Models

Of the previously proposed reinforced-concrete beam-column joint seismic models, the following three are considered for use in the current study: the two finite area super-elements with multiple zero-area rotational springs (Altoontash and Deierlein 2003, Lowes et al. 2004) and the zero-area rotational spring with rigid zones defining the joint area (Alath and Kunnath 1995). These formulations were primarily chosen because 1) they were implemented in OpenSees at the time this project started, 2) data were available indicating that these models could be expected to exhibit acceptably robust behavior under cyclic loading and 3) the research team had immediate access to individuals experienced with the models. The three models and explanations of their desirability are:

- **Lowes et al. 2004**, multi-spring super element (denoted *UW*)
    - Relatively computationally efficient
    - Explicit modeling of the three primary joint response mechanisms using 13 independent one-dimensional bar-slip, interface-shear, and shear-panel response components
    - Any material model may be used to simulate the response of the 13 components, thus joint damage may be defined as a function of deformation history, number of load cycles, energy dissipation or any combination of these
- **Altoontash and Deierlein 2003**, multi-spring super element (denoted *ST*)
    - Relatively computationally efficient
    - Explicit modeling of the three primary joint response mechanisms using five independent one-dimensional joint-interface-rotation and shear-panel response components
    - Accurate simulation of large or small displacements and large joint deformations

    - Any material model may be used to simulate the response of the five components, thus joint damage may be defined to be a function of deformation history, number of load cycles, energy dissipation or any combination of these
- **R**otational **S**pring model with area defined using rigid offsets (denoted *RS*)
    - Particularly high computational efficiency
    - Relatively accurate simulation of joint kinematics
    - Ease of calibration using experimental joint moment-rotation histories
    - Practical and immediately implemental in current SA software.

The advantageous characteristics of the three joint formulations make them desirable joint response simulation approaches for full frame analyses in OpenSees. Detailed discussion of the three joint formulations follows below.

UW Joint Element

The *UW* model was developed at the University of Washington for use in simulating the response of two-dimensional reinforced concrete frames using OpenSees, the earthquake engineering finite-element analysis software framework discussed in Section 1.4.1 (http://opensees.berkeley.edu); the model is identified as the *beamColumnJoint* element within OpenSees. The *UW* model is a 4-node, 12-degree of freedom, finite-area joint element that is appropriate for use in two-dimensional modeling of reinforced concrete frames. To introduce the element into a building sub-assemblage, four nodes are created at the perimeter of the joint. Each node is connected to the joint element and a single beam or column. Thus, in comparison to a sub-assemblage model with no joint model, the *UW* model introduces an additional 9 degrees-of-freedom into the analysis.

The *UW* model enables independent simulation of the three mechanisms that may determine joint behavior under seismic loading: the shear-panel deformation, bar-slip of the longitudinal reinforcement and interface-shear cracks as shown in Figure 3.5.2. The shear-panel component, which has a finite volume, is assumed to resist loading only in shear, and is calibrated to simulate the shear load versus shear deformation response of the joint core. The eight bar-slip components are intended to simulate the inelastic response of the joint due to slip of the longitudinal reinforcement of the beams or columns that is embedded in the joint. Calibration approaches of the bar-slip and shear-panel "springs" are discussed in Section 3.5. The interface-shear components are included to simulate the loss of shear-transfer capacity due to large permanent cracks that open at the beam-column interface under severe loading. Due to limited data with which to calibrate the shear-transfer springs, they have been consistently defined as elastic and stiff.

The UW model can be simplified to a one-dimensional model similar to the RS model by defining the bar-slip and interface shear components to have stiff elastic response and calibrating the joint shear-panel spring to represent the moment-rotation response of the entire joint. The shear stress carried by the panel component, v_j, can be defined as the ratio of the joint shear force, V_j, over the joint area, A_j, as shown in Equation 3.5.1. The joint shear force is defined by Equation 3.5.2 using the mechanics in Figure 3.5.1(a-d), and A_j is calculated at the horizontal plane at which V_j is located in Figure 3.5.1(d). The shear stress may be converted to a joint moment, M_j, which is related to the moment carried by the RS model, by multiplying by the joint volume, $\mathrm{Vol_j}$, which is equal to the beam depth times the beam height times the column width, as shown in Equation 3.5.3.

$$v_j = \frac{V_j}{A_j}$$ **Equation 3.5.1**

$$V_j = C_R + T_L - V_c$$ **Equation 3.5.2**

$$M_j = v_j / Vol_j$$ **Equation 3.5.3**

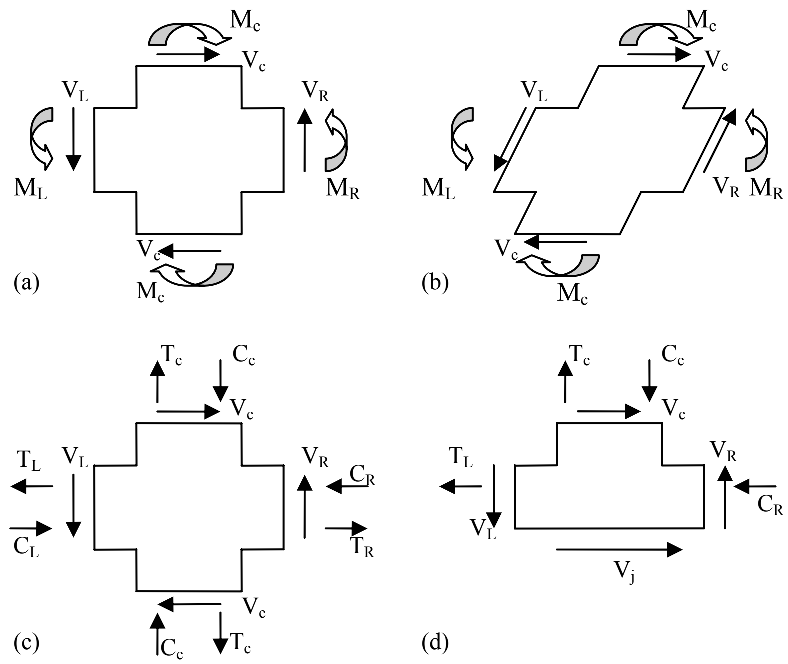

Figure 3.5.1: (a) Joint free-body diagram, (b) Deformed joint free-body diagram, (c) free-body diagram with moment shown as equivalent force couples, (d) free-body diagram of half the joint.

If the UW model is used in this way so that the shear panel represents the total joint behavior, empirical data such as that provided by Walker (2001) and Alire (2002) may be used to calibrate the panel. Otherwise, calibration of the various springs requires more complex calibration discussed in Section 3.6.

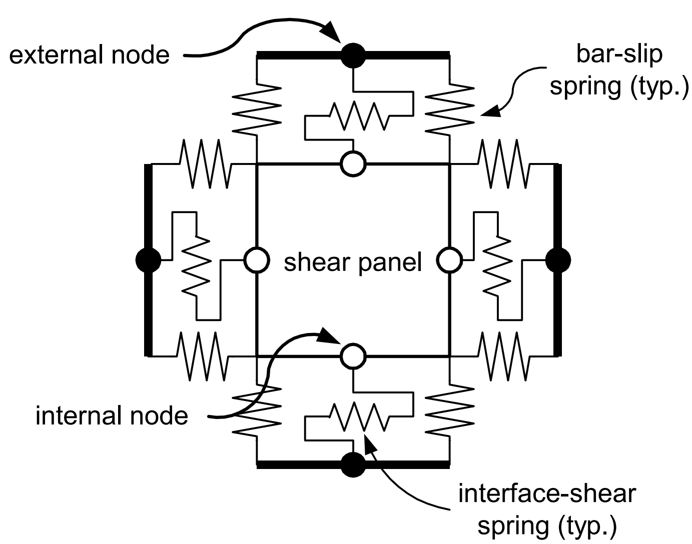

Figure 3.5.2: UW (beamColumnJoint) joint formulation (Lowes et al. 2004)

ST Joint Element

The *ST* model was developed at Stanford University (Altoontash and Deierlein 2003) also for use in OpenSees (http://opensees.berkeley.edu), in which it is denoted as the *Joint2D* element in OpenSees. The model defines joint response on the basis of a single shear-panel component, which is intended to simulate the inelastic response of the joint core concrete under shear loading, and four rotational spring components, which are intended to simulate the stiffness and strength loss resulting from slip of the beam and column reinforcement anchored in the joint. The ST model uses slaving of the degrees of freedom to enforce the constraints of no axial joint deformation. Figure 3.5.3 shows an idealization of the element.

To introduce the *ST* joint element into a building sub-assemblage, four nodes are created at the middle of each side of the joint and one node is created at the center of the joint. Each perimeter node is connected to the joint element and a single beam or column. The center node adds four degrees of freedom, three for the rigid body motion of the joint and one for the shear deformation, and connects the central node to the four external nodes using multi-point constraints. The nodal degrees of freedom are slaved to enforce the constraint of no axial deformation of the joint. The resulting element requires that global equilibrium equations be modified to enforce the slaving, and it introduces 13 additional degrees of freedom into the global problem beyond that required for a sub-assemblage model with no joint element.

The *ST* formulation also has the advantage of including modifications to enable simulation of large joint deformations and large displacements of the global system. The formulation has the default setting of a constant multi-point constraint matrix with no correction in the lengths between the constrained nodes. However, the large joint deformation modification allows the constraint matrix to vary with time, i.e. the constraint matrix is updated for every time step and calculations are carried out using the current configuration. The large displacement modification allows for continuous length correction procedure that maintains the length of the multi-point constraints.

Calibration of the model to represent the response of a particular joint with unique material, geometric and design parameters requires definition of the one-dimensional response of the four rotational bar-slip components and the one shear-panel component that make up the model. The rotational, bar-slip springs, can be calibrated using experimental data; however, as discussed previously these data are not readily available. For the current study these springs are assumed elastic and stiff. Thus, the *ST* formulation ends up identical to the simplified *UW* formulation; the central, joint shear-panel "spring" predicts the entire seismic joint response. Approaches to calibrating the shear-panel spring are discussed in Section 3.6.

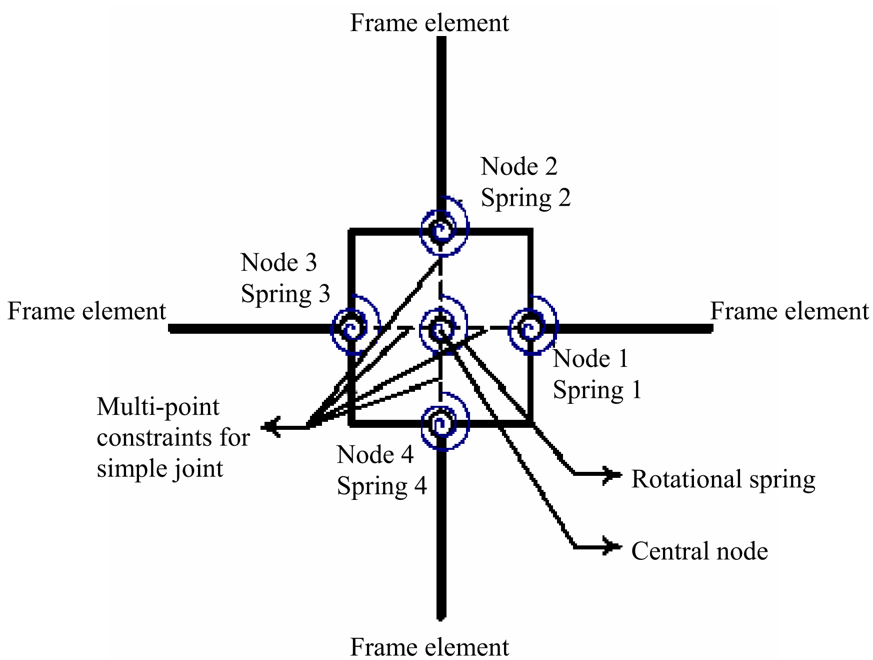

Figure 3.5.3: ST (Joint2D) joint formulation (Altoontash and Deierlein 2003)

RS Joint Element

The *RS* model is the simplest and computationally most efficient joint formulation used in this research. It simulates the behavior of the entire joint using a single zero-length rotational spring with rigid zones defining the joint area as illustrated in Figure 3.5.4 where d_b is the joint height and d_c is the joint width. This element is notable for it is of immediate use to practicing engineer.

To introduce the *RS* joint model into a building sub-assemblage, a duplicate node is added at the center of the joint. Thus, two nodes, each with three degrees-of-freedom for a two-dimensional model, are located at the center of the joint. Two beam elements connect at one of the joint nodes and two column elements are connected at the other. The joint element spans the duplicate nodes. Since the joint is expected to deform only in shear, horizontal degrees of freedom at the duplicate nodes are slaved, so that they have the same value and no horizontal deformation occurs across the joint. This is done also with the vertical degrees of freedom. Only the rotational degrees of freedom remain independent; thus, the one-dimensional constitutive model associated with the rotational spring determines the inelastic deformation of the joint.

The constitutive model used with the joint element defines the relationship between the transferred moment and relative rotation between the beam and column. The joint moment may be transformed into a nominal joint shear stress by dividing by the joint volume; the joint rotational deformation is equivalent to the joint shear deformation. Since a single one-dimensional constitutive model is used, this represents the combined inelasticity due to shear failure of the core and slip of the longitudinal reinforcement. This joint moment-rotation response model is calibrated most easily using empirical data that combine inelastic response due to both joint shear and bar-slip.

Additional rotational springs could be added to enable simulation of the two primary mechanisms that determine response: response of the joint core and bar-slip. This is done by Biddah & Ghobarah (1999). However, this requires having data defining the shear stress-strain response of the joint core as well as data defining the joint moment-deformation response where the joint deformation represents the total joint deformation associated with slip of the beam reinforcement. In practice, such data are not readily available, either from experimental testing or numerical modeling.

Beyond the issue of model calibration, the *RS* model has one main deficiency in comparison to the other finite-area joint models. The *RS* model fails to capture the joint kinematics. Specifically, it does not simulate the horizontal translation that can occur between the centerlines of the columns above and below the joint as shown in Figure 3.5.5. The other models with multiple nodes allow for more complex kinematics.

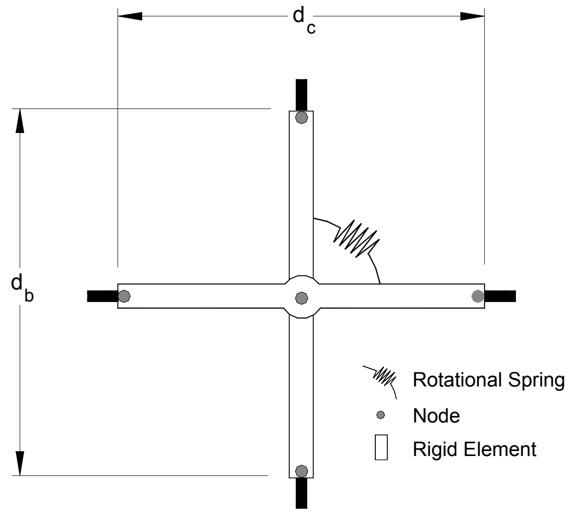

Figure 3.5.4: RS (Rotational Spring) joint formulation

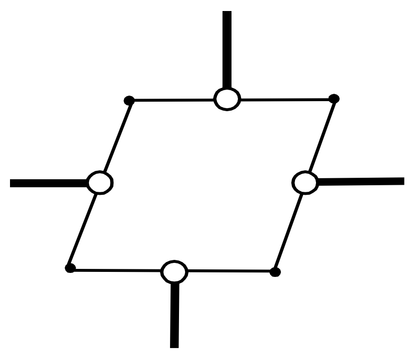

Figure 3.5.5: Joint translation that cannot be modeled by the *RS* model

3.6. One-Dimensional Constitutive Model Details

Each of the two-dimensional beam-column joint element formulations selected for the current research study predicts the seismic joint response using one or more one-dimensional constitutive models to simulate the primary joint response mechanisms. The *UW* element formulation requires the calibration of thirteen load-deformation response models to simulate the inelastic shear stress-strain response of the joint core, the load versus slip response of the longitudinal reinforcement of the beams and columns that is embedded in the joint, and the shear-interface action which simulates the loss of shear-transfer capacity at the joint perimeter. The *ST* element formulation requires the calibration of five response models to simulate the inelastic shear stress-strain response of the joint core and the member-end moment-rotation responses. In contrast, the simple *RS* formulation combines the action of the individual joint response mechanisms together, and thus requires a single moment-rotation response model to predict the inelastic response of the entire joint.

To facilitate the modeling process, a single one-dimensional load-deformation constitutive model (Lowes and Altoontash 2004) was used to define the response of the one-dimensional components that make up the different joint element formulations. This constitutive model, identified as *Pinching4* in OpenSees, is defined by a response envelope, an unload-reload path, and three damage rules that control how the joint response path evolves. The envelope is multi-linear, the unload-reload path is trilinear, and the damage rules control the unloading stiffness degradation, reloading stiffness degradation, and strength degradation as a function of the maximum historic deformation demand and either the hysteretic energy dissipated or number of deformation cycles experienced. Calibration of this general one-dimensional load-deformation response model to predict the response of a joint element component for a joint with specific material, geometric and design parameters is presented in the following sections.

3.6.1. Shear Panel Component Calibration for the *UW* and *ST* Joint Formulations

The shear-panel component of the *UW* and *ST* joint element formulations is intended to simulate the inelastic response of the joint core under shear loading. Calibration of the one-dimensional pinching material model to predict the joint core shear response of a specific joint requires definition of the response envelope, the unload-reload paths, and the damage rules of the *Pinching4* constitutive model. Three different approaches are used to define the envelope of the material response models for joint shear-panels with specific design details: the *MCFT*, the approach proposed by Lowes and Altoontash (2004), a method in which the envelope is defined by the flexural strength of the beams that frame into the joint, and the approach using shear stress-strain data from a joint in the UW test program that exhibited a joint shear failure. The unload-reload and damage rules for the Pinching 4 model were defined using two approaches: that proposed by Lowes and Altoontash (2004) and an empirical approach in which experimental data from the UW test program were used.

Shear-Panel Calibration: Response Envelope

For the current study, definition of the shear-panel envelope was accomplished by identifying the four load-deformation points that one the positive response envelope and assuming that response under positive and negative loading is identical. The three methods used to identify the load-deformation points are discussed in the below.

The Modified Compression Field Theory (*MCFT*) (Vecchio and Collins 1986) and empirical data from the University of Washington PEER-4150 test specimen (Alire 2002) are both used to develop a multi-linear shear stress-strain response envelope for the shear-panel similar to that pictured in Figure 3.6.1. The envelope shown in Figure 3.6.1 must be mirrored about the axes to get the complete 16-parameter, positive and negative envelope. For the empirical data calibration approach, the data are used to determine M_{nj}, the nominal joint moment, while the y-axis points, p_1, p_2, p_3, and p_4, are found as a percentage of M_{nj}, where the percentages are determined by Bennett (2004). The x-axis values are determined in the same study. The MCFT defines the envelope using a plane-stress constitutive model for shear-panels. The slope values, denoted k_1-k_4, are found

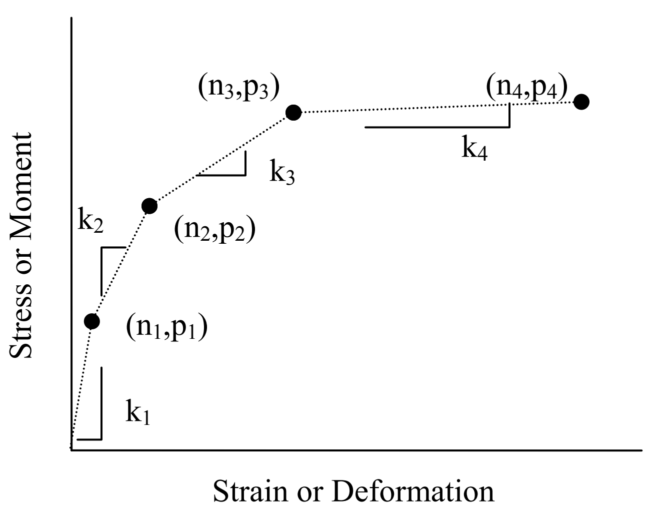

Figure 3.6.1: The general joint response envelope

Table 3.6.1: Positive Envelope Parameters

i	p_i (k-in)	n_i
1	$0.30M_{nj}$	0.0021
2	$0.7076M_{nj}$	0.0091
3	$1.0M_{nj}$	0.0278
4	$1.0M_{nj}$	0.0896

from the other values and are important for the calibration of the rotational spring joint formulation in Section 3.6.3.

MCFT Approach Proposed by Lowes and Altoontash (2004)

Lowes and Altoontash (2004) recommend using the Modified Compression Field Theory developed by Vecchio and Collins (1986) to develop the response envelope for the shear-panel of the *UW* joint model for the case of joints with moderate transverse steel and moderate shear stress demands. This approach was applied for the current study, although the joints do not have transverse reinforcing.

The *MCFT* is appropriate for predicting the response of reinforced concrete panels loaded uniformly in shear or shear in combination with tension or compression. Use of the *MCFT* for the case of monotonic loading requires few assumptions, and behavior is defined entirely on the basis of the concrete material properties, the vertical and horizontal steel ratios within the joint, and the steel reinforcement material properties. The *MCFT* was extended for cyclic loading by Stevens et al. (1991).

Lowes and Altoontash (2004) recommend calibration of the envelope of the joint shear-panel component using the *MCFT* adjusted using data provided by Stevens et al. (1991) to account for the observed reduction in concrete compressive and tensile strength under reversed-cyclic loading.

This approach to calibration of the joint panel is the most appealing from a modeling perspective, but is wholly inadequate for prediction of observed response. From the modeling perspective, this approach requires that the user make only a single assumption that joint core may be assumed to carry a uniform shear stress. From this assumption and know joint material, design and geometric parameters, the joint panel behavior is defined completely by the mechanistic *MCFT* constitutive model. However, as will be discussed in subsequent sections, this method under-predicts observed joint panel strength for all of the UW joint specimens.

Joint Panel Strength Defined by Beam-Moment Demand

The second approach considered for calibration of the joint panel component defined the joint strength using the moment demand on the joint based on the nominal flexural strength of the beams. This approach is denoted *MnB*. It is considered to be appropriate for joints in which 1) shear stress demand is sufficiently low that the joint could be expected to carry the load associated with beams developing flexural strength and 2) insufficient transverse reinforcement is provided to ensure that joints maintain strength under cyclic loading. For joints with theses design parameters, it is appropriate to define joint panel shear strength to be equivalent to the shear strength demand imposed by the beams and to calibrate the constitutive model damage rules such that this strength deteriorates under cyclic loading.

As discussed previously, defining the load-deformation response of the *Pinching4* material model envelope requires definition of four load-deformation points. An empirical approach was used to fill in the remainder of the points on this multi-linear curve. First, envelopes were constructed of the joint moment versus joint shear deformation data from the five sub-assemblage tests from the UW test series in which response was determined by beam yielding and subsequent strength loss due to joint damage. These envelopes were normalized with respect to the maximum joint moment. Then, three points, defining a tri-linear enveloped starting at the origin were computed to minimize the variation between the tri-linear model and the data. These three points, as well as fourth point defined by a normalized moment of 1.0 and a joint shear deformation of 0.0278, as shown in Figure 3.6.1, were used as the basis for defining the envelope for a joint in the test program.

While the *MnB* calibration approach is less desirable from a modeling standpoint than the *MFCT* approach, it is very useful for some of the joints tested by Stanton, Lehman, Walker(2001) and Alire(2002) and those found in the case study building, given its ability to simulation behavior of older under-reinforced joints with low joint shear stress demands. However, this approach is entirely inappropriate for joints that experience high joint shear stress demand. The *MnB* approach is also limited by the uncertainty inherent in the empirical approaches used to determine the modeling parameters for the backbone curve coordinates, cyclic damage, and unloading-reloading.

Joint Panel Strength Defined by Observed Shear Panel Strength

The final approach, denoted *MnJ*, used to define the envelope for the joint panel component is a purely empirical approach in which the joint shear stress versus shear deformation data from the PEER-4150 test specimen, used to define joint core response. This specimen was observed to experience a joint shear failure, prior to beam yielding. From the data gathered, M_{nj} can be determined by the point the joint core fails in shear. The M_{nj} value that is found from this approach is applicable for joints that have the same geometry, aspect ratio, and material properties as the PEER-4150 with no transverse reinforcement. The resulting nominal joint moment for the PEER-4150 joint core was 7215208.15 lbs-in.

The M_{nj} value can be calibrated for joints of varying volume and material properties. Varying volumes can be taken into account by multiplying by the ratio of the volume of the joint in question to the volume of the PEER-4150 model. Also, the M_{nj} value can also be calibrated for joints of different concrete strength. Joint shear strength is known to be influenced by concrete strength; however the relationship between the two is still debated by researchers. Traditionally, joint shear strength is considered to be a function of the $\sqrt{f'_c}$ (ACI 1999), yet some researchers postulate that the relationship is a function of f'_c (Mosier 2000). Thus, the joint shear strength must be multiplied by either the ratio of the concrete strengths or the square of the ratio. In this research, both relationships are explored for the PEER-0995 specimen to determine which results in a better fit of the experimental data.

As with the *MnB* approach, the *MnJ* approach is less desirable from a modeling standpoint because of the required assumptions. Nonetheless, this approach is appropriate for joints tested by Stanton, Lehman, Walker (2001) and Alire (2002) and those found in the case study building, some of which experience large joint shear stress demands.

Shear-Panel Calibration: Unload-Reload Path

Predicting seismic response of the joint shear-panel using the *Pinching4* constitutive model requires definition of the joint unload-reload behavior. The unload-reload path for the current research is calibrated using two approaches. The first approach was to use the parameters recommended by Lowes and Altoontash (2004). These parameters were defined to simulate the observed load-unload response of the reinforced concrete panels tested by Stevens et al. (1991); these data were used by Stevens et al. (1991) to extend the *MCFT* for the case of cyclic loading. The second approach was to define unload-reload path parameters to simulate the joint shear stress-strain data collected form the UW test series. Optimization algorithms were implemented in Matlab to determine the six unload-reload parameters that minimized the sum of the error between the observed and predicted stress-strain histories for the six UW tests that implement the PEER load-history (Bennett 2003).

Shear-Panel Calibration: Damage Parameters

Calibration of the damage parameters is critical for predicting the strength, unload stiffness, and reload stiffness degradation the joint shear-panel exhibits during reverse cyclic loading. These aspects of behavior are closely related to the unload-reload path, and the 16 parameters that control the damage are calibrated using the same two approaches as discussed above.

3.6.2. Bar-Slip Calibration: *UW* Joint Formulation

Calibration of the one-dimensional force-displacement history for the eight bar-slip component springs requires definition of a bar stress-slip relationship and a spring force versus bar stress relationship. Joint formulations that use this calibration are denoted with *BS.* This approach developed by Lowes and Altoontash (2004) was used to calibrate the envelope, load-unload response and damage rules for these components. It is implemented in a material model identified as *Barslip* in OpenSees.

The *Barslip* model defines the uniaxial material model for the reinforcement bars as a function of the joint material, geometric and design properties. The model uses the *Pinching4* model and exhibits cyclic degradation of strength, unloading stiffness, and reloading stiffness. However, the response envelope for the bar-slip springs does not explicitly represent strength deterioration. Strength deterioration due to cyclic loading initiates only when the slip demand exceeds 3mm (0.12 in). Thus, the bond-slip springs always exhibit positive stiffness, but strength deterioration occurs upon reloading to a previously observed slip demand. The parameters which control the deterioration are defined to represent observed bond-slip behavior and cannot be changed by the casual user.

3.6.3. Component Calibration: RS Joint Formulation

The calibration process of the *Pinching4* material for the rotational spring of the *RS* joint formulation is similar to that used for the simplified *UW* and the *ST* formulations; it can be assumed to represent the inelastic response of either the entire joint or just the shear-panel. Therefore, the calibration procedure given in Section 3.6.1 is applicable. However, the rotational spring formulation requires additional calibration steps beyond those previously presented because the kinematics of the rotational spring model are different from those of the other two finite area joint formulations. These additional steps are explained below.

Additional Joint Material Model Calibration

Calibration of the *Pinching4* joint material model with the *RS* formulation requires additional modification of the *n* and *p* values shown in Figure 3.6.1 (Charney 2001). The additional modification steps are represented by Equations 3.6.1-3 where α is the column depth over the beam span, β is the beam depth over the column span, *i* corresponds to the points along the backbone, 1-4, and *k* and *p* are taken from Figure 3.6.1.

$$k_{i\,\mathrm{mod}} = \frac{k_i}{(1-\alpha-\beta)^2} \qquad \textbf{Equation 3.6.1}$$

$$p_{i\,\mathrm{mod}} = \frac{p_i}{(1-\alpha-\beta)} \qquad \textbf{Equation 3.6.2}$$

These modification factors are directly applicable for the case of the simple linear material. For the more complex, multi-linear *Pinching4* material, the following additional step must be taken to determine the *n* values given the modified values above.

$$n_{i\,\mathrm{mod}} = \frac{\left(p_{i\,\mathrm{mod}} - p_{(i-1)\,\mathrm{mod}}\right)}{k_{i\,\mathrm{mod}}} + n_{(i-1)\,\mathrm{mod}} \qquad \textbf{Equation 3.6.3}$$

where *i* goes from 1 to 4, and $n_{o\ mod}$ and $p_{o\ mod}$ are both zero.

Chapter 4

Exploration of Seismic Joint Behavior

4.1. Introduction

Chapter 4 presents the evaluation of the joint element formulations and the behavioral models used to calibrate these elements for specific design details that were introduced in Chapter 3. The joint models are evaluated through the comparison of simulated and observed response for five of the 2/3-scale building joint sub-assemblage tests completed by Walker (2001) and Alire (2002) These five laboratory tests specimens have joint design details, including shear stress demands, transverse steel ratios, bond stress demands for beam longitudinal steel and column axial loads, that are representative of reinforced concrete buildings designed prior to 1967 (Mosier 2000) and span the range of values found in the case study building. The joint models were evaluated on the basis of simulated shear strength, stiffness, and the degradation of these due to simulated seismic loading.

Specifically, this chapter discusses the process used and assumptions made in developing calibration models of the test specimens using the modeling tools available in the OpenSees framework, discusses the application of the different joint model calibration methods presented in Chapter 3, evaluates the joint element formulations and calibration methods using specific qualitative and quantitative measures, and identifies two preferred methods for simulating the response of older beam-column building joints.

4.2. Cruciform Test Modeling Details

Five of the University of Washington laboratory test specimens (Walker 2001 and Alire 2002) were modeled to evaluate the proposed joint models. The specimens, identified as PEER-4150, PEER-0995, PEER-2250, CD30-2250, and PADH-2250 were chosen because they 1) span the range of nominal joint shear stress demand levels observed in RC buildings constructed at the time of the Van Nuys Holiday Inn, 2) include a range of bond stress demands for beam longitudinal reinforcement anchored in the joint, and 3) were tested using differing load histories as discussed in Sections 3.2 and 3.3. This section presents important details of the OpenSees models used to simulate the response of these laboratory test specimens.

Figure 4.2.1 shows the process used to simulate the lab tests in OpenSees. The simulation can be thought to take place in five levels. The first level is where the end-user controls the simulation. At this level the desired analysis parameters can be varied, such as type of joint element, type of joint shear panel calibration, load history, and data output control. This level is signified by the lightest shaded box. The second level, corresponding to the second lightest box, is where the building blocks for the simulation are created. Here, nodes are created to define the skeleton of the simulation, and the basic constitutive models, which will be used by the next levels, are developed. The third level is an intermediate level that is not always needed. For example, if the end-user chooses *beamWithHinges2* frame elements, then this level is required to define frame member fiber sections that simulate axial load strain, moment-curvature response. These fiber sections employ the steel and concrete constitutive models defined in level two. If fiber beam-column elements are not used, then definition of the fiber sections is not required and skipping to the fourth level is possible. The fourth level takes the previously defined constitutive models and sections and fits them onto the skeleton of the model defined at the second level. This is done through formal definition of the joint and frame elements chosen at the first level using the materials and sections defined levels two and three. The final, fifth level of the model building process, signified by the darkest box, takes the cruciform model, applies the loads indicated at the first level and runs the displacement-controlled, nonlinear analysis.

Details of the OpenSees model of the UW cruciforms, based on the scheme in Figure 4.2.1, are presented in the following sub-sections. The details explained include boundary conditions, steel and concrete material models, beam and column formulations, and the joint formulations.

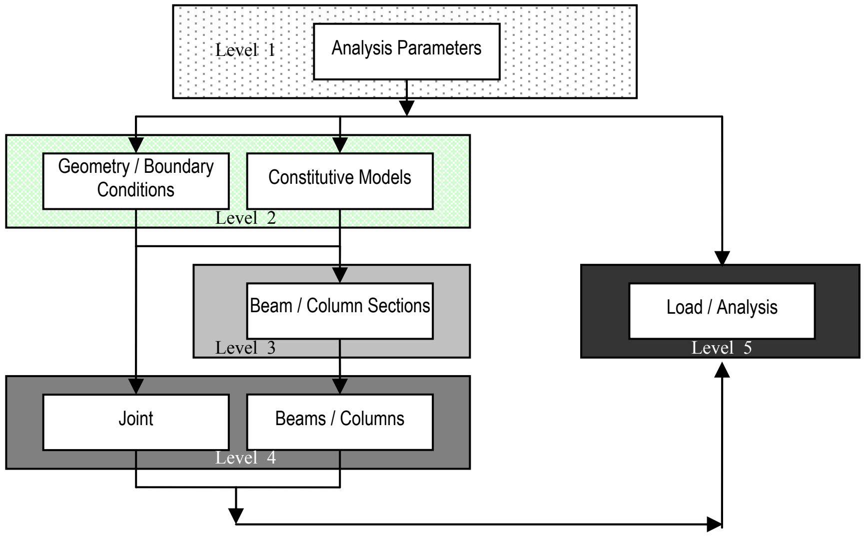

Figure 4.2.1: Scheme for cruciform simulation within OpenSees.

4.2.1. Boundary Conditions for the Building Joint Sub-Assemblage

The UW laboratory tests specimens are sub-assemblages from two-dimensional building frames and include the beam-column joint, two continuous beam segments that frame into the joint and extend to mid-span, and the two continuous column segments that frame into the joint extending to mid-height. In the laboratory, a constant axial load was applied to the column to represent gravity loading. Additionally, equal and opposite vertical shears were applied to the ends of the beam segments and reacted by horizontal shears at the top and bottom of the column segments. These loads were applied under displacement control and were representative of the loads that develop in a two-dimensional frame under earthquake loading. Figure 4.2.2 shows an idealization of the numerical model used to simulate the response the UW laboratory specimens.

The model shown in Figure 4.2.2 was created using elements and material models implemented previously in OpenSees. The model includes force-based fiber beam-column elements that are used to simulate the response of beam and column segments under flexural and axial loading. The response of the beam-column joint region is simulated using the proposed joint element formulations or by using rigid links. The rigid links are not intended to accurately represent observed response, but instead are intended to provide a basis for comparison.

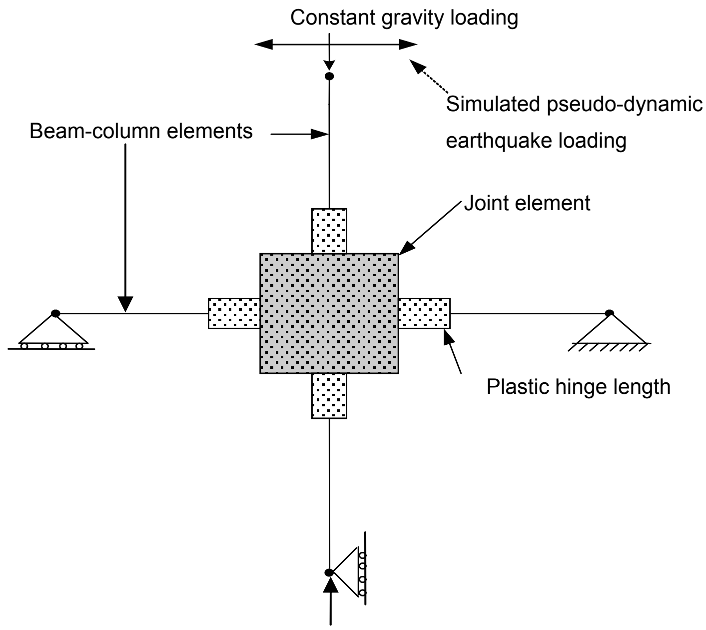

Figure 4.2.2: Schematic of UW cruciform test simulations.

4.2.2. Beam-Column Joint Element Formulations

Eight permutations of the joint models were developed to simulate the joint specimens tested by Walker (2001) and Alire (2002). Each model permutation consisted of a unique combination of three modeling tools available in OpenSees: a joint formulation, a joint shear panel material model, and a bar-slip material model. The three joint formulations introduced in Section 3.5, rotational spring (*RS)*, *beamColumnJoint* (*UW)*, and *Joint2D* (*ST)*, have been combined with the three joint material constitutive models introduced in Section 3.6.1, *MCFT*, *MnB*, and *MnJ*, and the *Barslip* material constitutive material model from Section 3.6.2 to develop the series of models shown in Table 4.2.1.

Table 4.2.1: Elements and materials used to model joint behavior in the UW cruciform simulations.

Simulation Tag	Joint Element Formulation	Joint Material Model	Barslip Material Model
RS-MnB	Rotational Spring	MnB	NA
RS-MnJ	Rotational Spring	MnJ	NA
UW-MCFT-BS	beamColumnJoint	MCFT	Barslip
UW-MnB	beamColumnJoint	MnB	Elastic
UW-MnJ-BS	beamColumnJoint	MnJ	Barslip
ST-MCFT	Joint2D	MCFT	Elastic
ST-MnB	Joint2D	MnB	Elastic
ST-MnJ	Joint2D	MnJ	Elastic

The flexibility of OpenSees allowed the various joint models and constitutive laws to be readily interchanged with no need to adjust the other elements. The following sections describe the implementation of the three joint formulations in the OpenSees environment.

RS Joint Formulation

Formulating a rotational spring joint element requires implementing the *rotSpring2D.tcl* script available on the OpenSees website (http://opensees.berkeley.edu). First, the user must create two nodes at the location of the joint, one node connects the two beam elements and one connects the two column elements. The joint can then be created from the following code:

proc rotSpring2D eleID nodeR nodeC matID

This code calls the file *rotSpring2D.tcl* shown in Table 4.2.2. The parameter *eleID* is a unique element tag integer in the domain for the rotational spring. The two node parameters *nodeR* and *nodeC* represent the two nodes that connect the beams and the columns. The *rotSpring2D.tcl* file creates a zero length element that deforms only in rotation in the desired plane. It also constrains the translation between *nodeR* and *nodeC* ensuring that the nodes stay pinned together like a pair of scissors. *matID* represents the one-dimensional constitutive model that defines the moment-rotation joint behavior. This model is created using the *Pinching4* material model and the parameters presented in Section 4.2.3.

Table 4.2.2: Tcl code to create a rotational spring.

```
# rotSpring2D.tcl
# Written: MHS  Date: Jan 2000
# Formal arguments
# eleID - unique element ID for this zero length rotational spring
# nodeR - node ID which will be retained by the multi-point constraint
# nodeC - node ID which will be constrained by the multi-point constraint
# matID - material ID which represents the moment-rotation relationship
#
# Creating the spring
proc rotSpring2D {eleID nodeR nodeC matID} {
# Create the zero length element
element zeroLength $eleID $nodeR $nodeC -mat $matID -dir 6
# Constrain the translational DOF with a multi-point constraint
# retained constrained DOF_1 DOF_2 ... DOF_n
equalDOF $nodeR $nodeC 1 2}
```

ST Joint Formulation

The information presented in Table 4.2.3 is adapted from the help file developed by Altoontash and Deierlein (2002) for the implementation of the Joint2D element in OpenSees (http://opensees.berkeley.edu). The first line below represents that which one would enter into OpenSees. The parameters to be entered are described below.

Table 4.2.3: Tcl command to create a ST joint element.

element Joint2D Tag? Nd1? Nd2? Nd3? Nd4? NdC? [Mat1? Mat2? Mat3? Mat4?] MatC? LrgDisp?	
Tag?	- an integer identifying the joint element tag in the domain
Nd1?	- an integer indicating the node 1 tag
Nd2?	- an integer indicating the node 2 tag
Nd3?	- an integer indicating the node 3 tag
Nd4?	- an integer indicating the node 4 tag
NdC?	- an integer tag for internal node (must not exist in the domain).
[Mat1?]	- an integer indicating the uniaxial material for rotational spring at node 1
[Mat2?]	- an integer indicating the uniaxial material for rotational spring at node 2
[Mat3?]	- an integer indicating the uniaxial material for rotational spring at node 3
[Mat4?]	- an integer indicating the uniaxial material for rotational spring at node 4
MatC?	- an integer indicating the uniaxial material for the panel rotational spring
LrgDisp?	- an integer indicating the flag for considering large deformation effects

The two-dimensional *Joint2D* element requires four nodes defining the midpoints of a virtual parallelogram upon which the element is then constructed. These external nodes (*Nd1-Nd4*) are connected to an automatically generated internal node, denoted by the unique integer *NdC*, which has an extra degree of freedom to represent the shear deformation. For this element, this study uses the convention that the first node, *Nd1*, represents the connection to the beam to the right of the joint and continues in a counter-clockwise order. These four external nodes can be assigned rotational springs with one-dimensional constitutive models that allow for member-end rotations. Defining the parameters *Mat1-Mat4* automatically created these springs, and leaving these parameters empty makes the end rotations fixed.

The parameter *MatC* indicates the material tag for the shear panel. For this study, this material is defined using the *Pinching4* material model using one of the calibrations discussed in Section 3.6.1, *MCFT*, *MnB*, and *MnJ*. The details of defining this material are presented in Section 4.2.3.

An important aspect of the *Joint2D* element is the multi-point constraints. These constraints enable the simulation of a pure shear deformation mode for the joint element. These four multi-point constraints are automatically added to the domain and they connect the central node to external nodes. These constraints may be set to account for the large deformations, using the *LrgDisp* flag. If flag is set to zero, the assumption is that large deformations do not occur and thus a constant constraint matrix, calculated based on the initial configuration, can be used. A non-zero value for *LrgDisp* enables simulations of large deformations through a time varying constraint matrix. In this case the constraint matrix is updated for every time step, based on the current nodal positions. A value of '1' indicates time varying constraint without length correction while a value of '2' includes length correction to maintain the initial length of the multi-point constraints. Also, to ensure that the multi-point constraints work correctly, the *Joint2D* element must be used along with the 'Penalty', or 'Transformation' constraint handler for the global problem.

UW Joint Formulation

The information presented in Table 4.2.4 is adapted from the help file for the implementation of the *beamColumnJoint* element in OpenSees (http://opensees.berkeley.edu). The element can be used in either two or three dimensional models, but the load is transferred only in the plane of the element. The first line below is the OpenSees command line that creates the element, while the parameters used in the command line are described below.

Table 4.2.4: Tcl command to create a UW joint element.

element beamColumnJoint $eleTag $Nd1 $Nd2 $Nd3 $Nd4 $Mat1 $Mat2 $Mat3 $Mat4 $Mat5 $Mat6 $Mat7 $Mat8 $Mat9 $Mat10 $Mat11 $Mat12 $Mat13 [$eleHeightFac $eleWidthFac]

$eleTag	an integer identifying the element tag in the domain
$Nd1,$Nd2,$Nd3,$Nd4	tag associated with previously defined nodes
$Mat1	uniaxial material tag for left bar-slip spring at node 1
$Mat2	uniaxial material tag for right bar-slip spring at node 1
$Mat3	uniaxial material tag for interface-shear spring at node 1
$Mat4	uniaxial material tag for lower bar-slip spring at node 2
$Mat5	uniaxial material tag for upper bar-slip spring at node 2
$Mat6	uniaxial material tag for interface-shear spring at node 2
$Mat7	uniaxial material tag for left bar-slip spring at node 3
$Mat8	uniaxial material tag for right bar-slip spring at node 3
$Mat9	uniaxial material tag for interface-shear spring at node 3
$Mat10	uniaxial material tag for lower bar-slip spring at node 4
$Mat11	uniaxial material tag for upper bar-slip spring at node 4
$Mat12	uniaxial material tag for interface-shear spring at node 4
$Mat13	uniaxial material tag for shear-panel
$eleHeightFac	floating point value (as a ratio to the total height of the element) to be considered for determination of the distance in between the tension-compression couples (optional, default: 1.0)
$eleWidthFac	floating point value (as a ratio to the total width of the element) to be considered for determination of the distance in between the tension-compression couples (optional, default: 1.0)

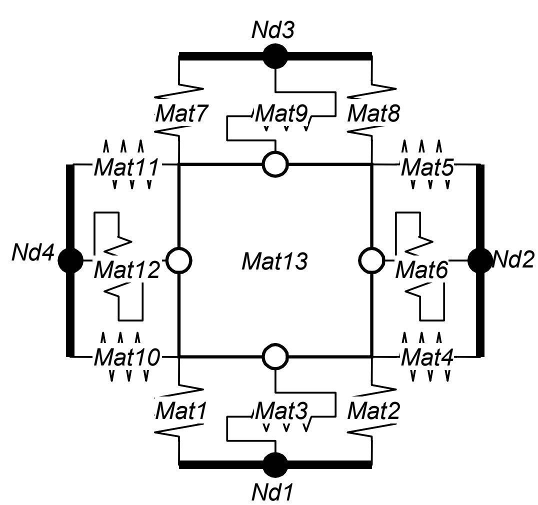

Figure 4.2.3: User-defined modeling parameters of the *beamColumnJoint* element.

The *beamColumnJoint* element requires the definition of four external nodes *Nd1-Nd4*, and it is assumed that *Nd1* is at the connection to the bottom column with the rest following in counter-clockwise order as shown in Figure 4.2.3. These four nodes define where the beam-column elements attach to the joint. This joint element also requires that 12 materials, *Mat1-Mat12* be assigned to the 12 bar-slip and shear-interface springs. The bar-slip materials may be elastic or nonlinear, while the shear-interface springs are assumed elastic and stiff. Parameters used to define the nonlinear cases are given in Section 4.2.3.

Figure 4.2.3 shows that the shear panel requires a thirteenth material represented by *Mat13*. As with the *Joint2D* element, this material is defined using the *Pinching4* material model using one of the calibrations discussed in Section 3.6.1. The details of defining this material are presented in Section 4.2.3. The final two parameters, *eleHeightFac* and *eleWidthhFac*, are used to define the distances between the tension-compression couples in the beams and columns.

4.2.3. Beam-Column Joint Material Model Parameters

Implementation of the eight joint models varied depending on the material models used in this study. This section describes the *Pinching4* material model and gives the parameters that define the different material models used in the current research. The parameters included are those that define the backbone curve, pinching behavior, stiffness degradation, and the strength degradation for the *MnJ*, *MnB*, and *MCFT* constitutive joint models described in Section 3.6.1.

Pinching4 Material Model

The *Pinching4* command (Lowes et al. 2004) is used to construct a one-dimensional material in OpenSees (http://opensees.berkeley.edu) to represent a 'pinched' load-deformation response that exhibits degradation under cyclic loading. The OpenSees command line that creates a *Pinching4* material is provided in Table 4.2.5 along with a description of the parameters included in the command line.

Table 4.2.5: Tcl command to create a *Pinching4* material model.

uniaxialMaterial Pinching4 $matTag $ePf1 $ePd1 $ePf2 $ePd2 $ePf3 $ePd3 $ePf4 $ePd4 [$eNf1 $eNd1 $eNf2 $eNd2 $eNf3 $eNd3 $eNf4 $eNd4] $rDispP $rForceP $uForceP [$rDispN $rForceN $uForceN] $gK1 $gK2 $gK3 $gK4 $gKLim $gD1 $gD2 $gD3 $gD4 $gDLim $gF1 $gF2 $gF3 $gF4 $gFLim $gE $dmgType

$matTag	unique material object integer tag
$ePf1 $ePf2 $ePf3 $ePf4	floating point values defining force points on the positive response envelope
$ePd1 $ePd2 $ePd3 $ePd4	floating point values defining deformation points on the positive response envelope
$eNf1 $eNf2 $eNf3 $eNf4	floating point values defining force points on the negative response envelope (optional, default: negative of positive envelope values)
$eNd1 $eNd2 $eNd3 $eNd4	floating point values defining deformations points on the negative response envelope (optional, default: negative of positive envelope values)
$rDispP	floating point value defining the ratio of the deformation at which reloading occurs to the maximum historic deformation demand
$rForceP	floating point value defining the ratio of the force at which reloading begins to force corresponding to the maximum historic deformation demand
$uForceP	floating point value defining the ratio of strength developed upon unloading from negative load to the maximum strength developed under monotonic loading
$rDispN	floating point value defining the ratio of the deformation at which reloading occurs to the minimum historic deformation demand (optional, default: $rDispP)
$rForceN	floating point value defining the ratio of the force at which reloading begins to the force corresponding to the minimum historic deformation demand (optional, default: $rForceP)
$uForceN	floating point value defining the ratio of the strength developed upon unloading from a positive load to the minimum strength developed under monotonic loading (optional, default: $rForceP)
$gK1 $gK2 $gK3 $gK4 $gKLim	floating point values controlling cyclic degradation model for unloading stiffness degradation
$gD1 $gD2 $gD3 $gD4 $gDLim	floating point values controlling cyclic degradation model for reloading stiffness degradation
$gF1 $gF2 $gF3 $gF4 $gFLim	floating point values controlling cyclic degradation model for strength degradation
$gE	floating point value used to define maximum energy dissipation under cyclic loading. Total energy dissipation capacity is defined as this factor multiplied by the energy dissipated under monotonic loading.
$dmgType	string to indicate type of damage (option: "cycle", "energy")

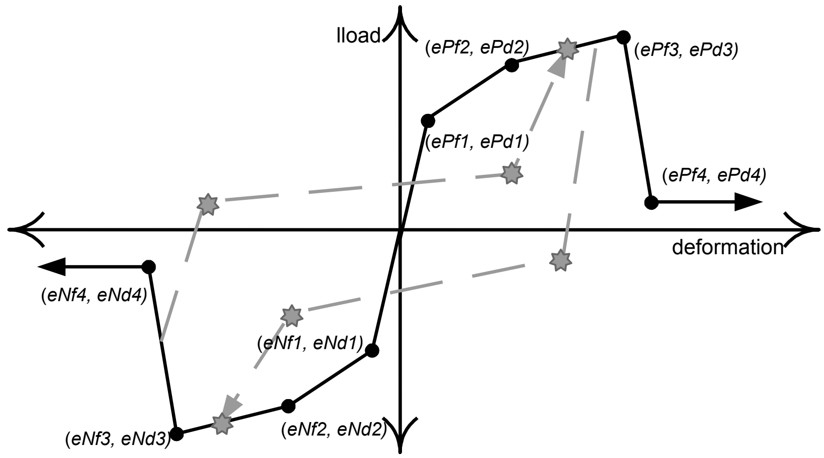

Figure 4.2.4: User-defined modeling parameters of the *Joint2D* element.

The response envelope for the *Pinching4* material is defined using the 16 parameters that come after the *matTag* parameter as shown in Figure 4.2.4. These parameters define the positive and negative backbone curves; for this study, responses in the positive and negative directions are assumed equal. Thus, eight unique parameters are required. These eight parameters for the *MnJ* and *MnB* joint constitutive models are given in Table 4.2.6 where M_{nj} is the nominal joint strength for each of the laboratory specimens from Table 4.2.7. Table 4.2.8 provides these values for the MCFT model. The parameters to be used do not depend on the joint element, only on the specimen design details.

The next 22 parameters, from *rDispP* to *gE*, define the pinching behavior, cyclic degradation, and energy dissipation of the joint model. The material model allows for simulation of these types of degradation: unloading stiffness degradation, reloading stiffness degradation, strength degradation. The six parameters that define the pinching, the 15 that define the three types of degradation, and the one energy dissipation parameter are given in matrix form in Table 4.2.9 for the *MnJ* and *MnB* models. These same parameters for the *MCFT* material model are given in Table 4.2.10. The final parameter, *dmgTyp*, is a string that determines if the joint damage is based on energy or cycle counting. For this study, damage is assumed to be based on the number of load cycles. Further details regarding the damage formulation can be found in Lowes et al. (2004).

Backbone Curve Parameters

Table 4.2.6: Response envelope parameters for the *MnB* and the *MnJ* models.

i	p_i *(k-in)*	n_i
1	$0.3000M_{nj}$	0.0021
2	$0.7076M_{nj}$	0.0091
3	$1.000M_{nj}$	0.0278
4	$1.000M_{nj}$	0.0896

Table 4.2.7: Nominal joint moment for *MnJ* and *MnB* models.

Nominal Moment M_{nj} *(lbs-in)*	Model	0995	2250	4150
	MnJ	*7215208.15*	*7215208.15*	*7215208.15*
	MnB	*6471847.90*	*5988509.90*	*10805412.20*

Table 4.2.8: Response envelope parameters for the *MCFT* model.

Parameter	0995	2250	4150
p_1 *(lbs-in)*	*2114035.2*	*1663606.2*	*1528070.4*
p_2 *(lbs-in)*	*1919577.6*	*1687392.0*	*1640736.0*
p_3 *(lbs-in)*	*1649491.2*	*1664524.8*	*1223193.6*
p_4 *(lbs-in)*	*1030982.4*	*917049.6*	*774892.8*
n_1	*0.00006*	*0.00006*	*0.000075*
n_2	*0.00064*	*0.00028*	*0.000759*
n_3	*0.00139*	*0.00057*	*0.00198*
n_4	*0.003*	*0.003*	*0.003*

Pinching, Stiffness and Strength Degradation Parameters

The values presented here are the values that have been used to define the pinching behavior, cyclic degradation and energy dissipation for the joint constitutive models in OpenSEES. They are based on a calibration study completed by Bennett (2003) that used data from the University of Washington joint testing (Walker 2001 and Alire 2002).

Table 4.2.9: Pinching, stiffness and strength degradation parameters for the *MnJ* & *MnB* models.

Parameters	MnJ & MnB Models
Pinching (+)	$\begin{bmatrix} 0.1070 & 0.2540 & 0 \end{bmatrix}$
Pinching (-)	$\begin{bmatrix} -0.1070 & -0.2540 & 0 \end{bmatrix}$
Unloading Stiffness Reloading Stiffness Strength	$\begin{bmatrix} 0.4148 & 0.3514 & 0.1977 & .0281 & 0.9999 \\ 0.0461 & 0.0051 & 1.3851 & 0 & 0.9999 \\ 1.0000 & 0 & 2.0000 & 0 & 0.9999 \\ 2.0000 & 1.0000 & 0 & 0 & 0 \end{bmatrix}$

Table 4.2.10: Pinching, stiffness and strength degradation parameters for the *MCFT* model.

Parameters	MCFT Model
Pinching (+)	$\begin{bmatrix} 0.25 & 0.15 & 0 \end{bmatrix}$
Pinching (-)	$\begin{bmatrix} -0.25 & -0.15 & 0 \end{bmatrix}$
Unloading Stiffness Reloading Stiffness Strength	$\begin{bmatrix} 1.299 & 0 & 0.235 & 0 & 0.894 \\ 0.12 & 0 & 0.23 & 0 & 0.95 \\ 1.11 & 0 & 0.319 & 0 & 0.125 \\ 10 & 0 & 0 & 0 & 0 \end{bmatrix}$

4.2.4. Simulation Parameters for Steel and Concrete

The response of the beams and columns in the sub-assemblage is simulated using a fiber beam-column element. This element requires a one-dimensional concrete and a one-dimensional steel stress-strain model to enable prediction of axial and flexural response at that section level and ultimately at the element level. The OpenSees material models *Steel02* and *Concrete01,* as implemented in Version 1.5 of the OpenSees platform, are used to simulate the one dimensional material response of the steel and concrete. The parameters required for definition of these models are listed in Table 4.2.11-Table 4.2.12.

The *Steel02* material model defines response under cyclic loading using a bilinear envelope to the stress-strain response and Menegotto-Pinto curves (1973) to define the unload-reload response. Calibration of the model requires definition of the steel elastic modulus, E_s, yield strength, f_y, ratio of the hardening modulus to the elastic modulus, *SHR*, the fracture strain, ε_u, and seven parameters that define the shape of the Menegotto-Pinto curves under unloading and reloading, R_i and a_i. For the experimental test specimens, data are available defining E_s, f_y, f_u, and ε_u. The hardening modulus was defined using these four data points. First, the yield strain, ε_y, is found using E_s and f_y, and then the hardening modulus is determined using f_y, f_u, ε_y, and ε_u. In order to define the seven Menegotto-Pinto curve parameters, the recommendations of Filippou et al. (1983) were used. Table 4.2.11 lists the parameters used in this study.

Table 4.2.11: Steel material modeling parameters for all specimens.

Steel Material Parameters	Columns	Beams
	4150	
f_y (psi)	79.0 e10^3	79.0 e10^3
E_s (psi)	29.0 e10^6	29.0 e10^6
SHR	13.8 e10^{-3}	13.8 e10^{-3}
R_o / R_1 / R_2	18.5/0.925/0.15	18.5/0.925/0.15
a_1 / a_2 / a_3 / a_4	0/0.4/0/0.5	0/0.4/0/0.5
	2250*: Steel 1	
f_y (psi)	78.0 e10^3	76.5 e10^3
E_s (psi)	29.0 e10^6	29.0 e10^6
SHR	15.7 e10^{-3}	14.9 e10^{-3}
R_o / R_1 / R_2	18.5/0.925/0.15	18.5/0.925/0.15
a_1 / a_2 / a_3 / a_4	0/0.4/0/0.5	0/0.4/0/0.5
	2250: Steel 2	
f_y (psi)	74.5 e10^3	-
E_s (psi)	29.0 e10^6	-
SHR	16.0 e10^{-3}	-
R_o / R_1 / R_2	18.5/0.925/0.15	-
a_1 / a_2 / a_3 / a_4	0/0.4/0/0.5	-
	2250: Steel 3	
f_y (psi)	79.0 e10^3	-
E_s (psi)	29.0 e10^6	-
SHR	20.0 e10^{-3}	-
R_o / R_1 / R_2	18.5/0.925/0.15	-
a_1 / a_2 / a_3 / a_4	0/0.4/0/0.5	-
	0995	
f_y (psi)	73.2 e10^3	73.1 e10^3
E_s (psi)	31.4 e10^6	31.6 e10^6
SHR	14.1 e10^{-3}	18.6 e10^{-3}
R_o / R_1 / R_2	18.5/0.925/0.15	18.5/0.925/0.15
a_1 / a_2 / a_3 / a_4	0/0.4/0/0.5	0/0.4/0/0.5

***Note**: The 2250 specimen was designed with three different types if reinforcement bars, thus three sets of parameters are included.

The *Concrete01* material model defines the one-dimensional response of concrete assuming no strength under tensile loading, a plastic-type response under compressive loading and a response envelop in which a second order polynomial defines response to the peak strength and a first order polynomial defines post-peak strength decay to a residual strength level. Calibration of the model requires definition of the stress-strain point corresponding to peak strength, f_c-ε_c, and the stress-strain point at which the residual strength is developed, f_{cu}-ε_{cu}. The model may be calibrated to predict the response of unconfined or confined concrete.

To predict the response of the unconfined cover concrete in the beams and columns, the compressive strength measured near the time of testing is assumed to be developed at a strain of -0.002 in./in. This strain level is used typically in analysis of reinforced concrete members (Kent and Park 1971). The approach recommended by Mander et al. (1988) in which complete strength loss is assumed to occur at the spalling strain is used to define the rate of post-peak strength deterioration. A spalling strain of -0.008 in./in. (Lehman 2004) and a residual strength of 20% is assumed. Typically, zero residual strength is assumed for unconfined concrete; however, for the current analyses, a residual strength of 20% was found to result to improve convergence of the nonlinear analysis and to have little impact on predicted response except when ductile demands are large. This is verified through a moment-curvature analyses of the elements which show that the 20% residual strength increases the moment strength by less than 5%, and that only occurs at ductility demands that are ten times the yield demand. Table 4.2.12 lists the parameters used in the analysis.

To predict the response of the concrete confined by transverse reinforcement in the beams and columns, the model proposed by Kent and Park (1971) and modified per the recommendations of Park et al. (1982) was used to define the increase in strength and ductility resulting from confinement. Table 4.2.12 lists the parameters used in the analysis.

Table 4.2.12: Concrete material modeling parameters for all specimens.

Concrete Material Parameters	4150			
	Columns		Beams	
	Unconfined	Confined	Unconfined	Confined
f'_c (psi)	-4783	-6242	-4783	-6230
ε_c	-0.0020	-0.0020	-0.0020	-0.0026
f'_{cu} (psi)	-3343	-1248	-3343.076	-1246
ε_{cu}	-0.0040	-0.0487	-0.0040	-0.0483
	2250			
f'_c (psi)	-5570	-6529	-5570	-6479
ε_c	-0.0020	-0.0023	-0.0020	-0.0023
f'_{cu} (psi)	-3769	-1305	-3769	-1295
ε_{cu}	-0.0040	-0.0262	-0.0040	-0.0252
	0995			
f'_c (psi)	-8767	-9841	-8767	-9835
ε_c	-0.0020	-0.0022	-0.0020	-0.0022
f'_{cu} (psi)	-5450	-1968	-5450	-1967
ε_{cu}	-0.0040	-0.0353	-0.0040	-0.0351

4.2.5. Simulation Parameters for Beams and Columns

The frame members of the cruciform are modeled using the *beamWithHinges2* element formulation as implemented in Version 1.5 of the OpenSees platform. The *beamWithHinges2* element formulation follows from the assumption that 1) the moment distribution along the length of the element is linear (i.e. the element is a force-based element) and 2) inelastic response is isolated to "plastic hinge" regions at the end of the members with the middle of the element assumed to response elastically. The hinge length for a member is defined as 0.5h where h is the height of the cross-section dimension perpendicular to the axis of bending. Multiple, more sophisticated plastic hinge length models have been proposed for defining hinge length are available (Priestley and Park 1987), however, research (Priestley and Park 1987) suggest that 0.5h provides a good estimate.

For all of the hinge-length models mentioned above, it is important to note that all of them assume a single inelastic section. In contrast, the *beamWithHinges2* model employs two sections to define the hinge. Using two hinges allows for the accurate estimation of the inelastic action at two points in the hinge region as opposed to one.

The inelastic response of the beams and columns is defined at the section level using a fiber discretization of the section in which fibers with a maximum dimension of 1/3” are used over the height of the section. Fiber response is defined using the concrete and steel material models present in Section 4.2.4.

Effective Stiffness Calibration

Observations of the experimental test specimens (Walker 2001 and Alire 2002) indicate that substantial flexural cracking occurs along the beam and column segments. The *beamWithHinges2* element formulation assumes that the element is elastic outside of the hinge region. To simulate the impact of flexural and shrinkage cracking an effective flexural stiffness, EI_{eff}, is used for the elastic regions of the elements:

$$EI_{eff} = \alpha EI_g \qquad \textbf{Equation 4.2.1}$$

where E is the elastic modulus of the concrete and I_g is the moment of inertia of the section computed using the gross section dimensions.

For the current study, two approaches were used to determine appropriate α values. First, α was define empirically, using the data from the tests specimens subject to the PEER displacement histories used traditionally in the laboratory to represent earthquake loading (Walker 2001 and Alire 2002). Here α was defined by forcing the cruciform’s predicted displacement at yield to coincide with the displacement at the observed yield point. The predicted yield point was defined as the point where the beam steel in the section adjacent to the joint yielded, and the observed yield point for the PEER specimens are determined by Walker (2001) and Alire (2002). Guidance was taken from the ACI-318-04 suggestions for reducing EI for an elastic analysis for strength design in order to set the reduction of the columns to be half that of the beams. Table 4.2.13 shows the α values for the two joint models, *UW* and *RS*.

The second approach used to define α employed the equation developed by Branson (1963):

$$I_{eff} = I_{cr} + (I_g - I_{cr})(M_n / M_a)^m \qquad \textbf{Equation 4.2.2}$$

where I_{cr} is the moment of inertia of the cracked section, I_g is the moment of inertia of the gross section, M_a is the maximum moment demand, M_n is the nominal flexural strength of the section and m is a model parameter. Branson recommends m equal to four for a constant moment region, to account for tension stiffening, and m equal to three for a simply supported beam to account for tension stiffening and variation in the moment distribution. This equation is the basis for the ACI proposed method of computing EI_{eff} for analysis of frame members under service level loads. ACI-318 (2002) provided recommendations for an average EI for cases in which I_{eff} is different in positive and negative moment regions. For the current study, EI_{eff} is computed using Branson's equation with m of three and M_a defined as the maximum moment within the region of the beam that the *beamWithHinges2* element formulation assumes to be elastic. Table 4.2.14 lists the α values computed using this approach.

One would expect that α would be relatively large for the test specimens in which the joints failed prior to the beams developing nominal flexural strength (PEER 4150) and relatively small for the test specimens in which the joints failure following beam yielding. For the former case, the beams and column experience small flexural demands at the point of failure, while for the later cases the demand-to-capacity ratios are larger and more cracking is realized. The α values based on Equation 4.2.2 support this assumption. Deviations from this expected behavior for the empirical values are a result of inaccuracies in the predicted joint stiffness, as indicated by the variations in α for different joint model calibrations. For example in Table 4.2.13, the *4150 UW-MnJ-BS* simulation requires a high α value because the inelastic action of the specimen is simulated primarily by the joint panel and bar-slip action. No additional flexibility of the beams and columns is required to simulate the stiffness of the cruciform. The *4150 RS-MnB* in contrast, requires a low α value to match observed displacement since observation suggests that the beams and columns do not exhibit significant cracking at yielding. This suggests that the *4150 RS-MnB* joint model too stiff when simulated using the beam strengths.

While the empirical manipulation of α allows for better predicted results for the current PEER specimens, the future applicability of the values is limited. The Branson equation on the other hand, presents a less ad hoc, more consistent approach to defining α that can be employed when empirical data are not available. Thus, the effective stiffness reduction factors based on the Branson equation are ultimately used in the current research.

Table 4.2.13: Empirical effective stiffness reduction factors.

Specimen		*0995*		*2250*		*4150*	
Joint Calibration		RS-MnB	UW-MnJ-BS	RS-MnB	UW-MnJ-BS	RS-MnB	UW-MnJ-BS
α	*beam*	1.00	0.35	0.13	0.13	0.13	1.00
	column	1.00	0.70	0.27	0.27	0.27	1.00

Table 4.2.14: Effective stiffness reduction factors based on the Branson equation.

Specimen		*0995*	*2250*	*4150*
α	*beam*	0.36	0.43	0.92
	column	0.36	0.40	0.78

4.3. Comparison of Simulated and Measured Responses

Simulations of the five UW cruciform tests: PEER-4150, PEER-0995, PEER-2250, CD30-2250, and PADH-2250 have been completed, and the results compared to the observed data (Walker 2001 and Alire 2002). Pushover simulations using a rigid joint and the eight joint elements in Table 4.2.1 for select specimens were carried out as an initial step in evaluating the joint elements. These simulations also allowed for validation of the moment-curvature response of the beams and columns, as well as quantitative comparison of the simulated and observed response.

Pseudo-static, reverse cyclic simulations were also completed for the five specimens and the results compared qualitatively and quantitatively to the experimental results. The qualitative comparison is based on the whether or not the correct failure mode of the specimen is predicted, and the quantitative comparison explores the predicted and observed yield strength, maximum strength, drift capacity, and rate of strength deterioration.

4.3.1. Initial Pushover Simulations

A basis for comparison was determined by completing initial pushover simulations with a rigid joint in the cruciform. The area of the joint in the plane of the frame was modeled as rigid using beam-column elements with high stiffnesses, while the rest of the simulation details were as discussed in Section 4.2. Thus, the non-linearities of the cruciform were confined to the material non-linearities of the beams and columns.

The results for the 4150 specimen with a rigid joint, as shown in Figure 4.3.1, indicate a dramatic inability of the simulation to capture the observed cruciform response. Figure 4.3.2 and Figure 4.3.3 compare that the non-linear moment-curvature response of the beams and columns as predicted using OpenSees with values calculated using basic concrete beam theory. Thus, the poor simulation of the cruciform response using a rigid joint and nonlinear beams and columns indicates a need for the implementation of the joint models discussed previously to enable accurate simulation of cruciform response.

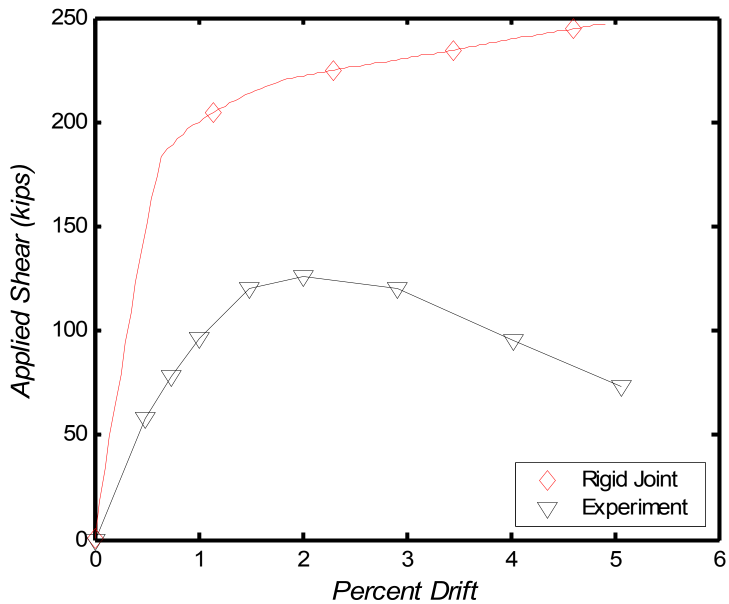

Figure 4.3.1: 4150 Response comparison between the rigid joint simulation and the observed.

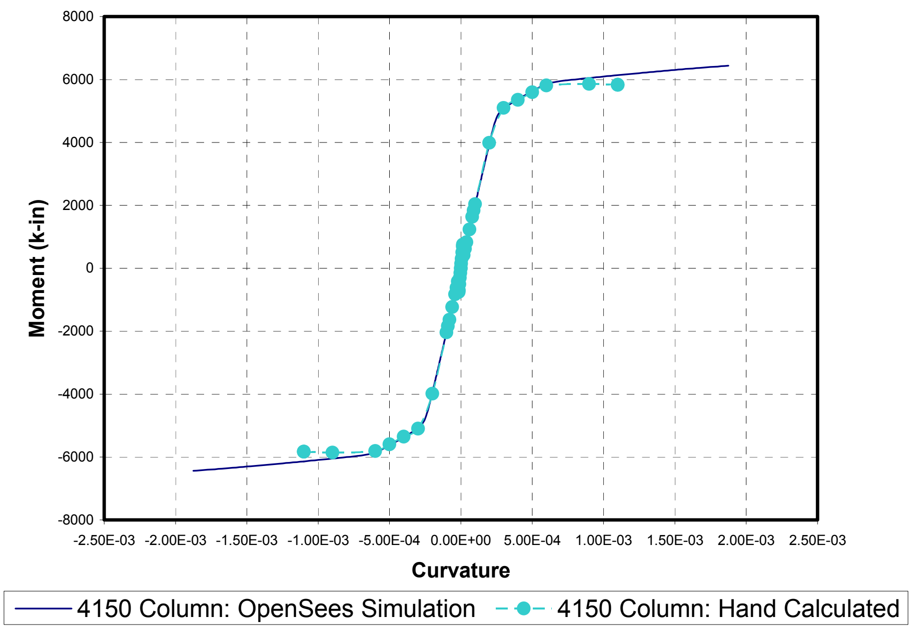

Figure 4.3.2: 4150 Column Moment-Curvature comparison of the OpenSees and hand calculations (axial load not included).

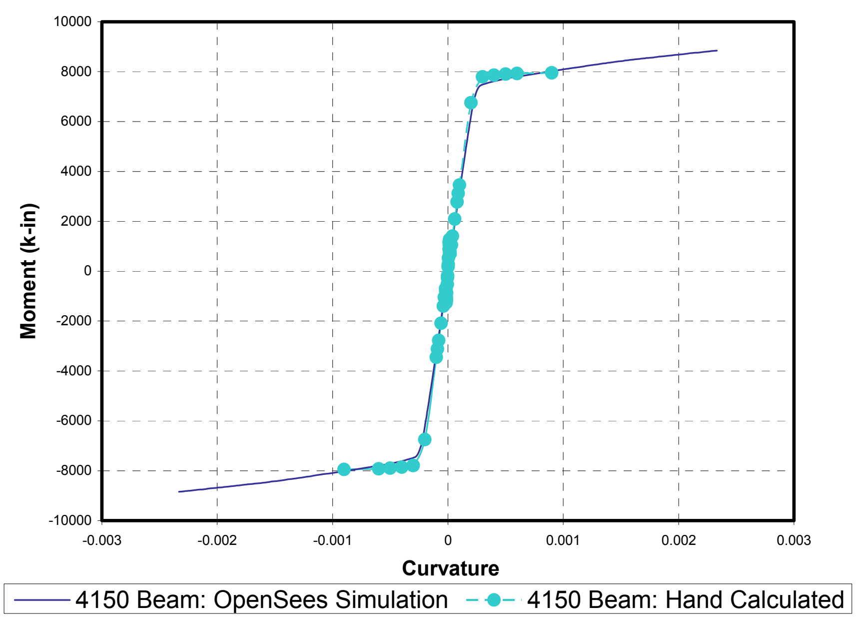

Figure 4.3.3: 4150 Beam Moment-Curvature comparison of the OpenSees and hand calculations.

Simulations of the 4150 and 0995 specimens under monotonic pseudo-static loading using the eight joint models from Table 4.2.1 were performed as the next step in the joint model investigation. The goal of these analyses was to identify any redundancy between the models, to identify any joint models that were inadequate for use in predicting observed response, and to provide initial understanding of the models.

Figure 4.3.4 and Figure 4.3.5 show the simulated response under monotonic loading as well as the envelope to the cyclic response histories observed in the laboratory. These two figures show the results for the 0995 and 4150 specimens, and the resulting qualitative comparison indicates much about modeling specimens of high and low joint shear stress demand. From the data in Figure 4.3.4-Figure 4.3.5(a), it is shown that the Modified Compression Field Theory is not suitable for use in simulating the observed strength of these joint. It is hypothesized that the joint shear is transferred primarily through a compression strut in the joint core and that this stress distribution is sufficiently different from the uniform stress distribution on which the theory is developed to make the theory invalid for predicting response. Also, from Figure 4.3.4 it appears that the *MnB* calibration is unsuitable for joints with high joint shear stress demand, while Figure 4.3.5 indicates that none of the calibration approaches seem better than any other for specimens with low joint shear stress demand.

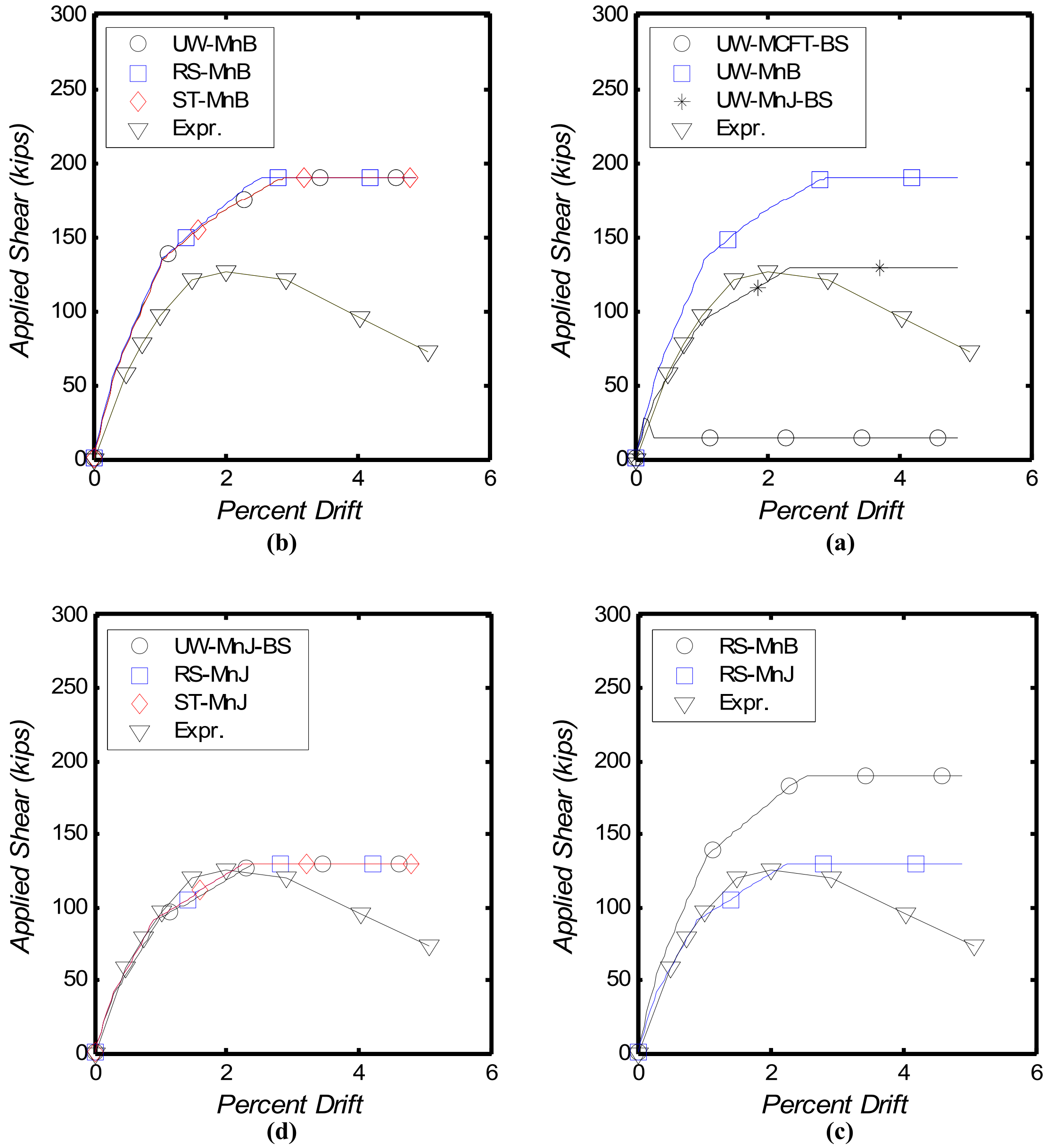

Figure 4.3.4: Cruciform Response comparison from pushover analysis for the 4150 specimen with (a) *UW* joint element with varying calibration (b) Varying joint elements with *MnB* calibration (c) *UW* joint element with varying calibration and (d) Varying joint elements with *MnJ* calibration.

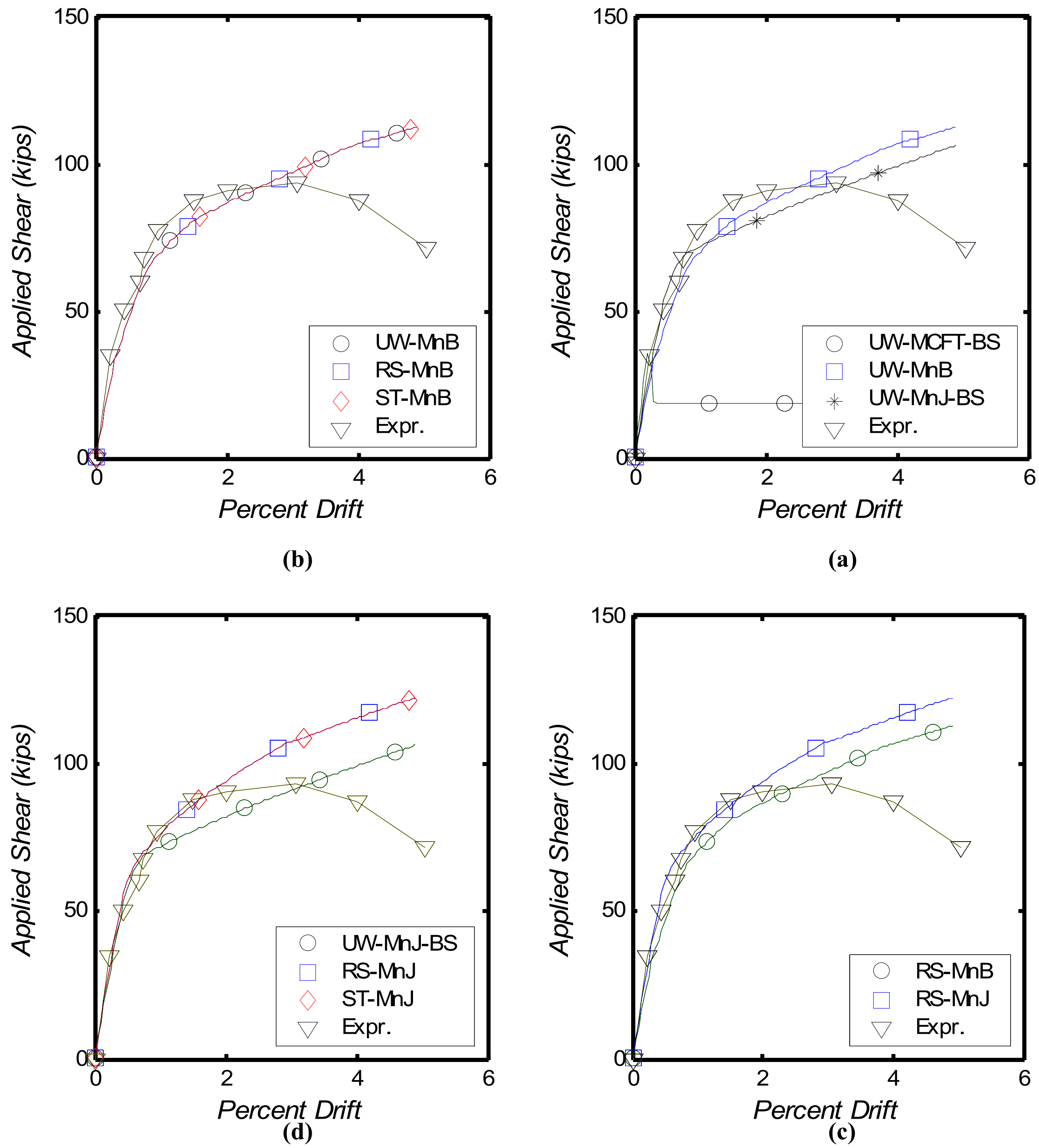

Figure 4.3.5: Cruciform Response comparison from pushover analysis for the 0995 specimen with (a) *UW* joint element with varying calibration (b) Varying joint elements with *MnB* calibration (c) *RS* joint element with varying calibration and (d) Varying joint elements with *MnJ* calibration

Closer inspection of the data presented in Figure 4.3.4-5 show that the *ST-MnB* and *UW-MnB* models predict exactly the same behavior. This is not unexpected given that both joint models allow inelasticity only in the joint panel, allow for the same joint mechanics, and they define the joint panel behavior using the same material model. In

Figure 4.3.4-5(d) one sees that *ST-MnJ* and *UW-MnJ-BS* almost predict the same behavior, but there are slight discrepancies due to the flexibility of the bar-slip springs. The more pronounced discrepancies in Figure 4.3.5 suggest the bar-slip springs play a larger role for specimens with low joint shear stress demand. The rotational spring version of these models, *RS-MnB* and *RS-MnJ*, also model closely the behavior of the UW and Stanford joint element models. However, as shown by the *RS-MnB* model in Figure 4.3.4, there are slight discrepancies. This may be due to uncertainties in the predicted initial stiffnesses of the models, or due to differences in joint kinematics between the models that the calibration in Equations 3.6.4-6 fails to include.

It has been asserted that the ability to model the various joint failure mechanisms separately is important to accurately simulate the seismic joint response. However, the data presented in Figure 4.3.4-Figure 4.3.5(d) do not clearly demonstrate the value of modeling the shear panel and the bar slip behavior separately. In both figures, the differences between the *UW-MnJ-BS* and *ST-MnJ* is slight, and neither one seems more promising than the other. The data in Figure 4.3.4(a) does show that the *UW-MnJ-BS* model is highly advantageous compared to the *UW-MnB* model, but that is due to the advantage of using the *MnJ* calibration for specimens with high joint shear stress demand. While, the importance of the bar-slip components on the overall cruciform shear strength at low joint shear stress demand is not clearly illustrated for these monotonic simulations, this lack of clarity is not unexpected given that degradation in the bar-slip springs occurs only after multiple cycles (Lowes et al. 2004). Thus, given that degrading behavior of the bar-slip springs occurs over multiple cycles, it is hypothesized that the bar-slip elements will control the overall response for specimens with low joint shear stress demand for the simulations with multiple cycles.

A quantitative comparison of the pushover data for rigid joint simulations and the analyses shown in Figure 4.3.4-Figure 4.3.5 is presented in Table 4.3.1, which lists the observed response values and compares them to the corresponding predicted values. The data compared are the initial stiffness, $K_{i,}$ yield shear strength, V_y, maximum shear strength, V_{max}, drift at yield, d_{Vy}, and drift at maximum strength, d_{Vmax}. The comparison of the rigid joint simulations to the observed simulations shows that the modeled shear strengths are well above those observed for the 4150 specimen. The drift capacities are also poorly predicted. For the 0995 specimen data in Table 4.3.1, the rigid joint appears to predict the shear strength values as well as the other models. As indicated above, this suggests that joint response does not impact the overall response as much for specimens with low joint shear strength demand as expected and reported in the experiments. The fact that the observed strengths between the different joint models are more consistent for the 0995 as opposed to the 4150 supports this assertion.

The data in Table 4.3.1 shows that the *MCFT* model is not appropriate for use in simulating joint responses. The ratios of the simulated to the observed shear strengths are never more than 0.50, even if the simulated initial stiffnesses are quite accurate. In contrast, the *UW-MnJ-BS* is the most consistent modeling approach as it predicts K_i, V_y, and V_{max} for both the 0995 and 4150 specimens within 15%. The *RS-MnJ* predicts the 4150 specimen response as well as the *UW-MnJ-BS*, but it fails to predict the maximum shear strength of the 0995 specimen. The *UW-MnB* and the *RS-MnB* predict the 0995 specimen behavior better than 4150, yet they are not clearly better when compared to the other models.

Table 4.3.1: Ratio of predicted monotonic loading response to experimentally observed response.

	Exp.	Rigid / Exp.	UW-MnB / Exp.	RS-MnB / Exp.	RS-MnJ / Exp.	UW-MnJ-BS / Exp.
	4150 Specimen					
K_i	139.85 k/in	2.59	1.23	1.29	1.00	0.92
V_y	117.74 kips	1.63	1.61	1.61	1.10	1.10
V_{max}	126.00 kips	1.97	1.51	1.51	1.02	1.02
d_{Vy}	1.49 in.	0.43	1.67	1.49	1.29	1.38
d_{Vmax}	1.71 in.	2.50	1.45	1.30	1.13	1.20
	0995 Specimen					
K_i	162.51 k/in	1.38	0.67	0.67	0.93	0.87
V_y	70.61 kips	0.89	0.88	0.88	0.89	0.90
V_{max}	93.44 kips	1.36	1.21	1.21	1.32	1.14
d_{Vy}	0.69 in.	0.50	0.93	0.93	0.68	0.74
d_{Vmax}	2.57 in.	1.67	1.67	1.67	1.67	1.67

The data in Table 4.3.1 show that none of the models predicted both displacements d_{Vy} and d_{Vmax} within 29%. This error is likely due, in part, to a comparison of displacements predicted for monotonic loading with displacement demands observed under cyclic loading; however, the error is sufficiently large to cause concern for the use of these models to predict system response beyond 3% drift.

On the basis of the data presented in Figure 4.3.4, Figure 4.3.5, and Table 4.3.1, four models were identified as preferred models: *UW-MnJ-BS, RS-MnB*, *UW-MnB, RS-MnJ*. The *UW-MnJ-BS* was chosen given its ability to predict the joint strengths for specimens with both high and low joint shear strength demands, and because it enables simulation of bond as well as joint shear failure. The two *MnB* models were chosen to further investigate the impact of joint element formulation on predicted cyclic behavior. The *RS-MnJ* model was included because it makes good response predictions at 2% and below, and in comparison with the *UW-MnJ-BS* model, it enables investigation of the impact of simulating bar-slip failure. These four models span the range of joint element complexity and include only the shear-panel response models that show significant potential for predicting observed response. These models were used to simulate cruciform response under the pseudo-static cyclic load histories employed in the laboratory.

4.3.2. Cyclic Load History Simulations

The results of the pushover analyses provided a basis for identifying four preferred models to simulate the actual laboratory tests, which were subjected to different pseudo-static cyclic loading. The results of these analyses are discussed in the following sections; complete numerical data sets for these analyses, including moment-curvature histories for critical beam and column sections, joint component load-deformation histories and specimen load versus drift histories, are provide in Appendix A. In the following sections, simulated and observed response qualities are compared. The response quantities used for comparison include, the initial stiffness, $K_{i,}$ yield shear strength, V_y, maximum shear strength, V_{max}, unloading stiffness at V_{max}, K_{max}, failure shear strength, V_u, drift at yield, d_{Vy}, drift at maximum strength, d_{Vmax}, and the drift at V_u, d_{Vu}. The data is presented in Table 4.3.2 and Figure 4.3.6-Figure 4.3.16. In Table 4.3.2 experimentally observed response quantity values are presented; also presented are the ratios of predicted to observed for each response quantity for each joint model.

Table 4.3.2: Ratio of predicted cyclic loading response to experimentally observed response.

	Exp.	RS-MnB/Exp.	RS-MnJ/Exp.	UW-MnB/Exp.	UW-MnJ-BS/Exp.	Mean	COV
	PEER-4150						
K_i	139.85 k/in	1.27	1.04	1.27	0.91	1.12	0.16
V_y	117.74 kip	1.53	1.01	1.53	1.02	1.27	0.23
V_{max}	126.00 kip	1.40	0.95	1.43	0.96	1.19	0.22
K_{max}	118.88 k/in	1.19	0.80	1.21	0.81	1.00	0.23
V_u	95.24 kip	1.40	1.09	1.40	0.33	1.06	0.48
d_{Vy}	1.49 in.	1.49	1.58	1.29	1.58	1.49	0.09
d_{Vmax}	1.71 in.	1.38	1.12	1.37	1.17	1.26	0.11
d_{Vu}	2.57 in.	1.67	1.33	1.31	1.33	1.41	0.12
	PEER -2250						
K_i	97.94 k/in	0.98	1.11	0.98	1.23	1.08	0.11
V_y	69.76 kip	0.99	0.98	0.99	0.99	0.99	0.01
V_{max}	80.81 kip	1.22	1.37	1.22	1.15	1.24	0.07
K_{max}	75.44 k/in	1.05	1.18	1.05	0.99	1.07	0.08
V_u	64.7 kip	1.21	NA	1.21	0.75	1.06	0.25
d_{Vy}	1.07 in.	1.07	0.80	0.68	0.80	0.84	0.20
d_{Vmax}	2.50 in.	1.37	1.71	1.37	1.03	1.37	0.20
d_{Vu}	2.57 in.	1.67	NA	1.47	1.00	1.38	0.25
	PEER -0995						
K_i	162.51 k/in	0.71	0.93	0.71	0.89	0.81	0.14
V_y	70.61 kip	0.87	0.82	0.87	0.88	0.86	0.03
V_{max}	93.44 kip	1.12	1.30	1.12	0.82	1.09	0.18
K_{max}	82.44 k/in	1.01	1.18	1.01	0.75	0.99	0.18
V_u	66.73 kip	1.25	NA	1.25	0.47	0.99	0.45
d_{Vy}	0.69 in.	0.69	0.90	0.61	0.90	0.78	0.19
d_{Vmax}	2.57 in.	1.33	1.67	1.33	0.50	1.21	0.41
d_{Vu}	3.45 in.	1.24	NA	1.16	0.37	0.92	0.52
	CD30-2250						
K_i	88.89 k/in	1.07	1.20	1.07	1.14	1.12	0.06
V_y	73.02 kip	0.96	0.96	0.96	0.95	0.96	0.01
V_{max}	84.45 kip	1.17	1.33	1.17	1.10	1.19	0.08
K_{max}	74.1 k/in	1.07	1.21	1.07	1.00	1.09	0.08
V_u	56.65 kip	1.21	NA	1.21	NA	1.21	0.00
d_{Vy}	1.14 in.	1.14	0.77	0.65	0.77	0.83	0.26
d_{Vmax}	2.16 in.	1.61	1.99	1.61	1.19	1.60	0.20
d_{Vu}	2.57 in.	1.67	NA	1.55	NA	1.61	0.05
	PADH-2250						
K_i	88.68 k/in	1.06	1.22	1.06	1.13	1.12	0.07
V_y	71.94 kip	0.97	0.96	0.97	0.97	0.97	0.01
V_{max}	84.24 kip	1.25	1.34	1.25	1.18	1.26	0.05
K_{max}	70.5 k/in	1.19	1.28	1.19	1.13	1.20	0.05
V_u	39.03 kip	1.54	NA	1.54	NA	1.54	0.00
d_{Vy}	1.16 in.	1.16	0.74	0.63	0.74	0.82	0.29
d_{Vmax}	2.34 in.	1.64	1.83	1.65	1.83	1.74	0.06
d_{Vu}	4.28 in.	1.00	NA	0.62	NA	0.81	0.33

Figure 4.3.6 through Figure 4.3.16 show simulated and observed response data for the five laboratory test specimens. For each of the three specimens subjected to the standard cyclic load history, data characterizing response are presented in three figures; Each PEER specimen has its corresponding data presented in three figures; Figure 4.3.6-Figure 4.3.8 show results for the PEER-4150 test, Figure 4.3.9-Figure 4.3.11 for the PEER-2250 test, and Figure 4.3.12-Figure 4.3.14 show results for the PEER-0995 tests. The first two figures for each specimen consists of four individual plots, one of the experimental data, two of simulated responses, and one comparing predicted and experimental response envelopes. These figures enable the evaluation of the simulation results in terms of strength, initial stiffness, and damage prediction. The third figure for each specimen compares the simulated and observed joint shear stress-strain, and shows the simulated bar-slip response for the beam and column steel. For the CD30-2250 and PADH-2250 specimens, subjected to non-structural load histories, only load-displacement data are presented. Figure 4.3.15 shows data for CD30-2250, while Figure 4.3.16 shows data for PADH-2250.

PEER-4150

Evaluation of the PEER-4150 test specimen and experimental load-displacement data indicate that the maximum column shear carried by the specimen was well below that required to develop nominal flexural strength of the beams. Observation of damage, as provided by Alire (2002), indicates that at a drift demand of 1.75% during the first load cycle to a maximum drift demand of 2%, the joint experienced significant spalling. During subsequent load cycles, the joint accumulated additional damage, exhibited a slight increase in strength, and maintained this reduced strength to a drift level of 2%. Strain gage data shows that the beam reinforcing steel yielded at the 1.75% drift level and continued to accumulate plastic strain. Despite the fact that the beam steel yielded, the maximum moment demand on the beam was 4467.13 kip-inches, which was well below the nominal flexural strength of 6819.32 kip-inches. Thus, it is assumed that beam bar yielding was due to the opening of cracks within the joint.

The observed damage indicates that the specimen experienced a shear failure of the joint. Thus the *RS-MnJ* and *UW-MnJ-BS* models could be expected to more accurately model the strength of the cruciform while the *RS-MnB* and *UW-MnB* models could be expected over-estimate the specimen strength. The simulation data presented in Figure 4.3.6 and Figure 4.3.7 and Table 4.3.2 conform to these expectations. Figure 4.3.6(d) and Figure 4.3.7(d) and Table 4.3.2 show that for joints with high joint shear stress demand the *RS-MnJ* and *UW-MnJ-BS* models more accurately predict the overall cruciform strength and the system stiffness at drift levels up to 4%. Beyond this point, the models consistently predict a rapid deterioration in joint strength that is not observed.

The data in Figure 4.3.8 show that for the *UW-MnJ-BS* model, the beam bar-slip springs are loaded to approximately 2/3 of the yield slip, while column bar-slip springs just reach the yield point, which is what was observed. Thus, response is determined primarily by joint panel shear response, and the response predicted using the *RS-MnJ* and *UW-MnJ-BS* models are fairly similar.

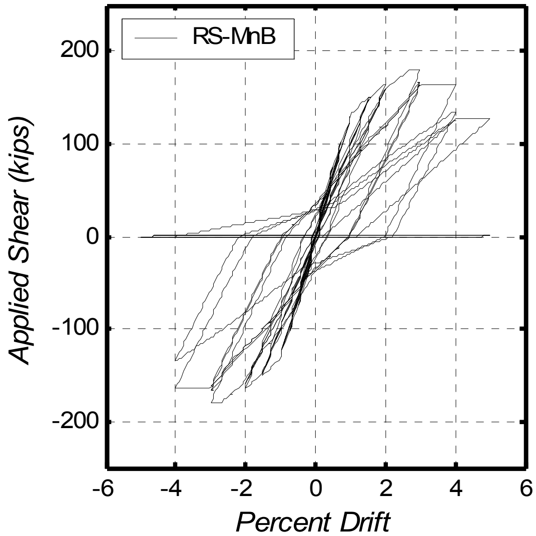

(b)

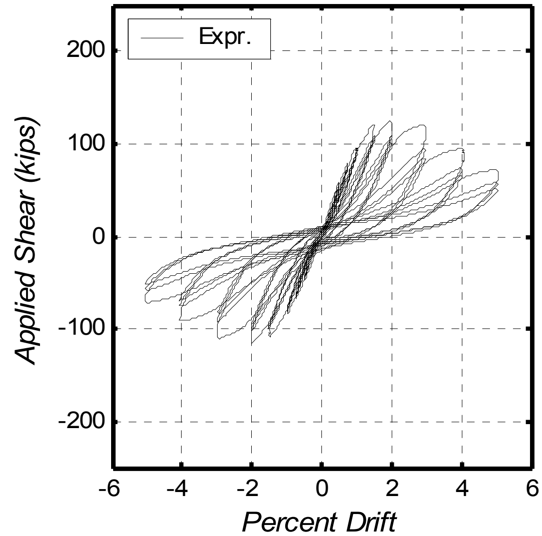

(a)

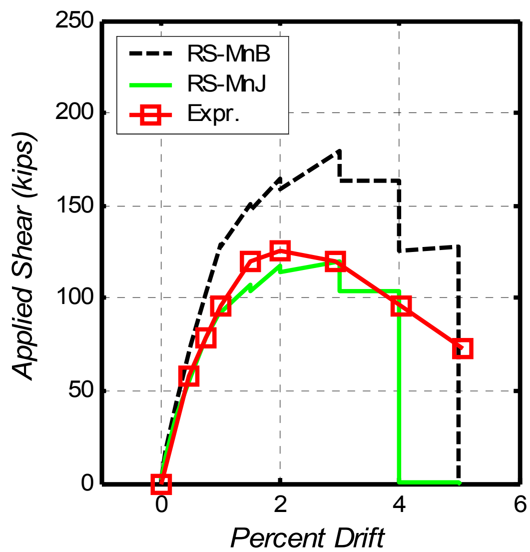

(d)

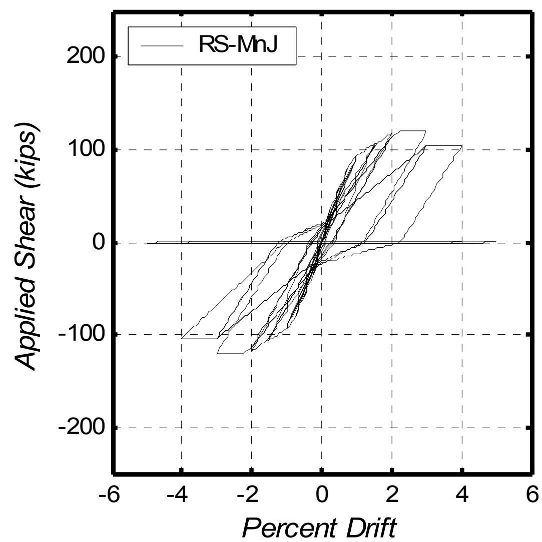

(c)

Figure 4.3.6: Cruciform shear strength vs. Drift data for (a) PEER-4150 Experiment (b) PEER-4150 *RS-MnB* and (c) PEER-4150 *RS-MnJ*. (d) Comparison of Cruciform shear strength envelopes.

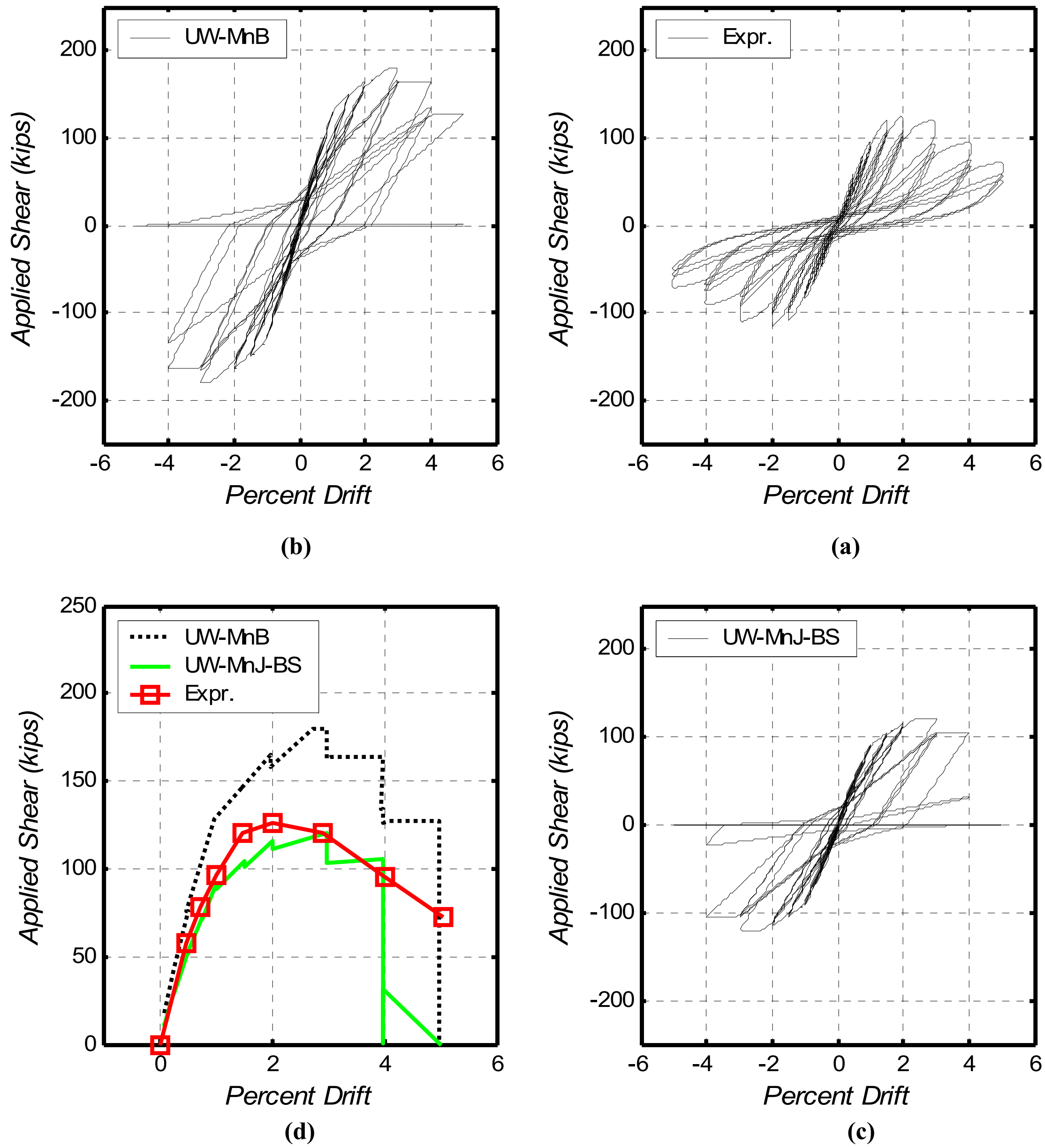

Figure 4.3.7: Cruciform shear strength vs. Drift data for (a) PEER-4150 Experiment (b) PEER-4150 *UW-MnB* and (c) PEER-4150 *UW-MnJ-BS*. (d) Comparison of Cruciform shear strength envelopes.

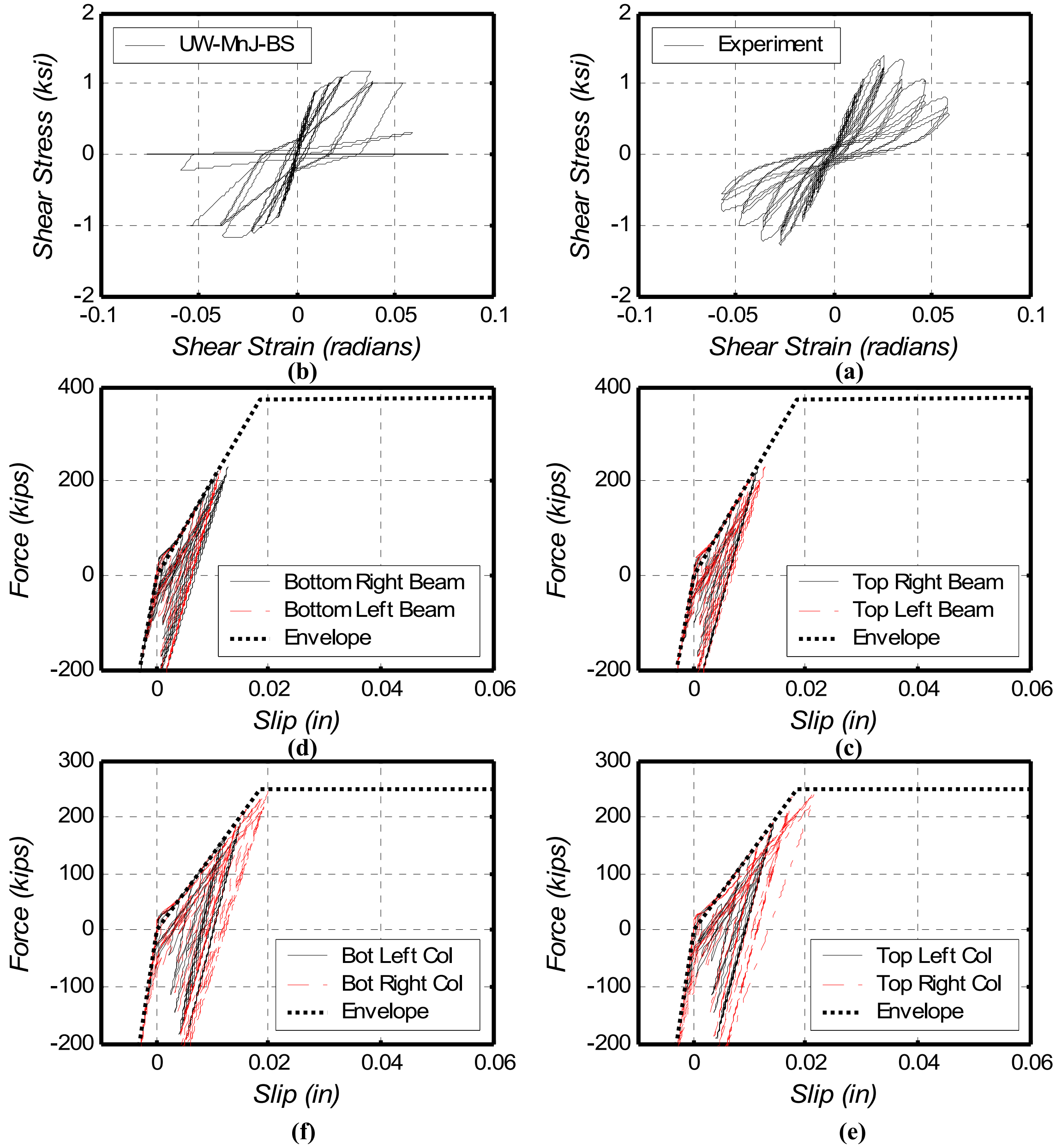

Figure 4.3.8: Experimental stress-strain response of (a) the joint panel. Simulated response of (b) the joint panel (c) top beam steel (d) bottom beam steel (e) top column steel (f) bottom column steel for the 4150 *UW-MnJ-RS* formulation.

PEER-2250

Evaluation of the PEER-2250 test specimen and experimental load-displacement data indicates that the beam longitudinal reinforcement yielded prior to the center of the joint spalling. Since concrete steel bond strength deteriorates when reinforcing steel yields, this suggests that the specimen may have failed due to joint shear failure or bar-slip or both.

The damage observed by Walker (2001) indicates that the specimen experienced joint cracking during the 0.5% drift cycles and yielding of the beam reinforcement bars during the first cycle at the 1.5% drift level. At the point the beam steel yielded, beam moment demand was 2646.74 kip-in, which coincides closely to the determined nominal strength of 2629.35 kip-in. During subsequent load cycles, the joint accumulated additional damage and exhibited a slight increase in strength to a drift level of 2% at which point initial spalling occurred. This strength was maintained to a drift level of 3% at which point extreme spalling occurred and the cruciform softened.

From the quantitative comparison in Table 4.3.2, all four simulation approaches achieve the same level of accuracy. They each are weak in modeling either the K_i or V_{max}, but otherwise they displace similar predicted values. A more useful comparison can be made qualitatively, particularly in terms of the joint failure mechanism. Looking at the simulation results from the various joint models in Figure 4.3.9-Figure 4.3.10 indicate the impact of modeling the bar-slip action for this cruciform. The three models without bar-slip action: *RS-MnJ*, *RS-MnB*, and *UW-MnB*, adequately simulate the initial phases of the specimen response, but fail to model the strength and stiffness degradation that dominates the experimental data at and beyond 2% drift. Figure 4.3.9(b)-(c), and Figure 4.3.10(b) show little degradation in the specimen stiffness and a specimen strength that is either continually increasing because the simulated joint panel failed to reach its yield strength, or has just begun to deteriorate at 5% drift. The fourth model, *UW-MnJ-BS* explicitly models the bar-slip, and the result is shown in Figure 4.3.10(c). This model with bar-slip springs predict dramatic strength and stiffness degradation beyond 3% drift. This simulated loss of cruciform shear strength corresponds to the rapid strength degradation of the beam bar-slip springs when they go beyond a deformation threshold of 0.12” as presented in Figure 4.3.11(d). The response of the joint shear panel remains linear as shown in Figure 4.3.11(b), thus the bar-slip is the primary joint failure mechanism. The differences in the positive and negative specimen response in Figure 4.3.10(c) are to differences in the predicted bar-slip response for the bottom bars of the right and left beams. Figure 4.3.11(d) shows that the spring representing the reinforcement at the bottom of the left beam fails to predict strength and stiffness degradations comparable to those for the right beam.

The PEER2250 laboratory specimen experiences a failure following the yielding of the beam longitudinal reinforcement. These observed results suggest the anchorage failure likely contributes to joint shear strength deterioration. This failure is simulated by the *UW-MnJ-BS* model which predicts strength loss due to bond failure for the yielded beam reinforcing steel. However, the simulation results show that while the *UW-MnJ-BS* model succeeds in predicting the initiation of strength and stiffness loss, it fails to accurately predict the rate of observed strength and stiffness degradation. Also, the model fails to capture the observed symmetry of the observed load-displacement response.

Thus, all of the joint formulations succeed in predicting the specimen response up to 1.5-3.0% at which time significant damage occurs. Only the *UW-MnJ-BS* model successfully predicts the observed initiation of joint strength loss at the 3.0% drift level. The *UW-MnJ-BS* model attributes strength loss to anchorage failure of beam steel, a likely source of deterioration. However, the model predicts a rapid strength loss and damage accumulation on one side of the joint that are not observed in the laboratory. Thus, none of the models succeed in accurately predicting observed response of the PEER2250 specimen.

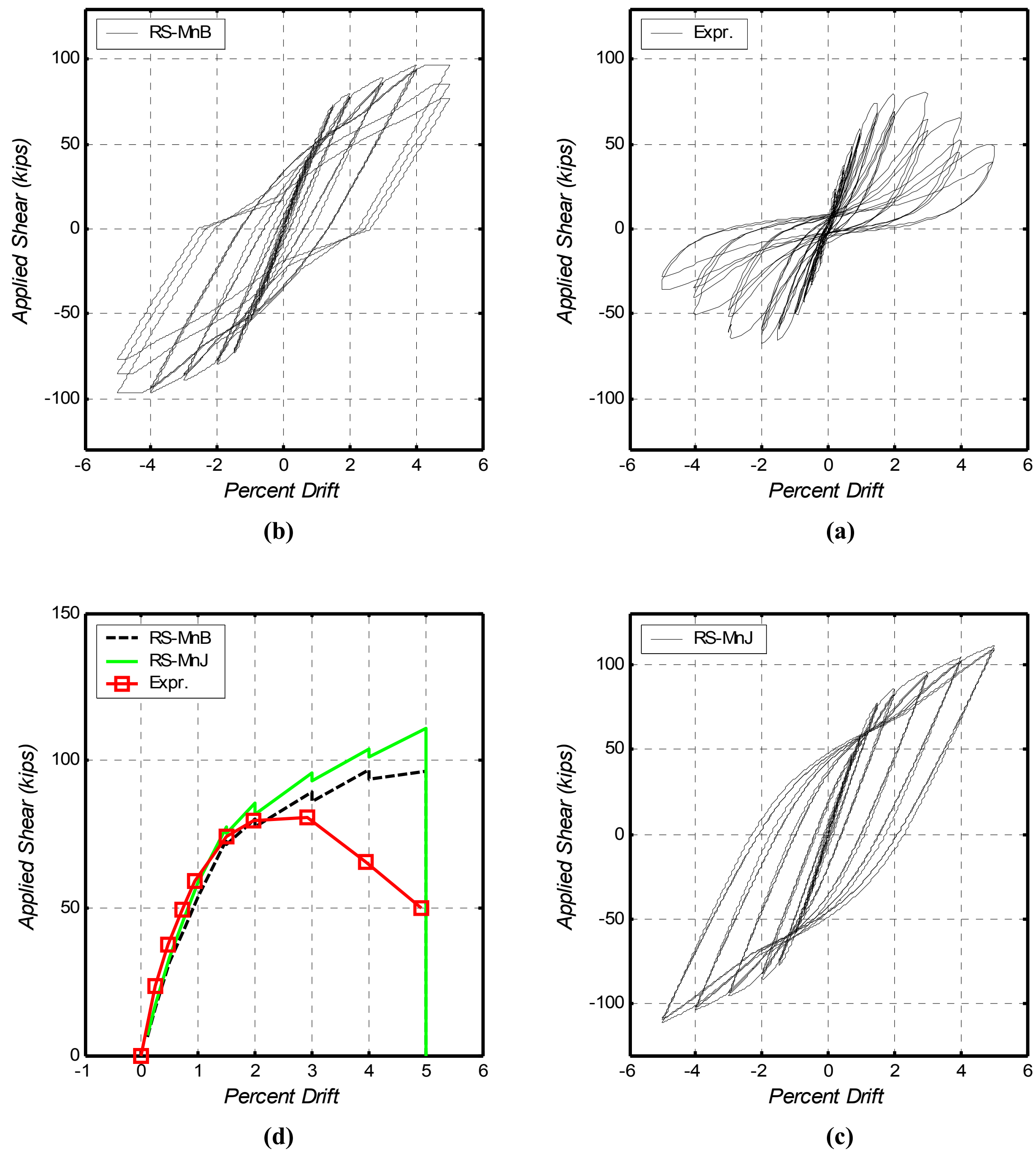

Figure 4.3.9: Cruciform shear strength vs. Drift data for (a) PEER-2250 Experiment (b) PEER-2250 *RS-MnB* and (c) PEER-2250 *RS-MnJ*. (d) Comparison of Cruciform shear strength envelopes.

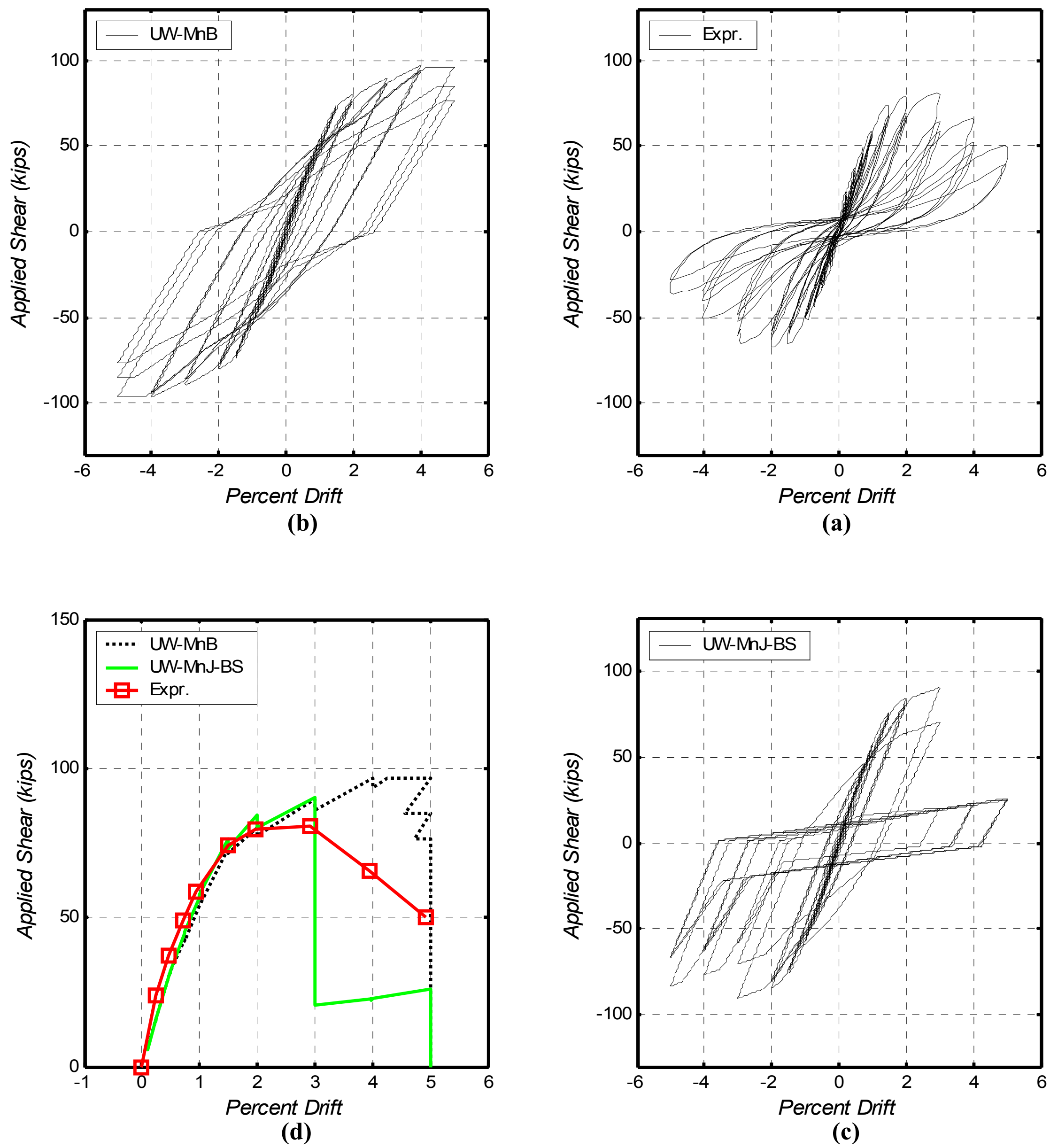

Figure 4.3.10: Cruciform shear strength vs. Drift data for (a) PEER-2250 Experiment (b) PEER-2250 *UW-MnB* and (c) PEER-2250 *UW-MnJ-BS*. (d) Comparison of Cruciform shear strength envelopes.

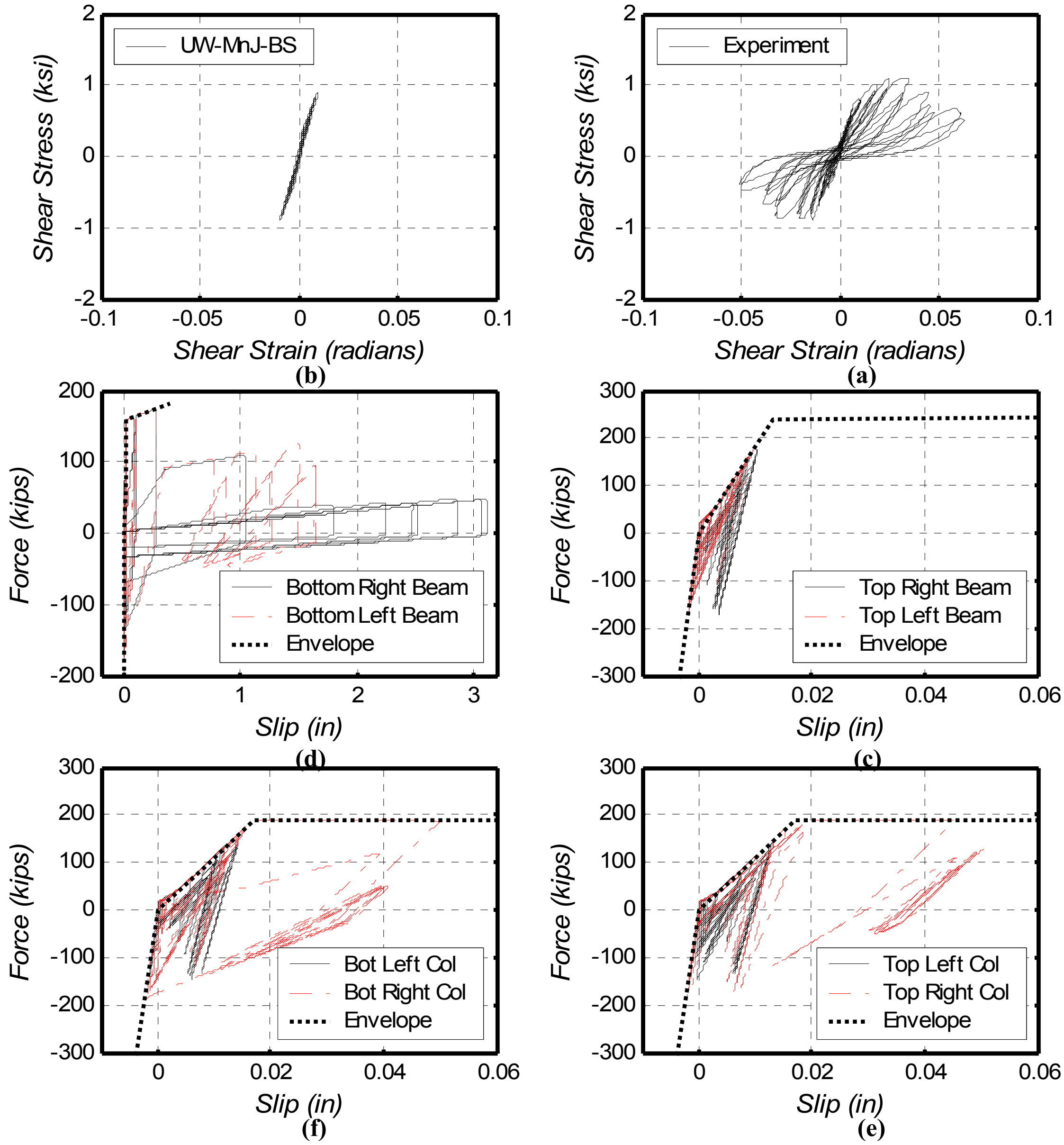

Figure 4.3.11: Experimental stress-strain response of (a) the joint panel. Simulated response of (b) the joint panel (c) top beam steel (d) bottom beam steel (e) top column steel (f) bottom column steel for the 2250 *UW-MnJ-RS* formulation.

PEER-0995

Evaluation of the PEER-0995 test specimen damage and experimental load-displacement data as provided by Alire (2002) indicate that the specimen failed due to bar-slip the beam longitudinal reinforcement. Below the observed results are summarized.

Alire (2002) indicates that center joint cracking occurs at the first positive peak to 0.5% drift. Cracking patterns which form around the layers of tensile reinforcement also indicated the initial loss of bond at this drift level. Furthermore, yielding of the longitudinal beam reinforcement bars was determined to occur at 0.81% drift during the first positive peak at the 1.0% drift level. At this point, the moment demand on the beams is determined to be 2678.99 kip-in, which is in close agreement with the nominal strength of 2313.80 kip-in. Initial spalling of the specimen began during the 2.0% drift levels and progressed until extreme spalling occurred at the 3.0% drift levels. The fact that the longitudinal beam reinforcing steel yielded prior to the center joint spalling is another indication the PEER-0995 specimen failed due to loss of bond through the joint for the beam bars.

From the quantitative comparison in Table 4.3.2, the two *MnB* simulation approaches seem to more accurately predict the 0995 response. The *RS-MnJ* and the *UW-MnJ-BS* models predict K_i more accurately, but the *MnB* approaches do a better job of predicting V_y, V_{max}, K_{max}, and V_u. All the models have difficulty consistently predicting the crucial drift values, and the *RS-MnJ* fails to predict a d_{Vu} and a V_u because it does not predict any joint failure.

The qualitative comparison of the PEER-0995 simulations further clarifies the preferred models. The two models *RS-MnB*, and *UW-MnB* in Figure 4.3.12-Figure 4.3.13 adequately simulate the initial phases of the specimen response. They do not predict degradation in the specimen stiffness and strength, however before 5% drift as shown in Figure 4.3.12(b)-(c), and Figure 4.3.13(b). As discussed earlier, this is indicative of the models failure to predict the crucial drift values. In contrast, the *RS-MnJ* model predicts on joint failure. The fourth model, *UW-MnJ-BS* explicitly models the bar-slip as a likely sources of strength and stiffness degradation, but as Figure 4.3.13(c) shows, the simulation slightly under predicts the maximum specimen strength and the deterioration rate is extremely rapid. Furthermore, the simulation fails to run beyond 2.0% drift for this model due to convergence issues with multiple non-linearities.

The PEER-0995 laboratory specimen experiences a failure that is apparently associated with the yielding of the beam longitudinal reinforcement, and therefore the *UW-MnJ-BS* is asserted as the best joint formulation to simulate the joint response due to the explicit modeling of the bar-slip. The *UW-MnJ-BS* model proves to be more appropriate than *RS-MnJ* for modeling joints with low joint shear stress demand. However, the rapid degradation predicted by *UW-MnJ-BS* and the computational difficulties beyond 2.0% drift indicate that the simple, more robust models, *RS-MnB*, and *UW-MnB*, are a more desirable choice for immediate practical implementation for the prediction of the specimen response.

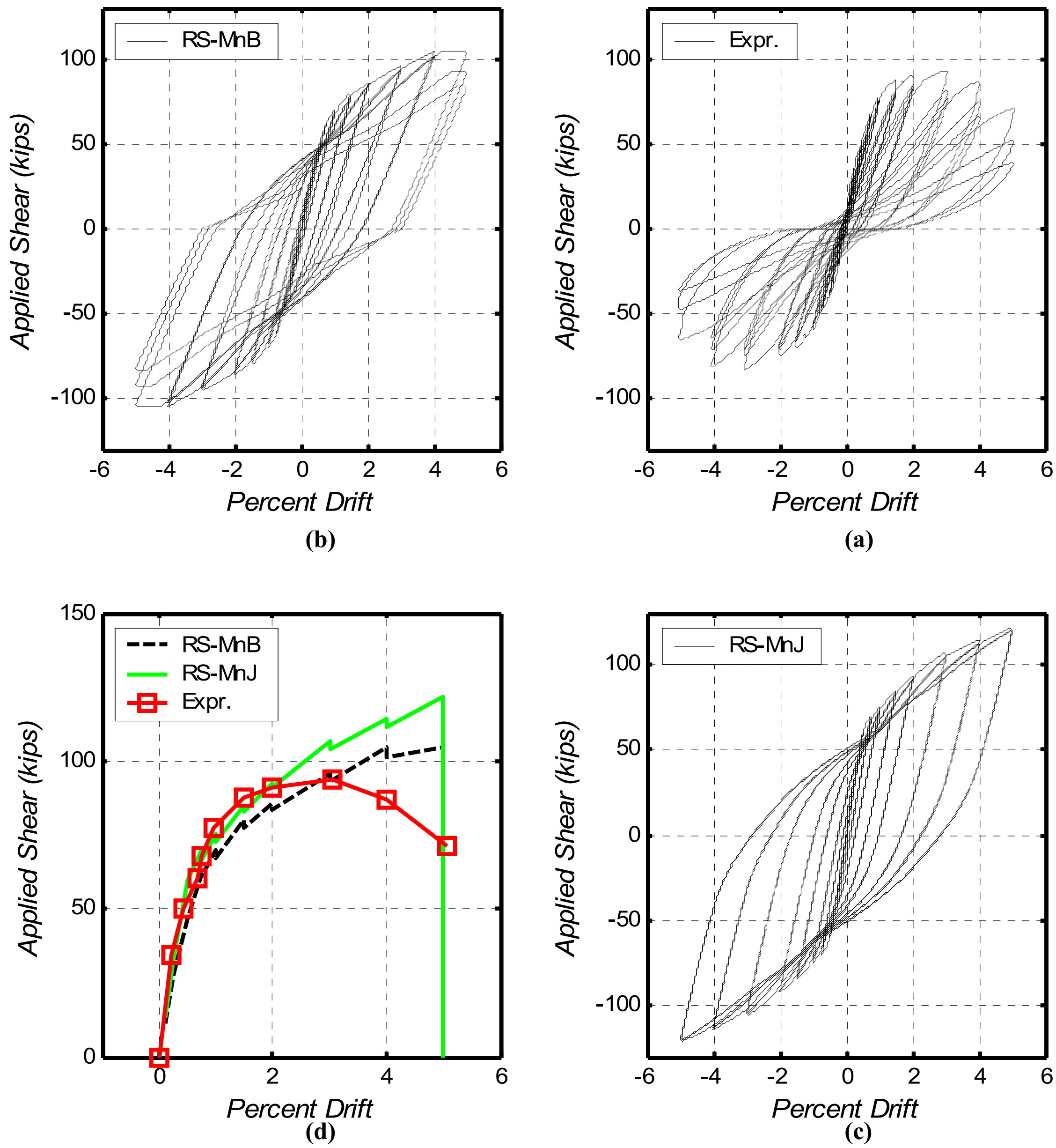

Figure 4.3.12: Cruciform shear strength vs. Drift data for (a) PEER-0995 experiment (b) PEER-0995 *RS-MnB* and (c) PEER-0995 *RS-MnJ*. (d) Comparison of cruciform shear strength envelopes.

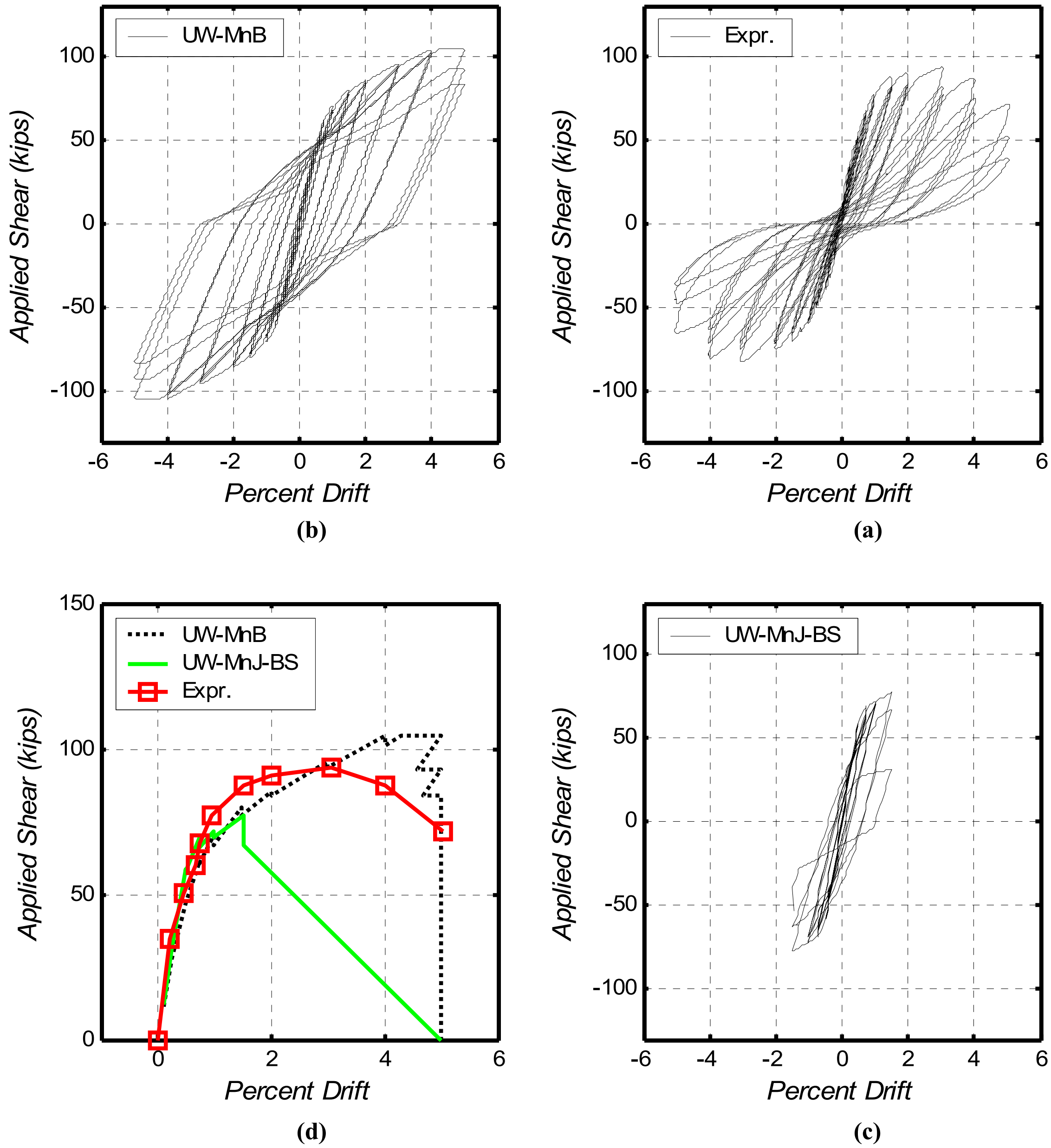

Figure 4.3.13: Cruciform shear strength vs. Drift data for (a) PEER-0995 experiment (b) PEER-0995 *UW-MnB* and (c) PEER-0995 *UW-MnJ-BS*. (d) Comparison of cruciform shear strength envelopes.

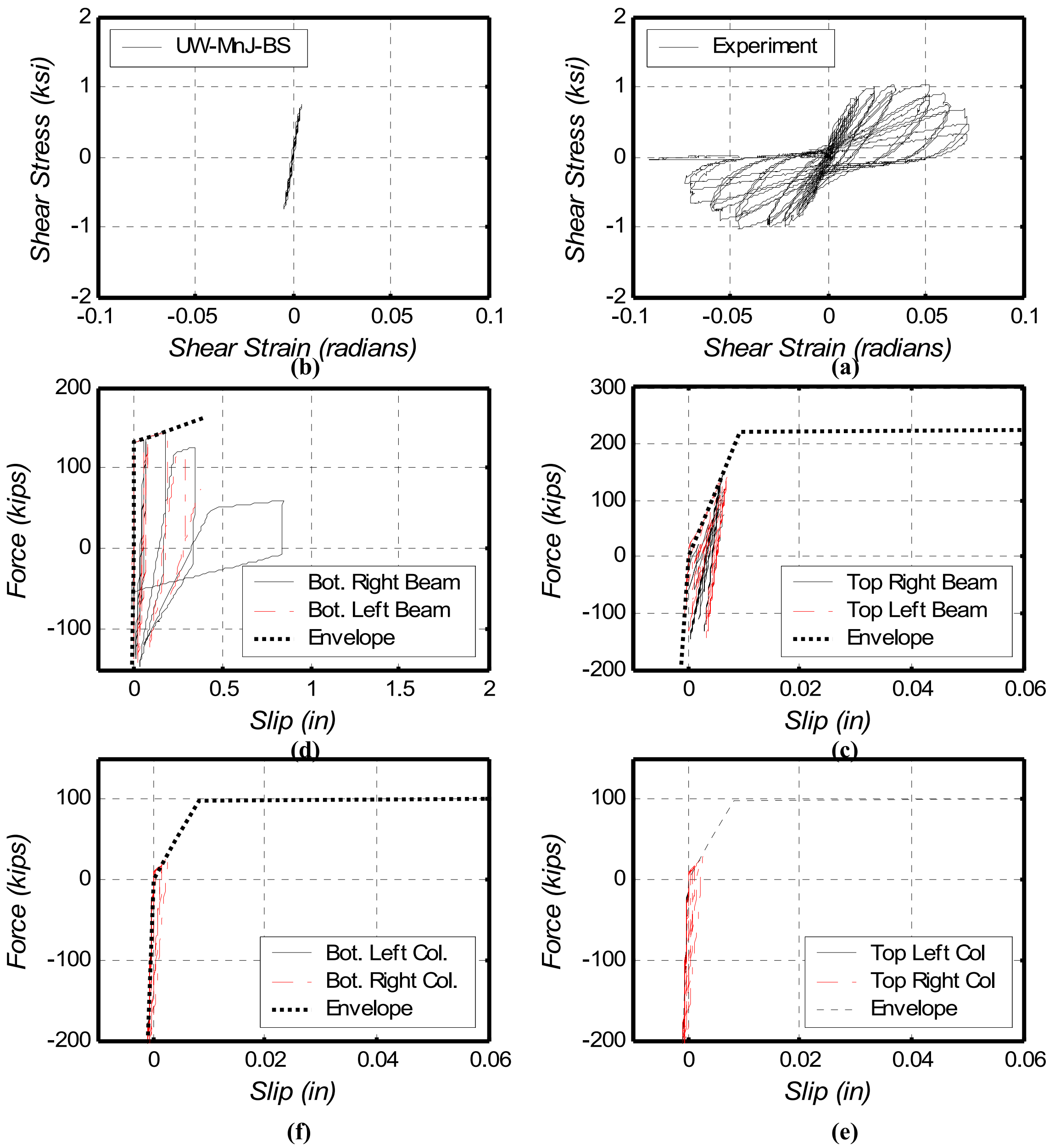

Figure 4.3.14: Experimental stress-strain response of (a) the joint panel. Simulated response of (b) the joint panel (c) top beam steel (d) bottom beam steel (e) top column steel (f) bottom column steel for the 0995 *UW-MnJ-RS* formulation.

CD30-2250

Evaluation of the CD30-2250 test specimen and experimental load-displacement data indicate that the beam longitudinal reinforcement yielded prior to the center of the joint spalling. As with the PEER-2250, this specimen failed due to the deterioration of bond between the reinforcement and the joint core concrete. Observation of damage, as provided by Walker (2001), indicates that during the first cycle to a drift demand of 3% yielding of the beam bars occurred at a drift demand of 1.14%. At the point the beam steel yielded, beam moment demand was 2770.42 kip-in, which is within 5% of the calculated nominal strength of 2629.35 kip-in. Joint cracking and spalling, corner cracks, and cracking along the beams and columns were also observed. Within the next two cycles to 3% drift, approximately 80% of the joint concrete spalled and much of the column reinforcement bars were exposed. By the end of the test, a 70% reduction in specimen strength was realized and a 1" offset between the upper and lower columns was observed.

Simulation data of the CD30-2250 specimen are presented in Figure 4.3.15 for the four preferred joint models. This figure directly compares the observed and simulated results. From the four subplots of Figure 4.3.15 and the comparison ratios in Table 4.3.2, one can say that the *RS-MnB* and *UW-MnB* models predict the response better than the *RS-MnJ* model. The *UW-MnJ-BS* model also appears to model the response well, while in fact it does not make it through the first full cycle, as shown in Figure 4.3.15(a) due to convergence issues. Nonetheless, all four joint models predict the yield strength within 5% of the observed values. However, the initial stiffnesses, maximum strength, unloading stiffnesses and critical drifts are slightly off of the observed values (5-25%). Even with these discrepancies, the largest issue is in regards to the predicted deterioration behavior. The *RS-MnB* and *UW-MnB* models do not predict significant strength or stiffness degradation until the final three cycles at 5% drift. The simulations fail to predict the extensive degradation that occurs at the later cycles at 3% drift. The *RS-MnJ* model in particular predicts no joint degradation at all.

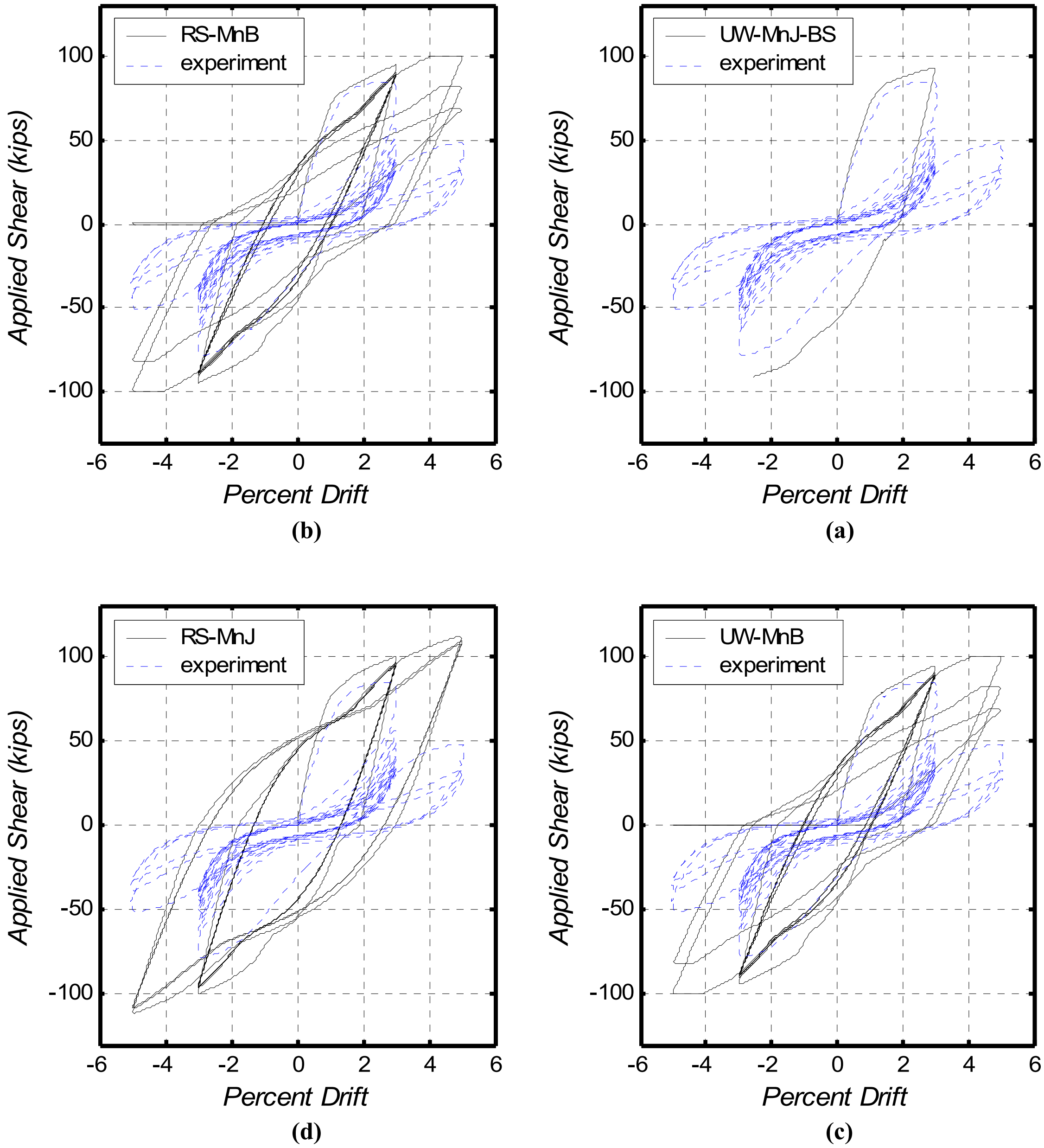

Figure 4.3.15: Comparison of cruciform shear vs. % drift between the observed *CD302250* and the (a) *UW-MnJ-BS* model (b) *RS-MnB* model (c) *UW-MnB* model and (d) *RS-MnJ* model.

PADH-2250

Evaluation of the PADH-2250 test specimen and experimental load-displacement data indicate that the beam longitudinal reinforcement yielded prior to the center of the joint spalling. As with the PEER-2250 and the CD30-2250 before, this suggests that there is the potential for anchorage failure to determine response. Observation of damage, as provided by Walker (2001), indicates that during the first positive cycle to a drift demand of 5% yielding of the beam bars occurred at a drift demand of 1.16%. At the point the beam steel yielded, beam moment demand was 2729.45 kip-in, which is within 5% of the calculated nominal strength of 2629.35 kip-in. As with the CD30-2250 specimen, joint cracking and spalling, corner cracks, and cracking along the beams and columns were also observed. The following six asymmetric cycles to a positive 1.5% and 3.0% drift did not result in an increase in crack number or length. The six cycles to negative 1.5% and 3.0% drift did result in some minor increase in crack length and number. New cracks in the beams formed in twelve inch intervals. The center longitudinal column bar was exposed in the joint during the first cycle to negative 5% drift, and extensive damage accumulated in the joint there after.

Simulation data for the PADH-2250 specimen are presented in Figure 4.3.16 for the four preferred joint models. The comparison approach is the same as that used with the CD30-2250. The four subplots of Figure 4.3.16 and the comparison ratios in Table 4.3.2 are used to make the qualitative and quantitative comparisons. As with the CD30-2250, all four joint models predict the yield strength within 5% of the observed values even though the *UW-MnJ-BS* model does not make it through the first full cycle due to convergence issues. Also, the initial stiffnesses, maximum strength, unloading stiffnesses and critical drifts are slightly off of the observed values (5-25%). As with the previous specimen simulations, the most significant issue is in regards to the predicted deterioration behavior. The *RS-MnB* and *UW-MnB* models fail to predict the rate of strength and stiffness degradation. The *RS-MnJ* model does not predict a joint failure and thus predicts no strength and stiffness degradation.

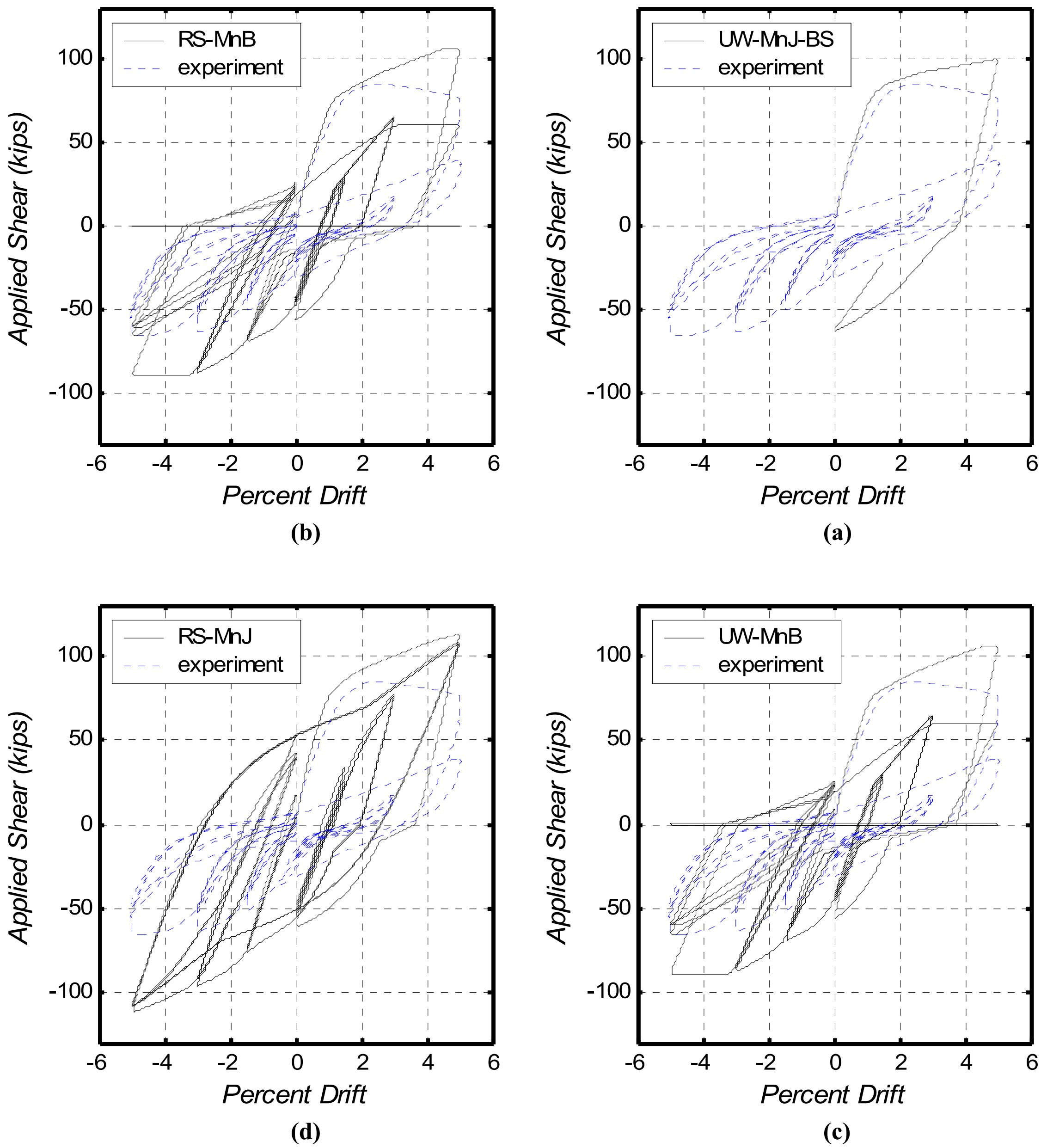

Figure 4.3.16: Comparison of cruciform shear vs. % drift between the observed *PADH2250* and the (a) *UW-MnJ-BS* model (b) *RS-MnB* model (c) *UW-MnB* model and (d) *RS-MnJ* model.

4.4. Summary and Conclusions

Summary

Four joint models have been used to simulate five cruciform tests with under-reinforced joints at the University of Washington (Walker 2001 and Alire 2002). The simulations have been used to evaluate the different joint models to determine the most desirable joint modeling approaches.

Conclusions

Of the four primary joint models tested, the preferred models are *RS-MnB* and *UW-MnJ-BS*. These models balance computational demand with model complexity and objectivity to represent adequate joint simulations. *RS-MnJ* fails to predict the joint failure for joints experiencing low shear stress demand, while *UW-MnB* is more computationally demanding than *RS-MnB* without any apparent advantages. Chapter 5 explains how the preferred models were implemented in a full-frame analysis of the case study building, the Van Nuys Holiday Inn, and discusses the impact on joint modeling on seismic simulation of older reinforced-concrete buildings.

One weakness of all four models is the rate of strength and stiffness degradation. Figure 4.3.6 through Figure 4.3.16 illustrate that the models are not calibrated to predict joint failure at the correct drifts, or not at all as in the case of the *RS-MnJ* model. When the models do predict joint failure, the result is rapid degradation of the cruciform shear strength and stiffness. In the case of the *UW-MnJ-BS* model for specimens with low joint shear stress demand, this degradation is dramatic and leads to convergence issues within the model. Nonetheless, the implementation of the preferred joints in not unreasonable given the high level of joint shear stress demand calculated in the case study and the acceptable model predictions for this type of joint.

Chapter 5

Seismic Joint Behavior in the Case Study Building

5.1. Introduction

Chapter 5 uses the two preferred joint models, *RS-MnB* and *UW-MnJ-BS*, identified in Chapter 4 to simulate the earthquake response of the case study building, the Van Nuys Holiday Inn. The two joint models are first used to simulate the response of a sub-assemblage from the exterior frame of the structure, and then to simulate the response of an exterior frame subjected to monotonic and dynamic loading.

This exercise of the modeling-building process identifies all modeling decisions that must be made and provides an opportunity to create OpenSees input scripts for use in sub-assemblage or full-frame analyses. The results of the sub-assemblage analyses provide understanding of expected joint behavior in the full-frame analyses and help to identify response characteristics and numerical issues that may affect prediction of full-frame response. Then, the models are incorporated in a full-frame model of the case study building and used in a series of analyses to determine frame response under pseudo-static and in dynamic loading. The impact of the joint model type and joint model damage parameters on building response is considered. Additionally, the impact of the simulation of brittle column failure, variation in gravity load, and variation in earthquake load intensity on a building with inelastic joints is considered. Building response is defined in terms of inter-story drift and roof drift.

5.2. Joint Cruciform Simulation Details

The response of a joint sub-assemblage from the external frame of the case study building is simulated using a sub-assemblage with the same configuration, boundary conditions, and loading history as was used for the cruciform analyses discussed in

Section 4.2 (see Figure 4.2.2). The sub-assemblage used here represents the third story joint from column line A6 of the building. This joint was chosen because it has geometry and reinforcement layout that is typical of the joints in the case-study building. OpenSees was used to simulate sub-assemblage response under pseudo-static analyses using the PEER load history. The assumptions and parameters used to model the cruciform are discussed in the following sections.

5.2.1. Modeling Assumptions and Parameters

Geometry, Boundaries, and Loading

The sub-assemblage geometry for the case study building is shown in Figure 5.2.1 and summarized in Table 5.2.2. The building consists of flat plate construction with eccentric spandrel beams placed flush with the interior face of the columns as shown in Figure 5.2.2. The resulting geometry of the joint region is complex, and a number of assumptions are made in developing the sub-assemblage model:

- The cruciform comprises the joint, the beams framing into the joint extended to mid span and the columns framing into the joint extended to mid-height. Earthquake loading is applied as a shear at the top of the column and reacted as shears at the cruciform beam and column ends. As discussed in Chapter 4, this is representative of the load distribution that develops in the full-frame if earthquake loads result in inflection points forming at beam mid-span and column mid-height.
- The slab does not contribute to the flexural strength or stiffness of the beam. Thus, only the spandrel beams and the columns are included in the sub-assemblage model.
- No beam and/or column eccentricity is included. The beam centerline is assumed to intersect with the column centerline, and the eccentricity of the beams is removed. Refer to Figure 5.2.1 and Table 5.2.2.

The loading parameters used to model a cruciform sub-assemblage of the Van Nuys building include:

- the axial load, P, is equal to 199.8 kips based on the gravity loading at this level of the building.
- the PEER pseudo-dynamic load history is applied (refer to Appendix C).

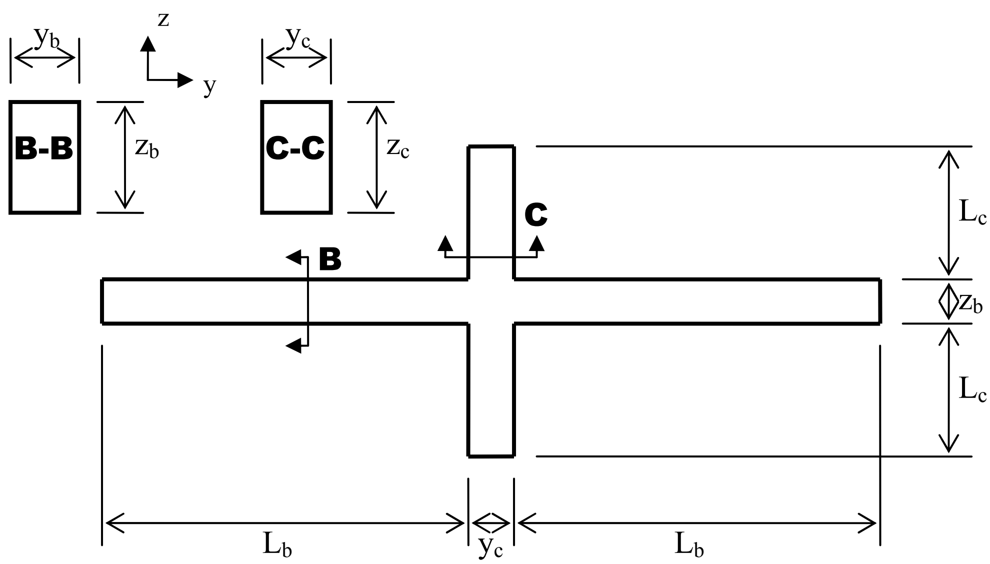

Figure 5.2.1: Geometry of Van Nuys cruciform model.

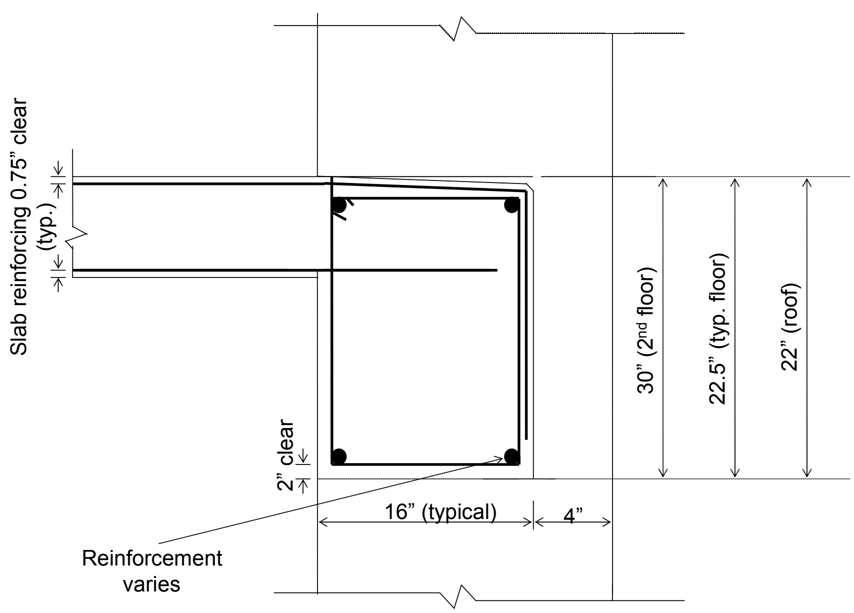

Figure 5.2.2: Longitudinal spandrel beam cross-section with joint eccentricity (NOAA report 1973)

Table 5.2.1: Geometry parameters for the Van Nuys cruciform.

Column Parameter	Values	Beam Parameter	Values
L_c	41.0”	L_b	105.5”
z_c	20.0”	z_b	22.5”
y_c	14.0”	y_b	16.0”

Beam and Column Modeling

The beam and column segments included in the sub-assemblage were modeled using the *beamWithHinges2* element from OpenSees. A detailed discussion of the element is provided in Section 2.4. This model requires definition of a section model that defines the inelastic response of the member sections at each end of the element, a plastic hinge length that defines the length at each end of the element over which inelastic section response extends, and elastic section geometry and material properties.

Table 5.2.2 contains geometric and material properties used to define the elements. The plastic hinge length was computed using *0.5h* (See Section 4.2.3). All other geometric properties were computed using gross section properties and previous assumptions. The material properties of the elements are computed using E_c equal to $57{,}000\sqrt{f_c'}$ (ACI318-02) and Poisson’s ratio, v, equal to 0.175 (Hibbeler 2002).

In doing the full-frame analysis of the Van Nuys building, it was found that the elastic stiffness required adjustment to bring the initial, first mode period of the structure into agreement with the value computed from response records at the beginning of the Northridge earthquake (Paspuleti, 2002). The same stiffness adjustments were made to the cruciform model. The adjustment factors used were $\alpha_{flex} = 0.279$ for flexure, $\alpha_{axial} = 0.558$ for axial, $\alpha_{shear} = 0.235$ for shear, and $\alpha_{torsion} = 0.558$ for torsion. The gross stiffnesses are multiplied by the adjustment factors, as shown in Equation 5.2.1-Equation 5.2.4 to get the effective stiffness that are used in the analyses.

$$EI_{eff} = EI_g \bullet \alpha_{flex} \quad \textbf{Equation 5.2.1}$$

$$EA_{eff} = EA_g \bullet \alpha_{axial} \quad \textbf{Equation 5.2.2}$$

$$J_{eff} = J_g \bullet \alpha_{torsion} \quad \textbf{Equation 5.2.3}$$

$$G_{eff} = G_g \bullet \alpha_{shear} \bullet \alpha_{axial} \quad \textbf{Equation 5.2.4}$$

Table 5.2.2: Elastic modeling parameters for the Van Nuys cruciform.

Column Parameter	Values	Beam Parameter	Values
Hinge length	11.525”	**Hinge length**	21.375”
E_{col} (ksi)	3823.20	**E_{bm}(ksi)**	3823.20
G_{col} (ksi)	1627.81	**G_{bm} (ksi)**	1627.81
$I_{y\ col}$ (in^4)	9333.33	**$I_{y\ bm}$ (in^4)**	15187.50
$I_{z\ col}$ (in^4)	4573.33	**$I_{z\ bm}$ (in^4)**	7680.00
J_{col} (in^4)	18293.33	**J_{bm} (in^4)**	60750.00

Other beam and column modeling assumptions include:

- Spliced column longitudinal steel does not exhibit splice failure. Despite, as discussed in Chapter 2, the inadequacies of the splices in the case study building, modeling of splice failure is not included in the sub-assemblage simulations.
- Columns do not fail in shear. Despite the inadequate transverse reinforcement provided in the design of the columns, shear failure is not included in the sub-assemblage simulations.

Beam and Column Section Response Modeling

Table 5.2.3 gives the parameters used to define the sections of the beams and columns. The positive and negative nominal moment strengths of the cruciform’s beams and columns are also given. The sections consist of steel and concrete materials. Table 5.2.4-5 present the parameters used to model the concrete and steel reinforcement, respectively. Only unconfined concrete is modeled. All concrete is assumed to be unconfined due to the inadequate transverse reinforcement that characterizes the case study building. Refer to Section 4.2.2 for explanations of the material parameters and the *Steel02* and *Concrete01* models used. Other parameters and assumptions impacting section response include:

- The model does not simulate the loss of strength due to buckling and fracturing of the beam and column longitudinal steel.
- Concrete crushing strength, f_{cu}, is 20% of the compressive strength, f'_c and the concrete has no tensile strength.

Table 5.2.3: Van Nuys Cruciform section modeling parameters.

Column Section Parameters	Values	Beam Section Parameters	Values
Total # rebar	6	**Total # rebar**	5
# rebar: top	2	**# rebar: top**	3
# rebar: middle	2	**# rebar: middle**	0
# rebar: bottom	2	**# rebar: bottom**	2
rebar area: top (in^2)	0.99	**rebar area: top (in^2)**	0.79
rebar area: middle (in^2)	0.99	**rebar area: middle (in^2)**	0.00
rebar area: bottom (in^2)	0.99	**rebar area: bottom (in^2)**	0.44
max fiber size (in.)	0.50	**max fiber size (in.)**	0.50
Conc. cover	2.563”	**Conc. cover**	2.563”
yield strength (+) (k-in)	2198.95	**yield strength (+) (k-in)**	2381.29
yield strength (-) (k-in)	2198.95	**yield strength (-) (k-in)**	959.13

Table 5.2.4: Concrete material modeling parameters (confined and unconfined).

Concrete Material Parameters	Van Nuys Cruciform			
	Columns		Beams	
	Unconfined	Confined	Unconfined	Confined
f'_c (psi)	-4783.0	-6242.553	-4783.0	-6230.355
ε_c	-0.002	-0.002610	-0.002	-0.002605
f'_{cu} (psi)	-3343.076	-1248.511	-3343.076	-1246.071
ε_{cu}	-0.004	-0.048688	-0.004	-0.048316

Table 5.2.5: Steel material modeling parameters.

Steel Material Parameters	Van Nuys Cruciform	
	Columns	Beams
f_y (psi)	79 e10^3	79 e10^3
E_s (psi)	29 e10^6	29 e10^6
SHR	0.0138	0.0138
R_o / R_1 / R_2	18.5/0.925/0.15	18.5/0.925/0.15
a_1 / a_2 / a_3 / a_4	0/0.4/0/0.5	0/0.4/0/0.5

5.2.2. Joint Model Implementation

On the basis of the results presented in Chapter 4, it was decided that only the *RS* and *UW* joint element formulations with the *MnB* and *MnJ-BS* joint element calibration methods, would be used in the Van Nuys cruciform and full-frame analysis. The calibration of each of the joint models for the Van Nuys sub-assemblage simulation is discussed in the following sections.

Joint Formulation 1: RS-MnB

This joint model includes the rotational spring joint element, *RS*, with the *Pinching4* material model calibrated to a specific Van Nuys joint by way of the nominal beam strengths, M_{nB+} and M_{nB-}. Implementation of the *RS* element and the *Pinching4* material are discussed in Sections 4.2.4-5. Nominal flexural strength was defined per ACI-318 (2002) as the moment developed when the extreme concrete fiber carries a compressive strain of -0.003 in/in. Nominal strengths were computed using OpenSees and verified by hand calculations. Geometric and material properties used in the analyses are listed in Table 5.2.1 through Table 5.2.5. OpenSees material models used in the sub-assemblage models were used in the moment-curvature analyses, and zero axial load was assumed.

To calibrate the rotational spring, M_{nB+} and M_{nB-} are used in Equation 5.2.5 to define the nominal moment strength of the joint, M_{nj} as:

$$M_{nj} = (M_{nB-} + M_{nB+}) - (V_c \bullet jd) \qquad \textbf{Equation 5.2.5}$$

where V_c, is the column shear when one of the beam is loaded to M_{nB+} or M_{nB-}, and jd is distance between resultant tension-compression couple that develops in the beam cross-section at the joint face. For these analyses, jd is assumed equal to 0.85 (MacGregor 1997). V_c is defined by applying equilibrium to an idealized cruciform:

$$V_c = (2 \bullet M_{nB}) / L_c \qquad \textbf{Equation 5.2.6}$$

where M_{nB} is the lesser of M_{nB+} or M_{nB-} and L_c is the distance between the assumed points of inflection in a continuous column. M_{nj} and the parameters listed in Table 4.2.6 define the backbone curve used in the *Pinching4* material model. The remainder of the parameters required to complete the definition of the *Pinching4* material model are provided in Table 4.2.9.

Joint Formulation 2: UW-MnJ-BS

The *UW-MnJ-BS* model uses the *beamColumnJoint* element which simulates joint failure due to shear failure of the core and due to anchorage failure. The *beamColumnJoint* employs the *Pinching4* material model to define the response of the shear panel component, eight bar-slip springs, and four interface shear springs that comprise the element. Thus, calibration of the *UW-MnJ-BS* joint model for a joint with specific geometry and design details requires definition of the parameters in the *Pinching4* material model for the specific joint conditions.

The joint model assumes that M_{nj} for a certain joint may be defined using the observed strength of an older reinforced joint of specific volume and concrete strength as shown in Equation 5.2.7:

$$M_{nj} = M_{nj(emp)} \bullet (\sqrt{f'_c} \,/\, \sqrt{f'_{c(emp)}}) \bullet (V_j \,/\, V_{j(emp)}) \qquad \textbf{Equation 5.2.7}$$

where the empirical joint strength, $M_{nj(emp)}$, concrete strength, $f'_{c(emp)}$, and joint volume, $V_{j(emp)}$, equal 7215208.15 lbs-in, 4783.0 psi, and 4608 in^3. These values are taken from the UW PEER 4150 test. f'_c, and V_j are the concrete strength and volume of the joint being modeled. All the other parameters required for the definition of the *Pinching4* material model care taken from Tables 4.2.6 and 4.2.9.

Calibration of the *Pinching4* material model to simulate anchorage failure is done following the work of Lowes and Altoontash (2003). The current implementation of the joint element included this approach and only data defining bar geometry, joint geometry, and material properties are required for model use. Values used for cruciform analyses are listed in Table 5.2.6.

Table 5.2.6: Van Nuys Cruciform bar-slip modeling parameters.

Bar-slip Parameters	Column	Beam, Top	Beam, Bottom
f'_c (psi)	4,500	4,500	4,500
f_y (psi)	50,000	50,000	50,000
E_s (psi)	29,000,000	29,000,000	29,000,000
f_u (psi)	60,000	60,000	60,000
E_h (psi)	580,000	580,000	580,000
Bar diameter	1.12”	1.00”	0.75”
Development length	14.0”	14.0”	14.0”
Number of bars	3	3	2
Joint width	16.0”	16.0”	16.0”
Joint depth	14.0”	22.5”	22.5”
Bar-slip flag	1.0	1.0	1.0
Type	Strong	Strong	Strong
Damage?	Yes	Yes	Yes

The four interface shear springs in the *beamColumnJoint* are set as elastic and stiff for all of the Van Nuys cruciform analyses. A lack of calibration data for these springs results in the conservative assumption that they are rigid.

5.3. Joint Cruciform Simulation Results

Evaluation of the geometry and design of the cruciform sub-assemblage from the case study building suggests a certain response under simulated earthquake loading. In terms of overall strength, the weakness of the beams in negative flexure compared to the relatively strong columns suggests that beam yielding will play an important role. The importance of the beam yielding on overall strength is also suggested by the joint shear stress demand parameters given in Table 5.3.1. The normalized joint shear stress demand, $V_{jt}/\sqrt{f'_c}$, for the case study building cruciform as modeled here is 0.04. This puts the cruciform at the extreme low end of joint shear stress demand spectrum over which the UW PEER tests range, and at this low end of the joint shear stress demand range, joint strength is closely associated with adjacent beam strength.

The strength deterioration behavior of the cruciform under simulated earthquake loading can be inferred from the beam bar bond demand parameters. The large Bond Indexes in Table 5.3.1 for the top and bottom steel indicate small ratios of column depth to beam bar diameter, h_c / d_b, that are below the ACI code limitation of 20 (ACI 318-02).

These small ratios indicate inadequate bond which results in reduced energy dissipation effects after beam yielding.

Based on the geometry and design of the cruciform, and the joint shear stress and Bond Index parameters that characterize it, behavior predictions for the *RS-MnB* and *UW-MnJ*-BS joint models can be made. For the *RS-MnB*, the joint panel, based on the strength of the beams in flexure, should experience yield as the beams undergo yield. As for the *UW-MnJ-BS* model, the bar-slip springs in the beams should yield given that this behavior is closely related to flexural beam yield. Predictions in regard to strength deterioration are difficult to make other than saying both models with experience rapid strength deterioration once yielding occurs.

Table 5.3.1: Joint shear stress and beam bar bond demand parameters.

Specimen Parameters	Van Nuys Cruciform	PEER-0995	PEER-2250	PEER-4150
V_{jt}/f'_{ct}	3.04	8.50	14.80	29.30
$V_{jt}/\sqrt{f'_{ct}}$	0.04	0.09	0.22	0.41
Bond Index (top)	42.06	24.28	24.28	31.30
Bond Index (bottom)	31.54	24.28	24.28	31.30

The analysis results for both models, shown in Figure 5.3.1-Figure 5.3.3, agree with the expected behavior. In both models, the beams undergo significant yielding at the larger drift demands of the PEER load history (see Figure 5.3.3). For the *UW-MnJ-BS* model, beam bar-slip springs experience yielding while the shear panel and the column bar-slip springs remain elastic (see Figure 5.3.2). For the *RS-MnB* model, behavior is controlled by the yielding of the beams and the joint shear panel (see Figure 5.3.2(b) and Figure 5.3.3). One point of disagreement between expected and modeled behavior is that the *UW-MnJ-BS* model experiences little deterioration. The bar-slip springs have yielded, but they have not exceeded a deformation of 0.12 inches that triggers the joint deterioration.

The model of the case study building sub-assemblage presented here introduces the steps carried out for the following sections on the full-frame simulations: parameters and assumptions are determined, joint models are formulated and implemented, and the resulting seismic behavior is presented. Furthermore, the results of the sub-assemblage indicate that for a typical case study building joint, the introduction of the joint models impacts the seismic behavior in the expected ways of joint panel yielding and bar-slip.

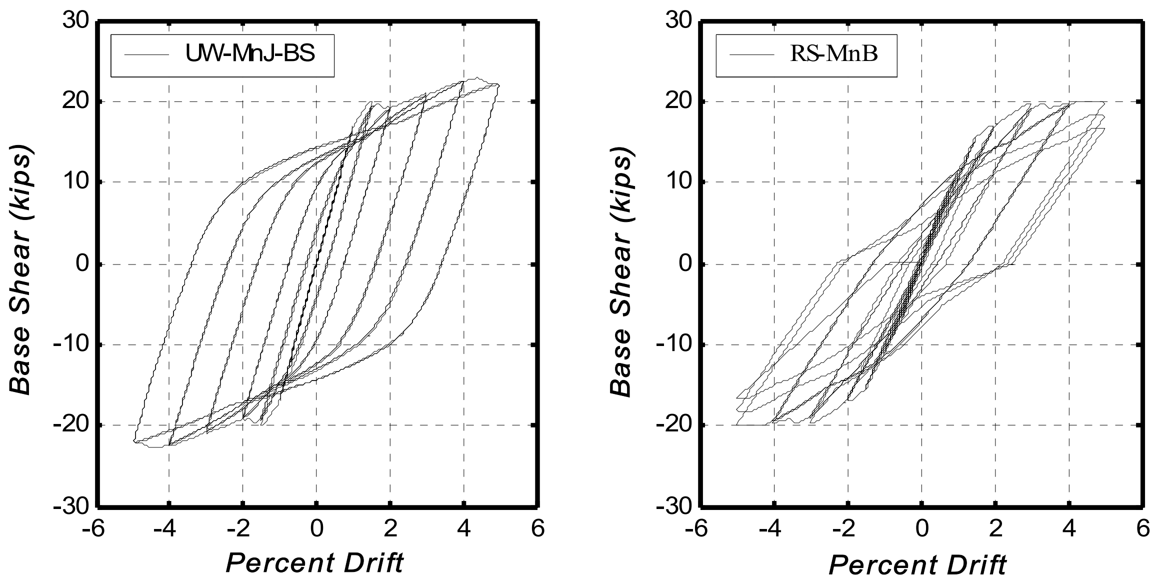

(b) **(a)**

Figure 5.3.1: Shear at the cruciform base vs. % drift response from the simulations with the two joint models (a) *RS-MnB* (b) *UW-MnJ-BS*.

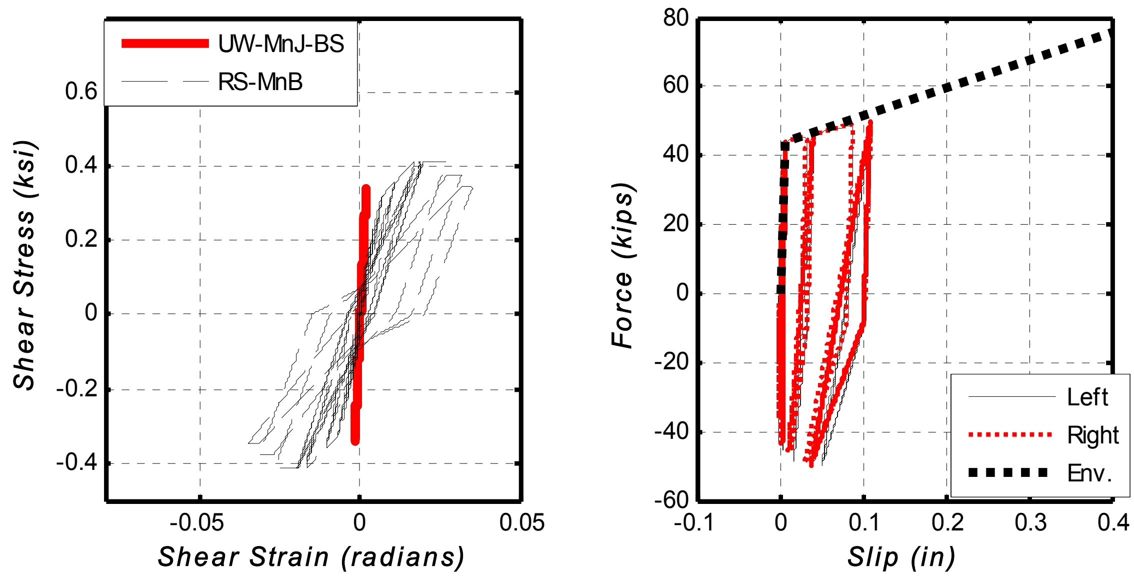

(b) **(a)**

Figure 5.3.2: (a) Simulated bar slip response of the bottom steel in the right and left beams for the *UW-MnJ-BS* model (b) Simulated stress-strain response of the joint panel for the *UW-MnJ-BS* and *RS-MnB* models.

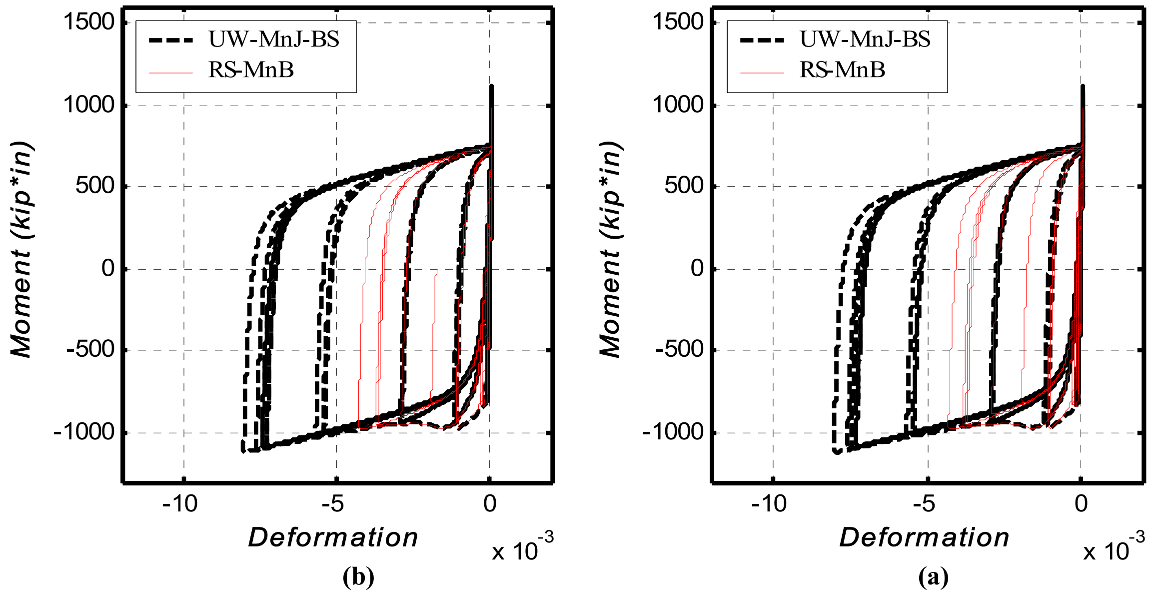

Figure 5.3.3: Simulated (a) right and (b) left beam response for *UW-MnJ-BS* and *RS-MnB* models.

5.4. Full-Frame Simulation Details

To investigate the impact of explicit modeling of inelastic joint behavior during the simulation of the earthquake response of the case study building, an existing model of the case study building was extended to include the *RS-MnB* and *UW-MnJ-BS* joint models. A previously developed model of the building created by Paspuleti (2002) for use with OpenSees was used. This model allows for simulation of the nonlinear flexural response of the beams and columns as well as brittle column failure due to shear and splice failure. Details of the full-frame model are presented in Chapter 2. The *RS-MnB* and *UW-MnJ-BS* are calibrated for use in the model in Chapters 3 and 4.

This section discusses the revision and extension of the full-frame model present in Chapter 2 to enable investigation of joint modeling and a discussion of the analyses conducted. Finally, the results of the simulations are presented and discussed.

5.4.1. Modeling Assumptions and Parameters

Paspuleti Model

The current research takes the model developed by Paspuleti presented in Chapter 2, revises it to improve the simulation and modifies it to allow for the simulation of joint response. As discussed in Chapter 2, analysis of the case study building considers response only along the North-South longitudinal direction of the frame, and the full-frame model of the seven-story building includes only two of the four frames, C and D (refer to Appendix D for plan and elevation drawings). These frames are approximately identical to the other two longitudinal frames that complete the structure, A and B; thus simulation of the response of these frames is sufficient to assess full-frame response. The two longitudinal frames in the model are linked together by constraining the in-plane displacements and out-of-plane rotations between the two frames to be equal.

Other important parameters and assumptions from this original model are presented in the following sections:

- Boundaries, Loading, Damping, and Tolerances
- Section and Material Modeling
- Beam and Column Modeling

Boundaries, Loading, Damping, and Tolerances

When modeling the case study building, the units used are pounds and inches. Also, no P-Δ effects are accounted for in the simulations, and the soil-foundation interaction is assumed to be rigid.

When modeling the loads on the building, load is applied only in the plane defined by the longitudinal frames. Furthermore, a lateral loading pattern for the pushover simulations is based on FEMA 356 guidelines and is discussed in Section 2.4.

Damping for the models is assumed to be 3% Rayleigh damping. The simulations use a global solution tolerance of 1E-6, and it is to be achieved within 10 iterations. The element solution tolerance is 1E-8, and it is to be achieved within 10 iterations.

Section and Material Modeling

When defining the beam and column sections, the maximum fiber dimension used is 0.5”. The longitudinal reinforcing steel used in the section definitions has a strain hardening ratio of 0.02. The maximum and minimum strains at which splice failure occurs in this steel are 0.02 and -0.02. The concrete for the section definitions uses a concrete over-strength factor of 1.5 as suggested by FEMA to predict the real concrete strength due to age and increased strength at time of casting.

Beam and Column Modeling

The beams and columns are modeled with *beamWithHinges2* elements. These elements are forced to iterate until element equilibrium is achieved. The number of integration points along the length of the beams and columns is five. The elements do not model beam or column eccentricity. The beam centerline is assumed to intersect with the column centerline, and the eccentricity of the beams is removed. In the elements that model the slab in the interior frame the reinforcing steel in the bottom of the slab that extends from the middle strip to the column line is not included in the model.

Modified Paspuleti Model

To modify the model developed by Paspuleti for the research here, some changes and additions to the Paspuleti modeling assumptions and parameters were made. These assumptions are broken up into the following sections:

- Boundaries and Loading
- Material Modeling
- Beam and Column Modeling
- Joint Modeling

Boundaries and Loading

The movement of Frames C and D is constrained by slaving the fifth column line of nodes between the two frames. The frames are slaved at only the middle column line in order to minimize the axial load in the beams which can impact overall element response. For the *UW* element, only the node defining the bottom of the joint is slaved, and for the *RS* element only one of the middle nodes, in order not to impact the joint response.

For this research, the gravity load is not included for the dynamic simulations. This modeling decision is made to reduce convergence problems which resulted in aborted analyses at the more intense ground motions.

Material Modeling

The reinforcing steel model simulates the loss of strength at material levels under cyclic loading that would be expected if the steel fractured and buckled. This reduction in strength is assumed to occur at a strain value of 0.1 or -0.15. Also, the concrete crushing strength, f_{cu}, is 20% of the compressive strength, f'_c and the concrete has not tensile strength.

Beam and Column Modeling

All the beams, slabs, and columns have fiber cross-section defining their flexural, axial, shear, and torsion behavior. The slab contributes to the flexural strength or stiffness of both Frames D and C. The beams for Frame C consist of the slab between the columns with a width defined as the total column strip width. The beams for the D frame consist of a spandrel beam and a portion of the slab to make an L-shaped beam rotated 90 degrees clockwise. The portion of slab included in the section models can vary from zero to half of the column strip width from an interior frame.

Different α-values are used to modify the stiffness of the beams, slabs, and columns in flexure, axial, shear, and torsion capacity. They are: $\alpha_{\text{flex}} = 0.2965$, $\alpha_{\text{axial}} = 0.593$, $\alpha_{\text{shear}} = 0.2372$, and $\alpha_{\text{torsion}} = 0.593$. These values are based on the FEMA 356 values, which are adjusted to ensure the period is 1.5 seconds. The adjustments to the FEMA 356 values are determined from an eigen analysis using rigid joints.

Plasticity in the flexural members is assumed to be lumped in a plastic hinge defined according to Priestly and Park (1987). The length is defined as $0.05L+0.5D$, where L is the distance from the end of the member to the inflection point assumed here to be at the midpoints, and D is the effective depth of the element assumed to be 90% of the gross depth.

Joint Modeling

Beam-column joint models are included in both Frame C and D even though the connections in Frame C are more accurately modeled as slab-column connections. As a result the models are assumed to over predict the amount of damage the Frame C joints experience.

The rigid joint simulations use elastic elements with large stiffnesses to define the area of the joint. This increases the degrees of freedom in the model, but ensures the joints exhibit rigid behavior.

5.4.2. Joint Model Implementation

The *UW-MnJ-BS* and the *RS-MnB* joint models are introduced and evaluated in Chapter 3. The calibration of the models is discussed in Section 5.2.2. Here, the models are implemented in the OpenSees model framework created by Paspuleti (2002). The basic structure of the model is contained in the *vannuys.tcl* script.

vannuys.tcl

The *vannuys.tcl* script shown below is a list of the primary scripts that when called in OpenSees, creates and analyses the full frame model. The script first defines the basic pathway and unit information and then calls the additional scripts using the "*source*" command that executes each line in the script. In most cases, the joint incorporation occurs by having these primary scripts call additional scripts in which joint parameters, materials, or elements are defined, resulting in multiple levels to the model. The incorporation of the joint models into the framework is discussed in the following paragraphs.

```
source setAnalysisParameters.tcl
source setFrameGeometry.tcl
source setFrameMemberSectionProperties.tcl
source setMaterialProperties.tcl
source setElasticElementProperties.tcl
source setLimitStateMaterialProperties.tcl
source setNodalMass.tcl
source defineStructuralMaterials.tcl
source defineSections.tcl
source defineNodes.tcl
```

source defineGeometricTransformations.tcl
source defineElements.tcl
source defineBoundaryConditions.tcl
source analyze.tcl

setAnalysisParameters.tcl

In the modeling framework developed by Paspuleti (2002), the user modifies the *setAnalysisParameters.tcl* file to define the column shear model, column splice-failure model, the type of gravity loading, and ground motion intensity that is to be used in the current analysis. For the current study, *setAnalysisParameters.tcl* has been modified to allow the user to also choose the type of joint model and the level of joint damage. Other model parameters, modeling decisions, and Paspuleti model extensions as discussed in Section 5.4.1, may also be defined in this script.

setMaterialProperties.tcl

The *setMaterialProperties.tcl* script has been modified to define the material parameters for each *RS-MnB* or *UW-MnJ-RS* joint in the case study building, as well as all of the materials for the beams and columns. The joint parameters created here include the nominal moment strength, *Mnj*, the other strength envelope parameters based on those from Table 4.2.6, the hysteretic behavior parameters, and the bar-slip parameters. *Mnj* is calibrated for each of the 126 joints in the model based on beam strength or geometry as discussed for the case study building cruciform in Section 5.2.2. The hysteretic behavior parameters are the empirical values based on the laboratory joint tests results from Walker (2001) and Alire (2002) given in Table 4.2.9. The bar-slip parameters for each joint are taken from the material properties and joint geometry, examples of which are given in Table 5.2.6.

defineStructuralMaterials.tcl

For the current study, this file has been modified so that the materials required to simulate joint response are created using the joint material parameters defined in *setMaterialProperties.tcl*. Each shear panel, bar-slip spring, or shear interface spring of each joint model is assigned a unique material, depending on the joint type specified in *setAnalysisParameters.tcl*.

defineNodes.tcl

This file defines the nodes in the case study building model. For this study, it has been updated to create the nodes required for the joint element specified in *setAnalysisParameters.tcl*. Section 3.5 discusses the node requirements of the *RS* and *UW* joints. Extra nodes are also included to enable simulation of rigid joints using stiff, elastic flexural elements within the joint core.

defineElements.tcl

For the current study, this file was modified to include the OpenSees commands that create joint elements at each of the beam-column intersection of the frame. Materials and nodes defined in the *defineStructuralMaterials.tcl* and *defineNodes.tcl* scripts are used in creating the joint elements. Note that the joint elements are included at the roof level and at the external columns where only one beam meets the column.

5.4.3. Simulation Series Explanation

To investigate fully the impact of simulation of inelastic joint response, it is appropriate to consider variation in the joint model parameters as well as to consider simulation of joint response in combination with variation in other computed failure models and load patterns. For the current study, the following modeling decisions were considered variable:

- Analysis type: pushover or dynamic
- Joint model: rigid, *UW-MnJ-BS*, or *RS-MnB*
- Shear and splice failure model: ACI or none
- Gravity loading: lumped or none
- Joint damage: yes or no

Table 5.4.1 defines the combinations of the modeling decisions used for each analysis performed as part of the study. For the dynamic analyses, an additional variable of ground motion intensity was used to investigate the impact of explicit joint modeling on the predicted seismic response of the case study building. Detailed discussion of the modeling decisions follows below.

Analysis Type

The two analysis types used in the current research are pushover and dynamic. Pushover analyses are a typical approach to evaluate the performance of a structure in terms of lateral strength and deformation capacity. These analyses also allow for the identification of failure mechanisms of the structure. The lateral, pushover load was applied with a parabolic load pattern as discussed in Section 2.4.

Determining the seismic response of the case study building using dynamic analyses require using direct integration to solve for dynamic equilibrium of the system for each time step of a ground motion history. The size of the time steps in a dynamic analysis can significantly impact the computational effort and accuracy of the simulation. The current research uses a variable time step Newmark integration procedure. The procedure has a maximum step of 0.02 seconds and allows for fractional time steps when convergence issues arose.

Table 5.4.1: Simulation Series of the full-frame case study building.

Model ID	Analysis	Joint Model	Shear/Splice	Gravity Load	Joint Damage
M1	pushover	*UW-MnJ-BS*	None	none	--
M2	pushover	*RS-MnB*	None	none	--
M3	pushover	*Rigid*	None	none	--
M4	pushover	*UW-MnJ-BS*	None	lumped	--
M5	pushover	*RS-MnB*	None	lumped	--
M6	pushover	*Rigid*	None	lumped	--
M7	pushover	*UW-MnJ-BS*	ACI	none	--
M8	pushover	*RS-MnB*	ACI	none	--
M9	pushover	*Rigid*	ACI	none	--
M10	pushover	*UW-MnJ-BS*	ACI	lumped	--
M11	pushover	*RS-MnB*	ACI	lumped	--
M12	pushover	*Rigid*	ACI	lumped	--
M13	Dynamic	*UW-MnJ-BS*	None	none	No
M14	Dynamic	*UW-MnJ-BS*	None	none	Yes
M15	Dynamic	*RS-MnB*	None	none	No
M16	Dynamic	*RS-MnB*	None	none	Yes
M17	Dynamic	Rigid	None	none	--
M18	Dynamic	*UW-MnJ-BS*	ACI	none	No
M19	Dynamic	*UW-MnJ-BS*	ACI	none	Yes
M20	Dynamic	*RS-MnB*	ACI	none	No
M21	Dynamic	*RS-MnB*	ACI	none	Yes
M22	Dynamic	Rigid	ACI	none	--

Joint Model

The current research models the joints in the case study building model in three possible ways: rigid, *UW-MnJ-BS*, or *RS-MnB*. The rigid joint model uses stiff, elastic flexural elements to define the joint core. The *UW-MnJ-BS* and *RS-MnB* joint models are discussed in Section 5.2.2.

Shear and Splice Failure Model

Some of the analyses included simulation of column shear and splice failure. The shear model is the conservative ACI model which simulates a rapid loss in shear strength, and thus flexural strength, when the shear capacity is reached (Paspuleti 2002). The shear capacity used here is from ACI318-02 which assumes that the concrete contributes to shear strength (ACI318 2002).Up to the point where the shear capacity is reached the column element behavior is controlled by the flexural strength. The splice model modifies the stress-strain history of the longitudinal reinforcement steel in the section of the column closest to the splice location. If a splice failure is predicted, the steel has a reduced yield strength and negative post-yield stiffness. The model is uses the ACI anchorage length equation 12.1 (ACI318 2002) to determine if a splice failure will occur. Both models are discussed in Section 2.4.

Gravity Loading

For the case study building models that include gravity loading, the load is applied lumped at the beam column intersections.

Joint Damage

The amount of strength and stiffness deterioration predicted by the joint models is controlled by parameters used to define the joint model materials. Depending on the parameters used with the *Pinching4* material model, damage resulting from cyclic loading may or may not be simulated. Thus, strength and stiffness deterioration in the joint panel and bar-slip springs of the *UW-MnJ-BS* and the joint panel of the *RS-MnB* may or may not be simulated. For the current research, simulation of damage is considered a variable and the impact of simulating damage is investigated. This is done only for the dynamic analyses, since strength and stiffness deterioration is a cyclical phenomenon.

Ground Motion Intensity

Each of the models identified in Table 5.4.1 as being used for dynamic analysis is subjected to the 1994 Northridge ground motion, as recorded at the location of the case study building (Figure 5.4.1), scaled to four intensity levels. Three of these intensity levels correspond to earthquake hazard levels and are identified *2% in 50 yrs.*, *10% in 50 yrs.*, *50% in 50 yrs.* (http://www.peertestbeds.net), where *2% in 50 yrs.* indicates that the ground motion is scaled to an intensity that has a 2% probability of being exceeded by an earthquake in the next 50 years. Thus, a *50% in 50 yrs.* ground motion is more common and less severe than a *2% in 50 yrs.* The records are scaled by matching the longitudinal component of the time history to uniform hazard spectrum at a period of 1.5 seconds (Somerville and Collins 2002). The fourth intensity level is the unscaled ground motion, which is slightly less intense than the *10% in 50 yrs.* level (the *10% in 50 yrs* scaling factor is 1.043) (http://www.peertestbeds.net).

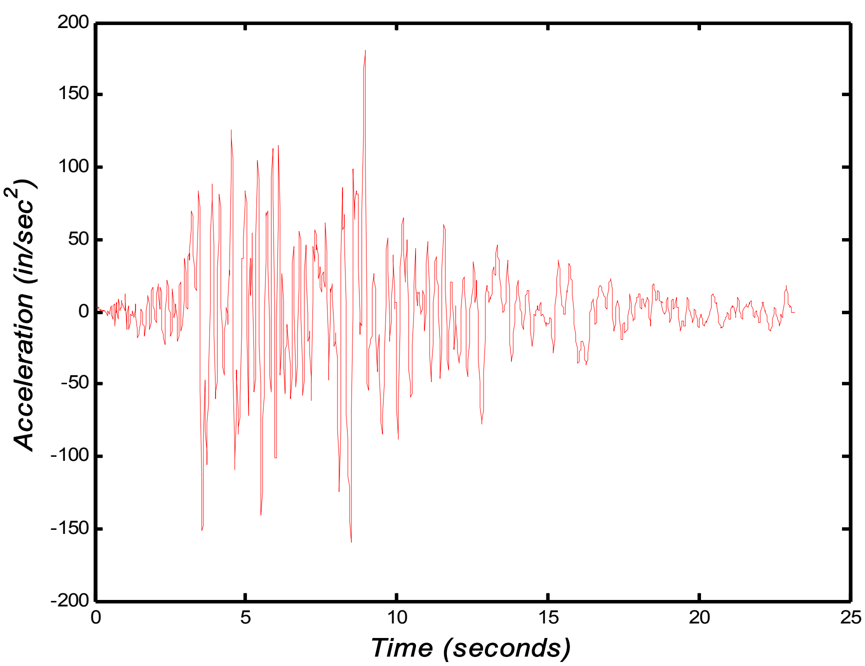

Figure 5.4.1: 1994 Northridge ground motion

5.5. Full Frame Simulation Results

5.5.1. Pushover Results

The results of the pushover simulation series given in Table 5.4.1 are summarized in Figure 5.5.1 and Figure 5.5.2. These plots show roof drift versus base shear ratio. The data in these plots illustrate the trends in the overall response of the building that arise from including the simulation of inelastic joint behavior. These trends are quantified in Table 5.5.1 and Table 5.5.2. In these tables, the maximum base shear and the roof drift at the point of maximum base shear are compared for the pushover tests. The following paragraphs discuss the results in terms of impact due to different joints and shear and splice failure models.

Impact of Joint Model Type

Figure 5.5.1 and Figure 5.5.2 show that regardless of gravity load, shear failure and splice failure models, the case study building simulations with *UW-MnJ-BS* joints are shown to have the lowest base shear strength, followed by the *RS-MnB* models. The models with rigid joints consistently have the highest base shear strength, the highest initial stiffness, and the lowest drift at the point of maximum base shear. These trends are quantified in Table 5.5.1 and Table 5.5.2. It is noted from the plots that none of the simulations proceed past the 2.0% roof drift point. The models fail to converge due numerical problems associated with significant non-linear behavior in the beams, columns and joints. Despite these computational failures, the resulting roof drifts summarized in Table 5.5.1 and Table 5.5.2 are sufficient when compared with past research and the observed drift during the Northridge earthquake observed drift for use in model evaluation.

Analysis data show that the type of joint model determines the progression of failure and failure mode for the structure. Figure 5.5.3 maps the progression of failure for the first three models in the pushover simulation series. This figure shows that the flexibility of the *UW-MnJ-BS* and *RS-MnB* joints increases the overall flexibility of the structure resulting in the beams yielding at drift levels of 0.5-0.6% as opposed to 0.2%

for the rigid joint model. The same trend is seen in the columns. Additionally, when the bar-slip springs are activated the result is reduced overall stiffness unique to the *UW-MnJ-BS* model.

The failure progression of the models in Figure 5.5.3 is determined using figures such as Figure 5.5.4-Figure 5.5.6. These plots indicate the type and location of failures on the two longitudinal frames that have occurred at a given step in the analysis. A series of steps in the different analyses were explored to determine the failures indicated on Figure 5.5.3.

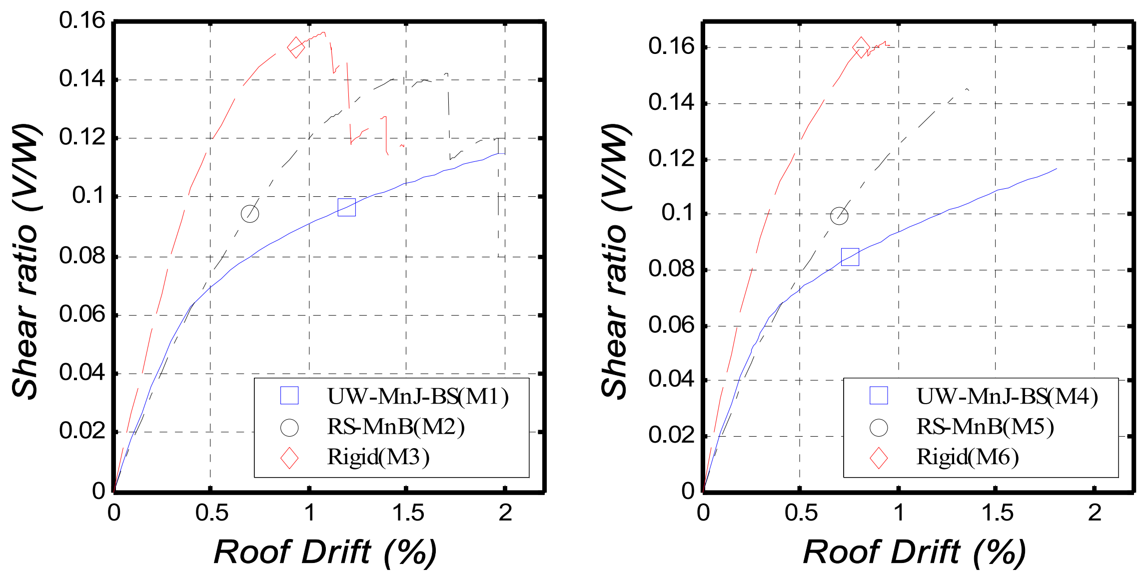

(b) **(a)**

Figure 5.5.1: Pushover response for the different joint models with no shear or splice models and (a) with gravity load and (b) without gravity load.

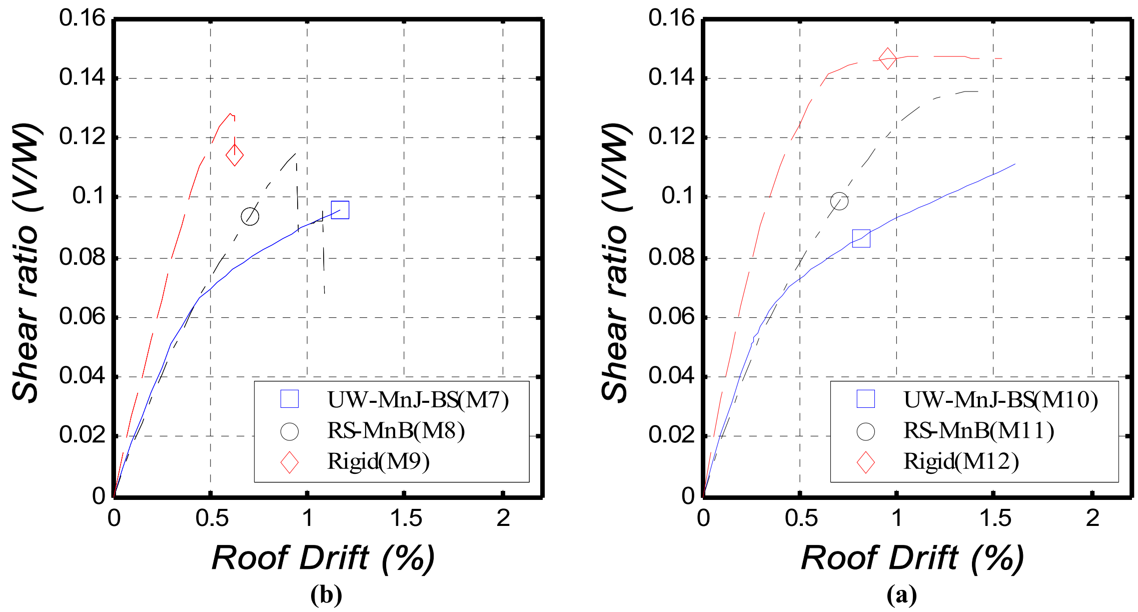

Figure 5.5.2: Pushover response for the different joint models with shear and splice models and (a) with and (b) without gravity load.

Table 5.5.1: Max shear ratio for pushover analyses of the case study building.

joint type / shear, splice & grav.	*UW-MnJ-BS*	*RS-MnB*	*Rigid*	**Mean:** (varying joints)	**C.O.V.:** (varying joints)
no shear, no splice no gravity	0.114	0.142	0.156	0.137	0.156
no shear, no splice gravity	0.116	0.146	0.162	0.141	0.165
shear, splice no gravity	0.096	0.115	0.128	0.113	0.142
shear, splice gravity	0.111	0.136	0.147	0.131	0.140
Mean: (same joints)	0.109	0.135	0.148	**Mean** (all models)	0.131
C.O.V. : (same joints)	0.083	0.102	0.100	**C.O.V.** (all models)	0.156

Table 5.5.2: Max roof drift (%) at max shear ratio for pushover analyses of the case study building.

joint type / shear, splice & grav.	*UW-MnJ-BS*	*RS-MnB*	*Rigid*	**Mean:** (varying joints)	**C.O.V.:** (varying joints)
no shear, no splice no gravity	2.007	1.716	1.087	1.603	0.293
no shear, no splice gravity	1.813	1.358	0.935	1.369	0.321
shear, splice no gravity	1.170	0.946	0.600	0.905	0.317
shear, splice gravity	1.613	1.421	1.190	1.408	0.150
Mean: (same joints)	1.651	1.360	0.953	**Mean** (all models)	1.321
C.O.V. : (same joints)	0.217	0.233	0.270	**C.O.V.** (all models)	0.312

Table 5.5.3: Comparison of simulated max shear ratio and roof drift from previous pushover analyses of the case study building.

Model ID	**Max shear ratio**	**Roof drift at max shear (%)**
Mean (M1-12)	0.131	1.321
C.O.V. (M1-12)	0.156	0.312
Barin and Pincheira (2002) (displacement controlled)	0.155	0.840
Paspuleti (2002) (Base model)	0.100	1.294
Islam (1996)	0.115	0.700
Observed (1994 Northridge)	--	1.060

Impact of Gravity and Failure Models

The maximum base shear data presented in Table 5.5.1 enable evaluation of the impact on earthquake response of the simulation of gravity load and column brittle failure modes. These data show that simulation of gravity loading has little impact on the maximum base shear of the building when there are no brittle column failure models included regardless of the joint type. The largest change in maximum base shear strength is between 0.156 and 0.162, or 3.8%, for the analyses with rigid joint models. The analyses with the other joint models show even less variability due to gravity load simulation. The gravity impact increases when column shear and splice failure models are included; comparison of the data in the fourth and fifth rows of Table 5.5.1 show that including gravity increases the maximum base shear of the full frame by 15-18%. For the models where the gravity is constant and the shear and splice failure models are varied, the addition of the failure models has a marginal impact on the maximum base shear as shown by the increase of 5-10% for the data in rows three and five.

It is unclear why including the gravity reduces the strength and ductility when the brittle failure models are included. One possible reason is that the increased axial loads result in increased moment and shear demands in the columns. As a result, shear failures are more likely to occur.

The trends in pushover response of the case study building in terms of the roof drift at the point of maximum base shear are shown in Table 5.5.2. These trends mimic those seen in Table 5.5.1. Gravity impacts the full frame response the most when the failure models are included, and the failure models do not impact the response as much if the gravity is included.

The coefficient of variations for the maximum base shear values for the simulations with same joints but differing shear, splice and gravity are bunched between 8.3% and 10.2% (see bottom row in Table 5.5.1). In contrast the roof drift values at the maximum base shear for the same models vary from 21.7% to 27.0% (see bottom row in Table 5.5.2). These large variations in roof drift levels for models with constant joint models indicate the importance of choosing the gravity, shear, and splice models because of the relationship of roof drift to inter-story drift levels, an important engineering design parameter and damage indicator.

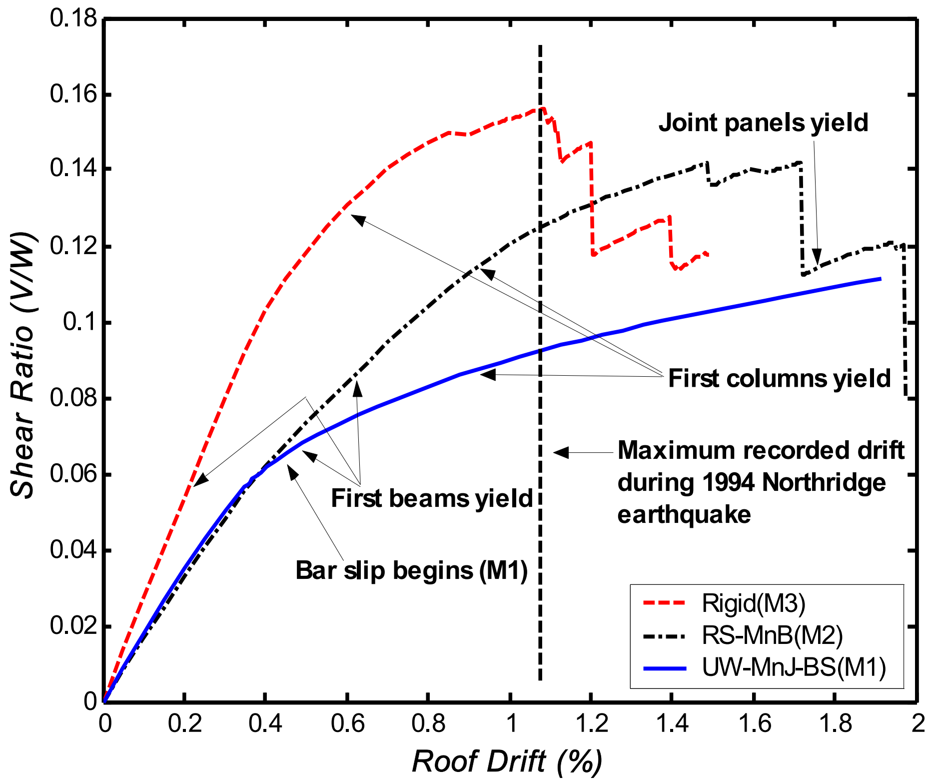

Figure 5.5.3: Progression of failure mechanisms for pushover response for the different joint models with no shear and splice models, and with no gravity load.

Figure 5.5.4 through Figure 5.5.6 show simulated curvature ductility demand and failure modes for the beams and columns of the exterior and interior frames at the maximum base shear for each of the joint models and the case of a pushover analysis with no gravity load and no simulation of brittle column failure (M1, M2, M3). These figures illustrate the relationship between joint type and curvature ductility demand in the beams and columns. For example, for model M1, the beams and columns in general experience lower curvature demands because of the relative flexibility of the *UW-MnJ-BS* joints. While, for model M3, the rigid joints result in the beams and columns experiencing large deformation demands which lead to a high number of element failures. Individual elements that are considered to have failed, are indicated by a "#" if they predict unrealistically large curvature demands. For the first three simple models in Figure 5.5.4 through Figure 5.5.6, the curvature ductility demand on the beams and columns are the only data plotted. However, for the more complicated models symbols representing shear and splice failures are included in the plots. Appendix E includes figures similar to Figure 5.5.4 through Figure 5.5.6 for multiple drift levels for all the pushover models.

Curvature Ductility Demand and Failure Legend

O : $\mu = 1$ to 1.5 O : $\mu = 1.5$ to 2 O : $\mu = 2$ to 3 O : $\mu = 3$ to 4 O : $\mu > 4$

X = shear failure, S = splice failure, # = numerical failure

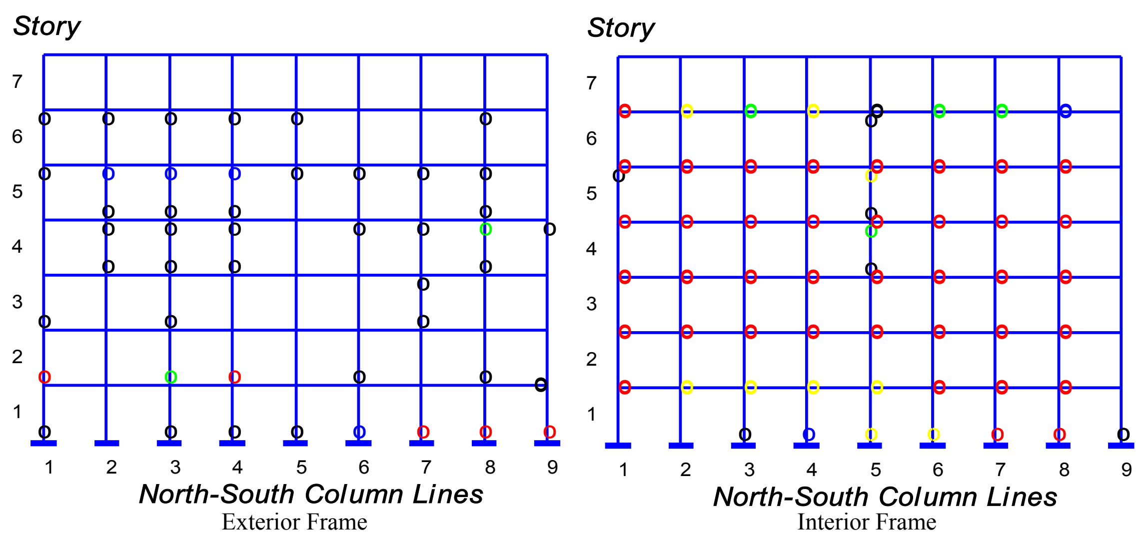

Figure 5.5.4: Locations and types of member failures for model M1 at maximum base shear.

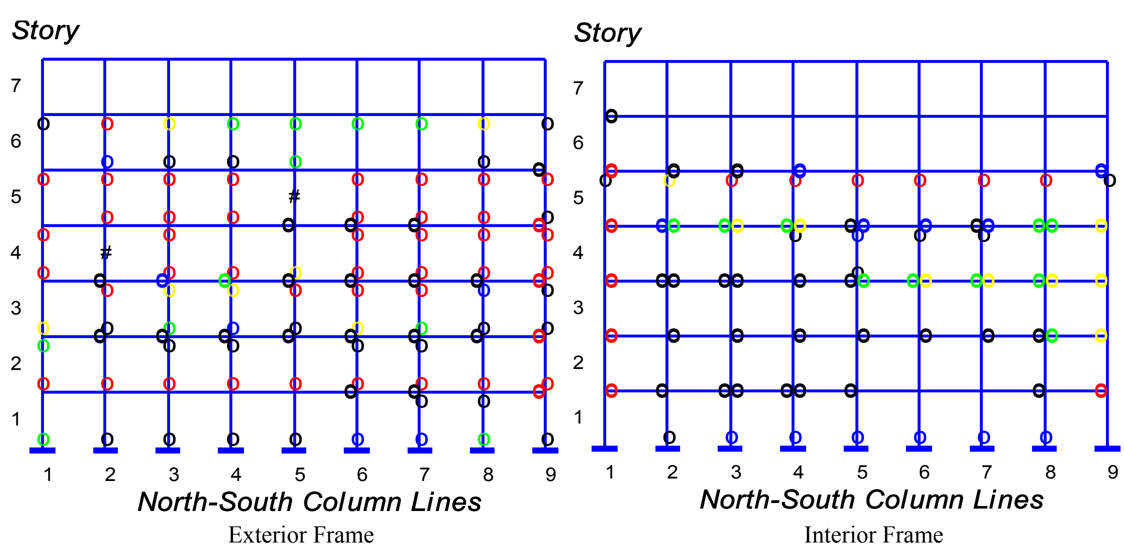

Figure 5.5.5: Locations and types of member failures for model M2 at maximum base shear.

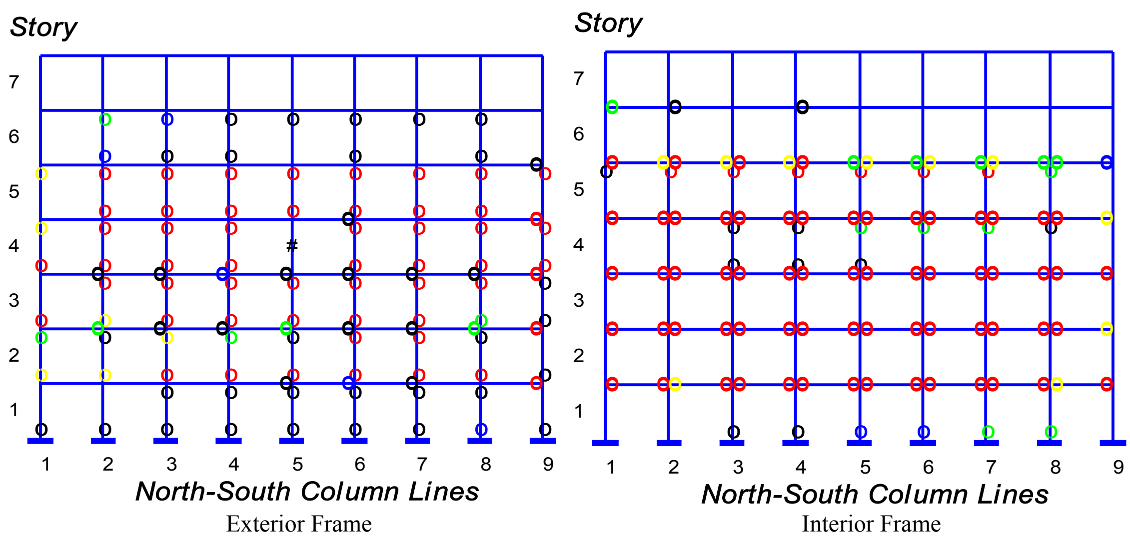

Figure 5.5.6: Locations and types of member failures for model M3 at maximum base shear.

5.5.2. Dynamic Results

This section discusses the impact on dynamic response of the case study building of the following four parameters: type of joint model, simulation of joint damage, simulation of column shear and splice failure, and ground motion intensity. The first section addresses the impact that ground motion intensity has on the simulated building response when different joint models are used. Results of simulations using the 1994 Northridge ground motion record scaled to four different intensities are presented. The next two sections focus on the impact that simulating joint damage and column shear and splice failure has on the system response when different joint models are used. This investigation is accomplished by exposing models M13-M22 from Table 5.4.1 to the first 23 seconds of the Northridge ground motion record scaled to an intensity level associated with a hazard level of 50% probability of exceedence in 50 years. The simulated response is then compared to the observed roof response from 1994. The final section looks at the joint impact on overall behavior for the various dynamic simulations of the case study building exposed to the 1994 Northridge earthquake. Specifically, the inter-story drift levels at the predicted maximum roof drift are compared to the values at the observed maximum drift from 1994.

Impact of Ground Motion Variability

Table 5.5.5-Table 5.5.7 summarize the results of the dynamic analyses of the case study building. Data of the response to the 1994 Northridge ground motion record scaled to three earthquake hazard levels and the unscaled record are provided. Each table presents the maximum inter-story drift at each floor and the maximum roof drift simulated for the ten different dynamic models from Table 5.4.1. Each table also identifies floor failures; inter-story drifts greater than 10% are assumed to indicate failure.

The data in the tables show that as expected, increasing the hazard level, or ground motion intensity, results in increased inter-story drift demands and reduced building performance, as defined by more building failures. None of the analyses fail at the *50% in 50 yrs.* hazard level. As intensity increases from the *50% in 50 yrs.* level through the unscaled and *10% in 50 yrs.* levels to the *2% in 50 yrs* level, the number of floor failures (where inter-story drift > 10%) increases from 0 to 5 to 6 to 8. Similarly, the maximum roof drift increases from an average of 0.614% to between 2 and 2.5% to 4.203%, and the average maximum inter-story drift increases from 1.074% to between 7.2 and 7.5% to 9.133%.

Table 5.5.4: Dynamic analysis data for the *50% in 50 yrs.* ground motion intensity.

model parameters \ building story	Maximum inter-story drift (%)							Max Inter-Story Drift (%)	Max Roof Drift (%)
	1	2	3	4	5	6	7		
M13 UW-MnJ-BS, no shear, no splice, no joint damage	0.762	0.513	0.481	0.599	0.434	0.305	0.176	0.762	0.481
M14 UW-MnJ-BS, no shear, no splice, joint damage	0.684	0.517	0.475	0.620	0.445	0.311	0.170	0.684	0.475
M15 RS-MnB, no shear, no splice, no joint damage	0.752	0.734	0.770	1.120	1.125	0.618	0.446	1.125	0.770
M16 RS-MnB, no shear, no splice, joint damage	0.955	0.850	0.747	0.985	0.824	0.738	0.516	0.985	0.747
M17 Rigid, no shear, no splice, no joint damage	1.200	0.904	0.726	0.707	0.572	0.429	0.256	1.200	0.726
M18 UW-MnJ-BS, ACI shear & splice, no joint dam.	0.666	0.589	0.799	0.659	0.476	0.299	0.172	0.799	0.487
M19 UW-MnJ-BS, ACI shear & splice, joint damage	0.669	0.584	0.535	2.247	0.641	0.344	0.205	2.247	0.535
M20 RS-MnB, ACI shear & splice, no joint damage	0.926	0.817	0.715	0.955	0.746	0.620	0.696	0.955	0.715
M21 RS-MnB, ACI shear & splice, joint damage	0.793	0.689	0.507	0.601	0.625	0.661	0.342	0.793	0.507
M22 Rigid, ACI shear & splice, no joint damage	1.176	0.890	0.691	0.697	0.526	0.408	0.258	1.176	0.691
Mean:	0.858	0.709	0.819	0.919	0.641	0.473	0.324	1.074	0.614
C.O.V. :	0.233	0.215	0.199	0.546	0.331	0.356	0.547	0.420	0.204
# of failures	0	0	0	0	0	0	0	**Tot. failures**	0

Table 5.5.5: Dynamic analysis data for the unscaled ground motion intensity.

model parameters \ building story	Maximum inter-story drift (%)							Max Inter-Story Drift (%)	Max Roof Drift (%)
	1	2	3	4	5	6	7		
M13 UW-MnJ-BS, no shear, no splice, no joint damage	1.111	1.862	1.203	8.322	0.996	0.464	0.255	8.322	1.028
M14 UW-MnJ-BS, no shear, no splice, joint damage	1.284	0.992	1.060	10.00	0.796	0.435	0.258	10.00	2.978
M15 RS-MnB, no shear, no splice, no joint damage	1.588	1.652	1.879	10.00	1.474	0.854	0.511	10.00	2.549
M16 RS-MnB, no shear, no splice, joint damage	2.182	1.566	1.690	1.573	1.198	0.855	1.326	2.182	1.397
M17 Rigid, no shear, no splice, no joint damage	1.067	1.724	1.843	2.262	2.034	0.480	0.353	2.262	1.120
M18 UW-MnJ-BS, ACI shear & splice, no joint dam.	0.935	1.336	7.627	2.296	0.711	0.397	0.287	7.627	0.965
M19 UW-MnJ-BS, ACI shear & splice, joint damage	3.374	2.049	1.064	10.00	0.737	0.410	0.222	10.00	3.963
M20 RS-MnB, ACI shear & splice, no joint damage	1.061	0.911	0.947	10.00	1.040	0.705	0.403	10.00	2.538
M21 RS-MnB, ACI shear & splice, joint damage	1.726	1.057	1.035	10.00	1.040	0.705	0.404	10.00	4.006
M22 Rigid, ACI shear & splice, no joint damage	0.938	2.027	1.785	1.391	1.115	0.689	0.449	2.027	0.954
Mean:	1.771	1.589	1.357	7.355	1.117	0.601	0.440	7.242	2.150
C.O.V. :	0.523	0.282	0.286	0.532	0.352	0.300	0.743	0.498	0.569
# of failures	0	0	0	5	0	0	0	**Tot. failures**	5

Table 5.5.6: Dynamic analysis data for the *10% in 50 yrs.* ground motion intensity.

building story / model parameters	Maximum inter-story drift (%) 1	2	3	4	5	6	7	Max Inter-Story Drift (%)	Max Roof Drift (%)
M13 UW-MnJ-BS, no shear, no splice, no joint damage	1.290	1.002	1.508	7.548	0.869	0.415	0.261	7.548	1.063
M14 UW-MnJ-BS, no shear, no splice, joint damage	1.027	0.816	0.943	2.899	0.866	0.412	0.265	2.899	0.883
M15 RS-MnB, no shear, no splice, no joint damage	1.517	1.558	1.971	2.093	10.00	0.981	0.487	10.00	2.566
M16 RS-MnB, no shear, no splice, joint damage	2.131	1.609	1.778	10.00	1.247	0.881	0.555	10.00	7.479
M17 Rigid, no shear, no splice, no joint damage	1.927	1.560	2.107	2.294	1.663	0.697	0.395	2.294	1.274
M18 UW-MnJ-BS, ACI shear & splice, no joint dam.	5.486	0.863	1.016	10.00	0.652	0.321	0.206	10.00	1.362
M19 UW-MnJ-BS, ACI shear & splice, joint damage	1.534	1.222	1.506	1.556	0.771	0.372	0.203	1.556	0.942
M20 RS-MnB, ACI shear & splice, no joint damage	2.159	0.982	0.920	10.00	1.077	0.725	0.478	10.00	1.820
M21 RS-MnB, ACI shear & splice, joint damage	1.378	0.946	0.919	10.00	1.078	0.725	0.485	10.00	1.963
M22 Rigid, ACI shear & splice, no joint damage	2.727	2.043	1.001	10.00	1.679	1.192	1.094	10.00	1.997
Mean:	2.118	1.260	1.367	6.639	1.990	0.672	0.443	7.430	2.135
C.O.V. :	0.607	0.325	0.341	0.587	1.425	0.433	0.594	0.494	0.915
# of failures	0	0	0	5	1	0	0	**Tot. failures**	6

Table 5.5.7: Dynamic analysis data for the *02% in 50 yrs.* ground motion intensity.

building story / model parameters	Maximum inter-story drift (%) 1	2	3	4	5	6	7	Max Inter-Story Drift (%)	Max Roof Drift (%)
M13 UW-MnJ-BS, no shear, no splice, no joint damage	2.976	4.321	2.208	10.00	1.220	1.158	1.131	10.00	4.788
M14 UW-MnJ-BS, no shear, no splice, joint damage	1.985	2.443	5.331	5.170	1.282	0.688	0.370	5.331	1.838
M15 RS-MnB, no shear, no splice, no joint damage	1.534	1.487	1.599	10.00	1.105	0.658	0.411	10.00	5.698
M16 RS-MnB, no shear, no splice, joint damage	1.787	2.092	1.738	10.00	1.103	0.667	0.442	10.00	9.705
M17 Rigid, no shear, no splice, no joint damage	2.976	4.321	2.208	10.00	1.220	1.158	1.131	10.00	4.788
M18 UW-MnJ-BS, ACI shear & splice, no joint dam.	7.296	1.268	1.405	10.00	0.867	0.556	0.574	10.00	4.114
M19 UW-MnJ-BS, ACI shear & splice, joint damage	3.174	2.615	1.631	5.999	1.019	0.984	0.892	5.999	1.278
M20 RS-MnB, ACI shear & splice, no joint damage	2.369	1.226	1.405	10.00	0.867	0.556	0.476	10.00	2.499
M21 RS-MnB, ACI shear & splice, joint damage	1.396	2.372	2.286	10.00	0.945	0.829	0.745	10.00	2.250
M22 Rigid, ACI shear & splice, no joint damage	10.00	1.278	1.061	2.283	2.287	0.689	0.532	10.00	5.073
Mean:	3.549	2.342	2.087	8.345	1.191	0.794	0.670	9.133	4.203
C.O.V. :	0.797	0.498	0.579	0.338	0.346	0.288	0.432	0.201	0.587
# of failures	1	0	0	7	0	0	0	**Tot. failures**	8

Impact of Joint Damage

Including joint damage in the simulations enables representation of joint strength and stiffness loss due to load history. Figure 5.5.8 and Figure 5.5.7 show the observed, simulated roof drift history during the Northridge earthquake for models with and without joint damage. From the data in these figures we see that the inclusion of joint damage introduces erratic behavior in the roof drift history after about 10 seconds into the ground motion as non-linear behavior accumulates.

In Table 5.5.8, the normalized error in the simulated histories, defined by Equation 5.5.1, is presented. These data are calculated through the first 12 seconds of the simulations after which time comparisons become difficult because of simulations that fail. The data in Table 5.5.8 show that the simulation of joint damage has little impact on the error. The error varies by less than 10% with and without damage.

To overcome the limitations of using error between the observed and predicted roof drift to evaluate the models, inter-story drift at the maximum roof drift is used to asses the models. Figure 5.5.9 shows that at this intensity of ground motion, including joint damage in the simulation does not impact the inter-story drift of the models with *RS-MnJ-BS* joints (M13-14). Exploration of the bar-slip spring responses for these models shows little or no cyclic behavior and thus no strength or stiffness degradation. The joints appear to be flexible and elastic in such a way as to put demand on the beams and columns which then control the response. In contrast, the inter-story drift behavior for models with *RS-MnB* joints (M15-16) does change when joint damage is included. Figure 5.5.9 compares the moment-curvature responses for a joint in the models with *RS-MnB* joints. When joint damage is included the joint exhibits reduced stiffness and energy dissipation ability.

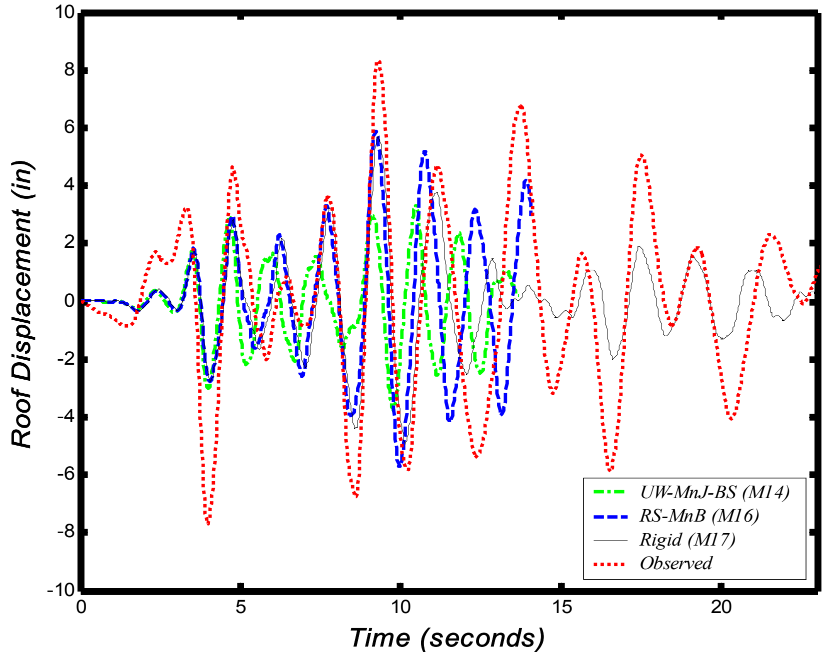

Figure 5.5.7: Comparison of roof drift versus time for various models with no shear or splice models, but with joint damage, exposed to the 50% in 50 Northridge ground motion.

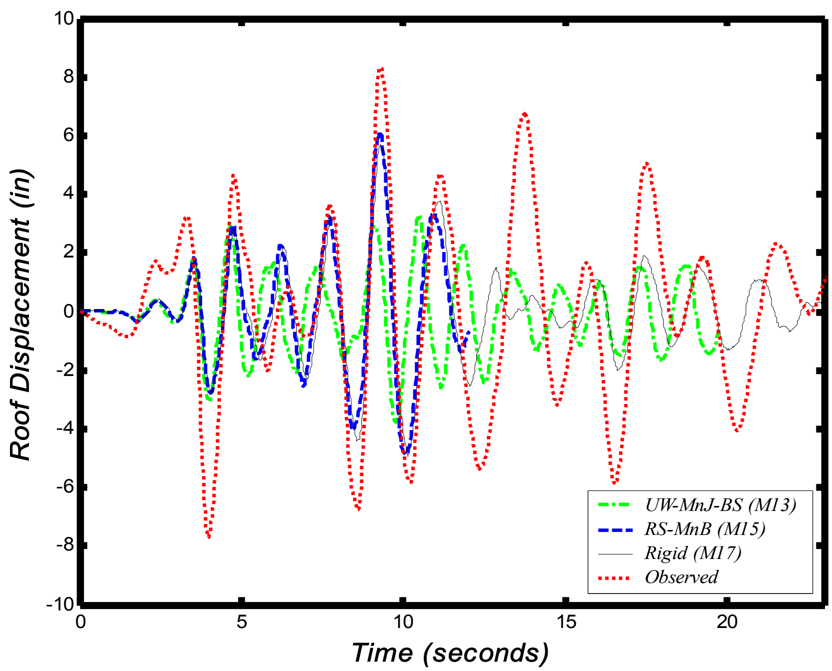

Figure 5.5.8: Comparison of roof drift versus time for various models with no shear, splice, or joint damage exposed to the 50% in 50 Northridge ground motion.

$$\text{Error} = \sqrt{\sum_{time}\left\{\frac{\left[(d_{roof,t})_{obs} - (d_{roof,t})_{simulated}\right]}{\max(d_{roof,observed})}\right\}^2} \quad \text{for time} < 12 \text{ sec.} \qquad \textbf{Equation 5.5.1}$$

Table 5.5.8: Error for simulations with varying failure models, joint damage and joint type.

50% in 50	joint type / shear, splice & dam.	*UW-MnJ-BS*	*RS-MnB*	*Rigid*
Error (values through first 12 seconds of the GM)	no shear no splice no damage	10.027	5.003	4.814
	no shear no splice Damage	9.426	5.538	--
	shear splice no damage	11.170	11.642	5.015
	shear splice Damage	10.867	8.719*	--

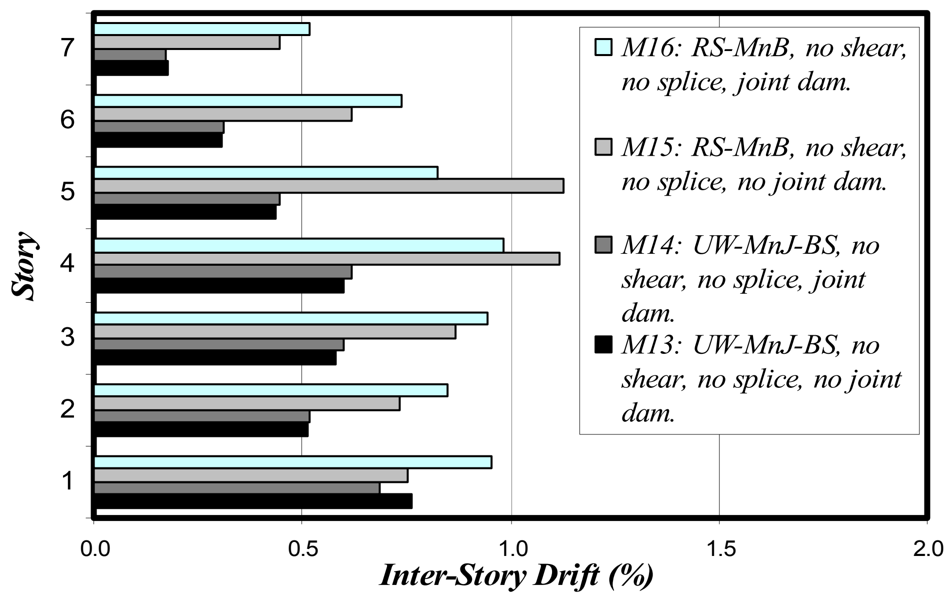

Figure 5.5.9: Comparison of maximum inter-story drifts to show the impact of joint damage.

* Error is calculated only through 9.54 minutes due to numerical issues that aborted the simulation.

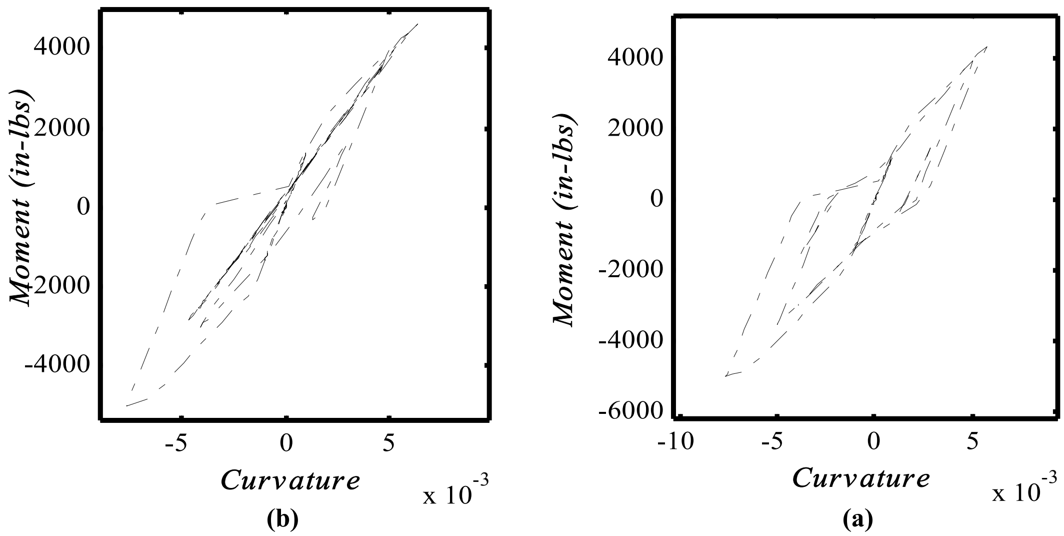

Figure 5.5.10: Joint moment-curvature response for a typical joint from the case study building with (a) no joint damage and (b) joint damage.

Impact of Shear and Splice Failure Models

Figure 5.5.11 provides data for use in evaluating the interaction between the joint models and brittle column failure models. Specifically, the data in Figure 5.5.11 show maximum inter-story drifts for the *50% in 50 yrs.* hazard level for the model with and without brittle column failure. At this intensity, the data show that if the rigid joint models are used, the models with and without the column failure models (M22 and M17) have approximately the same simulated response. This suggests that for these models, the flexural response of the beams and columns control the predicted drifts and the column shear demands do not exceed capacities of most of the columns. Results of analyses conducted using the *UW-MnJ-BS* models (M18 and M13) and the *RS-MnB* models (M20 and M15) indicate that simulating column shear and splice failure does have some impact on predicted inter-story drifts, primarily at the fifth floor for the *UW-MnJ-BS* model and the third floor for the *RS-MnB* model. The impact appears to be moderate because the joint models yield only slightly before brittle column failures occur. While this impact might be more pronounced at higher hazard levels, the slight differences shown in Figure 5.5.11 between the models with and without shear and splice failure models suggests that joint type is a more important parameter in predicting inter-story drift demands.

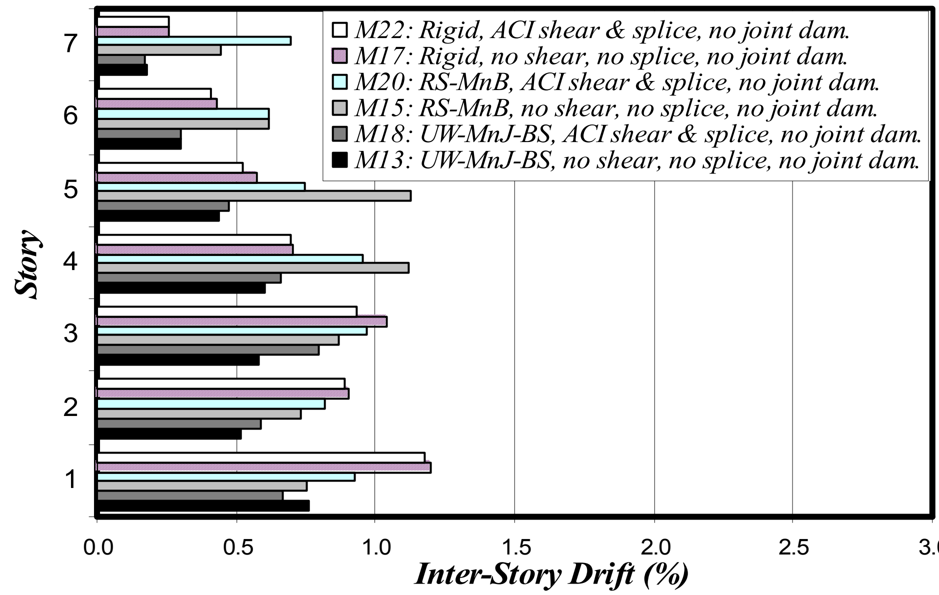

Figure 5.5.11: Comparison of maximum inter-story drifts to show the impact of including the shear and splice failure models.

Impact of Joint Models

The models listed in Table 5.4.1 are used to investigate the impact of the joint model on the maximum inter-story drift. Each model is used to simulate the response of the case-study building under the unscaled 1994 Northridge earthquake ground motion record. Data in Figure 5.5.12 and 5.5.13 provide data for models in which brittle column failure modes and joint damage are not simulated. Data in Figure 5.5.12 compare the predicted inter-story drifts at the maximum roof drift to the observed values; while data in Figure 5.5.13 compare the inter-story drifts predicted at the time of the maximum observed roof drift to the observed values (t = 9.280 seconds). Observed inter-story drift values are computed from acceleration records; values for floor levels on which accelerations were not monitored are interpolated from the available data. Data in Figure 5.5.12 show that including the *UW-MnJ-BS* and *RS-MnB* joint models in simulations of the case study building during the Northridge earthquake results in dramatic failure at the fourth floor for all models except for M18. The accelerations placed on the model result in yielding of the joints at the middle stories, thus placing additional demand on the adjacent beams and columns. The data in Figure 5.5.13 show similar trends, with simulation of inelastic joint action resulting in large drifts on the fourth floor, if not failure. Again this is attributed to the joints yielding and the surrounding beams and columns experiencing increased demand.

Data in Figures 5.5.13 and 5.5.15 compare simulated and observed response for models in which column shear failure and splice are simulated. Data in Figure 5.5.13 compare inter-story drifts at the maximum rood drift, while data in Figure 5.5.15 compare inter-story drifts at the time of the observed maximum roof drift. The data in Figures 5.5.13 and 5.5.15 show that use of the *RS-MnB* joint model results in a dramatic failure at the fourth floor, while use of the *UW-MnJ-BS* model indicates a reduction in inter-story drift demand. The simulations with the *UW-MnJ-BS* joints appear to have elements experiencing nonlinear behavior in a less local manner than when the *RS-MnB* joint model is used.

Figure 5.5.14 and Figure 5.5.15 compare the inter-story drifts predicted at the time of the maximum observed roof drift to the observed values (t = 9.280 seconds). These figures show that the joint models lead to large drifts on the fourth floor, if not failure, if no brittle column failure is modeled. When shear and splice is modeled, the *RS-MnB* shows dramatic failure at the fourth floor, while the *UW-MnJ-BS* model indicates a reduction in inter-story drift demand. The primary difference between the inter-story drifts at maximum drift and at the time of the observed maximum drift is that the models without the brittle column failure mechanisms do not exhibit extreme drifts on the fourth floor (see Figure 5.5.12 and Figure 5.5.14). The observed maximum drift occurs earlier in the analysis than the maximum drift for most models, and thus less damage and inter-story drift has been realized.

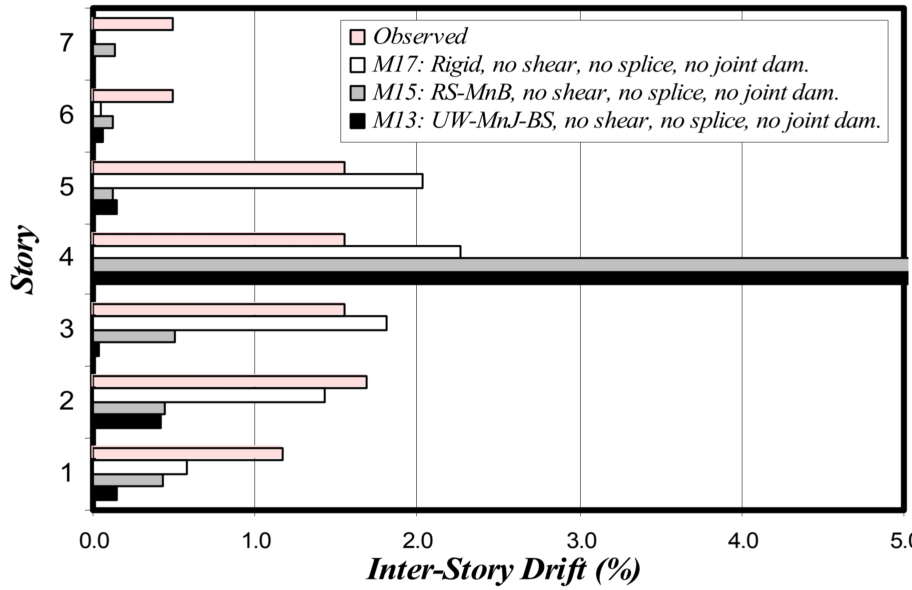

Figure 5.5.12: Simulated and observed inter-story drifts at maximum roof drift for models with no joint damage, shear, or splice failure for the unscaled 1994 Northridge ground motion.

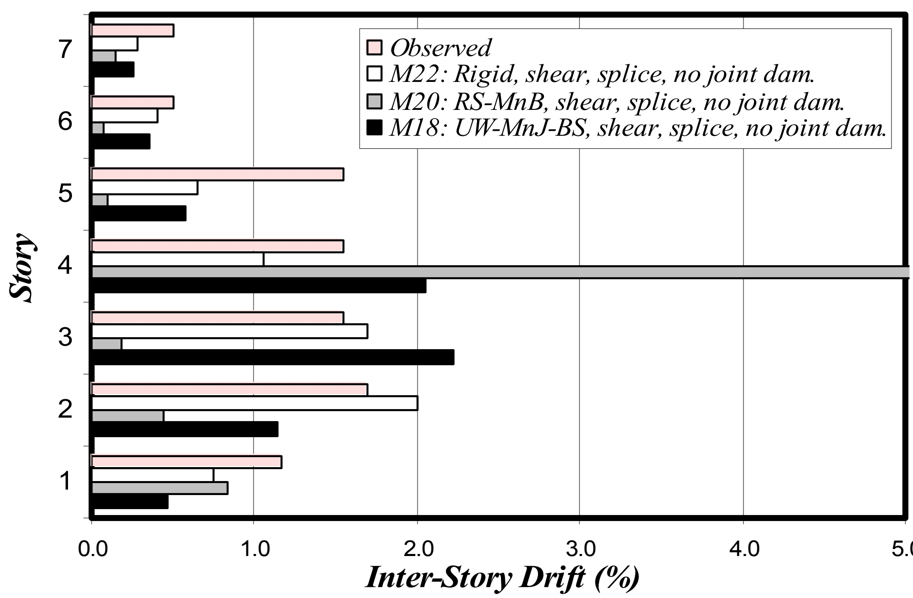

Figure 5.5.13: Simulated and observed inter-story drifts at maximum roof drift for models with shear or splice failure, but no joint damage for the unscaled 1994 Northridge ground motion.

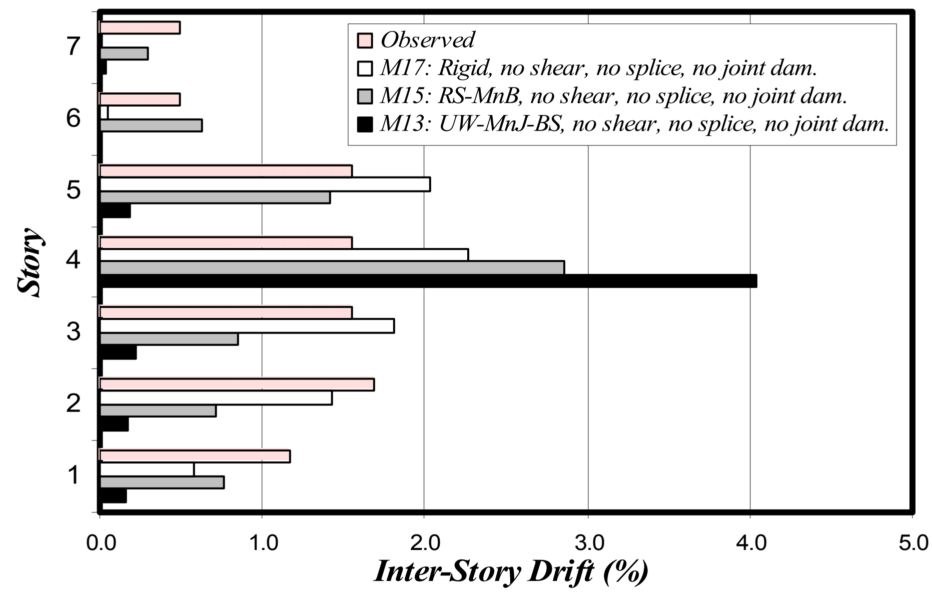

Figure 5.5.14: Inter-story drifts at the time of the observed max roof drift. Models have no joint damage, shear, or splice failure for the unscaled 1994 Northridge ground motion.

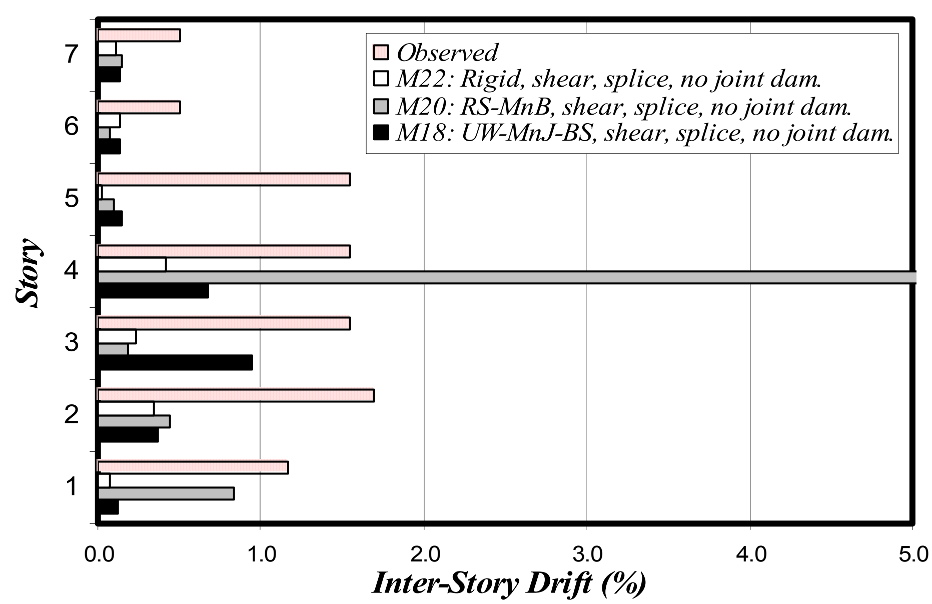

Figure 5.5.15: Inter-story drifts at the time of the observed max roof drift. Models have shear and splice failure, but no joint damage for the unscaled 1994 Northridge ground motion.

5.6. Summary and Conclusions

Joint Cruciform Simulation

The two joint models, *RS-MnB* and *UW-MnJ-BS*, were used to simulate the response of a typical joint sub-assemblage from the third story of the case study building. The sub-assemblage with the joint models were analyzed using the PEER pseudo-static, cyclic load history. The sub-assemblage analyses provided a template for the applying the joint models in the full-frame analyses of the case study building and provided improved understanding of simulated joint behavior.

The results of theses analyses show that for a typical case study building joint, the inclusion of the two preferred joint models impacts the seismic behavior through joint panel yielding and bar-slip. The *RS-MnB* analysis shows how joint panel yielding can control the deterioration in cruciform stiffness and strength. The *UW-MnJ-BS* model shows how inelastic bar-slip action can impact seismic joint behavior in the case study building.

Case Study Building Pushover Simulation

Full-frame pushover analyses were completed for a series of models with varying joint model type, brittle column failure models, and gravity loading (Table 5.4.1). Simulation of inelastic joint action was accomplished by modifying the model of the case study building developed by Paspuleti (2002) to include the joint models.

The pushover analyses allow for study of the impact of the joint model type, failure models and gravity on the lateral strength and deformation capacity of the case study building. The results of the pushover analyses show the following:

- If inelastic joint action is simulated, the simulated drift capacity of the building exceeds the maximum drift observed during the Northridge earthquake.
- The type of joint model affects the predicted failure mode and failure progression for the structure.

- Simulation of gravity load has little impact on frame response when brittle column failure models are not included, but does impact response when brittle column failure modes are simulated.
- Building response is determined also by modeling decisions associated with simulation of gravity load, column shear failure, and splice failure.

Case Study Building Dynamic Simulation

Dynamic analyses of study building were conducted to investigate the impact on response of 1) the type of joint model, 2) simulation of joint damage, 3) simulation of brittle column failure, and 4) ground motion intensity. The *RS-MnB*, *UW-MnJ-BS*, and rigid joint models were used, and the two non-rigid joints were allowed to have varying joint damage. The brittle column failure modeling options were combined with joint model type and joint damage to produce twelve different models that were then subjected to the 1994 Northridge earthquake ground motion as observed at the case study building, scaled to four different hazard levels.

Results of the dynamic analyses show that as the hazard level increases building performance is reduced and demands on the structure increase. The roof and inter-story drifts increase and the number of failed analyses with inter-story drifts greater than 10% increase from zero to eight.

The dynamic analysis results also show that joint damage has an impact on inter-story drift. Joint damage is shown to significantly impact inter-story drift for the models with the *RS-MnB* joint model even at the least intense ground motion because the joints exhibit reduced stiffness and energy dissipation. However, no joint damage is predicted in the *UW-MnJ-BS*. The response is controlled by the response of the beams and column instead.

The impact of the shear and splice failure models was explored in terms of inter-story drifts. For the analyses with the rigid joint model, the brittle column failure models have little impact on the predicted inter-story drifts. For these simulations flexural response of the beams and columns control the predicted drifts and the column shear demands do not exceed capacities of most of the columns. The analyses with the *UW-*

MnJ-BS and *RS-MnB* joint models show some impact on inter-story drifts with the inclusion of the brittle column failure models, but the impact appears to be moderate because the joint models yield only slightly before brittle column failures occur.

Comparison of inter-story drifts for models with and without flexible joints show that the inclusion of the different joint model types greatly impact the predicted inter-story drifts. The inclusion of the *UW-MnJ-BS* and *RS-MnB* joint models in simulations of the case study building during the Northridge earthquake results in dramatic deformation demands at the fourth floor, the floor of maximum observed damage during the earthquake. The nonlinear behavior of the joints results in increased demands on the beams and columns leading to the large deformation demands in these elements. Comparison of the predicted inter-story drifts at the predicted maximum roof drift and the time corresponding to the maximum observed roof drift to the observed values suggests that the observed maximum drift occurs earlier in the analysis than the maximum drift for most models, and thus less damage and inter-story drift has been realized.

Chapter 6

Summary and Conclusions

6.1. Summary

Past experimental investigation and observed earthquake response indicate that beam-column joint damage may have a significant impact on building response. This research investigates explicit simulation of inelastic joint action to enable accurate prediction of component demands and global building response. Specifically, this research investigates simulation of the inelastic response of beam-column joints in older, reinforced concrete frames.

The research effort presented here comprised a survey of previous research of an older reinforced concrete building (Chapter 2) and of beam-column joints (Chapter 3), development of a joint element model and simulation of sub-assemblage response (Chapter 4), and simulation of frames from the case-study building using the joint models (Chapter 5).

Chapter 2 introduces the case-study building, the Holiday Inn in Van Nuys, California. This building was used in the current study to support evaluation of the joint models through comparison of simulated and observed response as well as to support assessment of the impact of simulation of inelastic joint action on building frame response. The case-study building was designed in 1965 and has design details typical of pre-1970 construction. In particular, beam-column joints in the building have no transverse reinforcing steel, a design characteristic which is considered inadequate for seismic zones by today's standards and could be expected to results in significant joint stiffness and strength loss under earthquake loading. This building was instrumented with accelerometers prior to the 1971 San Fernando earthquake and again in 1980, and, as a result, has been studied extensively by researchers and practicing engineers. Acceleration data are available characterizing building response to the 1994 Northridge earthquake. Documentation of damage observed following the 1994 earthquake also is available.

Chapter 3 presents a survey of previous experimental investigations of the earthquake response of reinforced concrete beam-column joints. The results of these studies provide three things for the current research: an understanding of the design and load parameters that determine earthquake response of joints such as joint shear stress demand and bond demand, approaches to modeling joint response, and a basis for choosing which modeling approaches are most promising for use in simulation the response of older reinforced concrete buildings, such as the case study building.

Chapter 4 focuses on evaluation of the modeling approaches presented in Chapter 3. The models were evaluated through comparison of simulated and observed response for a series of building sub-assemblages tested in the laboratory by researchers at the University of Washington. This test program was chosen for use as the sub-assemblages included beam-column joints with reinforcement details, joint shear stress demand and bond stress demand typical of those observed in older, reinforced concrete buildings. The process used and assumptions made in building models of the laboratory test specimens using the OpenSees framework are presented. Simulated and observed response was compared using response measures such as simulated shear strength, stiffness, and drift demands. Finally, two preferred methods for simulating the response of older beam-column building joints were identified.

Chapter 5 presents the results of two studies in which the preferred joint modeling approaches, identified in Chapter 4, were used to simulate the earthquake response of the case-study building. First, analyses of a typical sub-assemblage from an exterior frame of the case study building were conducted. The results of these analyses provide understanding of joint behavior in multi-component frames and enabled identification of the response characteristics and computational issues that may affect prediction of global system response. The joint models also were used to simulate the response of an interior and exterior frame of the case study building subjected to pseudo-static and dynamic lateral loading. The impact of the joint model and model characteristics on building response were evaluated; additionally, the impact of simulating brittle column failure modes, variation in gravity load, and variation in earthquake load intensity in combination with simulation of inelastic joint action was investigated.

6.2. Conclusions

6.2.1. Review of Previously Proposed Joint Models

A review of previous research investigating modeling of the earthquake response of reinforced concrete beam-column building joints (Chapter 3) resulted in the identification of three different approaches to modeling joint action that were chosen for further study as part of this research effort. These modeling approaches included two finite-area super-elements comprised of multiple non-linear components (Altoontash and Deierlein 2003, Lowes et al. 2004) as well as one model in which a zero-length rotational spring is combined with rigid links that define the joint area (Alath and Kunnath 1995). These modeling approaches were chosen because 1) at the time this project began, the element formulations were available for use in OpenSees, 2) data were available indicating that these models could be expected to exhibit acceptably robust behavior under cyclic loading and 3) the research team had immediate access to individuals experienced with the models.

The OpenSees *Pinching4* material model, a general one-dimensional load-deformation response model that can be calibrated relatively easily to simulate stiffness and strength degradation under cyclic loading, was chosen for use in this study. A review of previous research resulted in the identification of three procedures for calibrating the joint models that were considered appropriate for further study. These calibration procedures enabled prediction of joint response on the basis of joint geometry, material properties and design characteristics and employed the Modified Compression Field Theory as well as empirical data.

6.2.2. Exploration of Seismic Joint Behavior

The three joint models with the three calibration approaches were used in combination to create a series of models that were used to simulate five laboratory tests conducted at the University of Washington (Walker 2001 and Alire 2002). Predicted and observed load versus drift data were compared and two preferred models were determined based. One of the preferred models, identified as *RS-MnB,* used the rotational spring element with an empirical calibration approach in which joint strength was defined by flexural strength of the beams framing into the joint. The second preferred model, identified as *UW-MnJ-BS*, used the super-element proposed by Lowes and Altoontash (2003) with a calibration approach in which joint-core shear strength and bar-slip response were defined by laboratory data.

The preferred models provide accurate representation of various joints depending on the model calibration. If joints with high joint shear stress demand are to be modeled, a model calibrated to the joint core shear stress is recommended, and for joints with low joint shear stress demand a model that is calibrated to the strength of the adjacent beams is recommended.

A number of issues resulted in joint models and calibration procedures being removed from the preferred model list. The calibration procedures in which the Modified Compression Field Theory was used to define joint core shear strength were shown to be unsuitable for use in simulating the observed strength of these joint specimens, as the MCFT under predicted observed strength. Those models that included the super-element create at Stanford were shown to be redundant to the University of Washington models. The University of Washington model was used because it included simulation of bar-slip behavior.

One weakness of all the models used to simulate the response of the laboratory test specimens was the rate of strength and stiffness degradation. The results showed that the models were not calibrated to predict joint failure at the correct drifts. Furthermore, when the models did predict joint failure, the result was rapid degradation of the cruciform shear strength and stiffness.

6.2.3. Joint behavior in the case study building

The two joint models, *RS-MnB* and *UW-MnJ-BS*, were used to simulate the response of a typical joint cruciform sub-assemblage from the third story of the case study building. The results of these analyses provide understanding of expected joint behavior and show that for a typical joint from the case study building, the inclusion of the two preferred joint models impacts the seismic behavior through joint panel yielding and bar-slip. The analyses done with the *RS-MnB* model show that joint panel yielding can control the deterioration in cruciform stiffness and strength. The analyses done using the *UW-MnJ-BS* model show how that inelastic bar-slip action can impact seismic joint behavior in the case study building.

Monotonic pushover analyses of an exterior frame of the case-study building were completed in which the joint model, column shear-failure model, and gravity load models were varied as shown in detail in Section 5.5. The results of these analyses indicate the following:

1. Even if inelastic joints action is explicitly simulated using the joint models, the frame has sufficient drift capacity to achieve the maximum drift observed during the 1994 Northridge earthquake without exhibiting significant strength loss.
2. The type of joint model determines the predicted failure mode and failure progression for the structure. The inclusion of the *RS-MnB* model results in predictions of large inter-story drifts at the fourth floor regardless of whether brittle column failure was possible. Including the *UW-MnJ-BS* model can result in large drifts at the fourth floor, but only if the columns can fail in shear and by splice.
3. Regardless of how the joint action is modeled, variation in the simulation of gravity load, column shear failure, and failure of column reinforcement splices have a significant effect on predicted response.
4. Simulation of gravity load has minimal impact on frame response when brittle column failure is not simulated. However, if brittle column failure is simulated, then simulation of the gravity load results in strength loss at a larger / smaller drift demand.

Dynamic analyses of the case study building were performed to investigate the impact of the joint model, simulation of joint damage, simulation of brittle column failure, and ground motion intensity on response. A total of twelve different models were used for the study; the different models employed 1) the two preferred joint models, *RS-MnB* and *UW-MnJ-BS*, as well as a rigid joint model were used; 2) simulation and no simulation of joint strength and stiffness deterioration under cyclic loading, and 3) simulation and no simulation of brittle column failure modes. The twelve models were subjected to the 1994 Northridge earthquake ground motion as observed at the base of the case study building, scaled to four different intensity levels. Results of the dynamic analyses show the following:

1. As ground motion intensity increased, roof and inter-story drifts increased and the number of analyses in which inter-story drift exceeded 10%, and thus the building was considered to have failed, increased from zero to eight.
2. For the analyses in which joints were assumed to be rigid, the brittle column failure models had little impact on the predicted inter-story drifts.
3. For the analyses in which inelastic joint action was simulated using either the *UW-MnJ-BS* or the *RS-MnB* model, simulation of brittle column failure models had some impact on inter-story drifts, but the type of joint model had a more significant impact on inter-story drifts. Specifically, the inclusion of the *UW-MnJ-BS* and *RS-MnB* joint models in simulations of the case study building during the Northridge earthquake resulted in dramatic deformation demands at the fourth floor, the floor of maximum observed damage during the earthquake.
4. Simulation of joint strength and stiffness deterioration resulting from cyclic loading had a significant impact on maximum inter-story drift demands for the *RS-MnB* model. The inclusion of joint strength and stiffness deterioration for the *UW-MnJ-BS* model is shown to have less impact on inter-story drift demands especially at low ground motion intensities.

6.3. Recommendations

6.3.1. Recommendations for Consulting Engineers

The results of the research presented here support some basic recommendations for the consulting engineers who are evaluating reinforced concrete frames with details typical of pre-1970 construction. The primary recommendation is that some consideration must be given to the inelastic response, including stiffness and strength loss, of beam-column joints in older reinforced concrete frames. The research results presented here show that if inelastic joint action is ignored in simulating the response of a joint sub-assemblage, the simulation will fail to accurately predict global system response. The results of the full-frame analyses support the same recommendation. However, for frame analysis, numerous other failure modes and modeling decisions may control the predicted response. Further research is needed to develop reliable models and comprehensive modeling recommendations for use in simulating the response of older reinforced concrete frames

6.3.2. Recommendations for Researchers

The results of this study support two recommendations for researchers. Both are limited to application of the joint models available currently in the OpenSees. The first addresses calibration of the joint element. For joints with detailing typical of older construction, different joint models and calibration approaches are appropriate depending on the shear stress demand. If joints with high joint shear stress demand are to be modeled, a model calibrated to the joint core shear stress is recommended, and for joints with low joint shear stress demand a model that is calibrated to the strength of the adjacent beams is recommended. The second addresses the different element formulations. The super-elements developed at Stanford University, denoted *ST*, and at the University of Washington, denoted *UW*, will predict the same behavior if only the joint shear panel component is defined to be flexible. However, the *UW* joint element should be used if bar-slip spring prediction is desired, and the *ST* element if large joint deformation predictions are desired. The researcher also should be aware of the difference in response that is predicted using the rotational spring element. The single spring element does not allow the upper column to translate with respect to the lower column. As a result, an additional calibration is recommended to bring the simple rotational spring element into kinematic agreement with the finite-area super-elements.

6.4. Future Work

The objective of the research presented here was to investigate the use of inelastic beam-column joint models to improve accuracy in predicting response and component demand for older, reinforced concrete frames. Accurate prediction of response is required for performance-based earthquake engineering (PBEE). The research results presented here advance understanding of nonlinear analysis of older, reinforced-concrete frames subjected to earthquake loading as well as identify a number of areas in which additional research is required to improvement to enable accurate prediction of response.

On area that must be addressed in the future is the objectivity in and refinement of the model calibration procedures. As discussed in the previous section, the results of this study suggest that it is appropriate to use one calibration procedure for joints with "low" shear stress demands and second for joints with "high" shear stress demands. However, at this time, there are not sufficient data available to accurately characterize "high" and "low" joint shear stress demand. Furthermore, the two preferred calibration methods rely heavily on highly empirical data and may not be appropriate for use in the simulating the response of joints with different geometric configurations or bond-zone characteristics.

Another area to be addressed in future work is the calibration of the stiffness and strength degradation models. The current calibration parameters result in inaccurate predictions of degradation. These predictions can be improved by assessing the experimental data from which the calibrations are determined, deciding if a large sampling of data is needed, taking a final set of data that contains experiments that will ensure applicability, updating the calibration parameters and testing them for a range of joints. The resulting calibration parameters should be more accurate in predicting degradation than the current ones do for the UW laboratory tests.

The beam-column joint models investigated as part of this research effort were developed using data from two-dimensional interior building sub-assemblage tests in which the impact of slabs and beam eccentricity was not considered. The exterior frame of the case study building include eccentric beam-column joints in which beams and slabs were composite and included interior and exterior joints. Additional research is required to investigate the impact of these, and other, design parameters on joint response and to extend the previously proposed models to better simulate the response of joints with these characteristics.

Finally, analysis results for the case-study building suggest that additional research is required also to improve beam-column component models and to develop comprehensive modeling recommendations for older reinforced concrete building frames. In simulating the response of the exterior frames of the case-study building, lumped plasticity beam-column elements were used. Effective stiffness parameters were determined for the elastic portion of these elements using the results of eigen analyses; additional research is required to develop recommendations for use in defining effective stiffness parameters for this type of model that are appropriate for a range of designs.

LIST OF REFERENCES

ACI Committee 435 (1966). *Deflection of Concrete Building Structures* (ACI 435-66), American Concrete Institute, Detroit, MI.

ACI Committee 318 (1971). *Building Code Requirements for Structural Concrete* (ACI 318-71), American Concrete Institute, Detroit, MI.

ACI Committee 318 (1999). *Building Code Requirements for Structural Concrete* (ACI 318-99), American Concrete Institute, Farmington Hills, MI.

ACI Committee 318 (2002). *Building Code Requirements for Structural Concrete* (ACI 318-02) *and Commentary* (ACI 318R-02), American Concrete Institute, Farmington Hills, MI.

Alath, S., and Kunnath, S.K. (1995). *Modeling inelastic shear deformation in reinforced-concrete beam-column joints.* Engineering Mechanics: Proceedings of 10th conference. University of Colorado at Boulder, May21-24, ASCE, New York, Vol. 2, 822-825.

Alire, D. A. (2002). "Seismic Evaluation of Existing Unconfined Reinforced Concrete Beam-Column Joints." Master's Thesis, Department of Civil Engineering, University of Washington.

Altoontash, A., and Deierlein, G.G. (2003). *A Versatile Model for Beam-Column Joints.* ASCE Structures Congress Proceedings, Seattle, Washington.

American Society of Civil Engineers (2000). *FEMA 356: Prestandard and Commentary for the Seismic Rehabilitation of Buildings*, Federal Emergency Management Agency, Washington, D.C.

Anderson, J.C., and Townsend, W.H. (1977). "Models for reinforced concrete frames with degrading stiffness." *Journal of thee Structural Division* ASCE, 103 (ST12), 1433-1449.

ATC 33. "NEHRP Guidelines for the Seismic Rehabilitation of Buildings." Building Seismic Safety Council, Washington, D.C., 1997.

Barin B., and Pincheira J.A. (2002). *Influence of modeling parameters and assumptions on the seismic response of an existing RC building.* Departmental Report, Dept. of Civil and Environmental Engineering, University of Wisconsin, Madison.

Bennett, B. (2003). Departmental Report. Department of Civil Engineering, University of Washington.

Biddah, A., and Ghobarah, A. (1999). "Modeling of shear deformation and bond slip in reinforced concrete joints." *Structural Engineering and Mechanics*. 7(4), 413-432.

Blume, J.A. and Assoc. (1973). *Holiday Inn*, Chapter 29 in *San Fernando, California earthquake of February 9, 1971*, Volume I Part A, U.S. Dept. of Commerce National Oceanic and Atmospheric Administration, Washington, D.C.

Bonnaci, J.F., and Pantazopoulou, S.J (1993). "Parametric Investigation of Joint Mechanics." *ACI Structural Journal* 90 (1): 61-71

Branson, D. E. (1963). *Instantaneous and Time-Dependent Deflections of Simple and Continuous Reinforced Concrete Beams*., Alabama Highway Research Report, No. 7, Bureau of Public Roads.

Browning, J.A., Li, R.Y., Lynn, A., and Moehle, J.P. (2000). Performance assessment for a reinforced concrete frame building. *Earthquake Spectra*, 16(3), 541-555.

California Strong Motion Instrumentation Program (CSMIP 1994). <http://www.consrv.ca.gov/cgs/smip/>

Clyde, C. Pantelides, C.P., and Reaveley, L.D., (2000). Performance-Based Evaluation of Exterior Reinforced Concrete Building Joints for Seismic Excitation." *Pacific Earthquake Engineering Research Report, PEER 2000/05*. Berkeley: University of California.

Charney, Finely (2001). "Calibrating SDOF joint spring models for complex kinematics." Proceedings of 9th US National conference on Earthquake engineering. Earthquake Engineering Research Institute, Oakland, CA.

De la Llera, J.C., Chopra, A.K., and Almazan, J.L. (2001). Three-dimensional inelastic response of an RC building during the Northridge earthquake. *Journal of Structural Engineering.* ASCE, 127(5), 482-489.

Deng, C.G., Bursi, O.S., and Zandonini, R. (2000). "A hysteretic connection element and its application." *Computers and Structures*, 78, 1-3, Nov 2000, 93-110.

Durrani, A.J., and Wight, J.K. (1982). *Experimental and Analytical study of internal beam to column connections subjected to reverse cyclic loading.* Technical Report, Department of Civil Engineering, The University of Michigan, July.

EERI (1994). *Northridge Earthquake January 17, 1994 Preliminary Reconnaissance Report*. Ed. J.F. Hall. Oakland, CA: EERI.

El-Metwally, S.E., and Chen, W.F. (1988). "Moment-rotation modeling of reinforced-concrete beam-column connections." *ACI Structural Journal*, 85(4), 384-394.

Elmorsi, M., Kianoush, M.R., and Tso, W.K. (1998). "Lightly Reinforced beam-column joint model for frame analysis" Proceedings of 6th US National conference on Earthquake engineering. Earthquake Engineering Research Institute, Oakland, CA.

Filippou, F.C., Popov, E.P., and Bertero, V.V. (1983), "Modeling of R/C joints under cyclic excitations," Journal of Structural Engineering, Vol. 109, No. 11, pp. 2666-2684.

Fleury, F., Reynouard, J.M., and Merebet, O. (2000). "Multi-component model of reinforced concrete joints for cyclic loading " *Journal of Engineering Mechanics*, 126(8), August 2000, 804-811.

Hibbeler, R.C., "Mechanics of Materials". 5th Edition, Prentice Hall, Inc., 2002.

Hsu, T.T.C., (1988) "Softening Truss Model Theory for Shear and Torsion," *Structural Journal of the American Concrete Institute*, Vol. 85, No. 6, Nov.-Dec., pp. 624-635.

Islam, M.S. (1996). "Analysis of the Northridge Eartthquake Response of a Damaged Non-Ductile Concrete Frame Building", *The Structural Design of Tall Buildings* 5 (3): 151-182, 1996.

Kent, D. C., and Park R. (1971). "Flexural Members with Confined Concrete," *Journal of the Structural Division*, ASCE, Vol. 97, No. ST7, July, pp. 1969-1990.

Kitayama, K., Otani, S. and Aoyama, H. (1987). "Earthquake resistant design criteria for reinforced concrete beam-column joints" Proceedings of Pacific conference on Earthquake Engineering. Wairakei, New-Zealand. Aug 5-8, Vol. 1, 315-326.

Kowalsky, M.J., and Preistly, M.N.J. (2000) "Improved Analytical Model for Shear Strength of Circular Reinforced Concrete Columns in Seismic Regions." *ACI Structural Journal* 97 (3): 388-396.

Leon, R.T. (1990). "Shear Strength and Hysteretic Behavior of Interior Beam-Column Joints." *ACI Structural Journal* 87 (1): 3-11.

Li, Y.R., and Jirsa, J.O. (1998). Nonlinear analyses of an instrumented structure damaged in the 1994 northridge earthquake. *Earhquake Spectra*. 14(2), 265-283.

Lehman, D. E. et al. (2004). “Experimental Evaluation of Seismic Design Provisions for Circular Reinforced Concrete Columns”. *Journal of Structural Engineering, ASCE*, June 2004.

Lowes, L.N., and Altoontash, A. (2003). “Modeling reinforced-concrete beam-column joints subjected to cyclic loading” *Journal of Structural Engineering,* ASCE, 129(12), December 2003, 1686-1697.

Lowes, L.N., Mitra, N., and Altoontash, A., (2004). “A Beam-Column Joint Model for Simulating the Earthquake Response of Reinforced Concrete Frames”. *Pacific Earthquake Engineering Research Report*, PEER 2003/10. Feb. 2004, Berkeley: University of California.

Lowes, L.N., and Moehle, J.P. (1999). Evaluation and Retrifit of Beam-Column T-Joints in Older Rieinforced Concrete Bridge Structures.” *ACI Structural Journal* 96 (4): 519-532.

MacGregor, James, G., “Reinforced Concrete: Mechanics and Design”. 3rd Edition, Prentice Hall, Inc., 1997.

Mander J.B., Priestley M.J.N., and Park R. (1988). "Theoretical stress-strain model for confined concrete," *Journal of Structural Engineering*, Vol. 114, No. 8, pp. 1804-1826.

Mazzoni, S., and Moehle, J.P. (2001), “Seismic Response of Beam-Column Joints in Double-Deck Reinforced Concrete Bridge Frames.” *ACI Structural Journal* 98 (3): 259-269.

Meinheit, D.F., and Jirsa, J.O. (1977). “Shear strength of Reinforced Concrete Beam-Column Joints”. *CESRL Report No. 77-1.*, Austin: University of Texas.

Menegotto, M., and Pinto, P.E., (1973). "Method of analysis for cyclically loaded R.C. plane frames including changes in geometry and non-elastic behaviour of elements under combined normal force and bending." Symposium on the Resistance and Ultimate Deformability of Structures Acted on by Well Defined Repeated Loads, International Association for Bridge and Structural Engineering, Zurich, Switzerland, pp. 15-22.

Mosier, W.G. (2000). “Seismic Assessment of Reinforced Concrete Beam-Column Joints.” Master’s Thesis, Department of Civil Engineering, University of Washington.

Open System for Earthquake Engineering Simulation (OpenSees) website: <http://www.opensees.berkeley.edu>. PEER, Berkeley: University of California.

Otani, S. (1974). “Inelastic analysis of reinforced-concrete frame structures” *Journal of the Structural Division*, ASCE, 100 (ST7), 1422-1449.

Pacific Earthquake Engineering Research Center website: <http://peer.berkeley.edu>. PEER, Berkeley: University of California.

Pacific Earthquake Engineering Research Center Test Beds website: <http://www.peertestbeds.net>. PEER, Berkeley: University of California.

Pagni, C.A. (2003). “Modeling of structural damage of older reinforced concrete components.” Master’s Thesis, Department of Civil Engineering, University of Washington.

Park, R., Priestly, M.N.J., and W.D. Gill (1982). “Ductility of Square-Confined Concrete Columns”. *Journal of the Structural Division*, ASCE, V. 108, No. ST4, pp. 135-137.

Park, R., and Ruitong, D. (1988). “A comparison of the behavior of reinforced concrete beam-column joints designed for ductility and limited ductility”. *Bulletin of the New-Zealand National Society of Earthquake Engineering*, 21(4), 255-278.

Paspuleti, C., (2002). “Simulating the Earthquake Response of an Older Reinforced Concrete Frame Building.” Master’s Thesis, Department of Civil Engineering, University of Washington.

Priestley, M.N.J., and Park, R. (1987). “Strength and Ductility of Concrete Bridge Columns Under Seismic Loading.” *ACI Structural Journal* 84 (8): 61-75.

Scott, M.H. (2001). “A Software Structure for Finite Element Material Models.” M.S. Thesis. Department of Civil and Environmental Engineering, Berkeley: University of California.

Somerville, P., and Collins, N. (2002). “Ground Motion Time Histories for the Van Nuys Building”. PEER Methodology Testbed Project, URS Corporation, Pasadena, CA.

Stevens N.J., Uzumeri, S.M., and Collins, M.P. (1991). “Reinforced-Concrete Subjected to Reverse-Cyclic Shear – Experiment and constitutive Model.” *ACI Structural Journal* 88 (2): 135-146.

Trifunac, M.D., Ivanovic, S.S. and M.I. Todorovska (1999). *Seven storey reinforced concrete building in Van Nuys, California: strong motion data recorded between 7 February 1971 and 9 December 1994, and Description of Damage following Northridge 17 January 1994 earthquake*, Dept. of Civil Engr., Report CE 99-02, Univ. of Southern California, Los Angeles, California.

Trifunac, M.D., and Hao, T.Y. (2001). *Seven storey reinforced concrete building in Van Nuys, California: Photographs of the Damage from the 1994 Northridge Earthquake*. Dept. of Civil Engr., Report CE 01-05, Univ. of Southern California, Los Angeles, California.

Uniform Building Code (1967). International Conference of Building Officials (UBC-67)

Vecchio, F.J., and Collins, M.P. (1986). "The modified compression field theory for reinforced concrete elements subjected to shear". *ACI Structural Journal*, 83(2), March-April, pp. 219-231.

Walker, S. G. (2001). "Seismic Performance of Existing Reinforced Concrete Beam-Column Joints." Master's Thesis, Department of Civil Engineering, University of Washington.

Ziyaeifar & Noguchi (2000). "A refined model for beam elements and beam-column joints." *Computers and Structures*, Vol. 76, 551-564.

Appendix A

UW Joint Modeling Data

A.1. Introduction

This appendix contains data plots for the simulations of the five cruciform tests explored in this research, PEER4150, PEER2250, PEER0995, PADH2250, and CD302250. Each plot in Section A.2 compares the simulated response of a given specimen using one of the nine joint models introduced in Chapter 4 to the experimental response of the same specimen. Table A.1 is a review of the nine joint models investigated. Section A.3 contains plots comparing relevant model pairs such as *RS-MnB* and *RS-MnJ*.

Table A.1: UW cruciform simulations

Simulation Tag	***Tag in Plots***	***Joint Element***	***Joint Material Model***	***Barslip Material Model***
UW-MCFT-BS	UW-A	beamColumnJoint	MCFT	Barslip
ST-MCFT	ST-A	Joint2D	MCFT	Elastic
UW-MnB	UW-B	beamColumnJoint	MnB	Elastic
ST-MnB	ST-B	Joint2D	MnB	Elastic
RS-MnB	RS-B	Rotational Spring	MnB	NA
UW-MnJ	UW-C	beamColumnJoint	MnJ	Elastic
ST-MnJ	ST-C	Joint2D	MnJ	Elastic
RS-MnJ	RS-C	Rotational Spring	MnJ	NA
UW-MnJ-BS	UW-D	beamColumnJoint	MnJ	Barslip

A.2. Simulation Data Plots

PEER4150

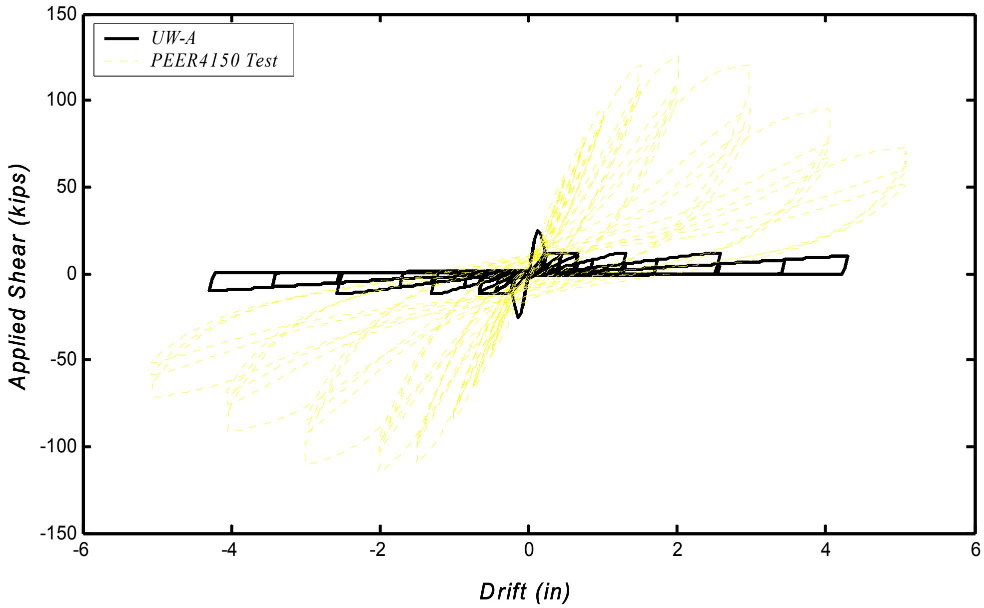

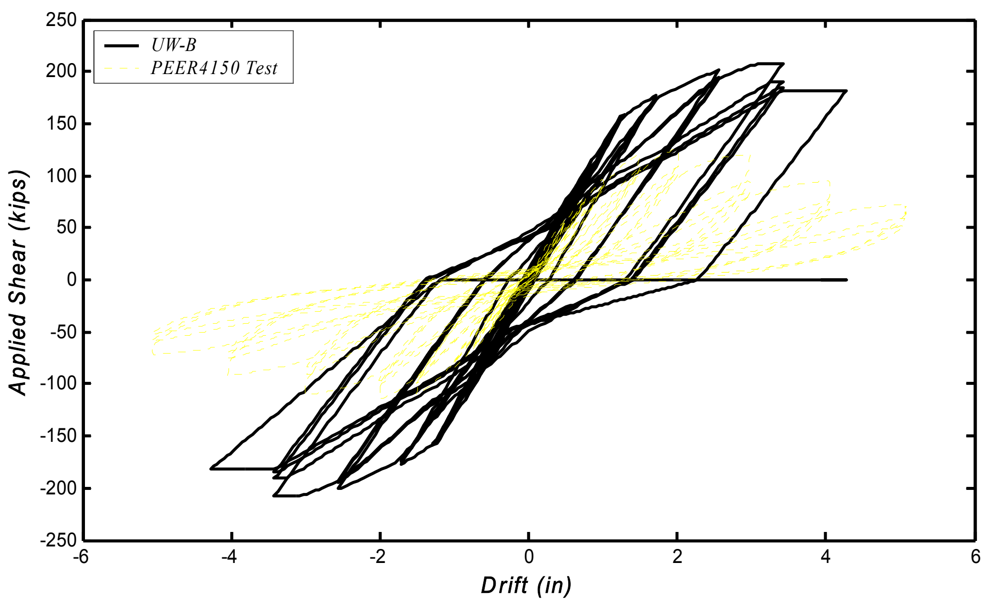

Figure A.1: PEER4150 Simulation results using (top) UW-A and (bottom) UW-B.

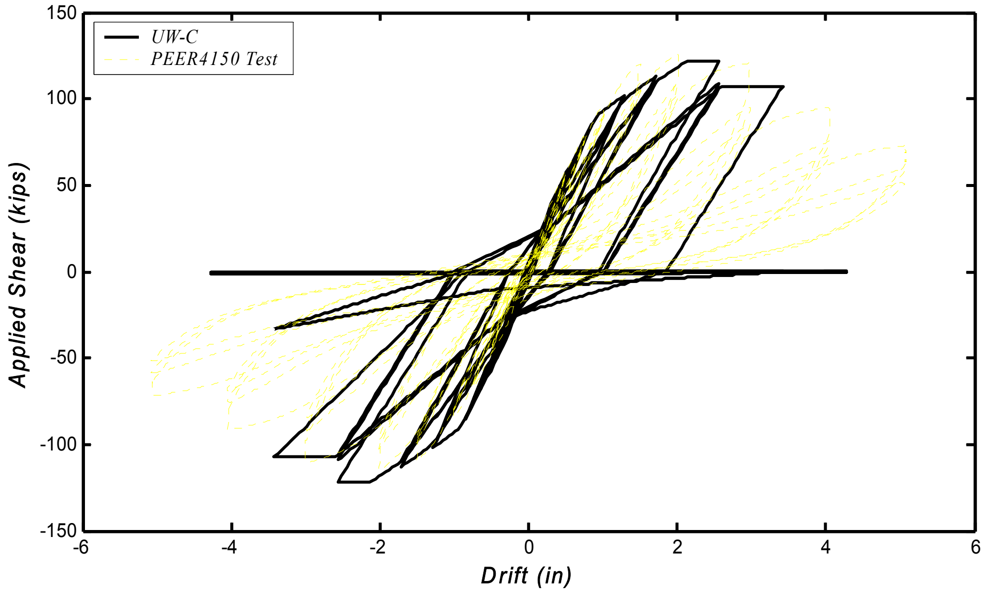

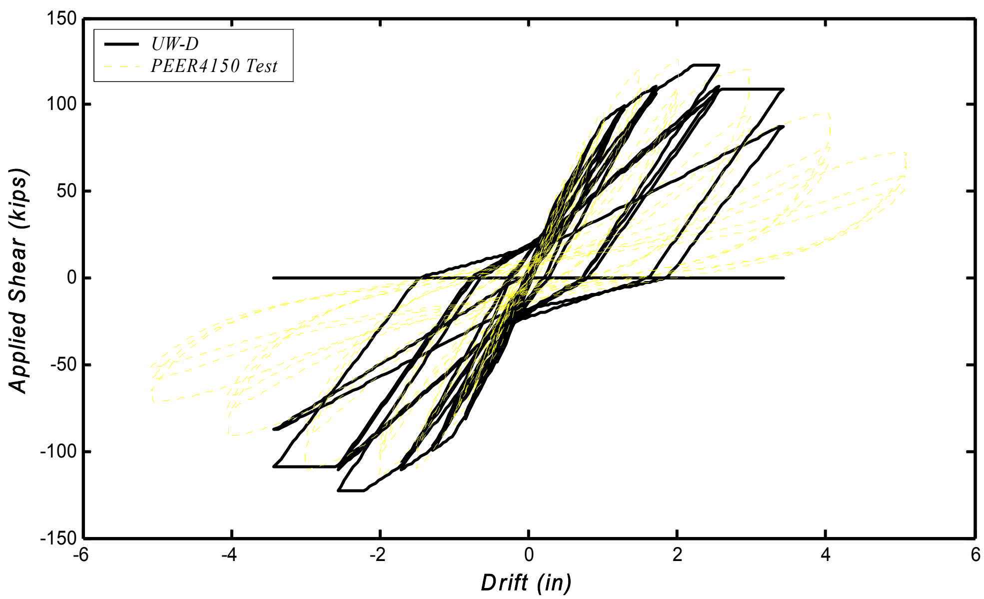

Figure A.2: PEER4150 Simulation results using (top) UW-C and (bottom) UW-D.

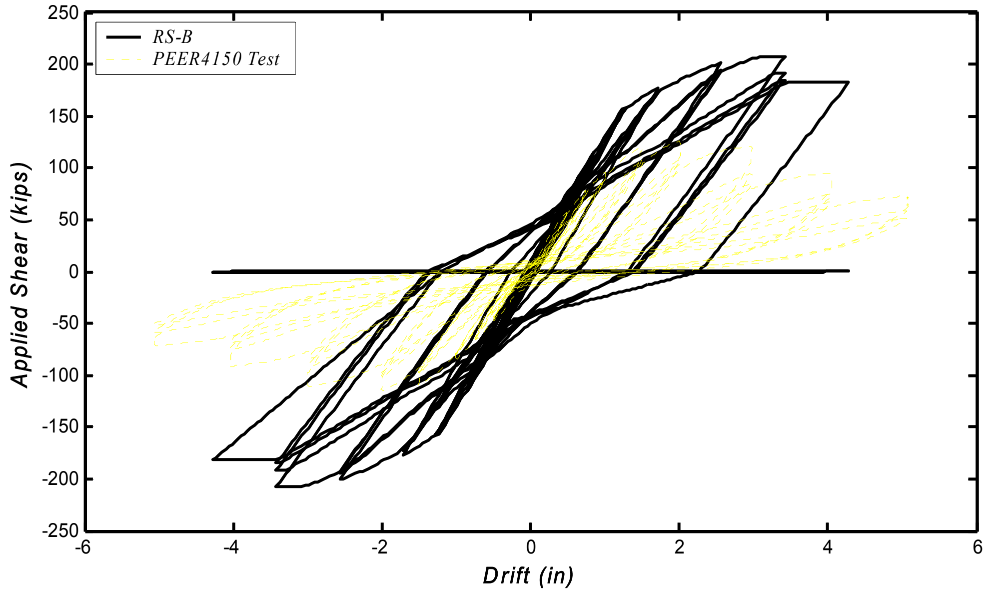

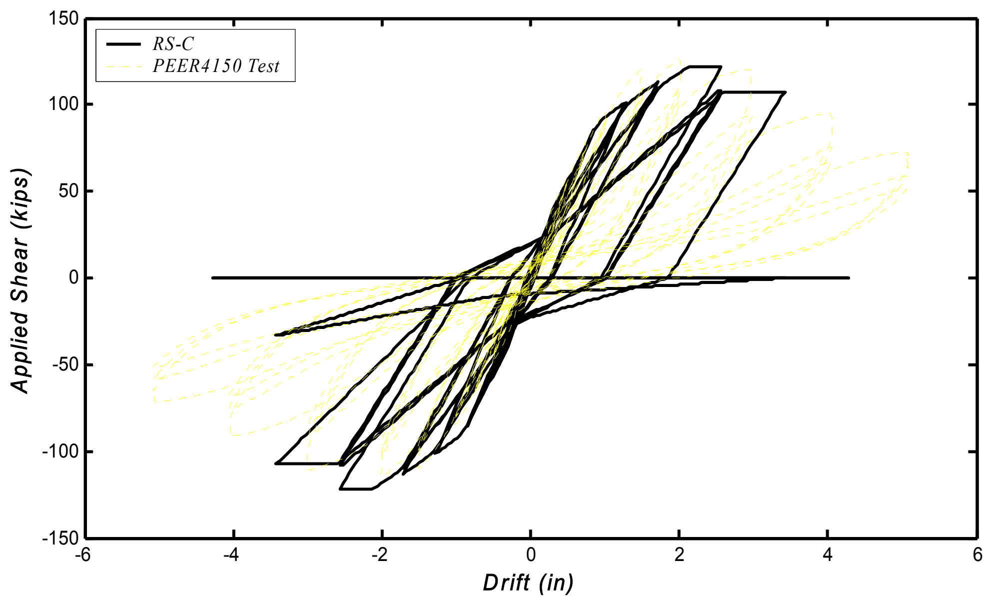

Figure A.3: PEER4150 Simulation results using (top) RS-B and (bottom) RS-C.

PEER2250

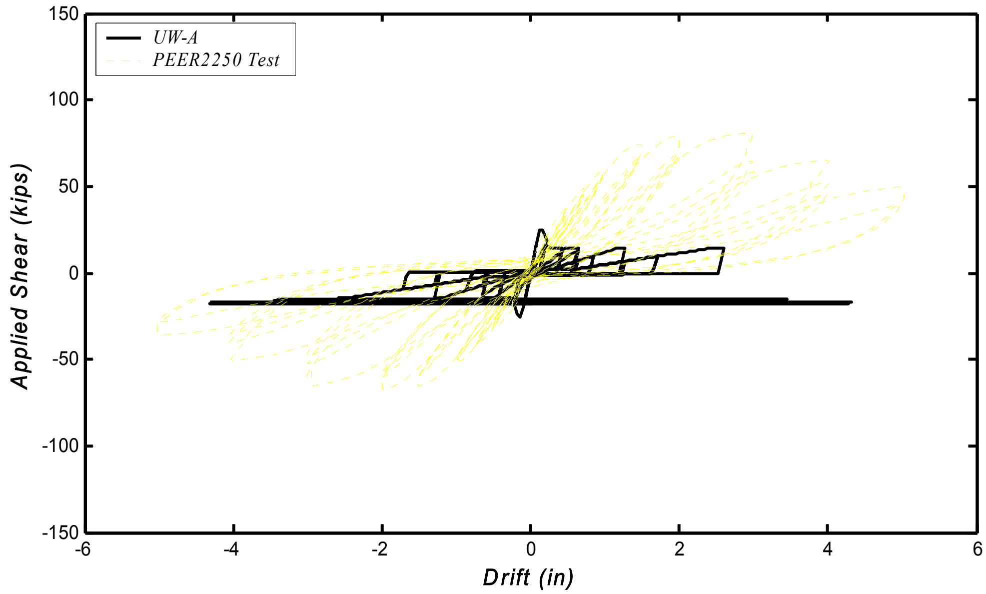

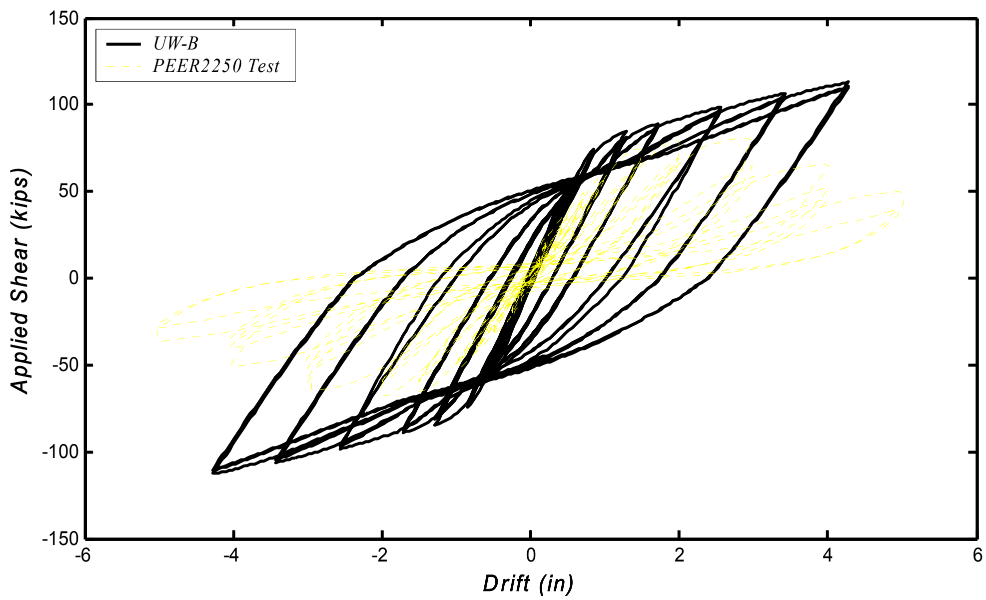

Figure A.4: PEER2250 Simulation results using (top) UW-A and (bottom) UW-B.

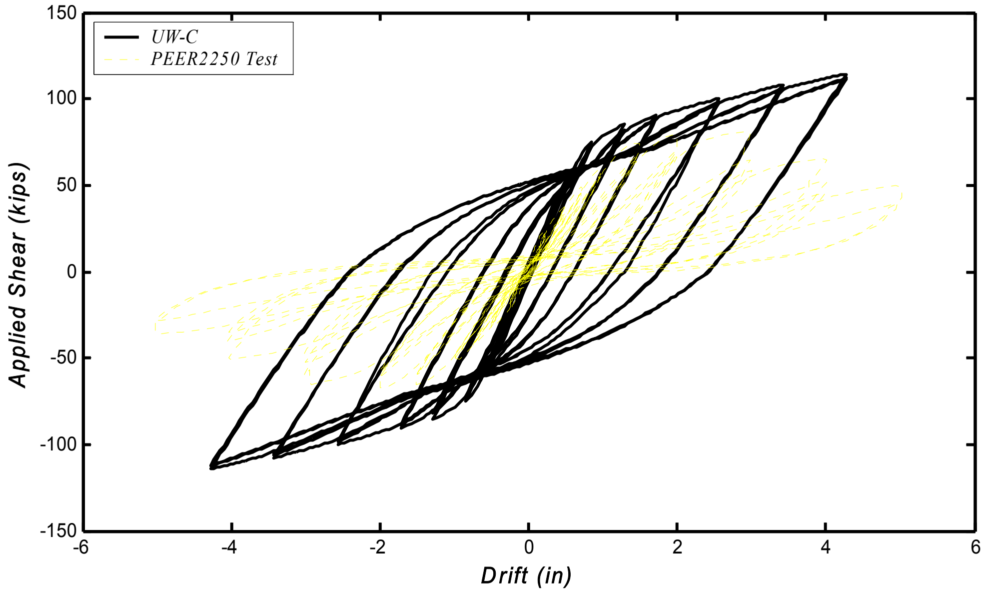

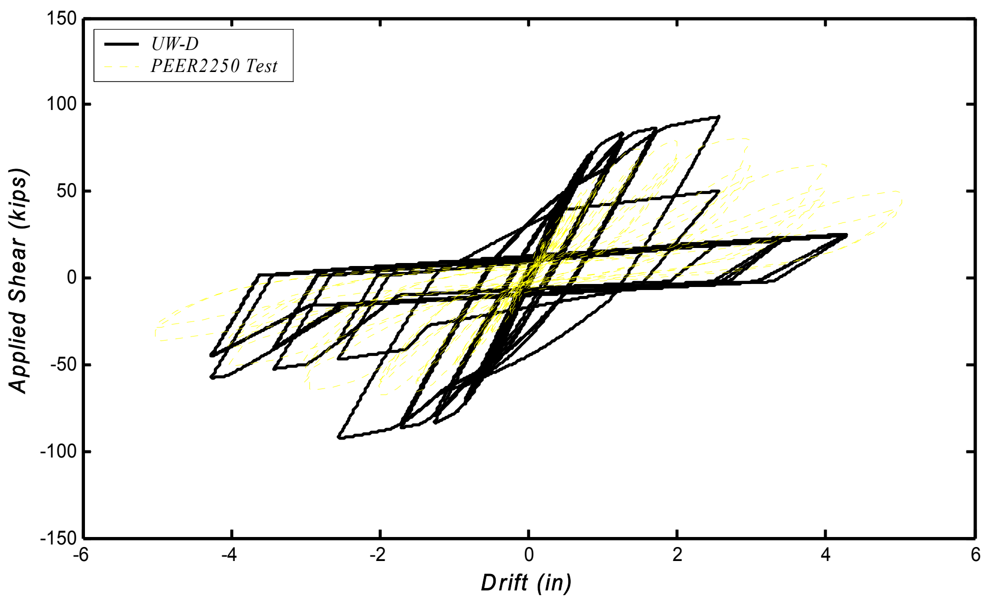

Figure A.5: PEER2250 Simulation results using (top) UW-C and (bottom) UW-D.

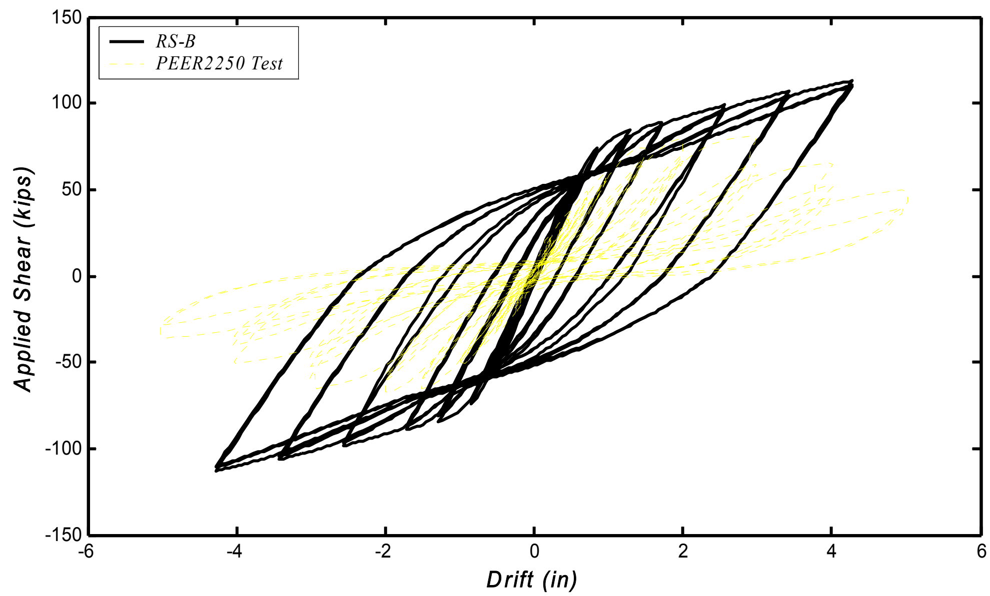

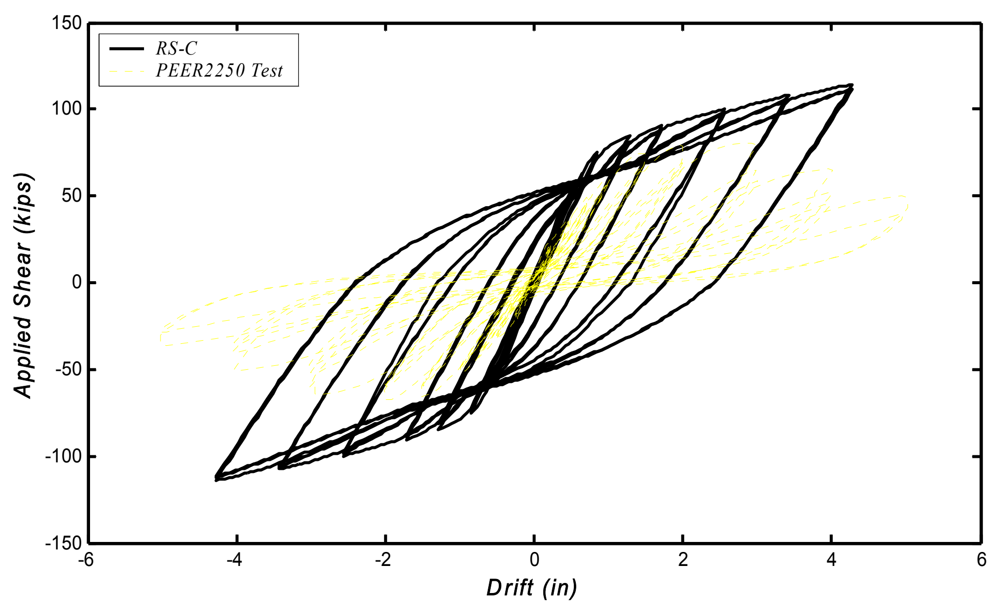

Figure A.6: PEER2250 Simulation results using (top) RS-B and (bottom) RS-C.

PEER0995

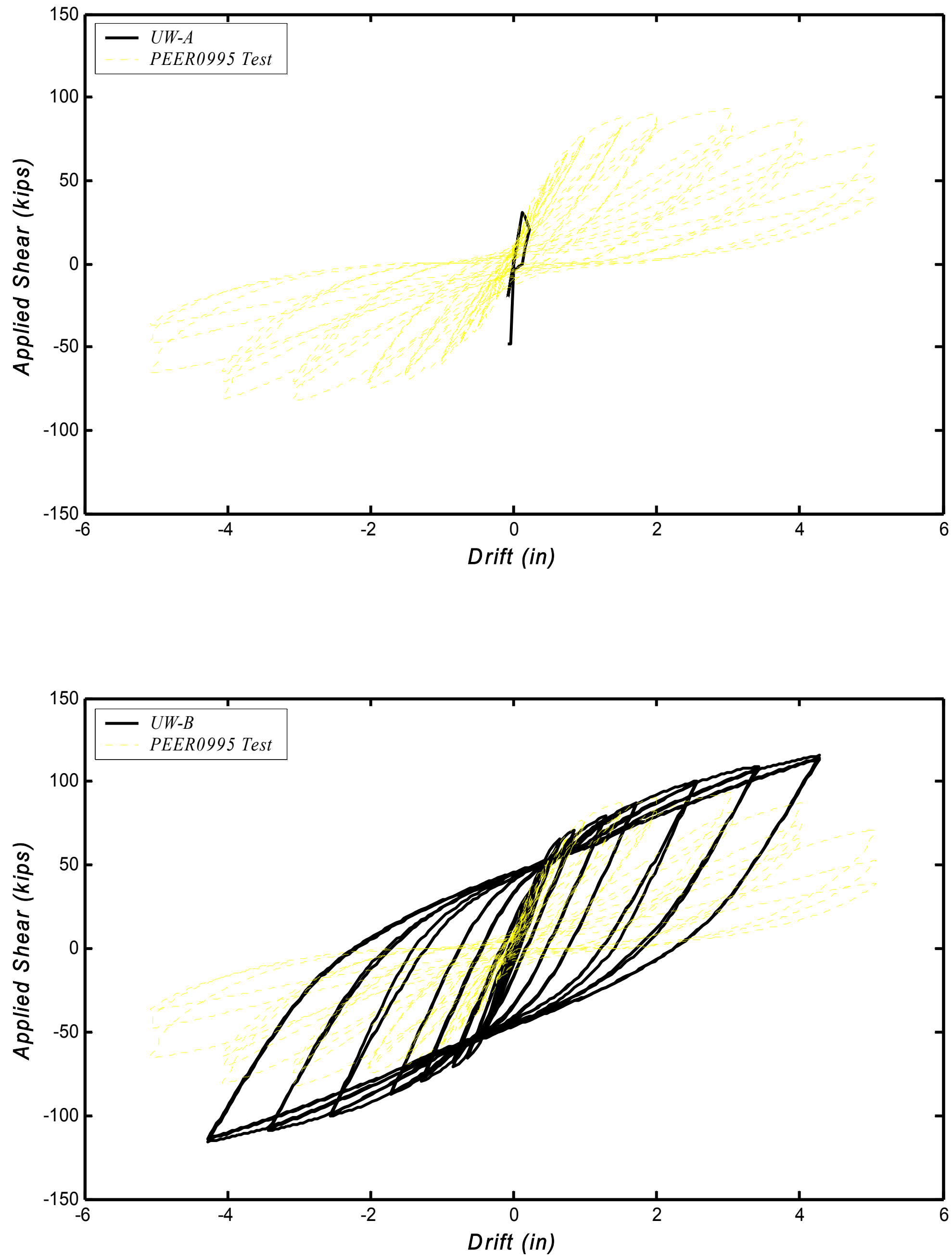

Figure A.7: PEER0995 Simulation results using (top) UW-A and (bottom) UW -B.

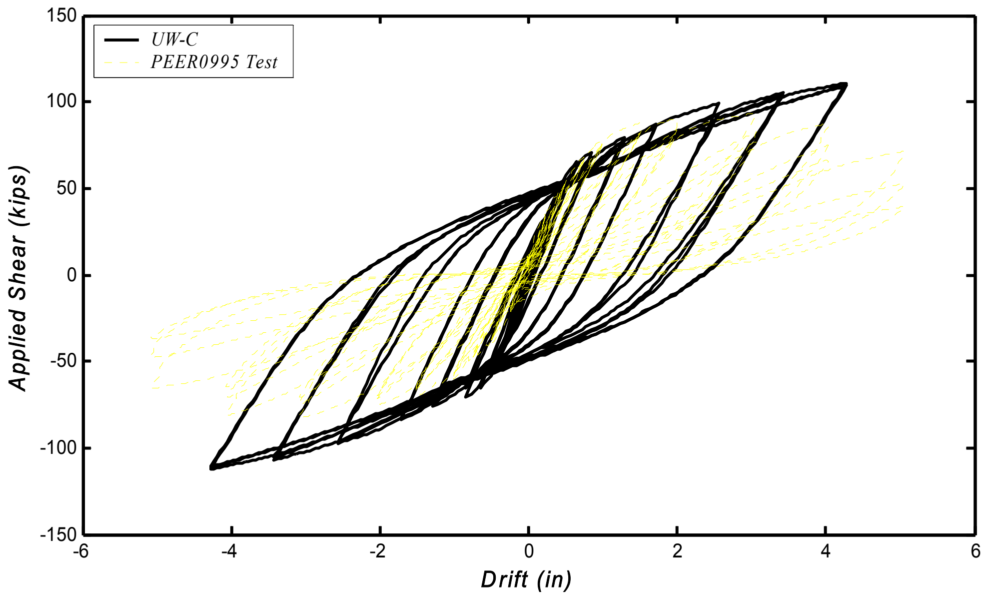

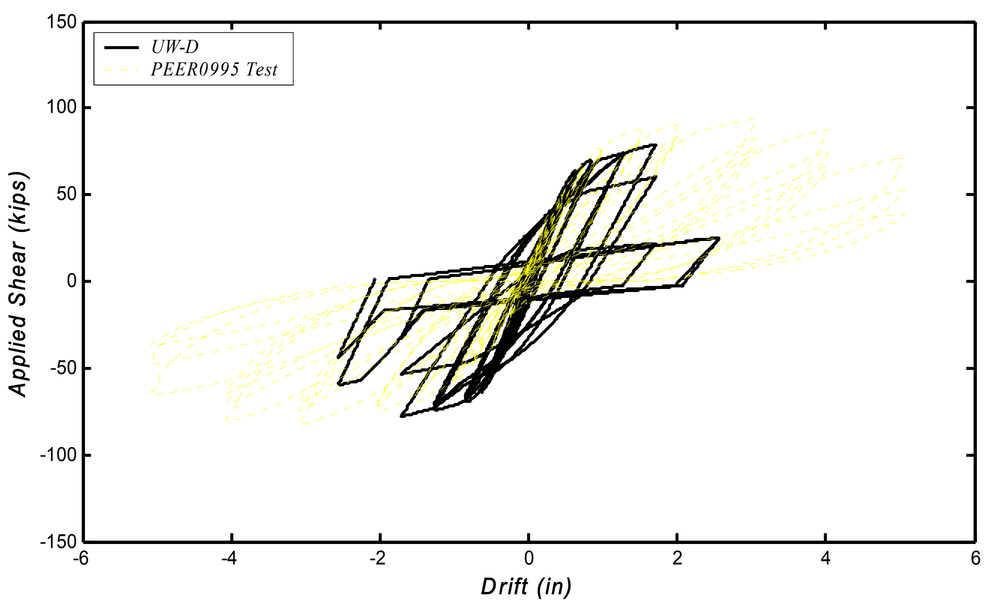

Figure A.8: PEER0995 Simulation results using (top) UW-C and (bottom) UW -D.

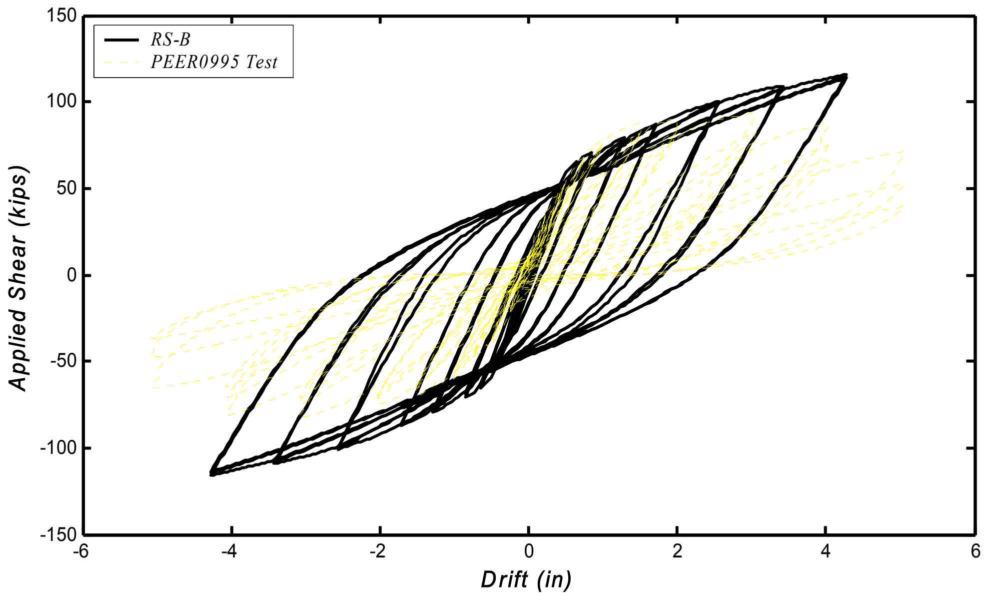

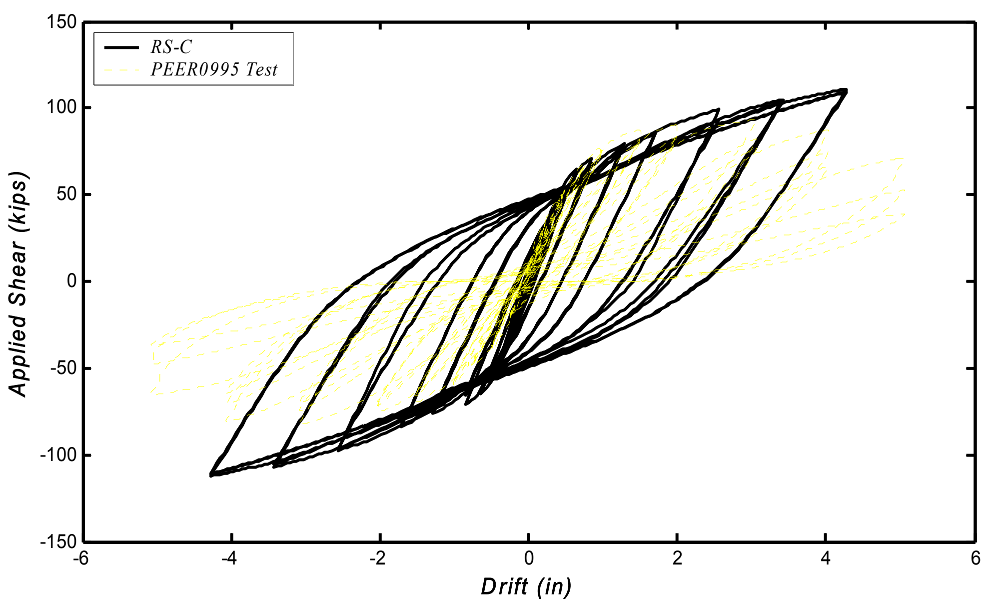

Figure A.9: PEER0995 Simulation results using (top) RS-B and (bottom) RS -C.

A.3. Model Comparison Plots

PEER4150

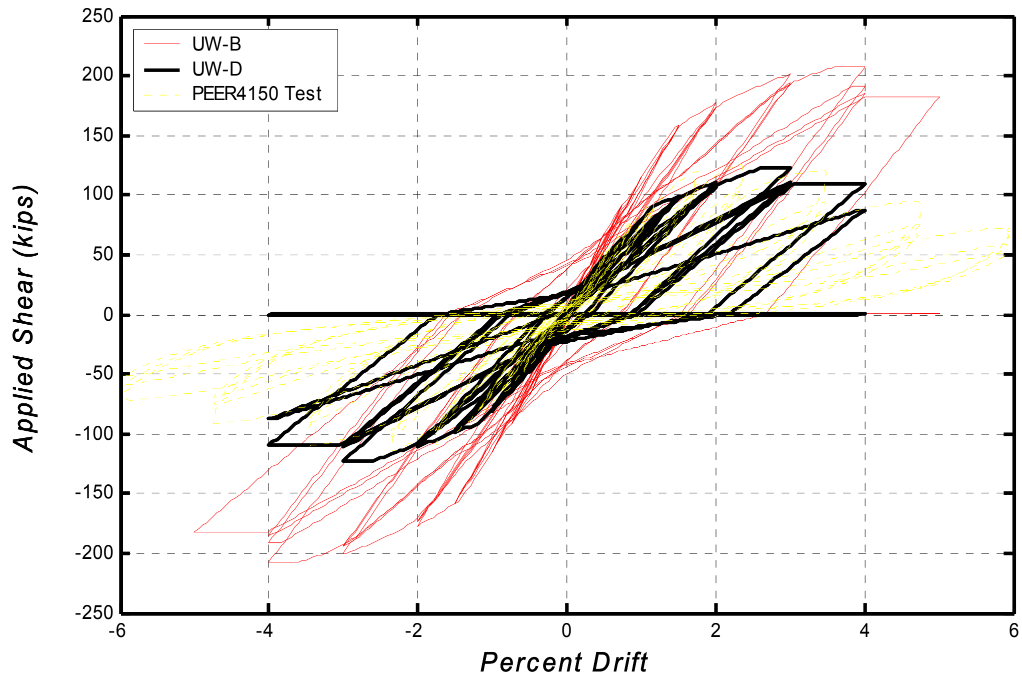

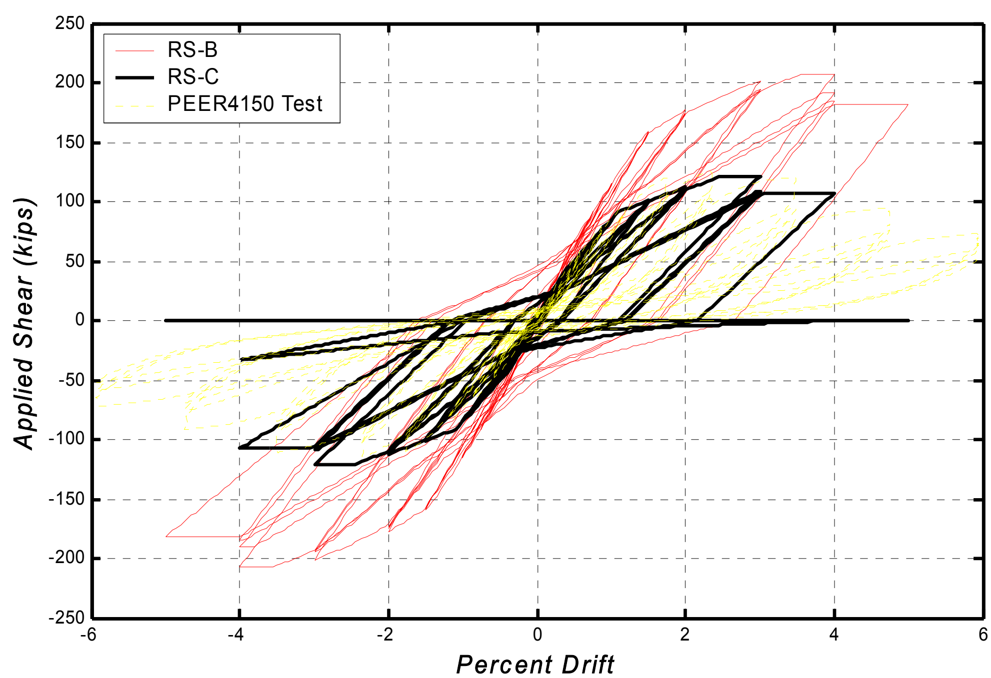

PEER2250

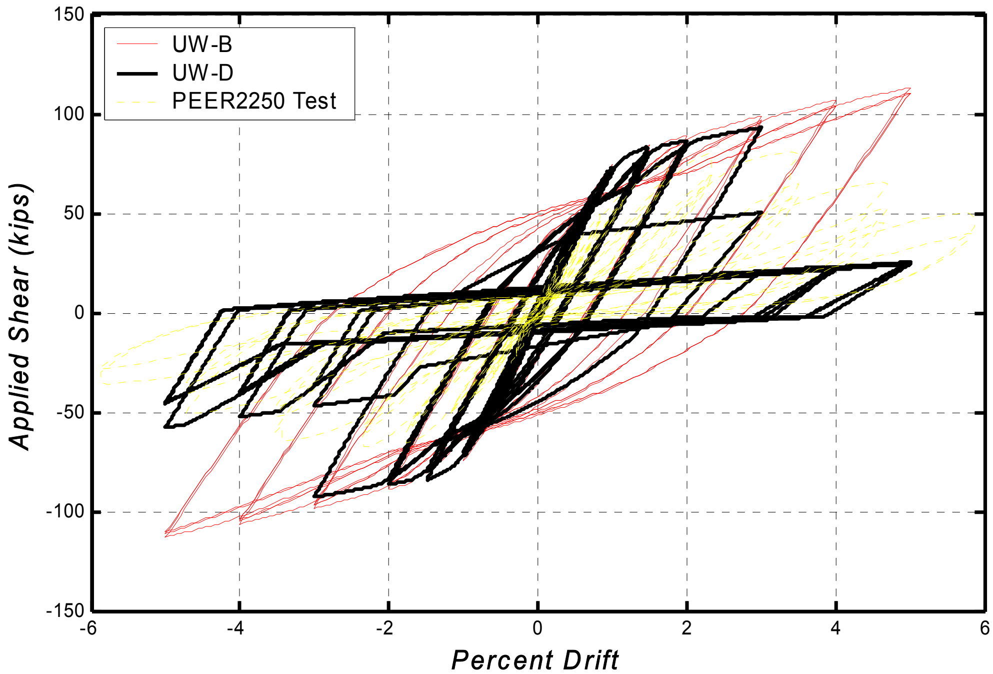
UW-B
UW-D
PEER2250 Test
Applied Shear (kips)
Percent Drift
150
100
50
0
-50
-100
-150
-6
-4
-2
0
2
4
6

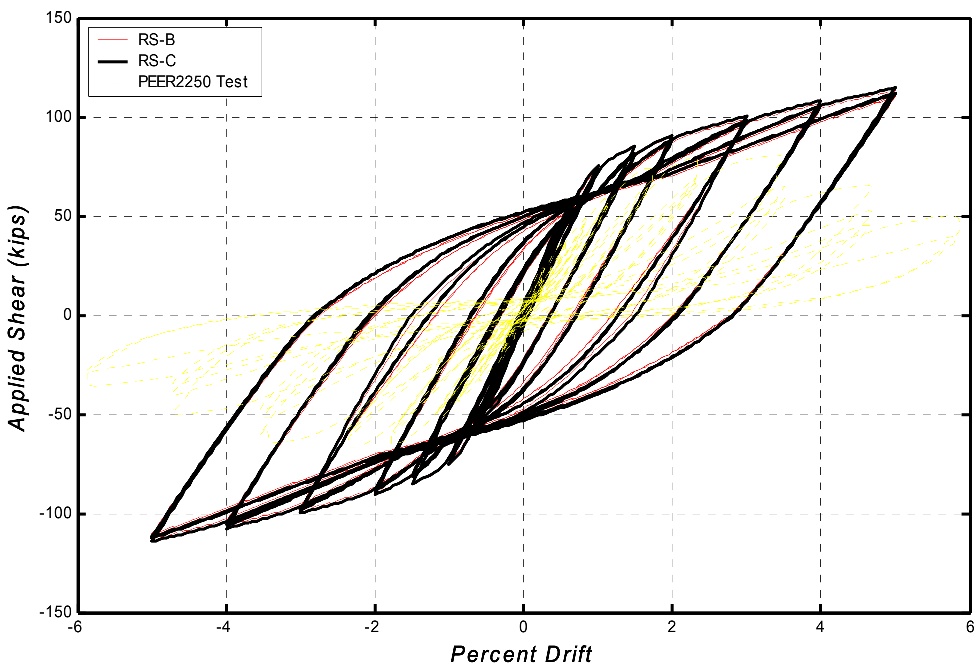
RS-B
RS-C
PEER2250 Test
Applied Shear (kips)
Percent Drift
150
100
50
0
-50
-100
-150
-6
-4
-2
0
2
4
6

PEER0995

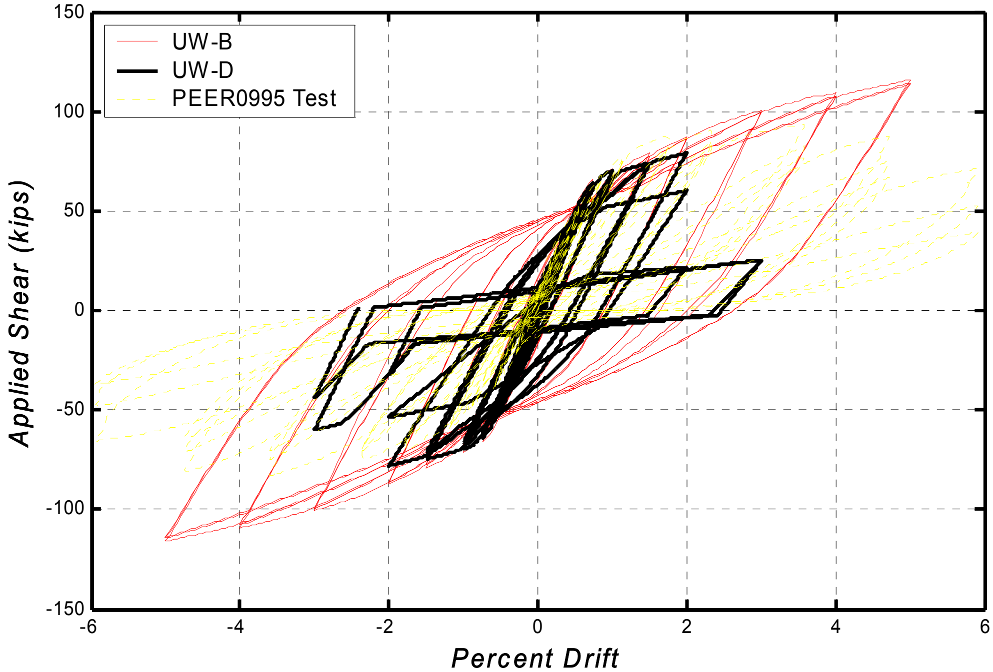
UW-B
UW-D
PEER0995 Test
150
100
50
0
-50
-100
-150
-6
-4
-2
0
2
4
6
Applied Shear (kips)
Percent Drift

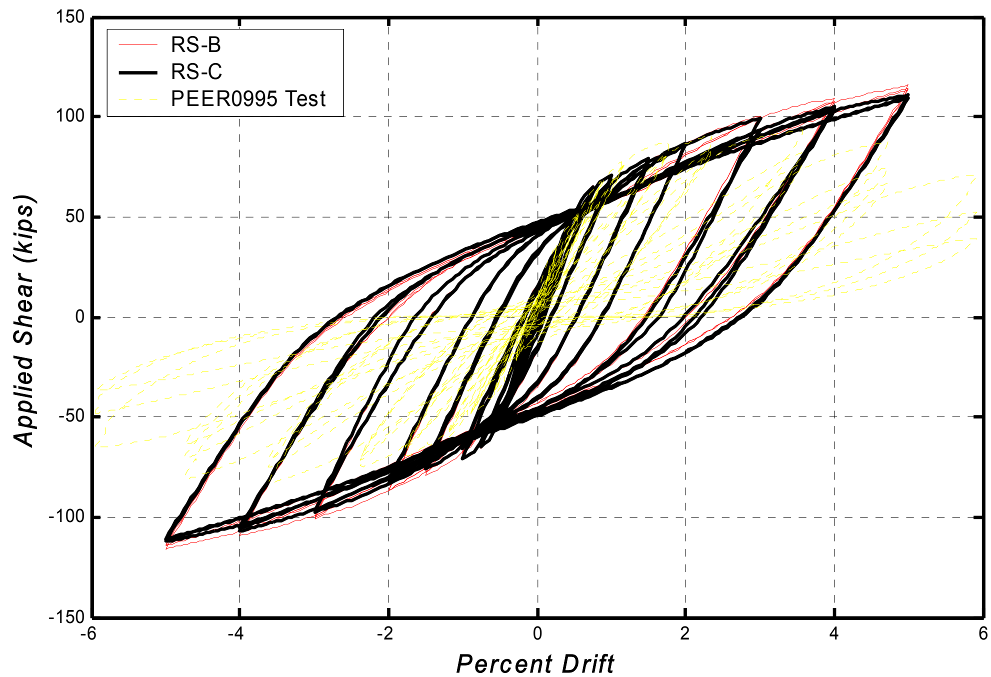
RS-B
RS-C
PEER0995 Test
150
100
50
0
-50
-100
-150
-6
-4
-2
0
2
4
6
Applied Shear (kips)
Percent Drift

A.4. CD30 and PADH Simulation Results

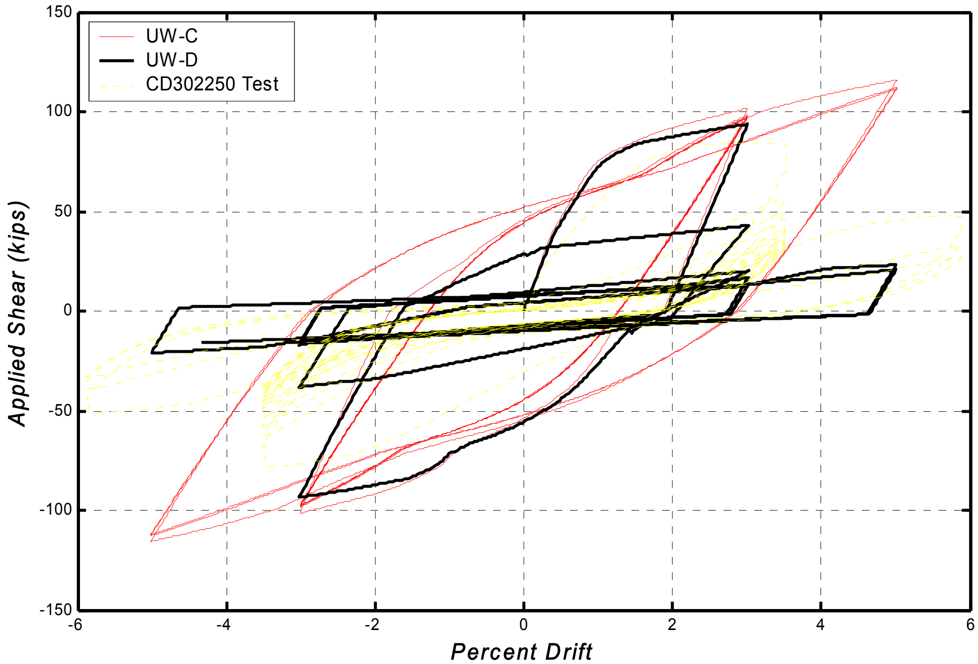

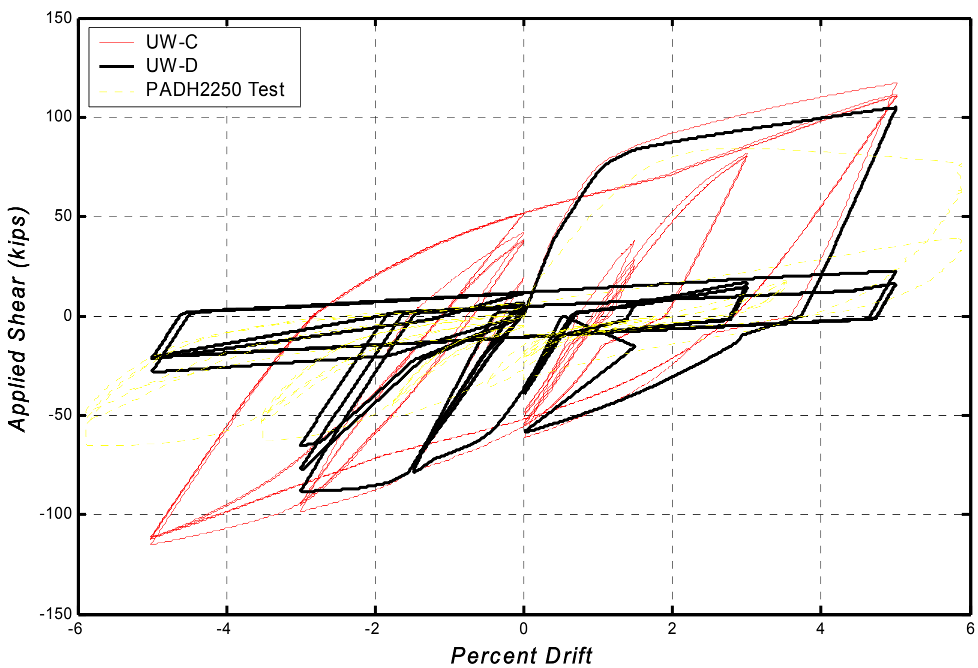

Appendix B

Specimen Design Properties: UW Joint Tests

B.1. Concrete Properties

Two different strengths of concrete were used for the three specimens. The concrete for the PEER-2250 and the PEER-4150 was made to reach a target compressive strength of 5,000 psi, and the concrete for the PEER-0995 was designed for 9,500 psi of compression. The actual day-of-testing concrete compressive strengths for the three specimens were found from ASTM C39 standard cylinder tests and are given in Table B.1 from Alire (2002) and Walker (2001).

Table B.1: Day-of-Testing Concrete Material Properties.

Specimen	f'_c(psi)	f_r(psi)
0995	8,767	514
2250	5,570	457
4150	4,783	533

B.2. Steel Properties

The steel reinforcement bar properties were determined for the bars of various sizes using standard uniaxial tension tests. Some of the reinforcement bars have machined grooves for the placement of strain gauges. The steel properties for the ungrooved and grooved bars from Alire's tests are given in Table B.2.

Table B.2: Measured steel properties from uniaxial testing (Alire, 2002).

	Ungrooved Bars					
Bar Size	**f_y(ksi)**	**f_u(ksi)**	**E_s(ksi)**	**ε_y**	**ε_{sh}**	**ε_u**
#4	77.8	121.7	33,190	0.0023	0.0059	0.08
#6	73.2	123.4	31,619	0.0024	0.0066	0.12
#7	73.1	123.5	31,619	0.0023	0.0045	0.09
#9	79.0	130.3	32,182	0.0025	0.0045	0.12
Bar Size	**Grooved Bars**					
#4	76.4	109.8	32,455	0.0024	0.0053	0.07
#6	59.4	98.9	24,931	0.0024	0.0062	0.09
#7	74.4	125.8	33,473	0.0022	0.0032	0.11
#9	78.5	139.3	35,169	0.0022	0.0022	0.11

The steel for Walker’s tests came from separate heats designated Silver (S) or Red (R). The bars had no grooves. The steel properties from Walker’s tests are given in Table B.3.

Table B.3: Measured reinforcing bar properties (Walker, 2001).

Bar Size	**f_y(ksi)**	**f_u(ksi)**	**ε_{sh}**	**ε_u**
#4 R	96	138.8	0.01	0.12
#7 S	76.5	123.4	0.005	0.12
#8 R	79	123.5	0.006	0.12
#8 S	74.5	123.5	0.003	0.12
#9 S	78	130.3	0.002	0.12

B.3. Reinforcement and Geometry

Table B.4: PEER/UW specimen reinforcement and geometry details.

	Beam Bars		Column Bars			Beam Geometry	Column Geometry
Specimen	Top	Bot.	Top	Mid.	Bot.	Cross-section/length	Cross-section /length
0995	5 #7	3 #7	3 #6	2 #6	3 #6	20”x16” / 160”	16”x18” / 85.5”
2250	6 #7	4 #7	3 #9	2 #9	3 #9	20”x16” / 160”	16”x18” / 85.5”
4150	6 #9	6 #9	4 #9	2 #9	4 #9	20”x16” / 160”	16”x18” / 85.5”

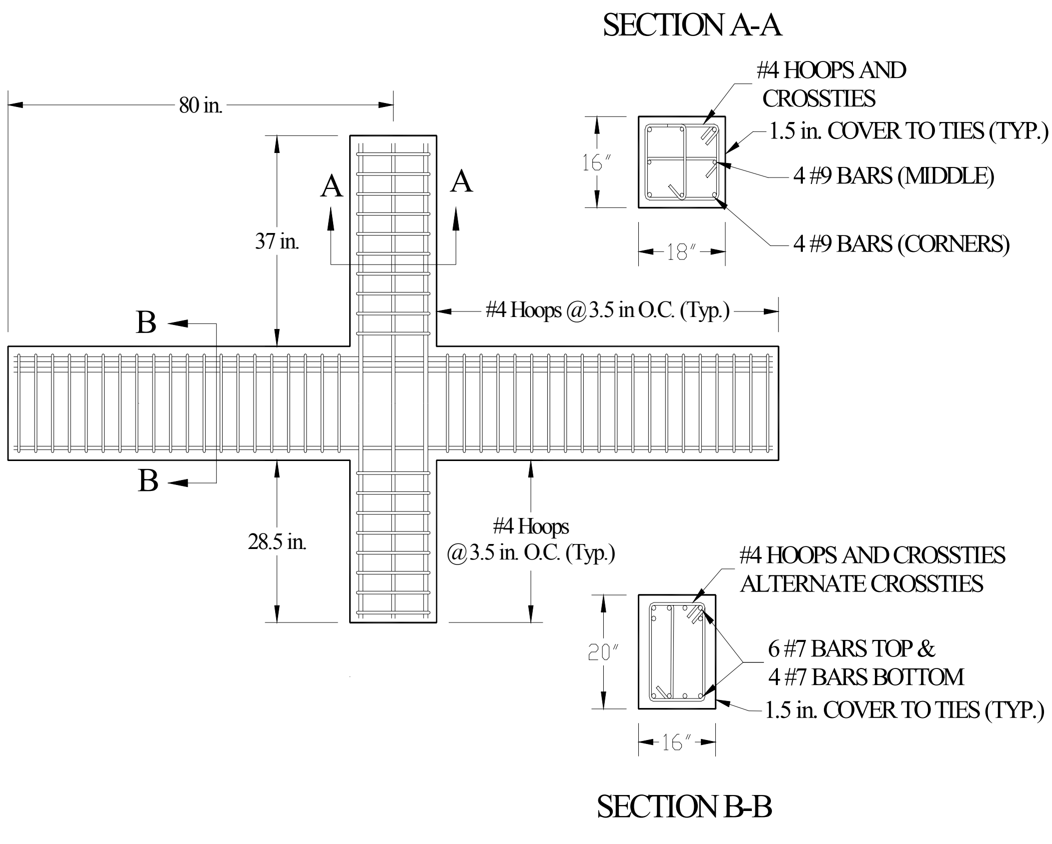

Figure C.1: Geometry and reinforcement for PEER 2250 (Walker, 2001).

B.4. Other Simulation Parameters

Table B.5 gives general parameters used to simulate geometry, column axial loading, and elastic element properties. The column axial load is based on a load ratio of 10% (Walker 2001). The elastic moduli for the concrete of the beams and columns are defined using Equation B.1.

$$E_i = 57000 / \sqrt{f'_{cc}} \qquad \textbf{Equation B.1}$$

Table B. 1: General modeling parameters for the UW cruciform tests.

Parameter	4150	2250	0995
Column Cross-Section	16”x18”	16”x18”	16”x18”
Column Length Top / Bottom	37” / 28.5”	37” / 28.5”	37” / 28.5”
Beam Cross-Section	20”x16”	20”x16”	20”x16”
Beam Length	71.0”	71.0”	71.0”
Column hinge length	10”	10”	10”
Beam hinge length	9”	9”	9”
Column Cover	1.564”	1.4325”	2.064”
Beam Cover	1.564”	1.4325”	1.9375”
Poisson’s Ratio	0.175	0.175	0.175
E_{col} (psi)	4503560.0	4605839.0	5654734.0
E_{bm}(psi)	4499158.0	4588082.0	5652785.0
G_{col} (psi)	1916409.0	1959932.0	2406270.0
j[1]	0.85	0.85	0.85
P (lbs)	137750.0	252490.0	160420.0

[1] This value is used only for the calculation of the impact of the column shear on the joint core shear strength for the MnJ joint formulations a shown in Equation 3.5.1.

Appendix C

UW Joint Testing Details

C.1. Test Setup and Procedure

This appendix summarizes the setup and procedure used for the UW cruciform tests. For these cruciform tests, the specimen was placed in an upright testing rig as illustrated in Figure C.1. Structures were constructed around the specimen to limit the displacement of the top of the column and the out of plane movement, to apply an axial load in the column, and to control the displacement of the beams. The tests were all completed using displacement control of the beams which does not take into account P-Δ effects and which allows for a simpler setup since the axial loading structure does not have to move with the column. Note that all drift levels were applied at a rate of 3.0% per minute. Instruments were placed on and in the specimen to collect data pertaining to joint shear, beam and column curvature, reactions and loads at the cruciform endpoints, and strain in the steel longitudinal reinforcement bars. Walker also determined the strain in the transverse steel, but this was found to be unnecessary. Note that the steel strain was determined both with internal strain gauges attached to the bars and with external LVDTs. Also note that all the instrumentation was calibrated prior to any testing to ensure accurate data collection. Refer to Alire (2002) and Walker (2001) for further data collecting and setup details.

Once the tests were set up the specimens were subjected to precise pseudo-static ground motions. The type of ground motion, or displacement history, that a joint is exposed to has been found to play an influential role in the joint strength and deformation (Mosier, 2000 and Walker, 2001). It sets the displacement the top of the column sees during the testing. The primary type of displacement history implemented in these simulations is referred to as a PEER history. This type of displacement history consists

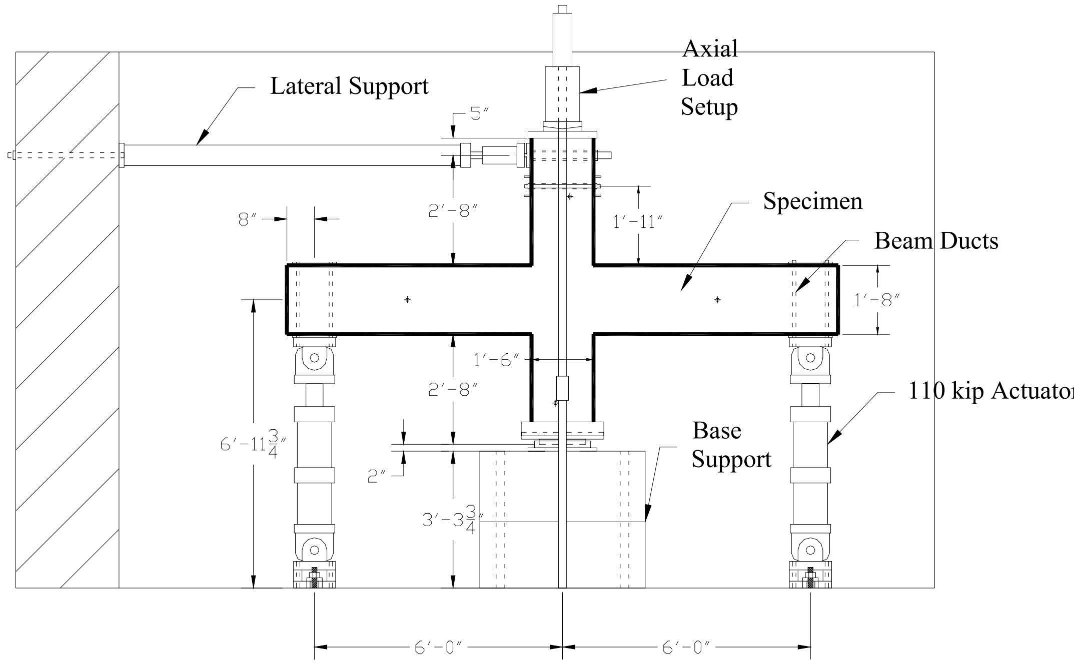

(a)

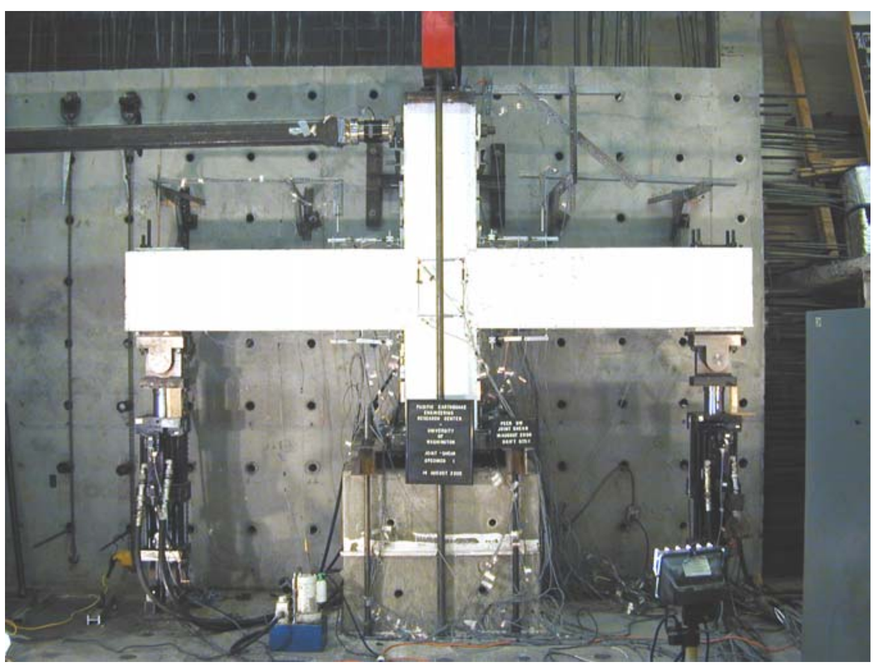

(b)

Figure C.1:Test Setup (a) schematic (b) Specimen CD15-14 in testing rig (Walker 2001)

of three cycles at a given drift level, for ten increasing drift levels. The required drift levels are given in Table C.1 and the resulting displacement history is given in Figure C.2. Other displacement histories include the CD30 and PADH histories. These more irregular histories are depicted in Figure C.3. Note that the tests were stopped periodically to facilitate the documentation of the testing progress.

Table C.1: PEER displacement history drift levels (Alire, 2002).

Drift Level	*Drift Ratio (%)*
1	0.10
2	0.25
3	0.50
4	0.75
5	1.00
6	1.50
7	2.00
8	3.00
9	4.00
10	5.00

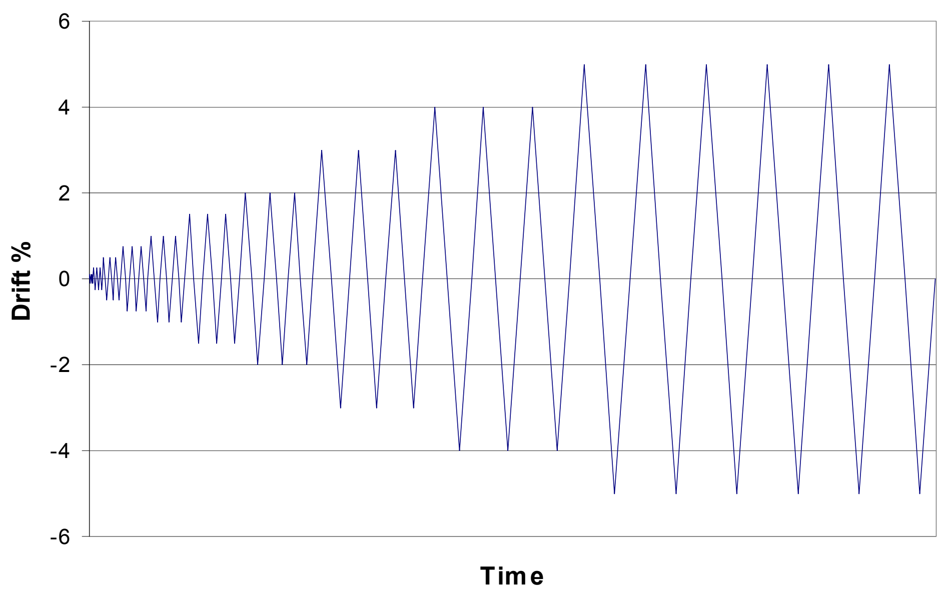

Figure C.2: PEER displacement history

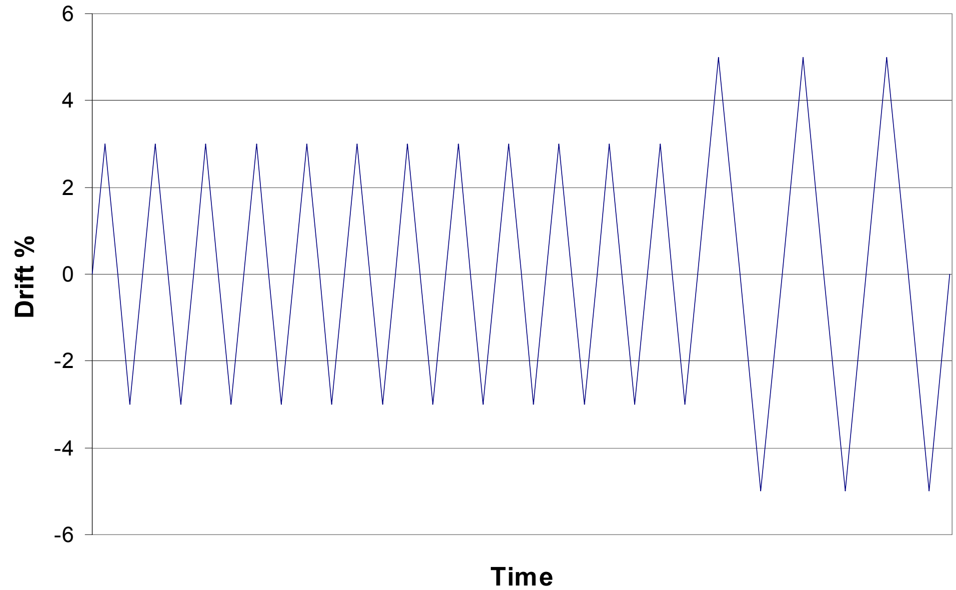

(a)

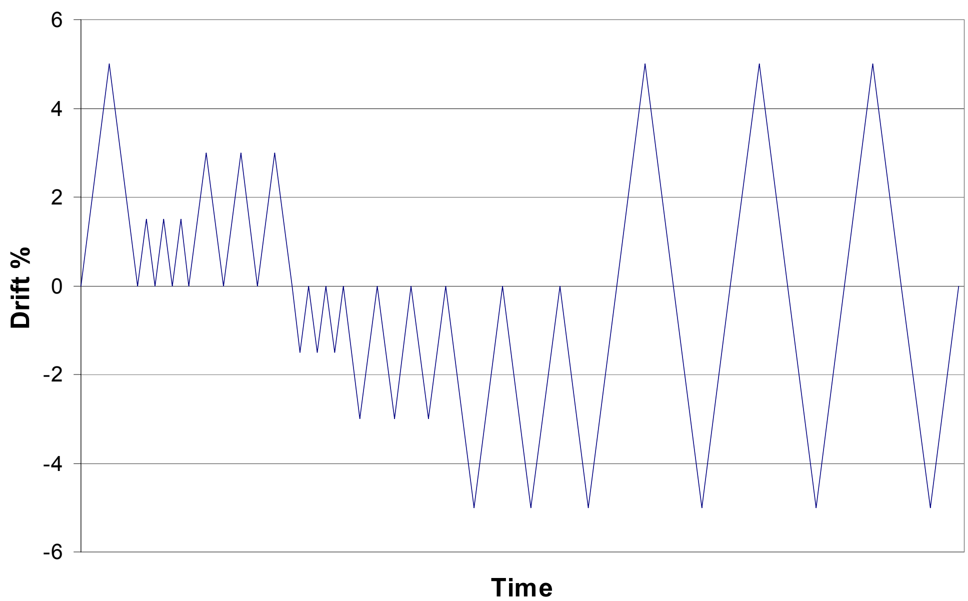

(b)

Figure C.3: Displacement Histories: (a) CD30 (b) PADH (Walker, 2001)

Appendix D

Case Study Building Drawings

D.1. Plan and Elevations Views

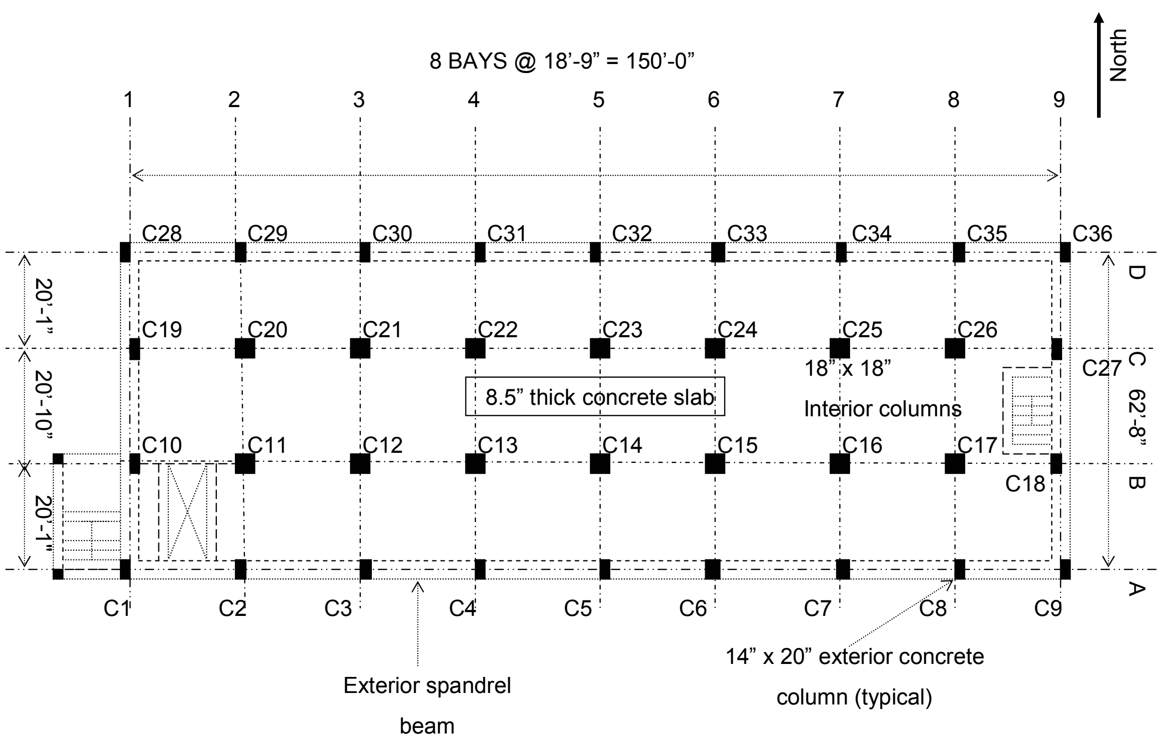

Figure D. 1: Typical floor plan view of Van Nuys Holiday Inn building with column schedule (Rissman 1965)

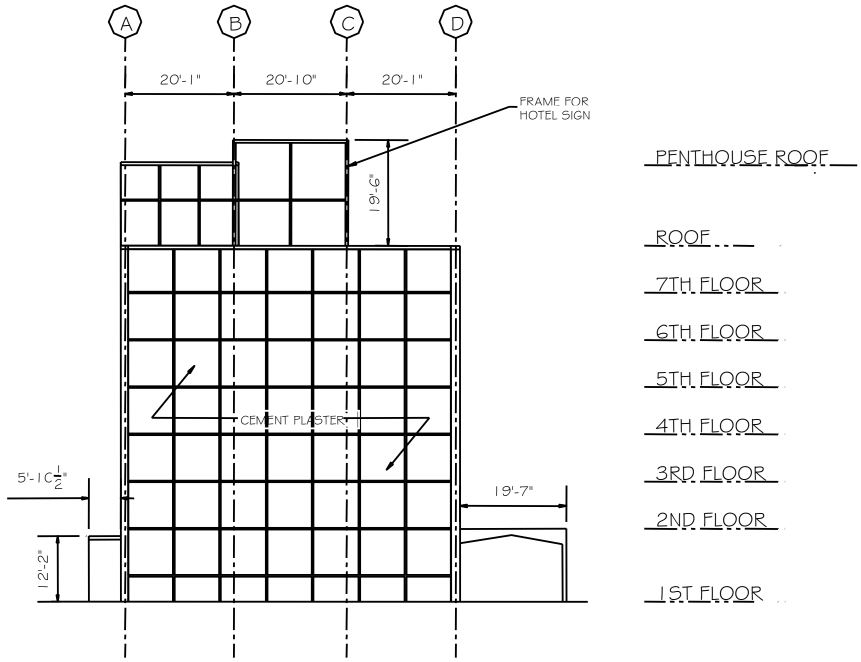

Figure D.2: East perimeter elevation view (Rissman 1965)

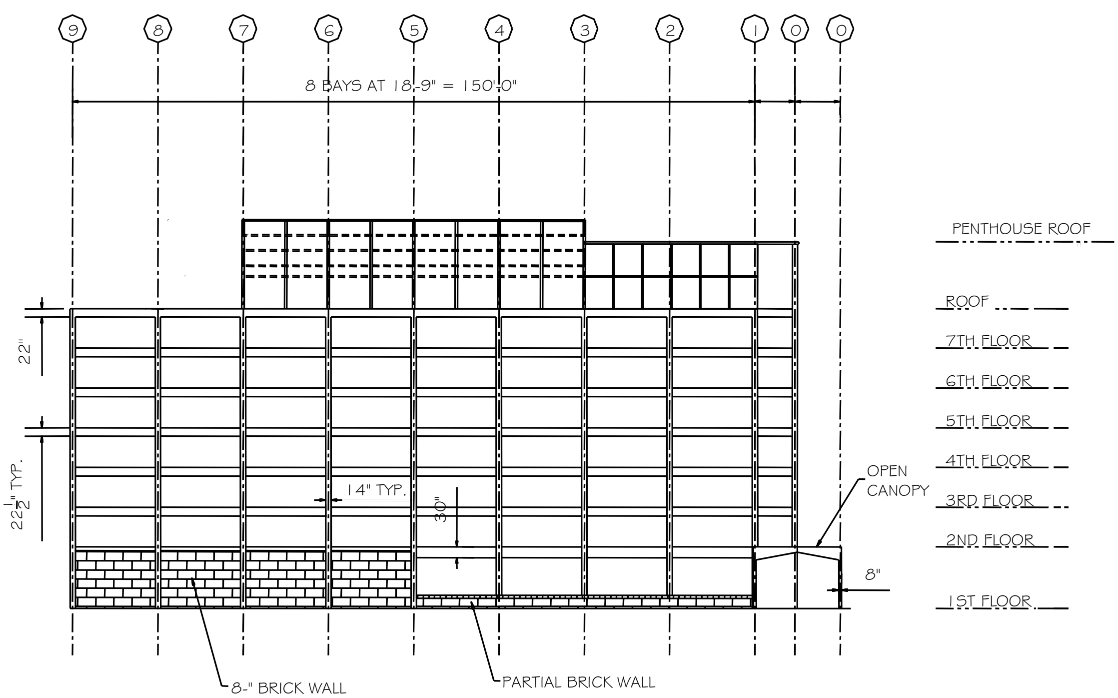

Figure D.3: North perimeter view (Rissman 1965)

D.2. Beam and Column Details

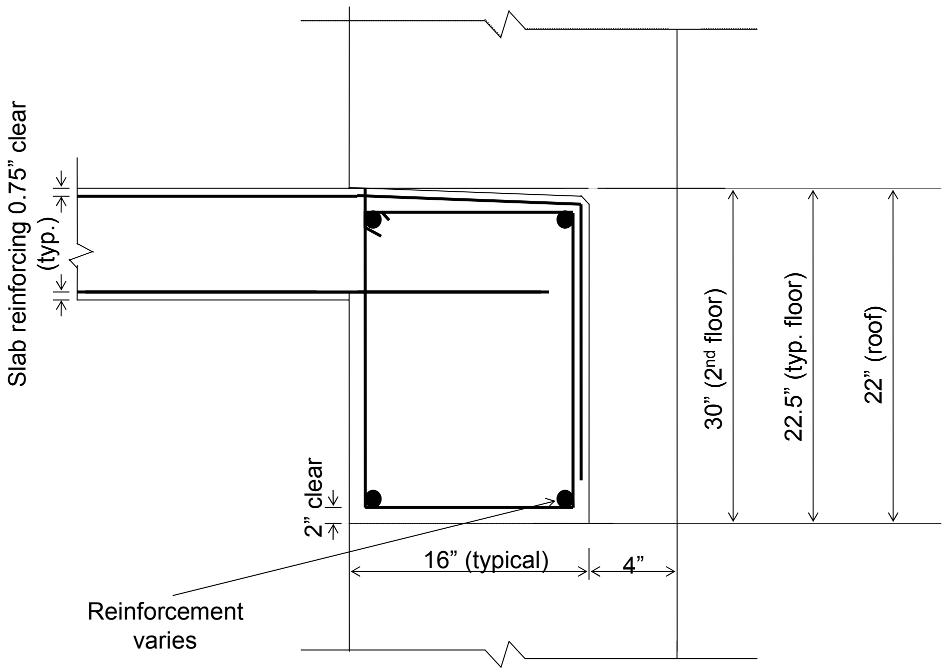

Figure D. 4: Typical longitudinal Spandrel Beam Cross-Section (NOAA report 1973)

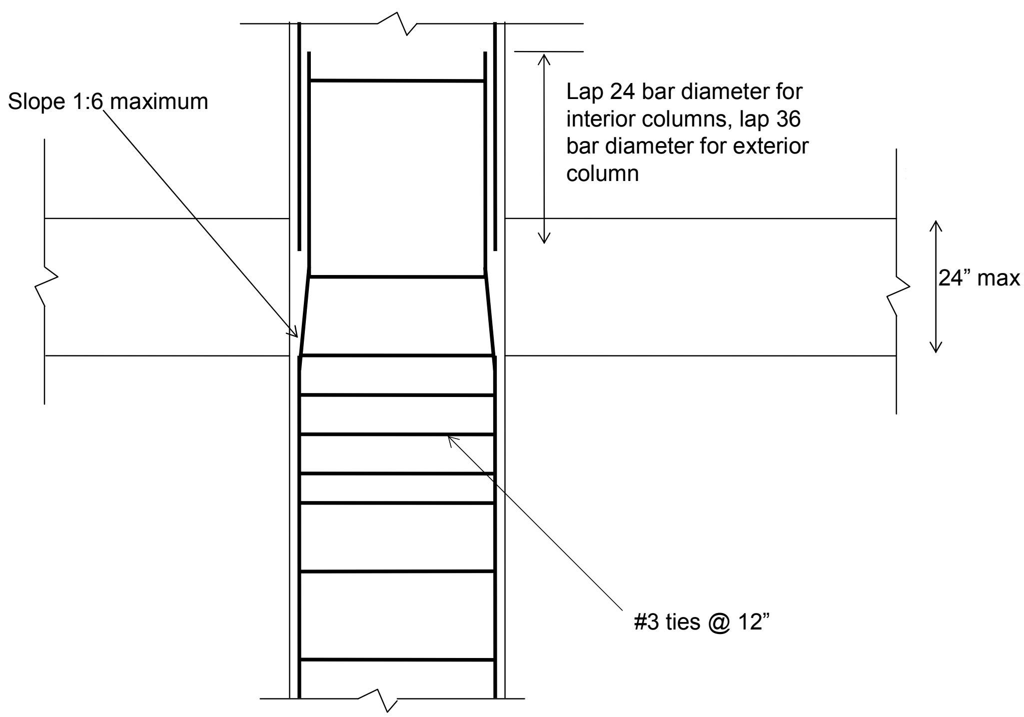

Figure D.5: Typical Column Detail (NAOO report 1973)

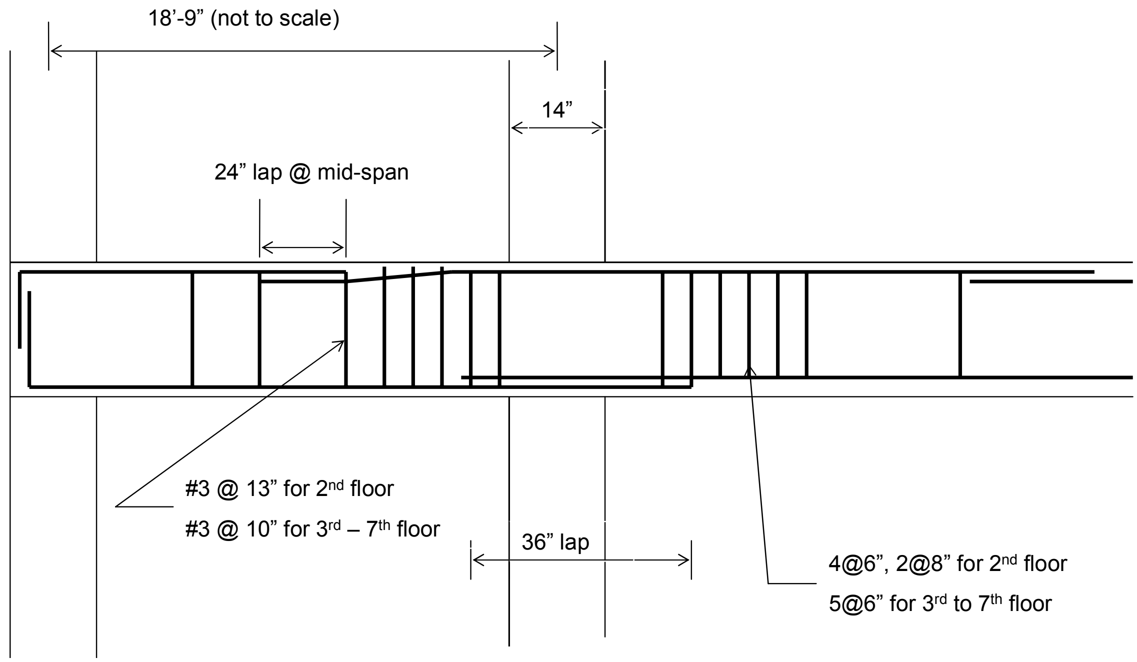

Figure D.6: Typical longitudinal spandrel beam elevation (NOAA report 1973)

Appendix E

Case Study Building Pushover Data

E.1. Data Explanation

Curvature Ductility Demand and Failure Legend
O : μ = 1 to 1.5 O : μ = 1.5 to 2 O : μ = 2 to 3 O : μ = 3 to 4 O : μ > 4
X = shear failure, S = splice failure, # = numerical failure

E.2. Model M1 (UW-MnJ-BS: no gravity/ no shear/ no splice)

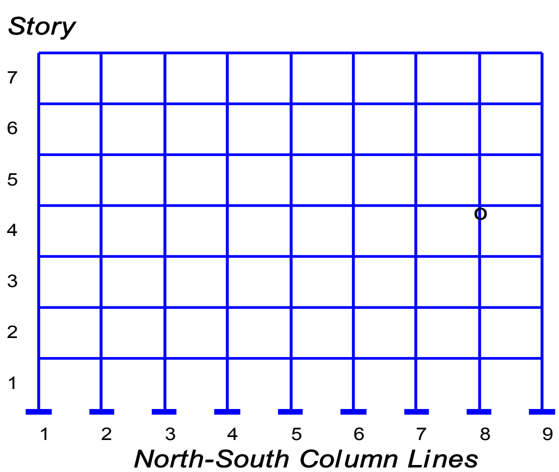

(b) External

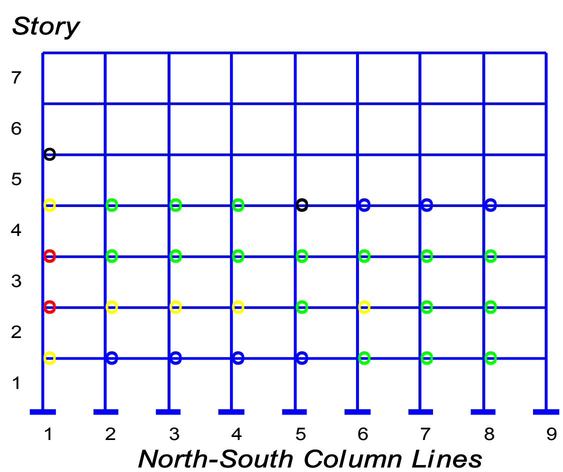

(a) Internal

Figure E. 1: Locations and types of member failures for model M1 at 0.6% roof drift.

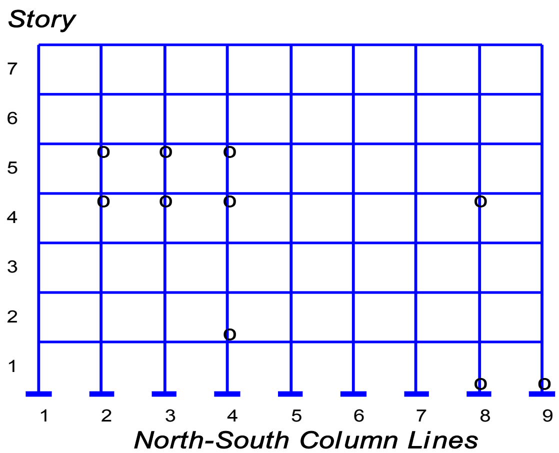

(b) External

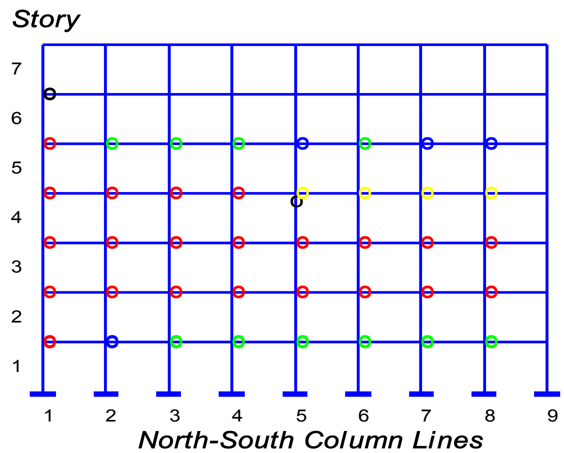

(a) Internal

Figure E. 2: Locations and types of member failures for model M1 at 0.9% roof drift.

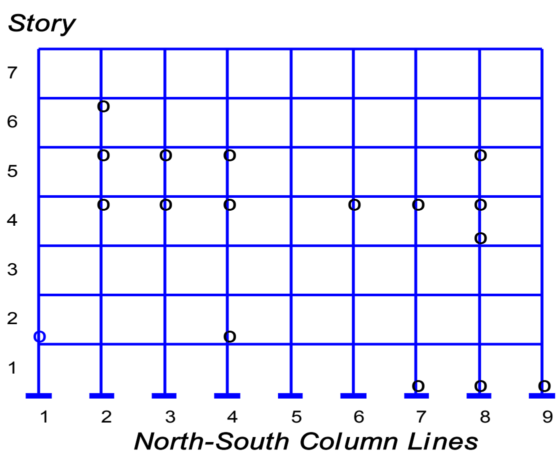

(b) External

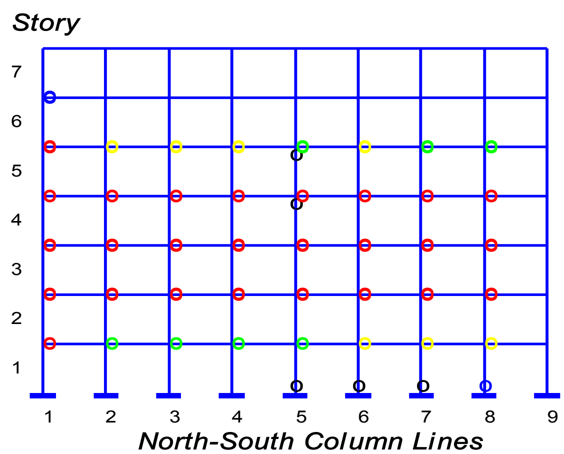

(a) Internal

Figure E. 3: Locations and types of member failures for model M1 at 1.2% roof drift.

E.3. Model M2 (RS-MnB: no gravity/ no shear/ no splice)

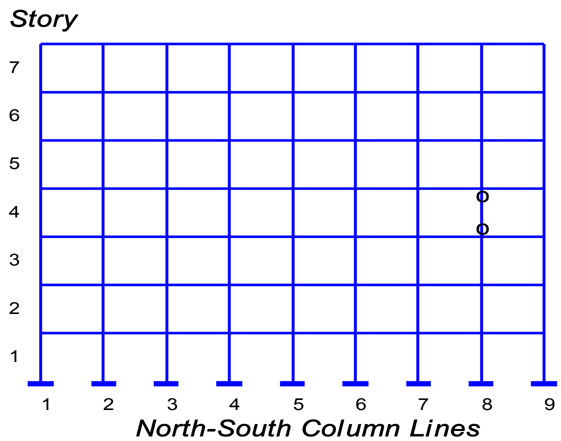

(b) External

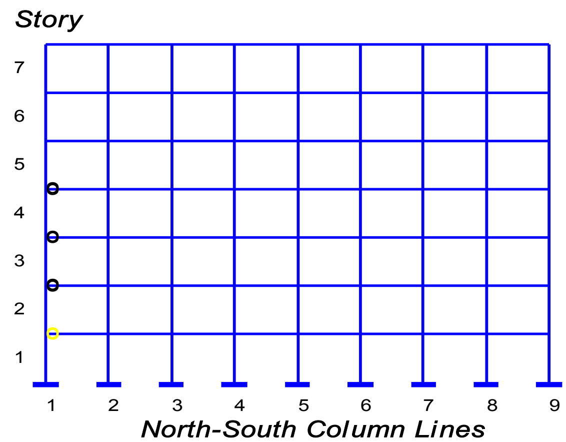

(a) Internal

Figure E. 4: Locations and types of member failures for model M2 at 0.6% roof drift.

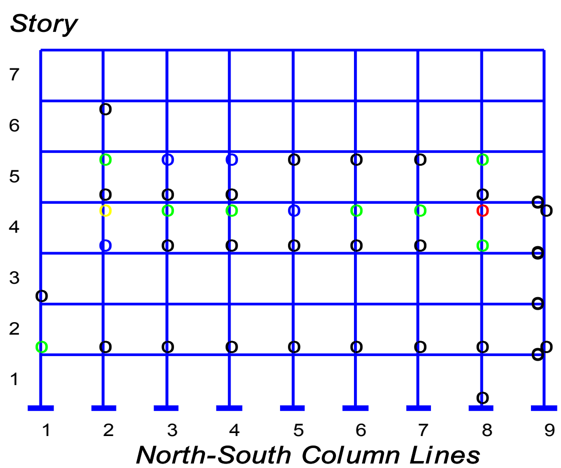

(b) External

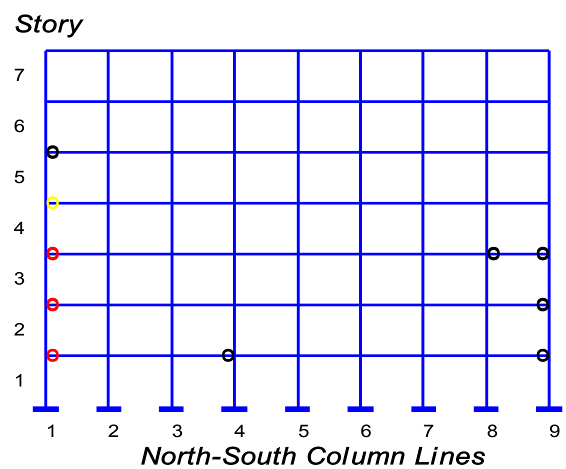

(a) Internal

Figure E. 5: Locations and types of member failures for model M2 at 0.9% roof drift.

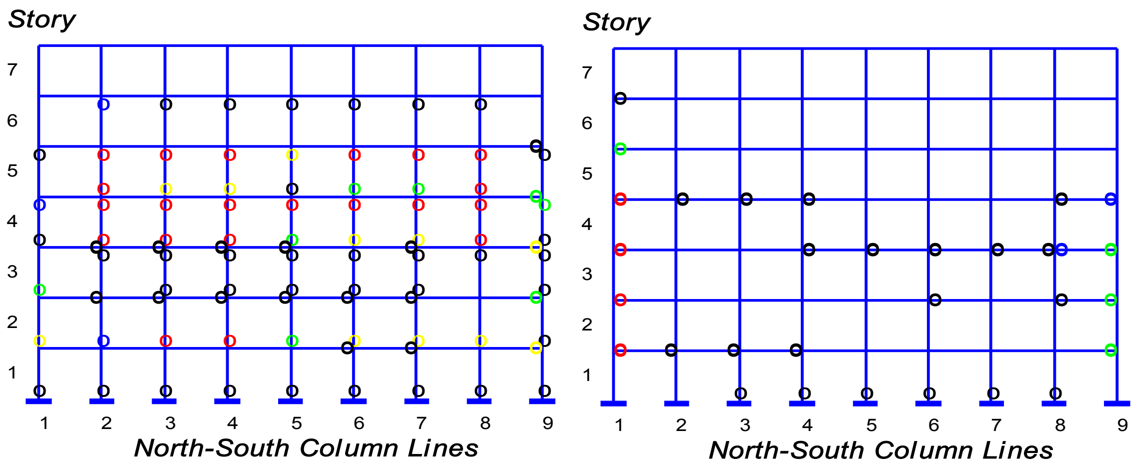

(b) External **(a) Internal**

Figure E. 6: Locations and types of member failures for model M2 at 1.2% roof drift.

E.4. Model M3 (Rigid: no gravity/ no shear/ no splice)

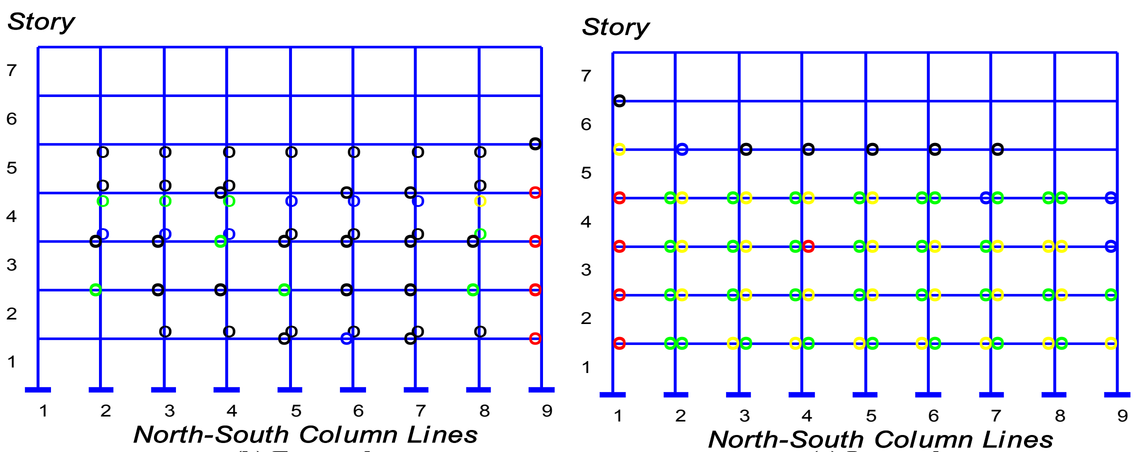

(b) External **(a) Internal**

Figure E. 7: Locations and types of member failures for model M3 at 0.6% roof drift.

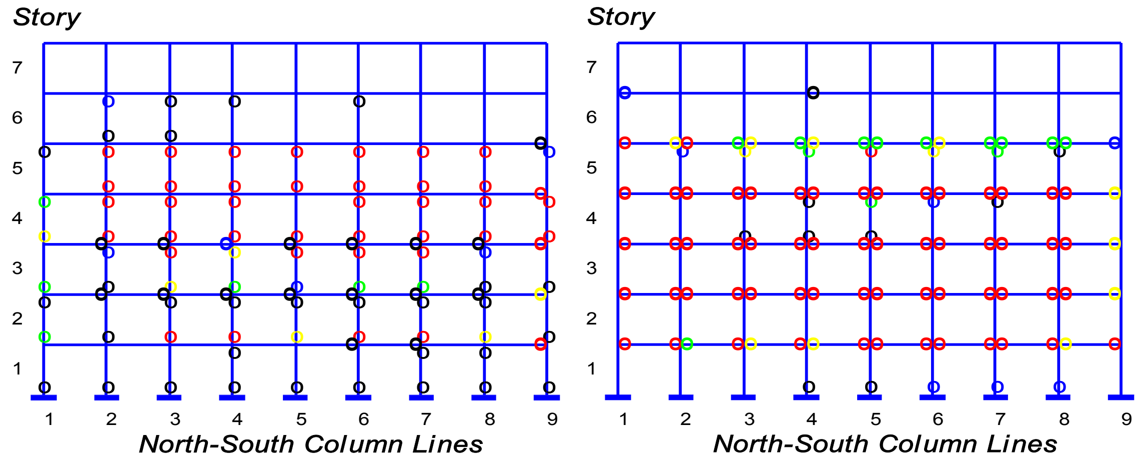

(b) External **(a) Internal**

Figure E. 8: Locations and types of member failures for model M3 at 0.9% roof drift.

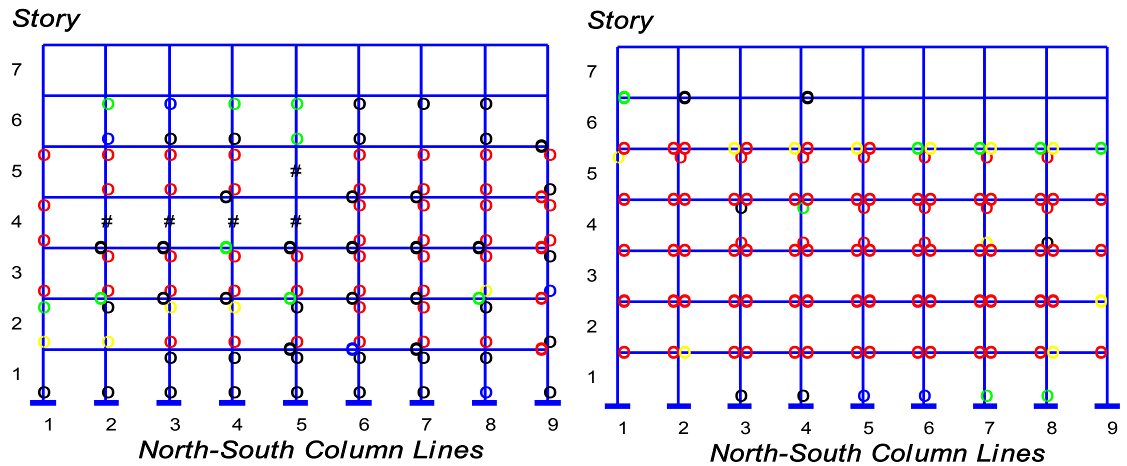

(b) External **(a) Internal**

Figure E. 9: Locations and types of member failures for model M3 at 1.2% roof drift.

E.5. Model M4 (UW-MnJ-BS: gravity/ no shear/ no splice)

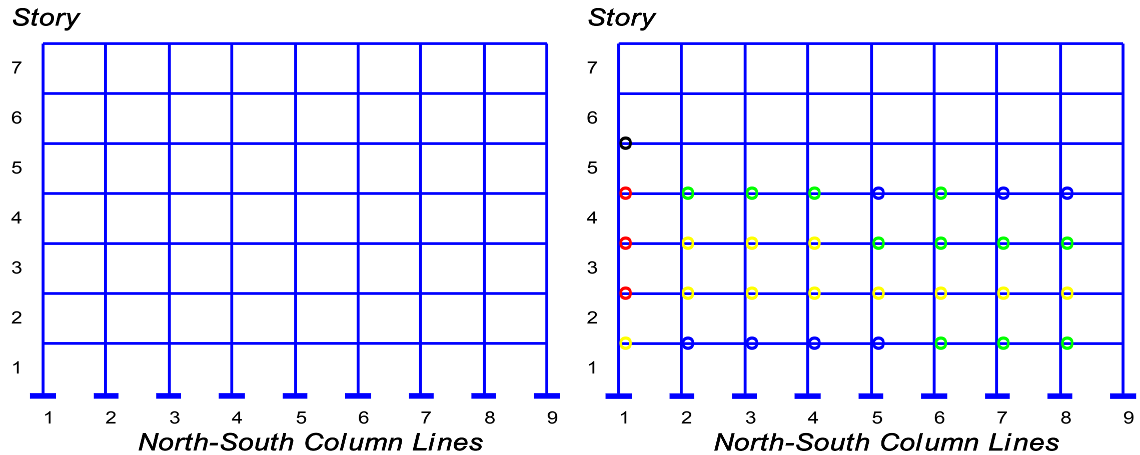

Figure E. 10: Locations and types of member failures for model M4 at 0.6% roof drift.

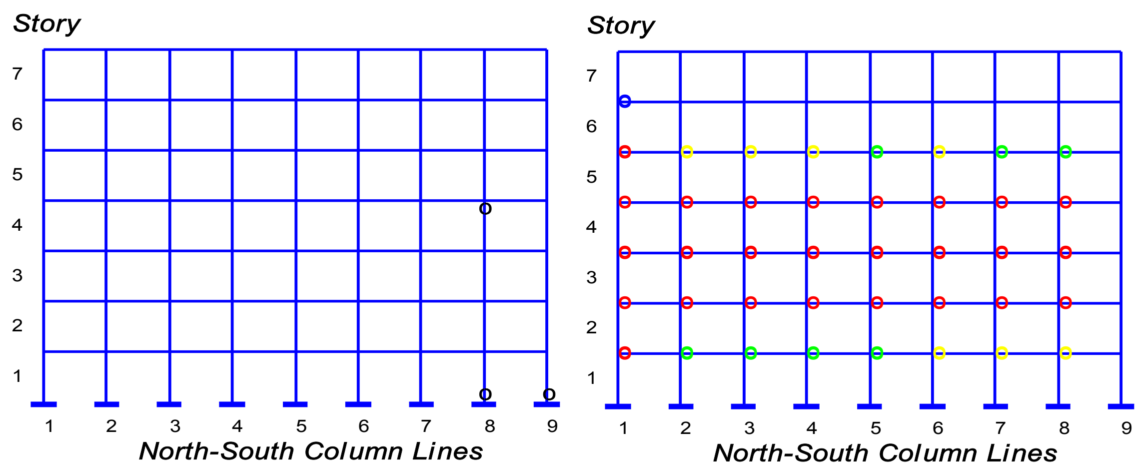

Figure E. 11: Locations and types of member failures for model M4 at 1.2% roof drift.

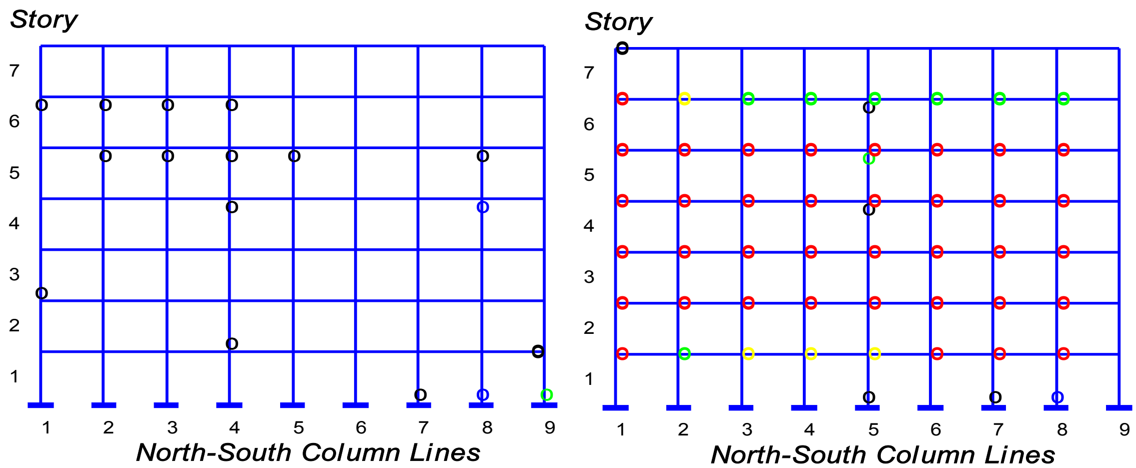

Figure E. 12: Locations and types of member failures for model M4 at 1.8% roof drift.

E.6. Model M5 (RS-MnB: gravity/ no shear/ no splice)

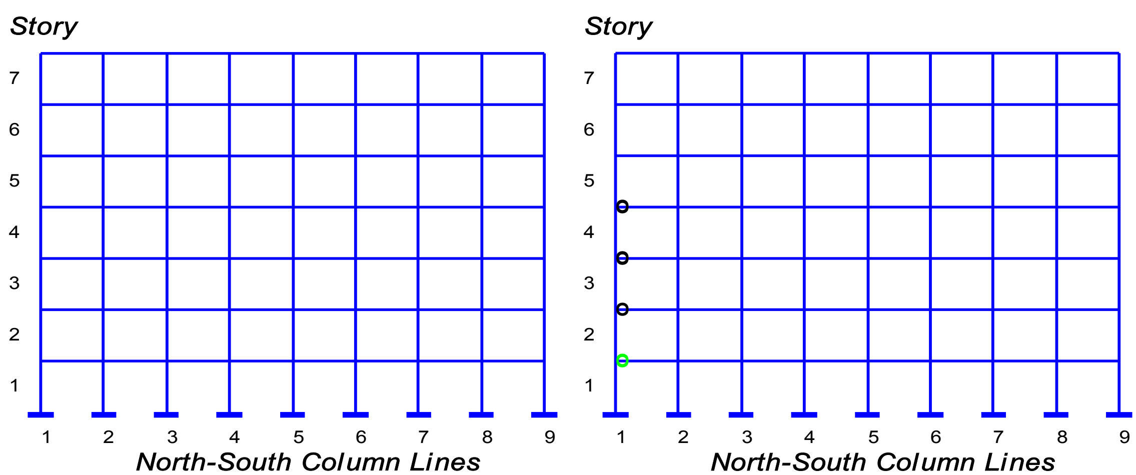

Figure E. 13: Locations and types of member failures for model M5 at 0.6% roof drift.

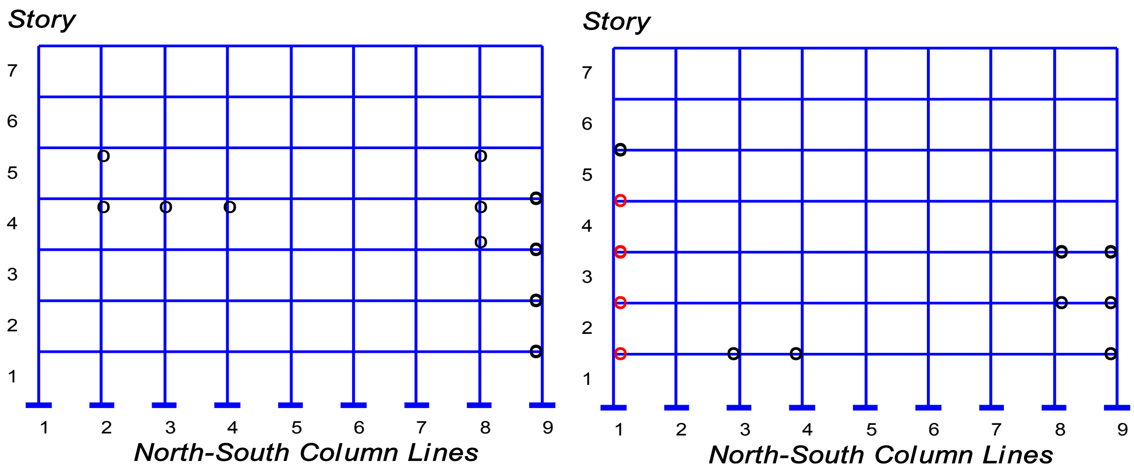

Figure E. 14: Locations and types of member failures for model M5 at 1.0% roof drift.

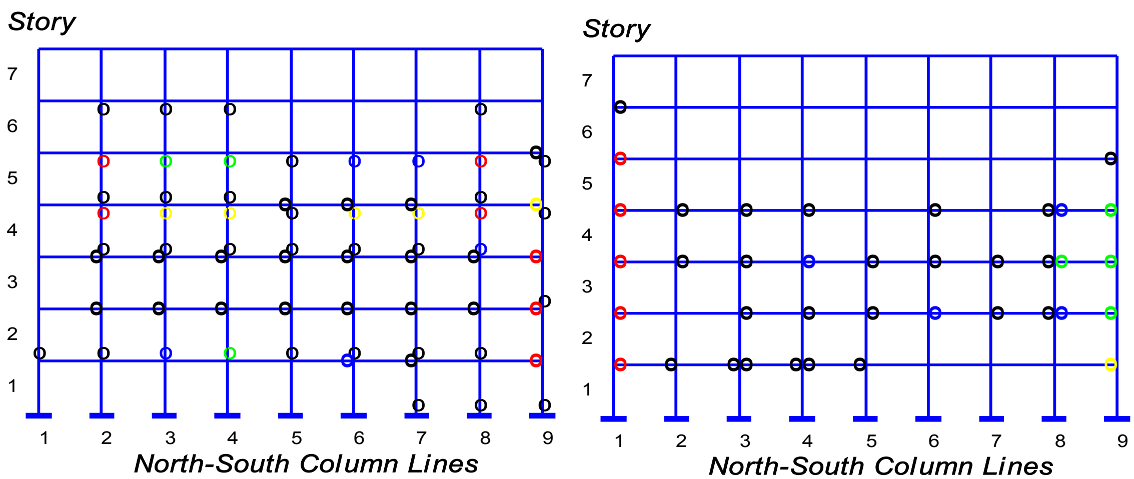

Figure E. 15: Locations and types of member failures for model M5 at 1.4% roof drift.

E.7. Model M6 (Rigid: gravity/ no shear/ no splice)

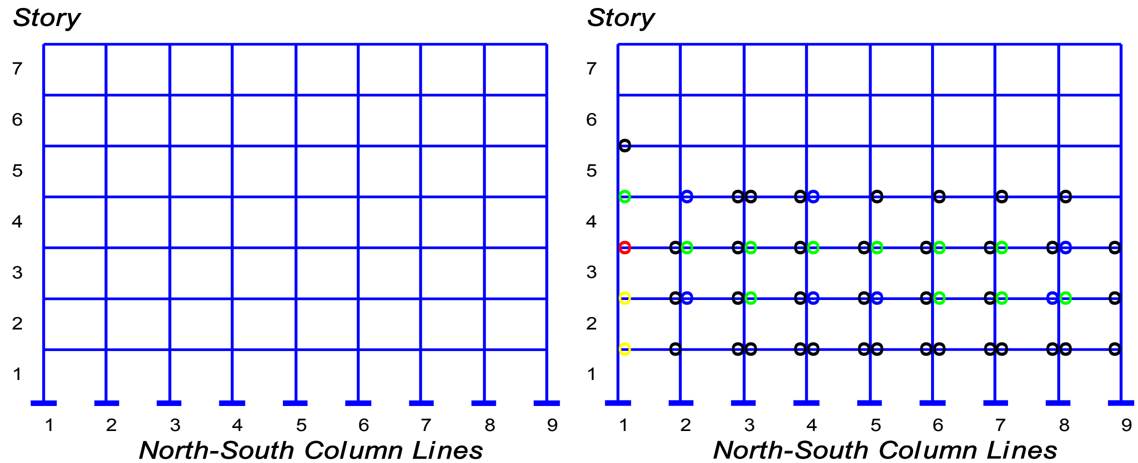

Figure E. 16: Locations and types of member failures for model M6 at 0.4% roof drift.

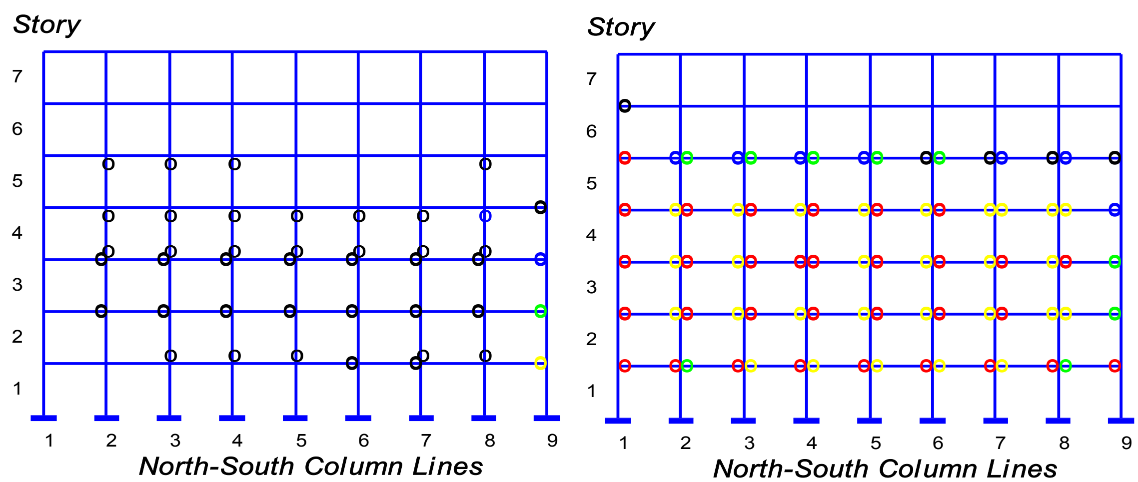

Figure E. 17: Locations and types of member failures for model M6 at 0.7% roof drift.

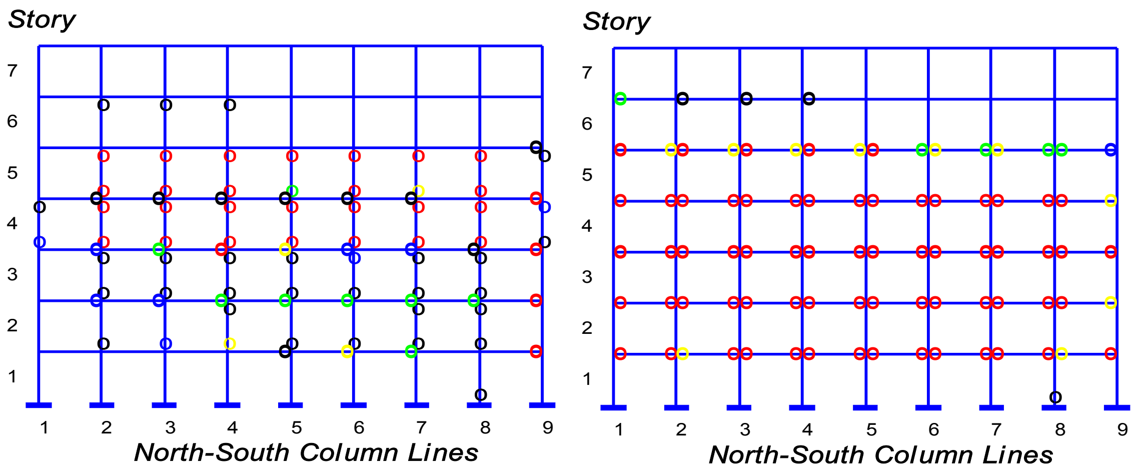

Figure E. 18: Locations and types of member failures for model M6 at 1.0% roof drift.

E.8. Model M7 (UW-MnJ-BS: no gravity/ shear/ splice)

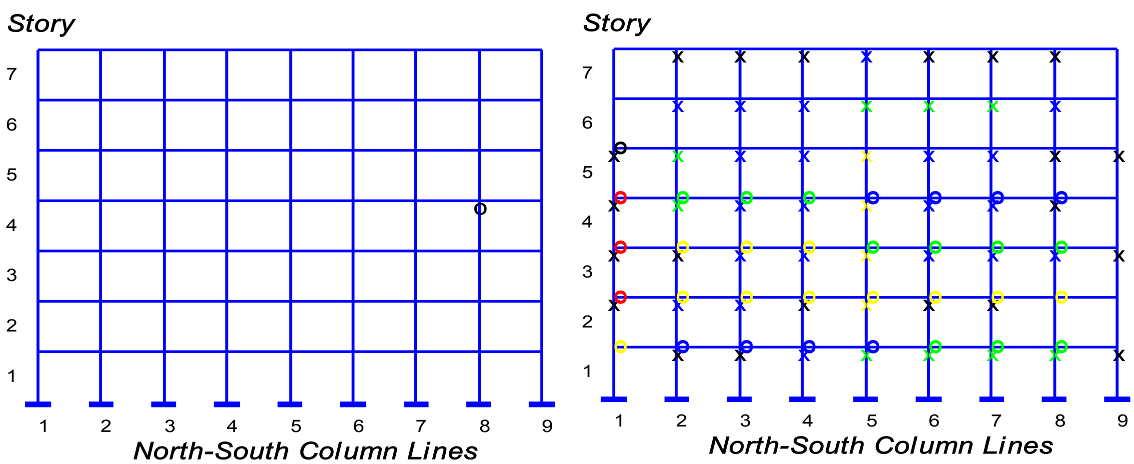

Figure E. 19: Locations and types of member failures for model M7 at 0.6% roof drift.

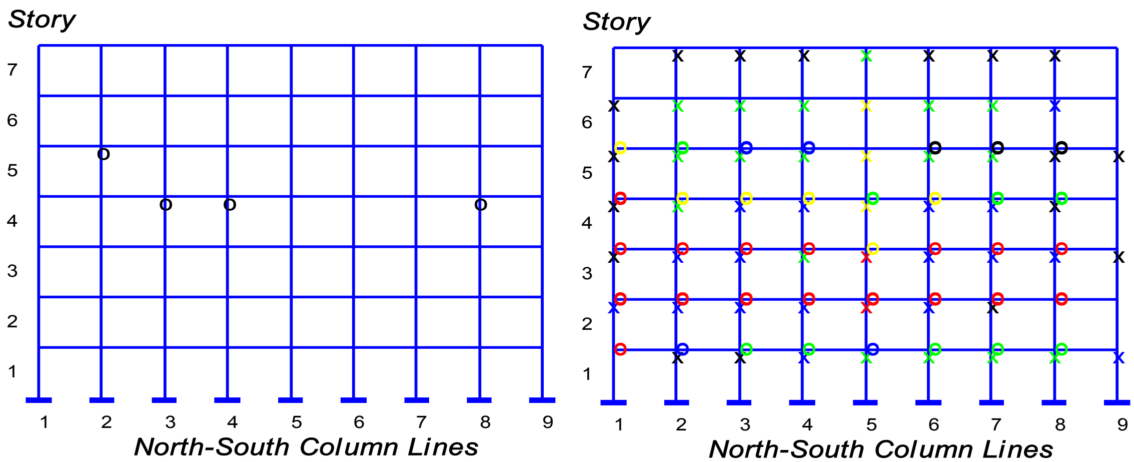

Figure E. 20: Locations and types of member failures for model M7 at 0.8% roof drift.

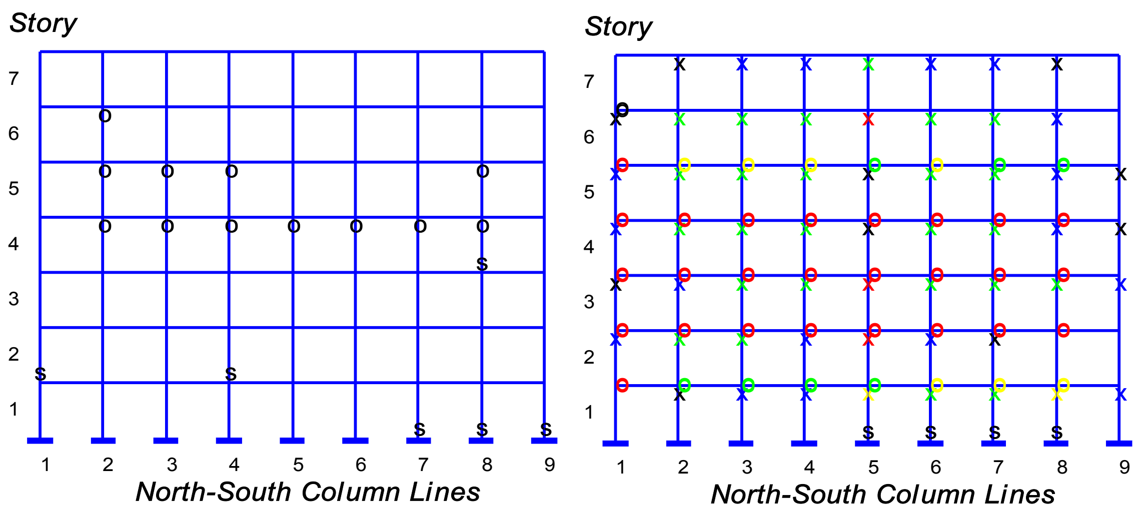

Figure E. 21: Locations and types of member failures for model M7 at 1.2% roof drift.

E.9. Model M8 (RS-MnB: no gravity/ shear/ splice)

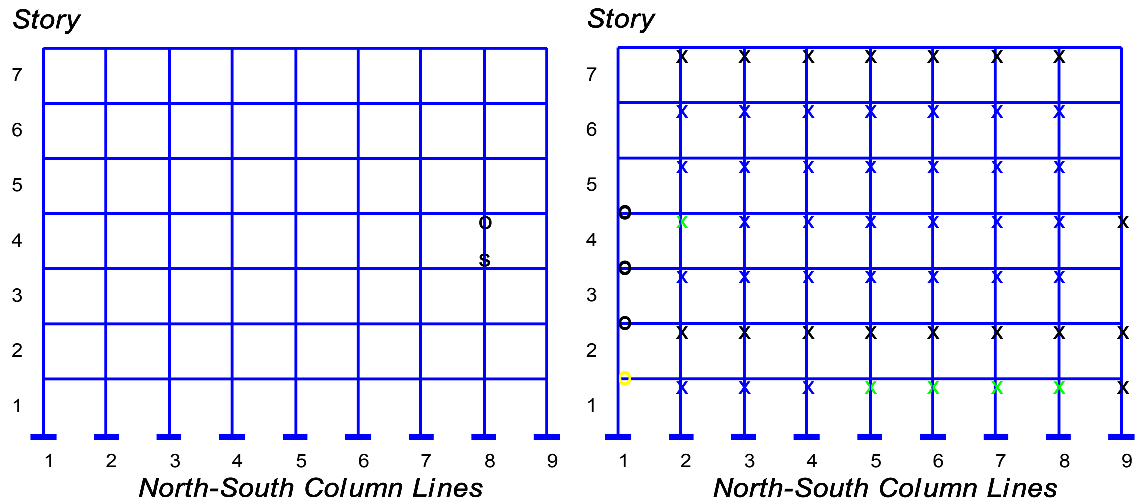

Figure E. 22: Locations and types of member failures for model M8 at 0.6% roof drift.

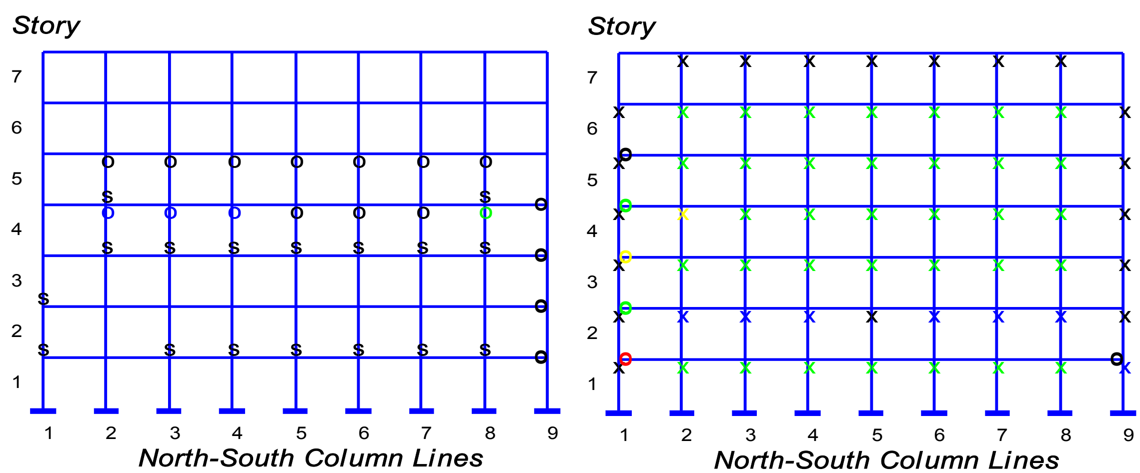

Figure E. 23: Locations and types of member failures for model M8 at 0.8% roof drift.

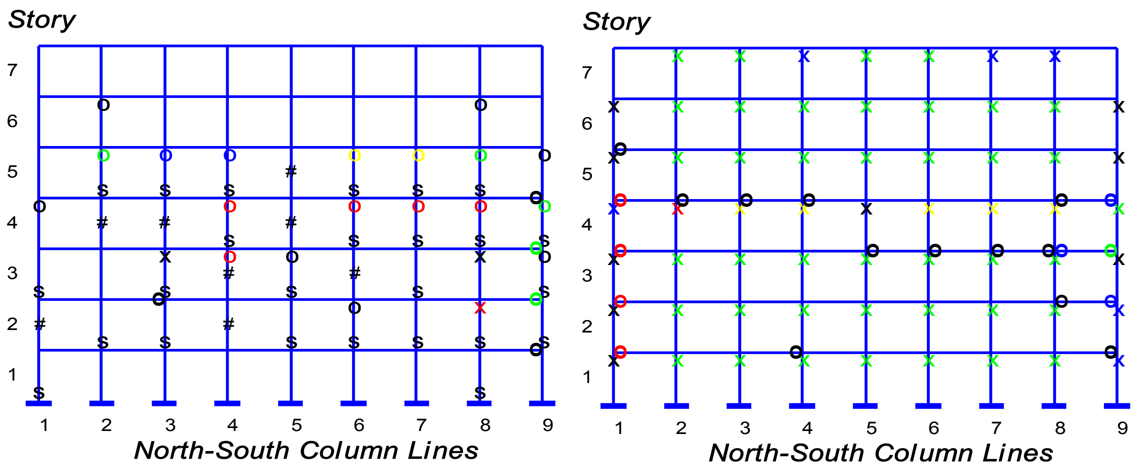

Figure E. 24: Locations and types of member failures for model M8 at 1.1% roof drift.

E.10. Model M9 (Rigid: no gravity/ shear/ splice)

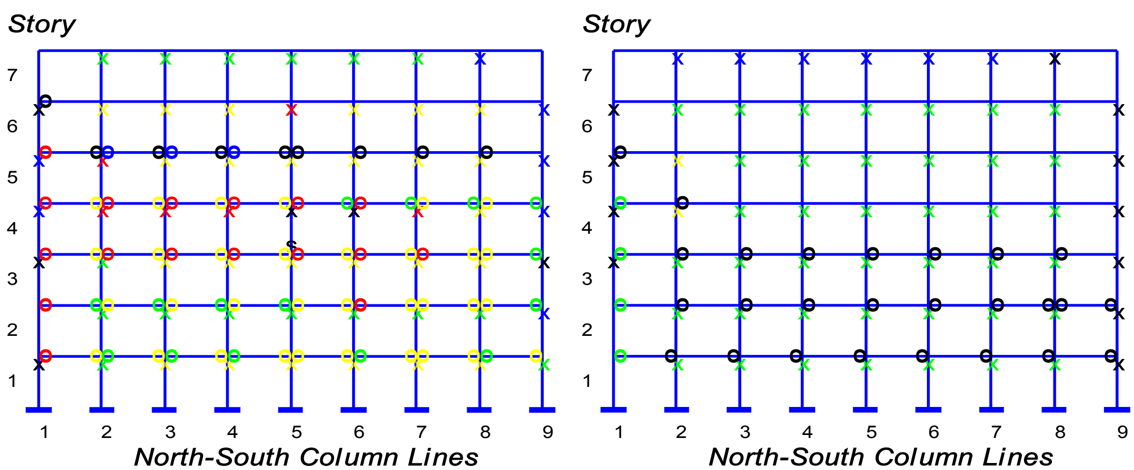

Figure E. 25: Locations and types of member failures for model M9 at 0.4% roof drift.

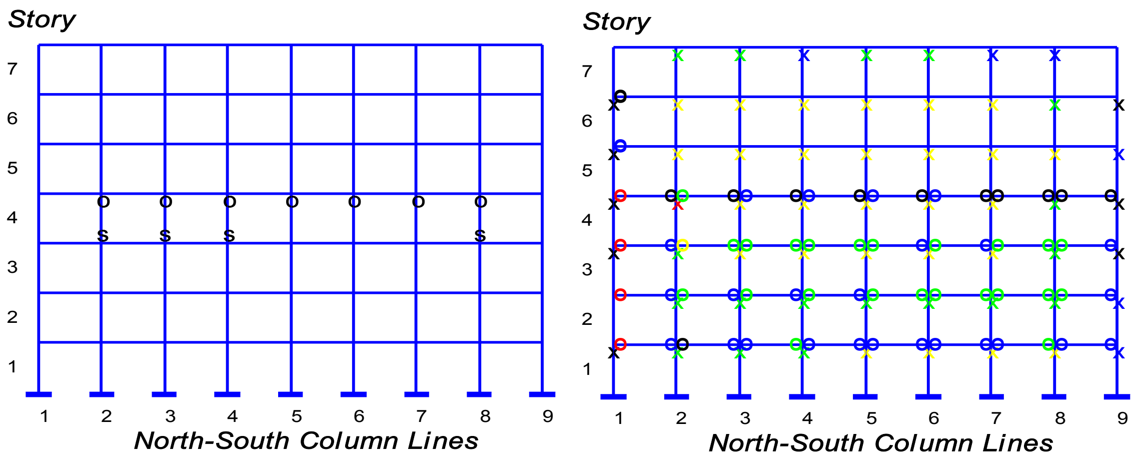

Figure E. 26: Locations and types of member failures for model M9 at 0.5% roof drift.

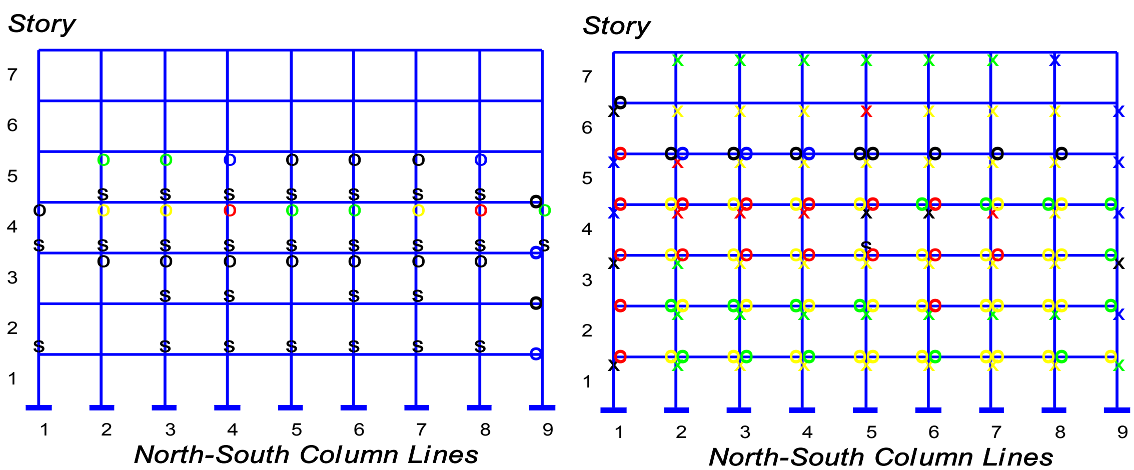

Figure E. 27: Locations and types of member failures for model M9 at 0.6% roof drift.

E.11. Model M10 (UW-MnJ-BS: Gravity/ shear/ splice)

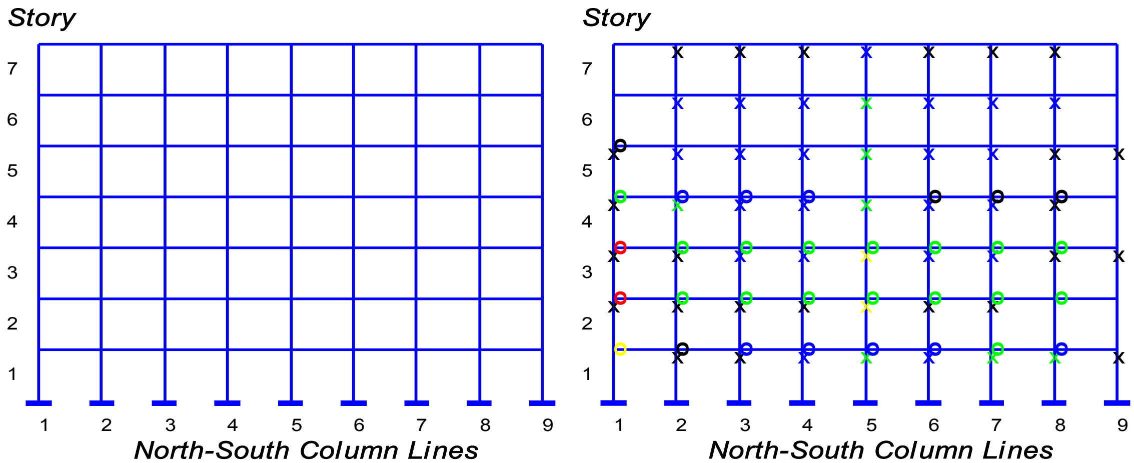

Figure E. 28: Locations and types of member failures for model M10 at 0.5% roof drift.

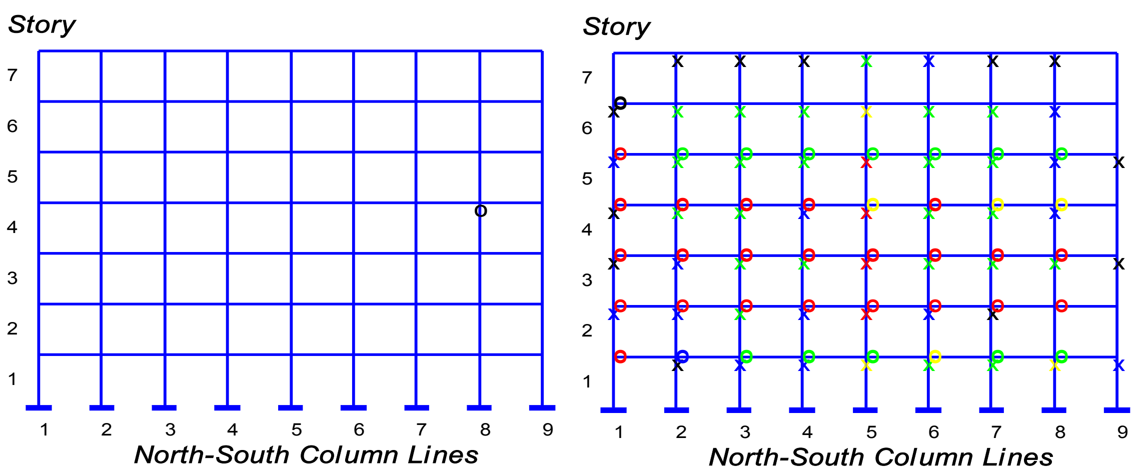

Figure E. 29: Locations and types of member failures for model M10 at 1.0% roof drift.

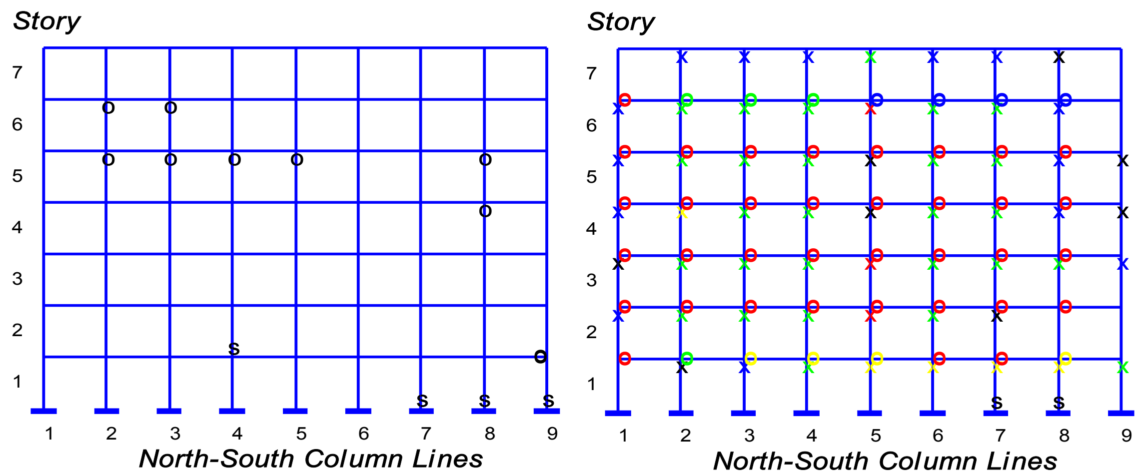

Figure E. 30: Locations and types of member failures for model M10 at 1.6% roof drift.

E.12. Model M11 (RS-MnB: Gravity/ shear/ splice)

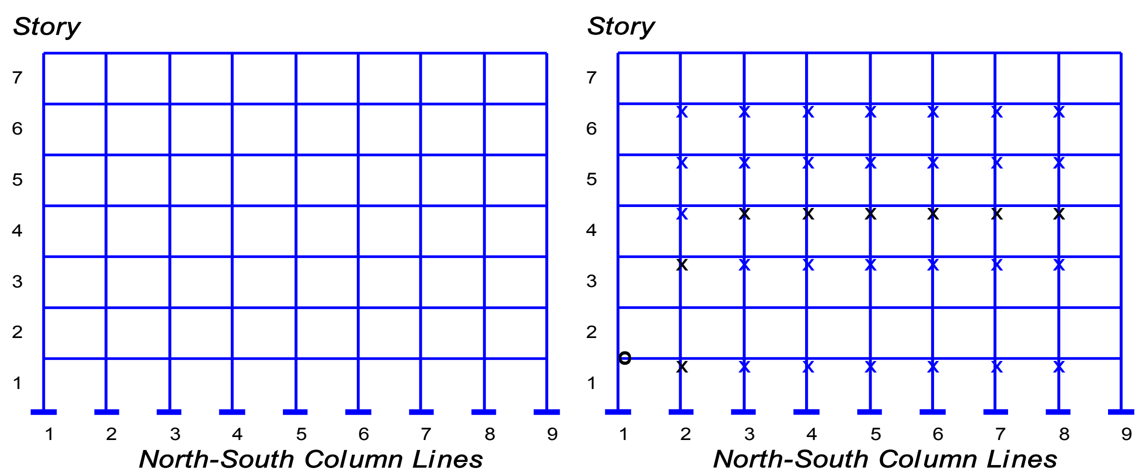

Figure E. 31: Locations and types of member failures for model M11 at 0.5% roof drift.

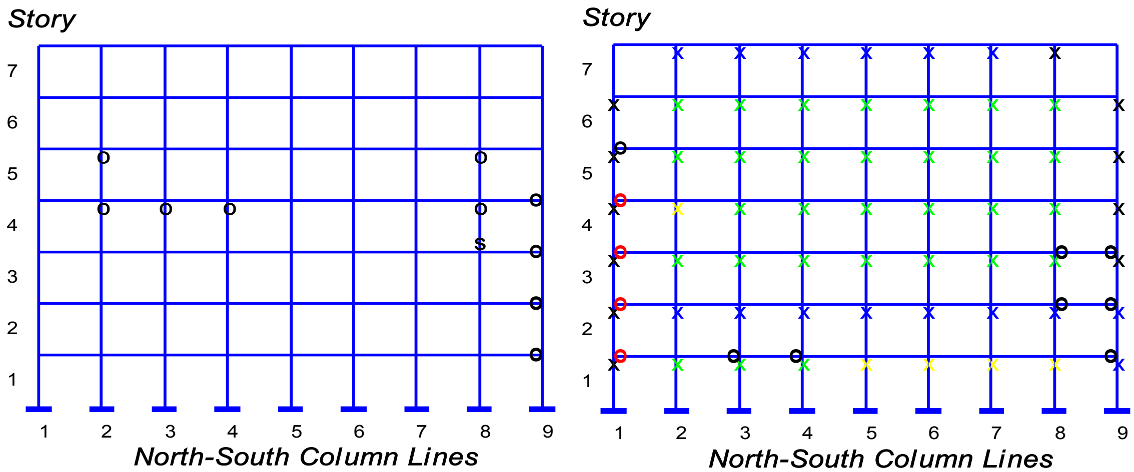

Figure E. 32: Locations and types of member failures for model M11 at 1.0% roof drift.

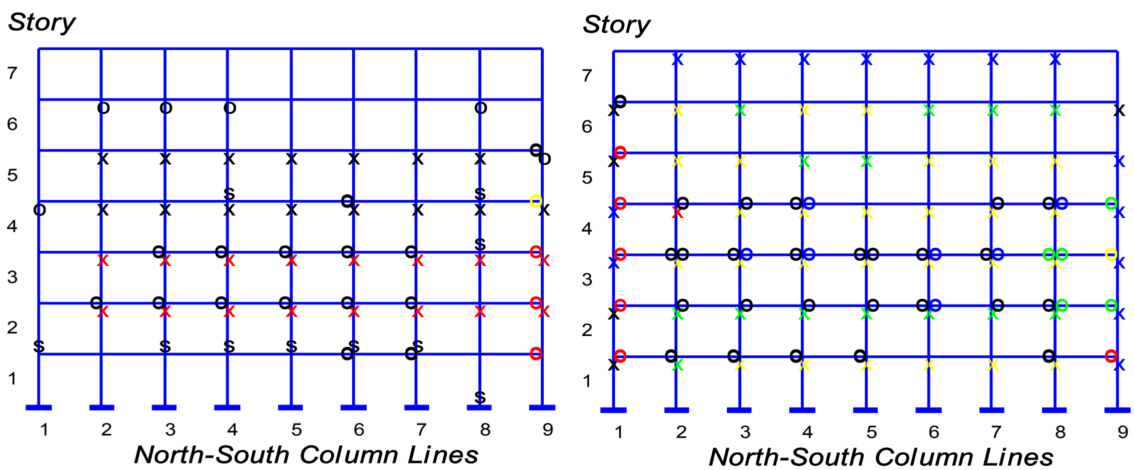

Figure E. 33: Locations and types of member failures for model M11 at 1.4% roof drift.

E.13. Model M12 (Rigid: Gravity/ shear/ splice)

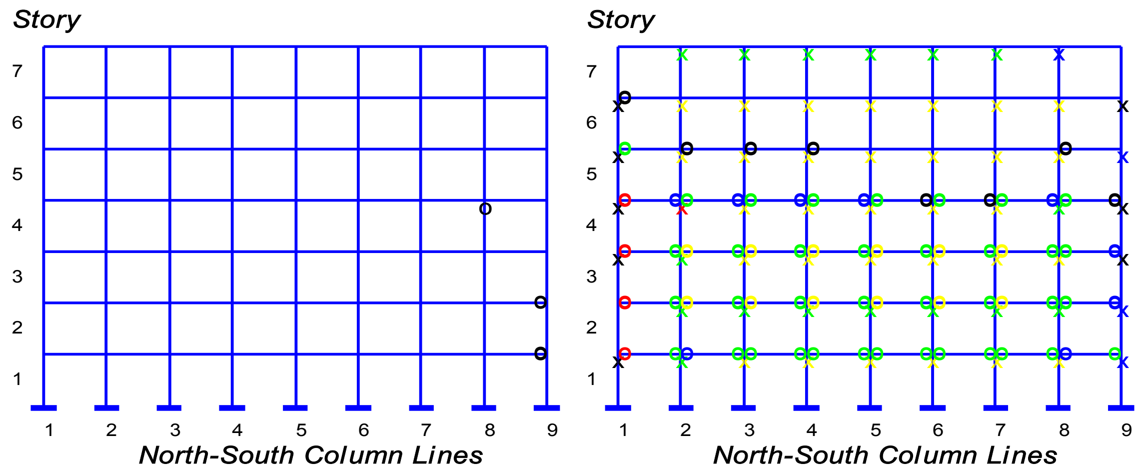

Figure E. 34: Locations and types of member failures for model M12 at 0.5% roof drift.

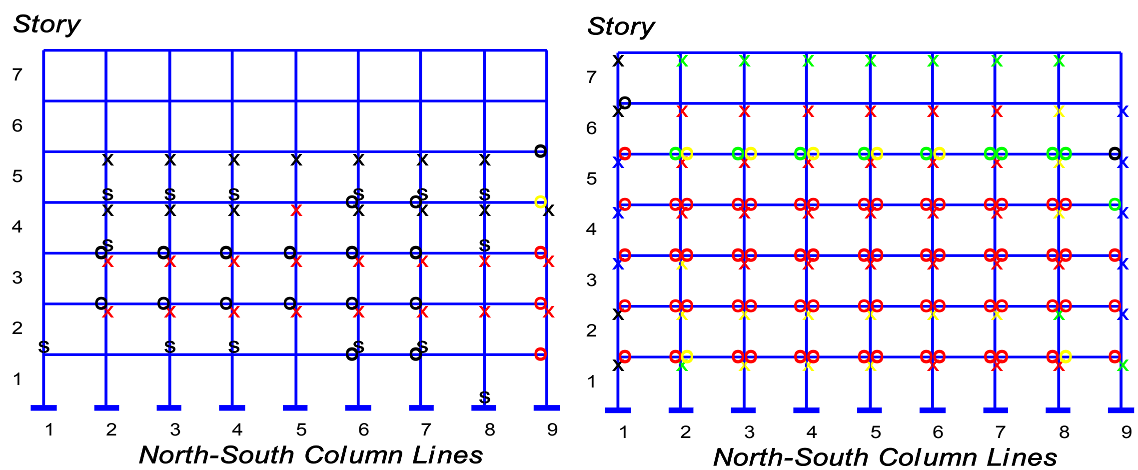

Figure E. 35: Locations and types of member failures for model M12 at 1.0% roof drift.

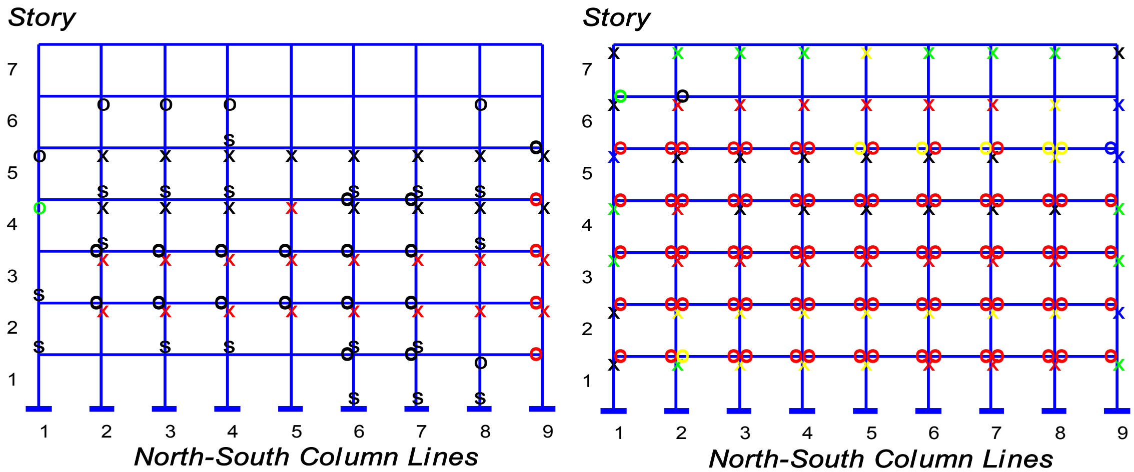

Figure E. 36: Locations and types of member failures for model M12 at 1.5% roof drift.